UNIVERSITY OF SOUTHAMPTON

FACULTY OF BIOMEDICAL SCIENCE

School of Medicine

Mechanisms of multidrug resistance in bladder cancer:

The role of the nuclear membrane

Jonathan Mark Featherstone

BM MRCS(Eng)

British Urological Foundation Scholar 2003-2004

Thesis submitted for the degree of

Doctor of Medicine

December 2007

UNIVERSITY OF SOUTHAMPTON

ABSTRACT:

FACULTY OF BIOMEDICAL SCIENCE

SCHOOL OF MEDICINE

Doctor of Medicine

Mechanisms of multidrug resistance in bladder cancer: The role of nuclear membrane

By Jonathan Mark Featherstone

Multidrug resistance (MDR) describes the phenomenon whereby cancer cells exposed to a single cytotoxic drug develop cross resistance to numerous other structurally unrelated chemotherapeutics. The development of MDR is a major cause of cancer chemotherapy treatment failure in all types of cancer.

Numerous mechanisms of MDR have been elucidated which include ATP-binding cassette (ABC) transporter proteins, cytoplasmic vaults, alterations in topoisomerase II and increased expression of glutathione-S-transferases, all of which result in reduced chemotherapeutic efficacy.

Superficial bladder cancer is commonly treated with adjuvant intravesical chemotherapy using mitomycin C or epirubicin (an anthracycline), following surgical resection. However, despite this treatment, the recurrence rates of these tumours can approach 60%. This high recurrence rate represents the development of MDR in many cases.

Previous work using anthracycline fluorescence has shown that MDR cells have reduced levels of anthracycline uptake and also demonstrate a characteristic nuclear sparing of drug uptake. This nuclear sparing phenomenon in MDR cells transcends tissue type and suggests that the nuclear membrane may also play a role in MDR.

The work described herein discusses the current role of chemotherapy in the treatment of superficial bladder cancer, mechanisms of MDR and the role of the nuclear membrane in MDR. Following this our investigation of the role of the nuclear membrane is described, using a number of novel techniques including cell fusion and microinjection. In addition, we investigated MDR modulation by verapamil, with analysis of changes in cellular, cytoplasmic and nuclear drug uptake mediated by this known MDR reversing agent.

LIST OF CONTENTS

List of figures: Page No.

List of tables:

DECLARATION OF AUTHORSHIP

I, Jonathan Mark Featherstone, declare that the thesis entitled

Mechanisms of multidrug resistance in bladder cancer: The role of the nuclear membrane

And the work presented in the thesis are both my own, and have been generated by me as the result of my own original research. I confirm that:

- This work was done wholly or mainly while in candidature for a research degree at this University;
- Where any part of the thesis has previously been submitted for a degree or any other qualification at this University or any other institution, this has been clearly stated;
- Where I have consulted or published the work of others, this is always clearly attributed;
- Where I have quoted from the work of others, the source is always given. With the exception of such quotations, this thesis is entirely my own work;
- I have acknowledged all main sources of help;
- Where the thesis is based on work done by myself jointly with others, I have made clear exactly what was done by others and what I have contributed myself;
- Parts of this work have been published as:

  Green Fluorescent Protein labelling is compatible with multidrug resistant clones in bladder cancer models
  C Davies, B Lwaleed, **J Featherstone**, A Cooper
  Uro-Oncology, June 2004; 4(2): 91 – 96.

  The nuclear membrane in multidrug resistance: microinjection of epirubicin into bladder cancer cell lines
  J M Featherstone, A G Speers, B A Lwaleed, M C Hayes, A J Cooper and B R Birch.
  BJU *International*, May 2005; 95(7): 1091 – 8.

Signed:

Date:

Acknowledgements:

I would like to express my thanks to the following people who have helped me both practically and theoretically with this work.
Dr Alan Cooper has been untiring in his supervision, support and motivation and has provided many of the ideas that have gone on to generate this piece of research. Mr Brian Birch for his continued interest and involvement throughout my research period. Mrs Jeanette Beverage for her instruction in the use of the confocal microscope and continued support with "confocal problems". Mrs Jill Rice for her help with laboratory cell culture and generally putting up with us invading her lab and "borrowing" her culture media periodically! Dr Kathy Triantifilous and Dr Jill Whitaker for instruction in the use of the BD FACScaliber flow cytometer. Dr Sara Campbell for allowing me some perform some cell culture in Southampton Nephrology laboratories.
Dr Graham Packham for allowing me to use the microinjection set-up in his laboratory.
The British Urological Foundation and Sanofi-Synthelabo for their combined scholarship from May 2003 – May 2004 which funded much of this research.
Finally I would like to thank my family. Firstly my wife, Vicky, for her continued support throughout my time in research and for shouldering the burden of family responsibilities in recent months, in order to allow me the time and space to complete this thesis. Thanks also to my children, Thomas and Sophie for tolerating my absence in recent months and providing me with regular welcome distractions from this work.

I would like to dedicate this research to my late grandfather, Donald Charles Featherstone who died of prostate cancer in January 2003, aged 82.

Abbreviations:

ABC	ATP binding cassette
AO	acridine orange
APS	ammonium persulphate
ATP	adenosine triphosphate
BCG	Bacille Calmette Guerin
BCRP	breast cancer resistance protein
b-FGF	basic fibroblast growth factor
BP	band pass
BSA	bovine serum albumin
Cis	carcinoma in situ
CT	computed tomography
DIC	differential interference contrast
DMEM	Dulbecco's modification of Eagle's medium
DMSO	Dimethyl sulphoxide
DNA	deoxyribonucleic acid
EB	ethidium bromide
EDTA	ethylene diamine tetracetic acid
EGF	epidermal growth factor
EGFR	epidermal growth factor receptor
EMDA	electromotive drug administration
EORTC	European Organisation for Research and Treatment of Cancer
EPI	epirubicin
ER	endoplasmic reticulum
FCS	foetal calf serum
FDA	fluorescein diacetate
FITC	fluoroscein isothiocyanate
FSC	forward scatter
GFP	green fluorescent protein
GSH	glutathione
GST	glutathione-S-transferase
HBBS	Hanks' balance salt solution
HeNe	Helium-Neon
HEPES	N-2-hydroxyethylpiperazine-N'-2-ethanesulphonic acid

IC50	inhibitory concentration (50%)
IC90	inhibitory concentration (90%)
IgG	immunoglobulin G
IVU	intravenous urogram
KDa	kiloDalton
LP	long pass
LRP	lung resistance protein
MAP	mitogen-activated protein
MDa	megaDalton
MDR	multidrug resistance
MeGLA	meglumine γ-linolenic acid
MMC	mitomycin C
MRC	Medical Research Council
MRI	magnetic resonance imaging
mRNA	messenger RNA
MRP	multidrug resistance-related protein
MSD	membrane spanning domain
MTT	3-[4,5-dimethylthiazol-2-yl]-2,5-diphenyltetrazolium bromide
MVAC	methotrexate, vinblastine, adriamycin and cisplatin
MVP	major vault protein
MXR	mitoxantrone resistance protein
NBD	nucleotide binding domain
NE	nuclear envelope
NPC	nuclear pore complex
PARP	poly(ADP-ribose) polymerase
PBS	phosphate buffered saline
PBSI	PBS containing protease and phosphatase inhibitors
P-gp	P-glycoprotein
PI	propidium iodide
PLC	prelysosomal sorting compartment
PMSF	phenylmethylsulphonyl fluoride
RanGAP	RanGTPase activating protein
RanGEF	Ran guanine nucleotide exchange factor

Rb	retinoblastoma gene
ROI	region of interest
RNA	ribonucleic acid
rpm	revolutions per minute
RT-PCR	reverse transcriptase-polymerase chain reaction
SSC	side scatter
TCC	transitional cell carcinoma
TEMED	N,N,N'N' – tetramethylethylenediamine
TEP1	telomerase associated protein
TMD	transmembrane domain
TNM	tumour nodes metastases (classification)
TOPO II	topoisomerase II
TUR	transurethral resection
TURBT	transurethral resection of bladder tumour
VEGF	vascular endothelial growth factor
VER	verapamil
VPARP	vault-poly (ADP-ribose) polymerase
WGA	wheat germ agglutinin
WHO	World Health Organisation
5-ALA	5-aminolevulinic acid

Chapter 1. Introduction and literature review

1.1: Bladder Cancer:

The majority of bladder cancers (90 – 95%) are transitional cell carcinomas (TCC) with the remainder being either squamous cell, adeno- or small cell carcinomas. The incidence of transitional cell carcinoma of the bladder had until recently been rising annually, in both the western world and developing countries. This increase mirrored the increasing prevalence of cigarette smoking in western societies and the spread of smoking to developing countries, throughout the last century.

However, since the introduction of the new World Health Organisation (WHO) grading system in 2004, some low-grade, non-invasive tumours are no longer classified as cancers, so do not appear in cancer registry statistics with a resultant fall in the reported incidence of bladder cancer.

Incidence

In England, bladder cancer is the fourth most common cancer in males, accounting for 4.9% of all malignant neoplasms, while in females it is ranked tenth accounting for only 2% of all cancers [1] (excluding non-melanomatous skin cancers).

In 2004, 8,137 new cases were diagnosed in England, affecting 5,800 males and 2,337 females. These figures give age standardised incidence rates of 18.8 per 100,000 of the male population and 5.5 per 100,000 of the female population [1].

In 2004, bladder cancer was the eighth most common cancer death accounting for 4,301 deaths in England and Wales, 2,840 in males and 1,461 in females. These figures give age standardised mortality rates of 8.4 per 100,000 males and 2.8 per 100,000 females [2].

The incidence of bladder cancer increased through the mid-1970s peaking in the late 1980s. There has also been a gradual decline in the male to female ratio of age standardised incidence rates from 4.1 **:** 1 in 1971 to 3.4 **:** 1 in 1997 (Figure 1). This narrowing of the sex ratio has been widely attributed to increased rates of cigarette smoking amongst women and was predicted to narrow further [3]. However, the latest figures from 2004 show that the sex ratio has remained steady at 3.4 **:** 1 [1].

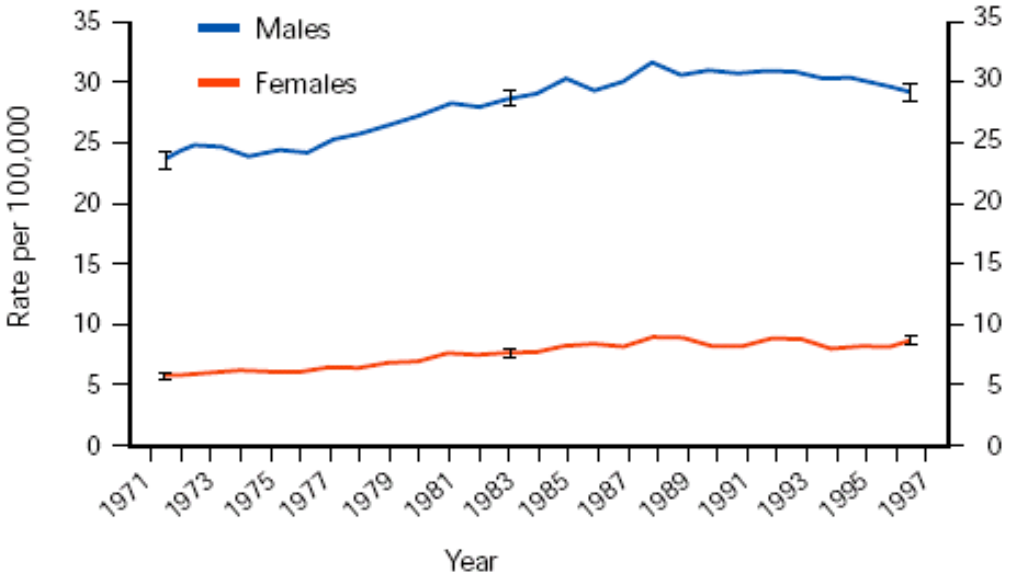

Figure 1: Age-standardised incidence of bladder cancer, England and Wales, 1971 – 1997 (Reproduced with kind permission of National Statistics [4]).

Despite this increasing incidence, mortality from bladder cancer has fallen in males since the early 1970s from just under 13 deaths per 100,000 to 8.4 per 100,000 in 2004. However, the female mortality rate has remained fairly static at around 3 per 100,000 females since 1950 (Figure 2).

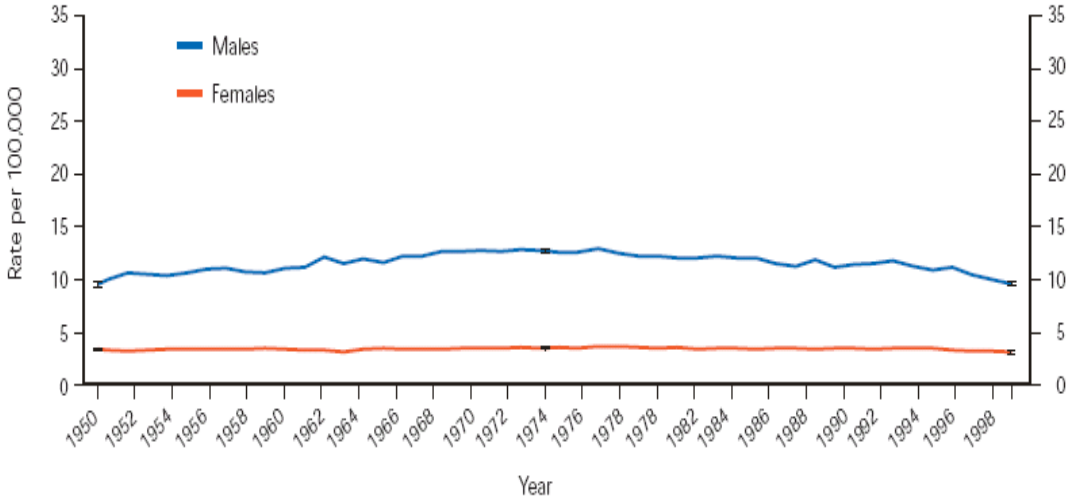

Figure 2: Age-standardised bladder cancer mortality by sex, England and Wales, 1950 – 1999 (Reproduced with kind permission of National Statistics [4]).

Regional bladder cancer statistics for the South West region supplied by South West Public Health Observatory (SWPHO), show that in 2005 bladder cancer was the seventh commonest cancer accounting for 708 new cancer

registrations in men and 267 in women. In the same year it was the tenth most common cause of cancer death accounting for 285 deaths in men and 153 deaths in women.

These figures for bladder cancer in the South West in 2005, give regional age standardised incidence rates of 20.0 and 5.6 per 100,000 for men and women respectively. These are similar to the national age standardised incidence rates for the same year (Table 1).

Age standardised mortality incidences for bladder cancer in the South West in 2004 were 7.7 and 2.8 per 100 000 population for men and women respectively. These figures are again similar to the national age standardised mortality rates for the same year (Table 1).

	Age standardised Incidence /100,000 population	Age standardised Mortality /100,000 population
	England	England and Wales
England and Wales 2004		
Male	18.8	8.4
Female	5.5	2.8
South West 2004		
Male	20.0	7.7
Female	5.6	2.8

Table 1: Comparison of National and Regional Age standardised incidence and mortality of bladder cancer from 2004.

From the age of forty the incidence of bladder cancer rises steadily up to the age of 60, where the rate of increase becomes steeper peaking in the over 85 age group in both sexes (Figure 3). Mortality incidences show a similar pattern peaking in the over 85 age group (Figure 4).

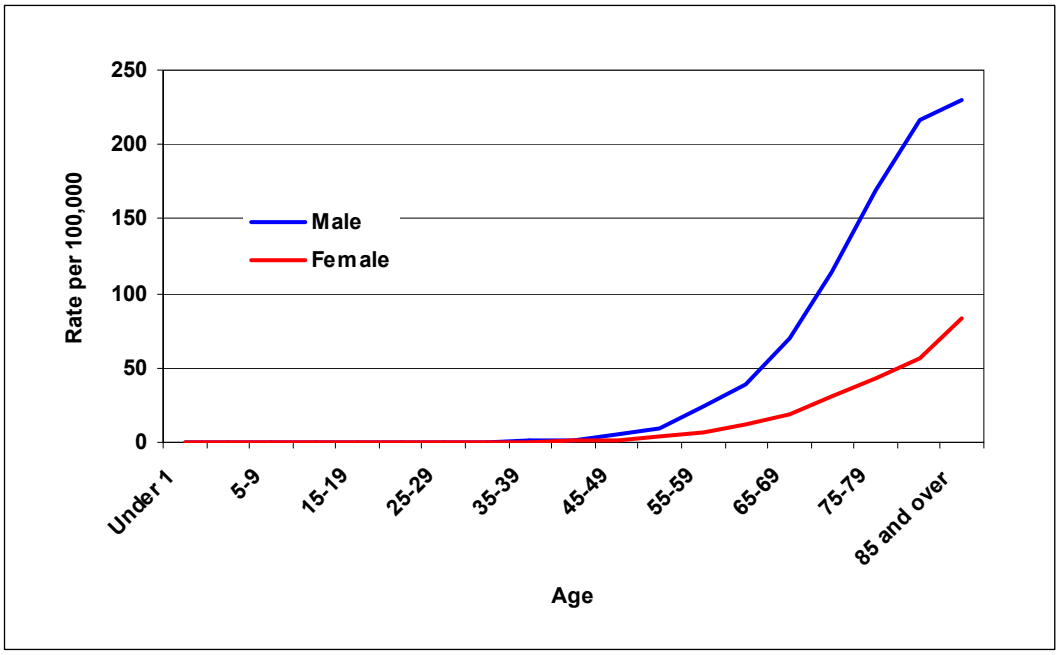

Figure 3: Age specific incidence of bladder cancer, England and Wales, 2004 (Produced from data published by National Statistics [1]).

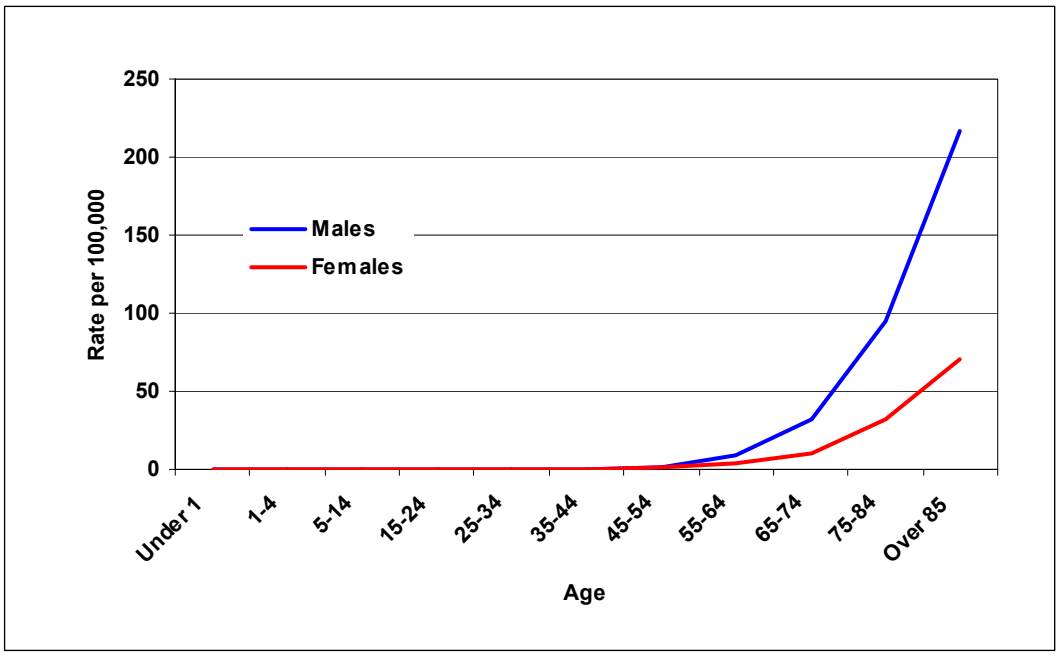

Figure 4: Age specific bladder cancer mortality, England and Wales, 2004 (Produced from data published by National Statistics [2]).

Aetiology

Bladder cancer aetiology is multifactorial, with both environmental and genetic factors playing a role in carcinogenesis.

Environmental Factors

A number of occupational and non-occupational environmental factors are associated with the development of bladder cancer (Table 2). The most important factors will be dealt with in this section.

Occupational	Non-occupational
2-Naphthylamine	Cigarette smoking
4-Aminobiphenyl	Phenacetin-containing analgesics /
Benzidine	Analgesic abuse nephropathy
4,4'Methylenebis(2-chloroaniline)	Cyclophosphamide
4-Chloro-o-toluidine	Chlornaphazine
o-toluidine	Thiotepa*
Methylene dianiline	Melphalan*
Benzidine-derived azodyes	Radiotherapy
	Balkan Nephropathy
	Arsenic
	Bladder calculi
	Recurrent UTI
	Schistosomiasis
	Long-term catheterisation

Table 2: Aetiological factors in bladder cancer
(*Associated with radiotherapy)

Occupational / Industrial factors

Historically, occupational or industrial exposure has contributed to bladder cancer causation, accounting for 18 – 35% of cases in men and 1 – 6% of cases in women [5]. Aniline dye workers were reported to be at increased risk of developing bladder cancer in 1895 [6]. However, the carcinogenic compound responsible, 2-naphthylamine, was only identified in 1938 [7]. In 1954, links were demonstrated between exposure to aromatic amines and bladder cancer in a large number of British industrial workers, not only in the dye industry but also the rubber, textile and chemical industries [8,9]. Exposure to other aromatic amines, such as benzidine and 4-amino-biphenyl

was subsequently shown to be the cause of these industry related bladder cancers.

Bladder cancers caused by industrial exposure are now declining due to increased awareness of the carcinogens responsible and the introduction of appropriate protective measures to reduce worker exposure to these occupational carcinogens.

Non-occupational factors

Cigarette smoking is the single most important cause of bladder cancer in industrialised developed countries, accounting for 25 – 60% of all cases of bladder cancer [10]. The increase in cigarette smoking throughout the twentieth century appears to be responsible for the rising incidence of bladder cancer in Western countries [3,11]. The precise mechanism by which cigarette smoking causes bladder cancer remains unresolved, although it is most likely related to one or more of the numerous chemicals present in cigarette smoke. There is considerable evidence that aromatic amines, especially 4-aminobiphenyl and *o*-toluidine, are associated with cigarette smoking and bladder cancer [12,13]. Other aromatic amines, including pyrolysis products, are possible contributors. Acrolein is the simplest of the α,β-unsaturated aldehydes, compounds that are ubiquitous in the environment. A single cigarette contains approximately 100µg of acrolein. These aldehydes are toxic, mutagenic and possibly carcinogenic. Acrolein has been shown to initiate bladder carcinogenesis in rats [14]. The risk of bladder cancer is 2 – 4 times greater among male cigarette smokers than among non-smokers [15,16]. A linear relationship between duration of smoking and bladder cancer risk has been demonstrated, with odds ratios ranging from 1.96 after 20 years to 5.57 after 60 years [17]. A dose relationship between the number of cigarettes smoked per day and bladder cancer has also been observed, up to a threshold limit of 15 – 20 cigarettes per day, odds ratio 4.5. Quitting smoking results in an immediate reduction in bladder cancer risk of up to 30% after 1 – 4 years and over 60% at 25 years, however even after 25 years the reduction in risk does not reach the level of non-smokers [17].

Analgesic abuse nephropathy is associated with an increased risk of developing urinary tract tumours, particularly in the renal pelvis but also in the ureter and bladder. Phenacetin-containing analgesics cause papillary necrosis and chronic interstitial nephritis leading to nephropathy. The relative bladder cancer risk of analgesia abuse nephropathy varies from 2.3 to 12.2 in different series [18-20].

Cyclophosphamide induced bladder cancer was first described in 1971 [21]. Cyclophosphamide is used to treat neoplastic and non-neoplastic diseases in approximately 500,000 patients worldwide annually. In a study of 6,171 2-year survivors treated for non-Hodgkin's lymphoma with chemotherapy regimens containing cyclophosphamide, 48 patients developed urinary tract cancers. There was a 4.5-fold increase in bladder cancer risk in these patients. A dose-response relationship was also demonstrated with the relative risk in patients who had received less that 20g being 2.4 compared to 14.5 in patients who had received over 50g. The mean latency period for bladder cancer development after cyclophosphamide treatment was 8.5 years, with a range of 3 – 21 years [22].

Conditions leading to chronic irritation of the urothelium may also induce carcinomas, although these tend to be of squamous cell type rather than transitional cell carcinomas, so will not be discussed here. Conditions that can precipitate malignant transformation of the urothelium include chronic infection, long-standing bladder calculi, long-term catheterisation and schistosomiasis infection.

Bladder cancer: Genetics

The exact sequence of events that leads to malignant transformation of the normal urothelium is unknown. Activation of oncogenes or inactivation or deletion of tumour suppressor genes is likely to play a role in this transformation process. Our understanding of the genetics of TCC has advanced significantly over the past few years with numerous oncogenes, tumour suppressor genes and chromosome abnormalities having been linked with bladder cancer genesis.

The majority of bladder cancers (over 70%) present as low-grade non-invasive papillary tumours that have not invaded the epithelial basement membrane (Ta). The rest are either muscle-invasive tumours (>T2) or non-

muscle-invasive tumours that have invaded the basement membrane (T1), which have a high risk of progression to muscle invasion.

Molecular analysis has demonstrated striking differences between these groups. This has led to the current two-pathway model for tumour development, with a postulated third pathway leading to the development of T1 tumours (Figure 5).

The first pathway which leads to genomically stable low-grade (Ta) disease occurs through mutations in the oncogene, fibroblast growth factor (FGF) receptor 3 (*FGFR3*). The second pathway which leads to muscle invasive bladder cancer is thought to arise via flat dyplasia which undergoes malignant transformation to carcinoma in situ (CIS) and the progresses to muscle invasive disease, as a result of mutations in the tumour suppressor gene *p53*.

Oncogenes

Several oncogenes have been implicated in TCC development and progression. Oncogenes contribute to the malignant phenotype in a dominant manner, either by being overexpressed or mutated to produce an oncoprotein [23]. Overexpression of the normal product is the most common mechanism, achieved either by gene amplification or chromosome translocation placing the gene downstream of a powerful promoter region [24].

Activating mutations of *FGFR3* are the most common genetic alterations identified in bladder cancer to date. The gene for *FGFR3* is found on chromosome 4p16. *FGFR3* mutations have been found in up to 80% of low-grade Ta tumours, but are only seen in 0 – 34% of T2 – T4 tumours. Activation of *FGFR3* is thought to induce signalling via the mitogen-activated protein (MAP) kinase pathway. Some studies suggest that mutation of FGFR3 confers an increased risk of recurrence, but no studies have demonstrated any increase in the risk of progression [25].

The oncogene *c-erb-B2* (chromosome 17q21) encodes a transmembrane receptor-like protein with homology to the epidermal growth factor receptor (EGFR). Overexpression of *c-erb-B2* has tyrosine kinase activity similar to that of EGFR and the ability to stimulate cellular growth. *C-erb-B2* is overexpressed in some TCCs by gene amplification and where present overexpression is associated with higher stage and grade tumours [26-30]. Overexpression has also been associated with poor clinical outcome [27] and

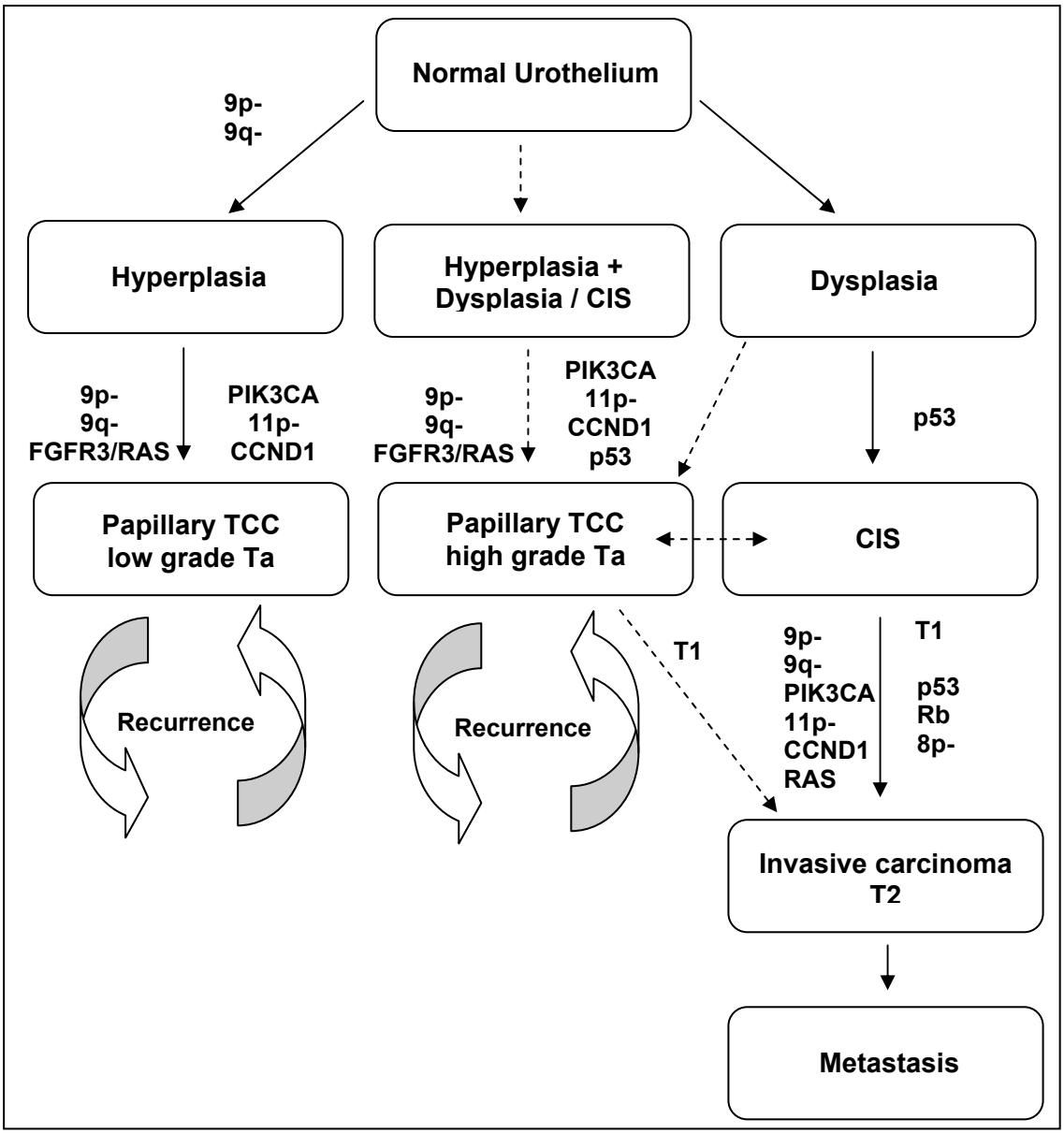

Figure 5: Model for pathogenesis of bladder cancer based on known histopathological and molecular data [25].

in multivariate analysis, *c-erb-B2* gene amplification and overexpression of its oncoprotein have a predictive value for death from bladder cancer [29]. Epidermal growth factor receptor status has also been shown in multivariate analysis to be an independent predictor of survival and stage progression [31]. In addition, EGFR status was found to be 80% sensitive and 93% specific in predicting stage progression in T1, grade 3 TCC [31].

The proto-oncogene *CCND1* (Chromosome 11q13) is also amplified and overexpressed in a subset of TCCs [32-34]. The product of *CCND1* is *cyclin D1*, a gene involved in cell cycle progression via the retinoblastoma (Rb)

pathway. Overexpression of *cyclin D1* has been associated with early tumour recurrence but not survival in TCC [35].

The *c-myc* oncogene (chromosome 8 long arm) codes for protein, $p62^{c\text{-}myc}$. This protein is associated with the nucleus and may be actively involved with DNA synthesis [36]. The overexpression of $p62^{c\text{-}myc}$ in bladder cancer was been linked to superficial disease [36]. It also appears to be overexpressed in some high-grade TCCs [37], but does not appear to predict any difference in survival or progression in these tumours [38].

Expression of a mutant protein product or oncoprotein is a less common mechanism of activation and is exemplified in TCC by the RAS gene family member *H-ras*. *H-ras* codes for a protein anchored to the cytoplasmic side of the cell membrane that is involved in signal transduction and may be involved with bladder cancer genesis. *H-ras* mutations have been found in up to 36% of bladder tumours [39,40].

Several studies have also identified common over-representation of certain chromosome arms and regions of high-level DNA amplification in TCC [41-44]. These changes have been shown mainly in T1 tumours and are much rarer in Ta tumours [42]. These alterations include over-representation of 1q, 8q, 3q, 5p, 6p and 10p and amplification at 1q22–24, 3p24–25, 6p22, 8p12, 8q21–22, 10p12–14, 11q13, 12q15–21, 13q31–33, Xp11–12 and Xq21–22.

Tumour suppressor genes

Deletion or inactivation of specific tumour suppressor genes or other specific genetic regions have been linked to cancer development. Multiple tumour suppressor genes have been implicated in the development of TCC.

The retinoblastoma (*Rb*) gene (Chromosome 13q14) encodes a nuclear phosphoprotein (*pRb*) that functions as a cell cycle regulator. Loss of heterozygosity at the *Rb* locus correlates strongly with the absence of *Rb* protein expression. *Rb* genetic mutations have been demonstrated in approximately 30% of TCCs [45]. Failure to detect *pRb* immunohistochemically is associated with increased tumour grade and stage (especially muscle invasion) and decreased survival [45-47].

Hyperphosphorylation of *pRb* which can be identified immunohistochemically as intense nuclear staining, is linked to TCC progression and carries with it a similarly ominous prognosis as absence of *Rb* staining [48,49].

Evidence of allelic loss of chromosome 17p in high grade compared to low grade TCCs, was the first suggestion that *p53* may play a role in bladder carcinogenesis [50]. The *p53* gene (chromosome 17p13) encodes a 53kDa transcription factor which plays a vital role in DNA repair and apoptosis. The half-life of mutated *p53* is significantly longer than that of wild-type *p53*, which allows its detection by immunohistochemistry. Nuclear overexpression of *p53* has been shown in up to 62% of muscle-invasive TCCs and is associated with increased stage and grade [51-53]. In superficially invasive disease (T1), p53 overexpression is less common, but where present is associated with a higher rate of disease progression and a poorer outcome. Mutated *p53* status is also an independent predictor of decreased survival. In muscle-invasive disease, it has been associated with a doubling in the risk of death from bladder cancer [54]. Altered *p53* is frequently seen in carcinoma in situ, which again reinforces the argument that *p53* plays a role in bladder cancer genesis and progression in high-grade TCCs [54].

Studies of *KAI1* (Chromosome 11p11.2), a metastasis suppressor gene, have shown a dramatic reduction in expression of this gene is common in both invasive and metastatic bladder cancer, suggesting that the loss of *KAI1* is an important and unfavourable step in tumour progression [55].

A loss of *KAI1* has also been associated with increased invasive behaviour in bladder cancer cell lines [56].

Deletions on chromosome 9 occur in greater than 60% of bladder cancers across all stages and grades and are likely to represent an initiating event [57]. Cytogenetic and molecular evidence has shown that it is often the only chromosomal aberration in early disease. Deletions of chromosome 9 alone are often associated with recurrence, but rarely associated with progression. The p21 region of chromosome 9 (9p21) has been found to be mutated in a variety of malignancies suggesting the presence of a common tumour suppressor gene. This complex genomic region encodes three distinct proteins, *p16*, *p14ARF* and *p15*, all of which are negative cell cycle regulators. In TCC, it is common for all three of these 9p21 genes to be deleted [58,59]. The potential prognostic implications of inactivation of one or all of these genes has not yet been studied in detail.

There are also 2 regions on 9q (9q11 – 13 and 9q33 – 34) that are also selectively deleted in a significant proportion of bladder cancers. The specific locations and functional proteins from these two putative tumour suppressor genes remain to be identified. Their deletion is more commonly associated with low-grade cancers [23].

The pattern of allelic loss at chromosome 9p21 (p16 gene locus) and 17p13 (*p53* gene locus) in primary bladder cancer has been shown to be maintained during cancer progression to metastasis with an identical pattern of allelic loss in primary cancer being conserved in paired metastatic carcinoma, suggesting that allelic loss of these chromosome regions occurs prior to the metastatic sequence [60].

Another tumour suppressor gene *PTEN* (chromosome 10q23) which is inactivated by loss of heterozygosity or mutation has been identified in some cases of TCC [61,62].

Several other chromosome arms show non-random deletions in bladder cancer including 3p, 4p, 4q, 8p, 11p, 11q, 14q and 18q [24].

The *GSTM1* gene is another form of tumour suppressor gene, which codes for the Glutathione-S-Transferase M1 enzyme which is effective at detoxifying some carcinogenic compounds and protecting against cancer development [63]. Approximately half of the Caucasian population are homozygous deleted for this allele and fail to express the protein [64]. Several studies have demonstrated that in subjects lacking *GSTM1* activity there is a significantly increased risk of developing bladder cancer [65,66]. These studies also estimate that as many as 17 – 25% of bladder cancers may be attributable to the *GSTM1* deficiency.

Molecular biology of cancer progression

Bladder cancer cells need to acquire certain properties to enable them to grow rapidly, invade and metastasise. These properties include uninhibited growth and cellular mobility, mediated partially by epidermal growth factor (EGF) and EGFRs, expression or loss of expression of specific cell adhesion molecules and increased production of angiogenic factors.

EGF and EGFRs

Abnormal expression or function of growth factor receptors can enhance malignant cell proliferation. EGF is a potent mitogen excreted in high

concentrations in human urine [67]. In patients with TCC, EGF is excreted in urine at much lower concentrations [68]. These lower urinary concentrations of EGF are thought to be due to increased ligand binding to EGFR receptors. EGFRs are normally found only in the basal layer of the urothelium, however in TCC these receptors become abnormally expressed throughout the entire urothelium, including those cells directly exposed to urine. EGFR expression as detected by immunohistochemistry has been shown to correlate with increased grade and stage and with a poor prognosis in bladder cancer [69]. High levels of EGFR expression have also been shown in cystoscopically normal urothelium in patients with TCCs elsewhere in the bladder [70]. This observation supports the existence of a urothelial field defect [71] and suggests that abnormal EGFR expression may be an early event in bladder carcinogenesis. Ligand stimulation of EGFRs also induces cellular motility, suggesting these receptors may also play a role in transepithelial motility and tumour invasion, as well as proliferation.

Extracellular Matrix and Cell Adhesion Molecules

Extracellular matrix and cell adhesion molecules have been extensively studied because they form natural barriers to tumour metastases. Urothelial cells are bound to each other and to the underlying basal lamina by cell adhesion molecules and extracellular matrix, in order to allow some cellular disaggregation and local movement these connections must be altered in some way. In addition, many of these molecules are involved with cell-cell communication, regulation of the expression and function of membrane bound growth factor receptors, manipulation of the activity of cell cycle regulatory molecules and other processes involved in urothelial carcinogenesis (e.g. angiogenesis).

E-Cadherin

The cadherins are a family of transmembrane glycoproteins involved in calcium-dependent cell-cell adhesion. Reduced expression of E-cadherin (an epithelial subclass) has been linked to increased tumour recurrence and invasiveness [38] and a reduction in overall survival of bladder cancer patients [72]. Advanced tumour stage and grade have also been associated with loss of cadherin-associated molecules (alpha, beta and gamma catenins) and the presence of multiple abnormalities in the E-cadherin-catenin complex [73].

Possible mechanisms accounting for decreased function of E-cadherin in bladder cancer cells include suppression or mutation of the E-cadherin gene, allelic loss of 16q, decreased E-cadherin protein expression and increased protease-mediated degradation. However, the mechanisms by which E-cadherin expression is decreased remain unknown.

Integrins

The integrins comprise a family of transmembrane heterodimeric proteins, functioning as receptors for each other and for extracellular matrix components, such as laminin, fibronectin and collagen. Alpha-6 beta-4 integrin associates with collagen VII on the basement membrane of the urothelium, forming a hemidesmosomal achoring complex, which prevents cell migration. In bladder cancer cells this association of apha-6 beta-4 integrin with collagen VII is lost, possibly explaining the problem with urothelial barrier function that occurs in malignancy [74]. This disruption of the structure and function of integrins may also enhance the ability of intraluminal urinary constituents with angiogenic, locomotive, mitogenic or mutagenic properties to gain unusual access to the interstices of the bladder wall.

Angiogenesis

Neovascularisation or angiogenesis are prerequisites to tumour growth and metastasis [75]. Angiogenesis inducers (e.g. vascular endothelial growth factor (VEGF) or substances that activate angiogenesis inducers (e.g. basic fibroblast growth factor (b-FGF)) are produced by the tumour cells or released from extracellular matrix or tumour associated stromal cells, or they may be products of inflammatory cells that infiltrate tumours [76].

Immunohistochemical methods looking at increased microvascular density (angiogenesis) have shown an association with tumour progression and decreased overall survival in bladder cancer patients [77,78]. In addition, increased urinary excretion of b-FGF, angiogenic factors such as autocrine motility factor (AMF) [79], and hyaluronic acid and its degradation products [80] have been found in patients with bladder cancer and could potentially provide a means of tumour detection and monitoring in the future.

Potent inhibitors of angiogenesis also appear to be expressed in abnormally low levels in bladder cancers compared with normal urothelium. Decreased expression of Thrombospondin-1, an extracellular matrix glycoprotein, has

been correlated with higher recurrence rates and decreased survival in bladder cancer patients, when compared with patients whose bladders have higher levels of expression [81].

Presentation

The majority of patients (75 – 90%) with bladder cancer will present with haematuria, which can be either macroscopic or microscopic. The degree of haematuria does not correlate with the extent of disease.

Bladder cancer may also present with recurrent urinary tract infections, sterile pyuria, pelvic pain or irritative voiding symptoms, such as frequency and urgency of voiding. Occasionally patients may present with anaemia, uraemia or symptoms related to metastatic disease, such as bone pain or weight loss.

Screening for asymptomatic haematuria is not recommended because its positive predictive value to too low (0.5%) to warrant mass screening [82,83]. However, routine screening for microscopic haematuria may be indicated for populations exposed to bladder carcinogens, including heavy smokers and workers in high risk occupations.

Physical examination is usually normal except in locally advanced disease, when a mass may be palpable.

Bladder cancers are usually diagnosed during investigation of patients with haematuria. Haematuria should always be investigated with either an intravenous urogram (IVU) or an ultrasound and plain X-ray of the kidneys, ureters and bladder combined with cystoscopy. Bladder cancers are usually diagnosed definitively at cystoscopy with either a rigid or a flexible cystoscope. However, bladder cancer may also be diagnosed as a filling defect in the bladder on an IVU or a mass lesion in the bladder on ultrasound. Computed tomography (CT) may also detect incidental bladder cancer when patients are being investigated for other conditions. These radiological investigations can miss smaller bladder lesions and areas of carcinoma in situ, so cystoscopy is mandatory in patients with haematuria.

Urine cytology may reveal the presence of malignant cells in the urine suggesting a urothelial tumour. Cytology is particularly useful when a high-grade malignancy or Carcinoma *in situ* (Cis) is present [84,85]. However, negative urinary cytology does not exclude the presence of a low-grade bladder tumour.

Newer urinary markers of bladder cancer may gain a role in bladder cancer screening and disease monitoring in the future. There are several tests already commercially available including bladder tumour antigen, NMP22 (Nuclear Matrix Protein), fibrin-degradation products, Quanticyt and Immunocyt. Most have better sensitivity for detecting bladder cancer, but lower specificity with false positive tests leading to unnecessary imaging and bladder biopsies.

New aids to the diagnosis of flat areas of TCC or Cis are currently being developed, as these lesions can often be missed using conventional white light cystoscopy. These techniques were pioneered using 5-Aminolevulinic Acid (5-ALA), a molecule that is metabolised via the Haem biosynthesis pathway into protoporphyrin IX. Protoporphyrin IX is a fluorescent molecule that is synthesised preferentially by tumour cells, accumulating about ten times the level of normal urothelium. Combination with blue light fluorescence cystoscopy allows areas of TCC or carcinoma in situ (Cis) to be clearly visualised as red fluorescent lesions. A newer molecule, Hexyl 5-aminolevulinate (HAL) is now available for clinical use, with the advantage that it doubles the fluorescence with only half the instillation time of 5-ALA and also uses a lower drug concentration.

Staging investigations

Once the patient is anaesthetised bimanual examination is performed to assess whether there is a palpable mass and if so, whether or not it is fixed to the pelvic wall. Another bimanual examination may be performed at the end of the resection to determine whether there is still a mass palpable, suggesting extravesical tumour. Transurethral resection (TUR) of the bladder tumour is then performed taking care to preserve the architectural detail and relationship of the tumour to the various layers of the bladder wall to allow accurate pathological staging.

Biopsy specimens of the tumour and suspected area should be taken to map the extent of the disease. Both cold cup biopsies to preserve the histological architecture and TUR biopsies to determine the extent of the disease should be performed [86]. Random biopsies of normal mucosa are indicated in the presence of positive cytology, even in the absence of tumour, or in any non-papillary tumour. Random biopsies in patients with solitary papillary lesions

are contra-indicated because of the absence of additional information [87] and because of the risk of tumour implantation [88]. Prostatic urethral biopsies by TUR are indicated if there is suspicion of Tis in view of the high frequency of prostatic urethral involvement [89].

Computed Tomography (CT) or Magnetic Resonance Imaging (MRI) are used to evaluate the extent of invasive bladder tumours and also to look for pelvic and abdominal lymph node metastasis. CT cannot detect microscopic lymph node disease and can therefore only provide information on lymph node enlargement and possible liver metastases [90].

Bone scanning is only recommended in patients who have a raised alkaline phosphatase or are suffering from bone pain [91].

Pathological staging and grading of bladder cancer

Bladder cancer is staged using the TNM staging system, first introduced by the Union International Contre le Cancer (UICC) in 1992. The TNM classification is updated periodically based on new prognostic information creating more sub-stages that more accurately predict survival. The latest version introduced in 2002 is shown below [92] (Figure 6 / Table 3). This update divided the T2 stage into T2a (inner half) and T2b (outer half).

The T (Tumour) stage relates to the degree of local invasion of the primary tumour, the N (Node) stage indicates the extent of nodal involvement and the M (Metastasis) denotes whether any metastases are present.

Initial TNM staging is based on a combination of clinical examination and radiological imaging. Tumours that are resected endoscopically or excised at open operation are submitted to histological staging, the tumour stages then receive the prefix pT. Muscle invasive tumours treated with radiotherapy or chemotherapy do not therefore receive a definitive pathological T stage, which has implications when comparing different treatment modalities in bladder cancer.

Approximately 75 – 80% of patients present with disease confined to the mucosa (stage Ta – Tis) or submucosa (T1), so-called non-muscle invasive (superficial) cancers. The other 15 – 20% have muscle invasion or nodal disease (T2 – 4, N+) at presentation [93].

The grouping of tumours confined to the mucosa and submucosa (Ta, Tis and T1) together as the so-called “non-muscle invasive” or “superficial” bladder

cancers remains controversial as the potential for recurrence and/or progression in each of these tumour types is vastly different.
Molecular biology techniques and clinical experience have demonstrated the highly malignant and invasive potential of Tis and T1 lesions [94,95].
For Ta disease the chance tumour recurrence and progression to invasive disease is 2 – 4% compared to 30% for T1 lesions.
Tis, also known as carcinoma in situ (Cis) should not be regarded as superficial disease as it carries a high risk of developing aggressive invasive disease over time [96]. Between 40 and 83% of patients with Tis treated by endoscopic resection alone will progress to muscle invasive disease [97].
Tis is therefore widely regarded as a separate entity to Ta and T1 disease and consequently treated more aggressively.

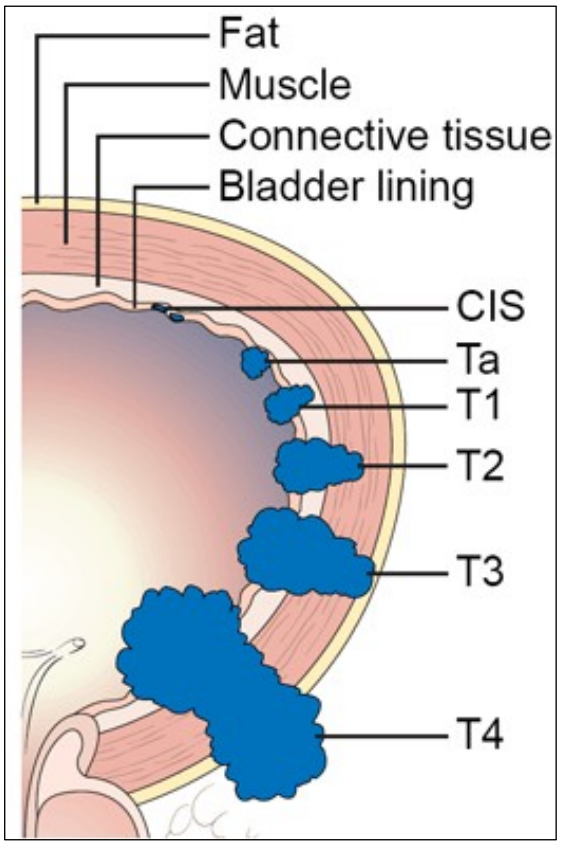

Figure 6: TNM Staging of Bladder cancer (Figure reproduced with kind permission of Cancer Research UK).

T (Primary tumour)

TX	Primary tumour cannot be assessed
T0	No evidence of primary tumour
Ta	Non-invasive papillary carcinoma
Tis	Carcinoma in situ (“flat tumour”)
T1a	Tumour invades subepithelial connective tissue
T2	Tumour invades muscle
T2a	Tumour invades superficial muscle (inner half)
T2b	Tumour invades deep muscle (outer half)
T3	Tumour invades preivesical tissue
T3a	microscopically
T3b	macroscopically (extravesical mass)
T4	Tumour invades any of the following: prostate, uterus, vagina, pelvic wall, abdominal wall
T4a	Tumour invades prostate, uterus or vagina
T4b	Tumour invades pelvic wall or abdominal wall

N (Lymph nodes)

NX	Regional lymph nodes cannot be assessed
N0	No regional lymph node metastasis
N1	Metastasis in a single lymph node 2cm or less in greatest dimension
N2	Metastasis in a single lymph node more than 2cm but not more than 5cm in greatest dimension, or multiple lymph nodes, none more than 5cm in greatest dimension
N3	Metastasis in a lymph node more than 5cm in greatest dimension

M (Distant metastasis)

MX	Distant metastasis cannot be assessed
M0	No distant metastasis
M1	Distant metastasis

Table 3: Bladder cancer staging: 2002 TNM classification approved by the Union International Contre le Cancer (UICC)

Bladder cancers of any pathological stage are also subjected to histological grading. In 1998, a new classification of non-invasive urothelial tumours was proposed by the World Health Organization (WHO) and the International Society of Urological Pathology (ISUP) (1998 WHO/ISUP classification) and published by the WHO in 2004 [98,99] (Table 4).

2004 WHO grading
Urothelial papilloma
Papillary urothelial neoplasm of low malignant potential (PUNLMP)
Low-grade papillary urothelial carcinoma
High-grade papillary urothelial carcinoma

Table 4: 2004 WHO Histological grading

This grading system differentiates between papillary urothelial neoplasms of low malignant potential (PUNLMP) and low-grade and high-grade urothelial carcinomas. PUNLMP are defined as lesions without cytological features of malignancy but having normal urothelial cells in a papillary configuration. They have a negligible risk of progression, but are not completely benign and still have a tendancy to recur. Tumour grade also has profound effects of recurrence rates [100-103].

Treatment

Following primary resection and staging investigations, the patients' cancer can be classified as either non-muscle invasive (Ta – T1), carcinoma in situ (Cis) or invasive (T2 – T4, N+). The treatment and follow-up of these three groups is vastly different and is outlined below.

Treatment of Ta – T1 lesions

The treatment of Ta – T1 lesions should take into account the risk of disease recurrence and progression, side effects and cost effectiveness. Non-muscle invasive cancers have a tendency to recur even after adequate treatment [95,104]. The risk of progression to invasive cancer is low in the majority of these cancers, but increases to 50% in high-grade T1 G3 tumours [94,95].

Following disease staging at initial TUR and with radiological investigations, the risk of disease recurrence and progression can be calculated from the clinical and pathological findings. Several prognostic factors have been identified that may predict tumour behaviour [105-108]. For disease recurrence they are:

1. Number of tumours present at diagnosis
2. Recurrence rate in the previous period; a recurrence at 3 months
3. Size of the tumour: the larger the tumour the higher the risk of recurrence
4. Histological grade of the tumour: Poorly differentiated or undifferentiated tumours showing higher recurrence rates

For progression to invasive disease, the histological grade and T-category are the most important. Tumours of the bladder neck have a worse prognosis than elsewhere [109].

Based on prognostic factors, superficial bladder cancers can be divided into the following risk groups:

Low-risk:	single, Ta, G1, < 3cm diameter
High-risk:	T1, G3, multifocal or highly recurrent, Cis
Intermediate:	All other tumours, Ta – T1, G1 – G2, multifocal, >3cm diameter

Following transurethral resection of non-muscle invasive bladder tumours, a single chemotherapeutic instillation with epirubicin or mitomycin C within 6 hours is able to reduce the recurrence rate by 50%. This treatment is therefore advocated in all cases of superficial bladder cancer, except where bladder perforation is suspected [110,111].

Low-risk tumours (Single, Ta – T1, G1 smaller than 3cm diameter and papillary tumours) need no further treatment as their risk of progression is very low with this management (<0.2% / year).

Tumours of intermediate- or high-risk of recurrence (recurrent multiple, Ta – T1, G1 – G2) should receive a further 4 – 8 week course of intravesical chemotherapy instillations followed by monthly maintenance instillations up to 6 months post-TUR [112].

Recurrent disease should be treated in the same way. In cases of highly recurrent tumours or multiple recurrence, Bacille Calmette Guerin (BCG) therapy should be instituted as this has been shown to be effective [113,114].

BCG instillations

The mechanism of BCG activity is not yet understood, although most evidence points towards some immunotherapeutic mode of action. BCG immunotherapy is more effective in high-risk non-muscle invasive bladder cancer and has been shown to prevent disease progression [115,116]. Six-weekly induction instillations are required to elicit an immunological response followed by three booster cycles to obtain a good immunological reaction. In papillary, Ta – T1, G1 – G2 tumours, the dose can be reduced to 25% whilst maintaining the same effectiveness as the full dose and reducing side effects [117-119].

BCG maintenance therapy up to 3 years given at 3 – 6 monthly intervals has been reported to lead to lower disease recurrence rates [116]. Whilst this heavy schedule is not suitable for all patients, it is suitable for patients with highly recurrent and high risk non-muscle invasive bladder tumours. Chemotherapy may still be effective after failure of BCG therapy and vice versa.

Treatment of Tis

The current standard treatment of Tis consists of intravesical BCG instillations given over a 6-week period. Complete remission is obtained in up to 70% of cases. If cytology and biopsies remain positive a further cycle of treatment may induce an additional 15% complete remission. Maintenance therapy with booster cycles at 3, 6, 12, 18, 24, 30 and 36 months are indicated in order to prevent recurrence of this highly malignant disease. If a second cycle of treatment does not achieve a cure or if there is early disease recurrence, cystectomy with urethrectomy is indicated. Bladder preservation is achieved in 70% of cases.

Treatment of T1 G3 bladder tumours

T1 G3 tumours represent 10% of all non-muscle invasive tumours and progress to invasive disease in up to 50% of cases [94,95]. Because of this high progression rate some experts tend to carry out early cystectomy with excellent long-term survival rates. However, several studies have demonstrated that 50% of patients with T1 G3 tumours can conserve their bladder with intravesical chemotherapy or BCG instillations [113-116,120]. Factors that may influence a decision towards cystectomy include solid

appearance of the tumour (as opposed to papillary), high recurrence rate, multiplicity of tumours and the presence of concomitant Tis.

Follow-up of non-muscle invasive bladder cancer after TUR

Cystoscopy is the gold standard of follow-up, with flexible cystoscopy being well tolerated and more convenient for patients.

Incomplete resection, tumour cell implantation at traumatised sites in the bladder and rapid growth of epithelial malignancy all contribute to higher recurrence rates of non-muscle invasive bladder cancer after TUR at 3 months. Early cystoscopy is therefore advised in all cases of superficial bladder cancer. In higher risk lesions (T1, G2 and G3), another resection at the site of the TUR should be performed within 3 months. In this group of tumours, repeat TUR will yield positive biopsies in up to 35% at 4 – 6 weeks after the initial resection [121]. Early repeat TUR can be justified on these grounds alone, but the effect of early re-TUR on the outcome of these tumours compared to cystoscopy and re-TUR at 3-months has not been established.

The frequency of follow-up cystoscopies should be tailored to the prognostic factors of the tumour [122]. In non-muscle invasive bladder cancer the recurrence rate is highest in the first 2 years of follow-up, with the number of positive cystoscopies becoming less frequent thereafter. In low-risk tumours (single, primary, Ta G1, < 3cm diameter) with no recurrence at 3 months, a follow-up cystoscopy can be delayed until 9 months later followed by yearly cystoscopies for up to 5 years because of the very low recurrence rate [123]. In over 95% of cases the histological findings of recurrent tumours are the same as those of the primary tumour. In patients with high-risk tumours, cystoscopy is performed every 3 months during the first 2 years. The frequency of cystoscopy is then reduced to every 4 months in the third year, every 6 months until the fifth year and thereafter on a yearly basis. The schedule of follow-up in the intermediate group lies between that of the low- and high-risk groups. After any disease recurrence, the cystoscopy schedule is restarted from the beginning.

Kaplan-Meier curves of bladder cancer recurrence rates demonstrate a continuous downward trend with time without plateau formation. Recurrences continue to occur during follow-up for up to 10 – 12 years [123-125]. Patients

with regular recurrence will continue to have recurrences until cystectomy or death. Patients with recurrences during the first 4 years after TUR continue to have lifelong recurrences [124].

From the available data, follow-up may be stopped after 5 years in single Ta G1 tumours with absence of recurrence. In all other cases, yearly follow-up is advised for up to 10 years, with lifelong follow-up for the high-risk group [125].

Treatment of Muscle-Invasive Bladder cancer (T2+)

Radical Cystectomy

Radical cystectomy is widely regarded as the gold standard treatment for muscle invasive bladder cancer. Muscle-invasive disease (T2 – T4a, N0-NX, MO) is the primary indication for radical cystectomy. Other indications include high-risk superficial tumours (T1 G3 and BCG-resistant Tis) and extensive papillary disease that cannot be controlled with conservative measures. Contraindications for cystectomy are major co-morbidity and patients not willing to accept the surgical risks. Patients who are keen to preserve their bladder may also opt for primary radiotherapy and/or chemotherapy, reserving cystectomy for salvage treatment if necessary.

The overall staging error between clinical and pathological staging can be as high as 44% [126] and appears to be highest for T2 tumours [127]. The frequency of regional lymph node metastases varies with T stage, from less than 10% in T1 to almost 33% in T3 – T4 disease.

The operative mortality from radical cystectomy is between 1.2 and 3.7% [128,129]. Early surgical morbidity is around 30% but is usually transient [130,131]. The risk of impotence is high and age dependant [132]. Late morbidity usually relates to urinary diversion.

Survival rates

The 5-year survival rate lies within the range of 40 – 60% and has not significantly improved in recent times. The use of pre-operative radio- or chemotherapy has not improved these outcomes. A recent study reported 5-year stage specific survival rates for radical cystectomy alone of 75% of stage pT1, 63% for stage pT2, 31% for stage pT3 and 21% for stage pT4 disease [133]. Approximately 10% of cystectomy specimens are without tumour (stage pT0) due to radical TUR. It is uncertain whether or not this confers any survival advantage [134,135]. Tumour stage and nodal involvement are the

only independent predictors of long-term survival [136]. P53 overexpression and mutation are not superior to staging as prognostic markers [137,138].

Radiotherapy

Definitive radiotherapy with curative intent and the aim of bladder preservation is performed in T1 – T4, N0, M0 TCC of the bladder. There are no adequate, modern, randomised trials comparing radiotherapy and cystectomy. When selection bias in radiotherapy series is taken into account, radiotherapy produces comparable survival values to cystectomy. A large multinational randomised investigation into the role of neoadjuvant chemotherapy in the management of muscle-invasive bladder cancer showed selection bias for radiotherapy as opposed to cystectomy, with patients undergoing radiotherapy having a generally poorer performance status [129]. The decision for or against radiotherapy is therefore based on prognostic factors, patient co-morbidities and desire to preserve their bladder.

Factors that give a more favourable outcome with external beam radiotherapy are low T-stage disease (T2), solitary tumour, lack of upper urinary tract dilatation and complete TUR of all visible tumour [139].

Other factors that may improve outcome are normal haemoglobin level, low tumour volume (<5cm diameter) and lack of concomitant Cis [140-143].

External beam radiotherapy is delivered in 30 – 40 fractions in doses up to 68Gy [140,141].

Local recurrence or recurrence elsewhere in the bladder will occur in more that 30% of patients undergoing bladder preserving treatment.

Modern radiotherapy techniques involve the use of CT-planned radiotherapy, which allows more accurate delivery of treatment and reduces the incidence and severity of side effects. Radiotherapy complications include enteritis, proctitis and cystitis, which are usually self-limiting. Late toxic effects including radiation cystitis (5%), proctitis (5%) and bowel obstruction (3%) are less common in more recent series [141,142,144]. Erectile dysfunction occurs in more than two-thirds of male patients [145].

The 5-year survival rate after definitive external beam radiotherapy is reported as 60 – 80%, 26 – 59% and 20 – 38% for T1, T2 and T3 tumours respectively. Patients with T4 tumours rarely survive for 5 years without tumour progression [140,141,144,146,147]. A recently published series reported a 10-year

disease specific survival of 42%, with an over 80% bladder preservation rate in the survivors [148]. With modern techniques with increased accuracy of treatment, via CT-guided radiotherapy, local disease control is much improved with approximately 70% of patients having no signs of disease in their bladders at first cystoscopy [148,149]. Local recurrence or the development of a second bladder tumour occurs in approximately 50% of patients [141]. These patients will require salvage cystectomy, with a favourable long-term outcome being achieved in up to 40% [144]. The morbidity of salvage cystectomy after radical radiotherapy is higher when compared to unirradiated patients. Despite this salvage cystectomy with bladder reconstruction is still possible [150], so patients should not be denied bladder-conserving treatment due to concerns about bladder reconstruction in the irradiated pelvis. Contraindications to radiotherapy for bladder cancer include inflammatory bowel disease, extensive previous pelvic surgery, previous radiotherapy or severe irritative bladder symptoms. Relative contraindications to radiotherapy are concomitant carcinoma *in situ*, a large primary tumour or ureteric obstruction. The elderly tolerate pelvic irradiation as well as younger patients so age alone is not a contraindication to radiotherapy [151] or even synchronous chemoradiotherapy [152].

Hypoxia has been shown to be clinically important in TCC of the bladder. Several trials have assessed the effects of modifying tumour hypoxia either with hyperbaric oxygen or hypoxic cell sensitizers, with promising results. A recently published phase II study [153] of bladder cancer patients treated with nicotinamide and carbogen (95% O_2 with 5% CO_2) in combination with radiotherapy showed significant improvements in local control, disease-free survival and overall survival, when compared to historical controls. The ARCON study (funded by Cancer Research UK), a multicentre, randomised, controlled trial comparing conventional radiotherapy with radiotherapy given in combination with nicotinamide and carbogen is currently recruiting in the UK.

There is increasing evidence that combination of cisplatin chemotherapy with radiotherapy improves local control rates up to 80% in T2 – T3 tumours [144,154-156], but it is unclear whether this regimen has led to improved 5 year survival rates. Randomised trials comparing radiotherapy with chemoradiotherapy are lacking.

Pre-operative radiotherapy has been shown to down-stage muscle-invasive bladder cancers. A meta-analysis of the results of randomised controlled trials of pre-operative radiotherapy in muscle-invasive bladder cancer concluded that the available clinical trial data does not support the routine use of pre-operative radiotherapy, but that additional well-designed trials are needed [157].

Follow-up after external beam radiotherapy

Life-long follow-up is required using cystoscopy, exfoliative urine cytology and other investigations to detect disease dissemination, as in patients who undergo cystectomy. Recurrent Tis and Ta TCC can be treated with intravesical immunotherapy (Tis) or TUR and adjuvant intravesical therapy. Patients with muscle invasive tumours should undergo radical cystectomy wherever possible.

Systemic chemotherapy

Up to 50% of patients who have undergone radical cystectomy for muscle invasive bladder carcinoma may develop metastases, usually occurring within 2 years of surgical resection [158]. Systemic, cisplatin-based chemotherapy regimens produce response rates in 40 – 70% of bladder tumours and are now being used in locally invasive disease in combination with cystectomy or radiotherapy, as either neo-adjuvant or adjuvant therapy. Most trials of chemotherapy in bladder cancer have used a combination of Methotrexate, Vinblastine, Adriamycin (Doxorubicin) and Cisplatin (M-VAC) which is only suitable for patients with good performance status and good renal function, as it carries a 3% risk of death due to toxicity. Recent studies have reported the use of Gemcitabine and Cisplatin in advanced bladder cancer which has shown equal efficacy with much less toxicity [159].

Neo-adjuvant chemotherapy

Non-randomised studies have clearly established the feasibility and safety of giving neo-adjuvant chemotherapy. Overall response rates of 60 – 70% with complete responses in around 30% of cases have been reported [158]. Neo-adjuvant chemotherapy can “downstage” tumours to the extent that inoperable cases may become operable [129,160]. Several studies of neoadjuvant chemotherapy have shown that the cystectomy specimen is pT0 in a higher proportion of patients who have had initial neoadjuvant

chemotherapy combined with a TUR (20 – 40 %) compared to TUR alone (7 – 17%) [154].

The Medical Research Council (MRC) Meta-analysis group obtained original patient data from 10 prospective randomised trials of neo-adjuvant chemotherapy, with >2600 patients eligible for analysis [139]. This analysis revealed conflicting results from several of the studies, some showing benefit and others not. The largest single study, a multinational trial co-ordinated jointly by the MRC and EORTC [129], recruited almost 1000 patients and was powered to detect a 10% survival improvement at 3 years. Initial analysis of the data, at median follow-up of 4 years, failed to show a clinically worthwhile benefit for patients who underwent three cycles of chemotherapy (cisplatin, methotrexate, vinblastine) before definitive treatment with cystectomy +/- pre-operative radiotherapy or radiotherapy alone. The respective 3-year survival was 50% and 55.5%. A more recent analysis, now with a median follow-up of 7 years, is of interest, as there were several late events [161]. The difference in absolute survival at 5 and 7 years remained 6% (44% vs 50% (p=0.075) and 37% vs 43% (p=0.048)) but the additional events added statistical power, meaning this difference has now reached statistical significance [161]. Patient data from the original South West Oncology Group neoadjuvant study showed a 14% survival benefit at 5 years, but this did not reach statistical significance (p=0.06) [162].

Response to chemotherapy is also an important predictor of survival in bladder cancer patients. The 5-year survival rate is 75% in patients who had down-staging of the primary tumour to pT0 or superficial disease compared to only 20% in patients who had residual muscle-infiltrating disease (>pT2) [163,164].

Neo-adjuvant chemotherapy and bladder preservation

Selected patients with invasive bladder tumours after neo-adjuvant chemotherapy may preserve their bladders [165]. Long-term disease free survivors, 55 – 70% at 33 – 60 months, have been reported among patients with muscle-invasive cancers that have been treated by neo-adjuvant platinum based chemotherapy regimens alone, where their planned radical procedure was not carried out [157].

Bladder preservation may be possible in approximately 40% of patients using a combination of chemotherapy and radiotherapy [156,166-170], with 5-year survival rates between 42% and 63%. Several groups have selected patients suitable for bladder preservation based on the response of the primary tumour to chemotherapy, with or without radiotherapy after TUR. If their tumour is responsive this treatment is followed up with a course of radiotherapy with curative intent. Prognostic factors for local disease curability were small tumour size, absence of hydronephrosis, papillary histology, visible complete TUR and complete response to induction chemotherapy. These combination regimens have however not been confirmed by randomised trials.

Bladder preservation in selected patients with muscle-invasive bladder cancer treated with either extensive TUR or partial cystectomy alone, have been reported in several published series. Survival rates in some of these series are equivalent to those in conventional cystectomy series [157].

Other series have reported results of treatment with systemic chemotherapy, either platinum-containing regimens or high-dose methotrexate, combined with conservative surgery, either extensive TUR or partial cystectomy. Survival rates for these selected patients are similar to those reported after cystectomy, many surviving with intact and functioning native bladder. Randomised controlled trials comparing survival and quality of life after radical surgery and bladder reconstruction with a modern bladder conserving approach combining extensive TUR, systemic chemotherapy and radiotherapy are needed.

A randomised, multicentre UK trial of Selective bladder Preservation Against Radical Excision (cystectomy) in muscle invasive T2 / T3 transitional cell carcinoma of the bladder (SPARE trial) aims to recruit 1015 patients by 2014. Recruitment began in July 2007 and to date 24 patients have been enroled in this study (personal communication - Rebecca Lewis, SPARE trial coordinator). Following 3 cycles of neo-adjuvant chemotherapy patients will undergo cystoscopy. Responders will be randomised to have either radical cystectomy or radical radiotherapy, with a fourth cycle of chemotherapy being given before definitive local treatment. Non-responders will undergo immediate radical cystectomy.

Adjuvant chemotherapy

Adjuvant chemotherapy is given to patients who have undergone potentially curative, definitive local treatment and who are apparently disease-free, but are at high risk of recurrence or metastasis. A few trials have attempted to assess the impact of adjuvant chemotherapy on survival of patients with bladder cancer [171-175]. However, these published series have been criticised because the trials were stopped early, they included too few patients, or inappropriate statistical analysis was used. Large multicentre trials are needed to clarify the role of adjuvant chemotherapy. A major international collaborative study is underway, coordinated by the European Organisation for the Research and Treatment of Cancer (EORTC) Genitourinary group, designed to establish the value of immediate post-operative chemotherapy versus chemotherapy deferred until relapse (EORTC 30994). Eligible patients must have had a radical cystectomy and bilateral lymphadenectomy for a TCC, pT3 or pT4 and/or node-positive (pN1 – 3), be free of any evidence of residual disease and be fit for treatment with cisplatin-based chemotherapy regimen. Patients will be randomised to receive either four cycles of chemotherapy given immediately after cystectomy, or deferred until relapse. The primary endpoint of the trial is survival. Recruitment of 1344 patients is required to detect a 7% improvement in absolute survival at 5 years, from 35% to 42% in the immediate chemotherapy arm [139].

Palliative treatment of bladder cancer

All treatment modalities are used in the palliative treatment of patients with metastatic or locally advanced bladder cancer.

Radiotherapy provides effective palliation of local, cancer-related symptoms in bladder cancer. Regimens in which fewer relatively larger fractions are given are more convenient and less distressing for patients. A large prospective randomised trial of palliative radiotherapy in bladder cancer [176], showed 68% of patients had symptomatic improvement with palliative radiotherapy. Haematuria is well palliated by radiotherapy in 50-90% of patients [176]. Dysuria and frequency are only improved by radiotherapy in approximately 20% of patients.

Prevention

As with all diseases prevention is better than cure. Bladder cancer has several known factors that lead to carcinogenesis. Reduction in population smoking figures would dramatically cut the numbers of patients presenting with bladder cancer. Reduction of worker exposure to industrial carcinogens would also lead to a reduction in bladder cancer incidence. It has been calculated that there are 820 preventable cases and 630 preventable deaths from bladder cancer each year as a results of socio-economic deprivation [4]. Additionally several dietary factors have been postulated to have a protective role against bladder cancer including green tea and Indole-3-carbinole (found in brassicas – cabbage, brussel sprouts, broccoli) [177].

Prognosis

Bladder cancer is one of the few cancers in which men have a substantial survival advantage over women. Comparison of both 1 and 5-year survival rates demonstrates a clear survival advantage. One- and five-year survival figures for patients diagnosed with bladder cancer in England and Wales and Wessex are shown in Table 5. In patients diagnosed between 1991 and 1999 figures for 1-year survival were 81 – 83% for men and 72 – 75% for women and 5-year survival figures were 64 - 70% for men and 56 - 65% for women. Survival in bladder cancer also appears to have a deprivation gradient with most affluent groups have around 6% better survival at both 1 and 5 years after diagnosis than more deprived groups.

England and Wales	1991-95 1-year survival (%)	1991-95 5-year survival (%)	1996-99 1-year survival (%)	1996-99 5-year survival (%)
Male	81.7	64.2	81.2	64.4
Female	73.1	59.0	72.9	56.0
South West	1992-94 1-year survival (%)	1992-94 5-year survival (%)	1994-96 1-year survival (%)	1994-96 5-year survival (%)
Male	82	70	83.7	68.8
Female	72	64	75.0	64.5

Table 5: One- and five-year survival figures for bladder cancer in England and Wales and the South West

The prognosis of individual patients with bladder cancer obviously depends largely on the stage and grade of their disease.

For superficial disease, the European Organisation for Research and Treatment of Cancer (EORTC) have developed tables that can predict the chances of disease recurrence and progression, based on variables including T category, grade, primary or recurrent tumour, number and size of tumours and the presence of concomitant Cis [103]. On the EORTC website (www.eortc.be), there is a calculator which utilises the EORTC Risk Tables for Stage Ta T1 Bladder Cancer, to predict the probability of recurrence and progression for the individual patient over the next 5 years.

Similar nomograms have been developed for predicting the 5-year risk of recurrence following radical cystectomy [178]. This nomogram predicts the probability of remaining disease free 5 years after cystectomy, based on variables including sex, age, number of days from diagnosis to cystectomy, pathological stage, tumour grade, histological type, and pathological node status. The Memorial Sloan-Kettering Cancer Centre (MSKCC) website (www.mskcc.org) provides an easy to use calculator based on this nomogram.

As highlighted earlier, cancers which express several oncogenes or tumour suppressor genes have been associated with a poorer prognosis. Several studies have investigated whether any of these markers could predict response to treatment. Altered p53 has been the most studied in this area. In terms of surgery, p53 status could not predict which patients would suffer recurrence or die following cystectomy and thus could not identify patients in whom cystectomy would be beneficial [179].

In studies of chemotherapy treatment, altered p53 expression was shown to be an independent prognostic marker for survival and an indicator of treatment failure in patients with invasive bladder cancer treated with neoadjuvant MVAC (methotrexate, vinblastine, adriamycin (doxorubicin) and cisplatin) [180]. However, some have reported opposing findings suggesting that only those with abnormal p53 expression associated with local and regionally extensive TCC benefit from cisplatin-based chemotherapy [181]. There are however several problems with using p53 as a prognostic utility in the clinical setting which would need to be resolved before it could be used

widely as a prognostic indicator and guide to treatment. Currently, there is no consensus as to how many tumour cells must exhibit nuclear overexpression of p53 before it can predict the response of that tumour to treatment. There are also several technical factors that need to be resolved and standardised including antibodies used to detect p53, means of tissue preservation (frozen or formalin fixed) and methods of optimising antigen detection and quantification.

1.2: Chemotherapy in bladder cancer

Chemotherapy has been used widely in bladder cancer, both as intravesical and systemic chemotherapy. Intravesical chemotherapy following transurethral resection has a clearly proven role in the prevention of superficial TCC recurrence and is now part of standard care. Systemic chemotherapy is starting to find a role in the neoadjuvant setting following recent meta-analyses confirming a survival benefit. However, adjuvant systemic chemotherapy is still awaiting trial data to support its use.

Intravesical chemotherapy

Various anticancer agents have been instilled directly into the bladder in order to reduce recurrence rates in superficial bladder cancers, so-called intravesical chemotherapy. These agents include cytotoxic drugs and immunotherapeutic agents including BCG alone or in combination with various interferons.

We will deal only with cytotoxic drugs in this section, as it is these drugs that are susceptible to the multidrug resistance phenomenon which is the main focus of this research.

The rationale for intravesical chemotherapy

Eighty percent of bladder cancers are superficial, meaning that their major risk is of recurrence rather than disease progression. It is for this reason that ways of providing local control were sought and hence intravesical chemotherapy came into being.

The rationale for intravesical chemotherapy was based on the easy accessibility of the bladder via catheterisation allowing administration of local therapy and the ability to give relatively high doses with minimal systemic absorption and side effects. Practically, local side effects of cystitis have limited the doses that can be given.

Intravesical chemotherapy can either be adjunctive, prophylactic or therapeutic. Adjunctive chemotherapy is when a single instillation is given immediately post-TURBT in order to kill tumour cells that are liberated as a result of tumour morcellation. The aim is to prevent tumour cell implantation and recurrence by that mechanism. Prophylactic use is where intravesical chemotherapy is given as a course of repeated instillations after complete tumour resection. This aims to prevent new recurrences forming from a

genetically unstable urothelial field change, as is found in a significant proportion of bladder cancer patients. Therapeutic use means repeated instillations to treat residual unresected disease, either carcinoma in situ (Cis) or extensive papillary tumour.

Intravesical chemotherapy regimens should be tailored to the patient's disease. Giving a single dose of intravesical chemotherapy post-operatively is now part of routine clinical practice, with further courses being dictated by clinical and histological features that predict a higher chance of recurrence.

In terms of the choice of drug to use, there is no single best agent for intravesical chemotherapy. The features that would be desirable in a "gold-standard" drug would be prevention of recurrence and disease progression in 100% of cases, requiring only a single instillation to do so. The cost of the drug should be reasonable and there should be no local or systemic toxicity.

The optimal course of intravesical chemotherapy is not known.

Chemotherapeutic agents need to be in direct contact with the urothelium to be effective. Most chemotherapeutic agents are cell cycle dependent meaning that they only affect dividing cells, meaning that repeated instillations are necessary to produce a response with tumour cell killing. The concentration of the drug and the dwell time in the bladder are also important determinants of tumour cell kill with chemotherapy but studies looking at these variables are lacking.

A brief history of intravesical chemotherapy…

The first use of intravesical chemotherapy in bladder cancer was reported by Jones and Swinney in 1961 [182]. They gave 16 patients with superficial tumours four doses of intravesical thiotepa, an alkylating agent. Eight patients showed a significant response with their tumours almost completely disappearing at 6 and 12 week cystoscopies. Two patients developed haematological problems following treatment, one a mild leucopenia and one severe thrombocytopenia requiring treatment. It was later discovered that these haematological side effects were due to transvesical absorption of thiotepa. Molecules smaller than about 200MW can be absorbed transvesically and thiotepa's molecular weight is only 189.

The first clinical trial of adjuvant intravesical chemotherapy using thiotepa was published in 1978 [183]. This study recruited 22 patients with recurrent TCC.

In group 1, patients were treated with 30mg of thiotepa twice daily for 3 days post-operatively. Their recurrence free interval increased to 33 months compared to 9.5 months before treatment. In group 2, patients were given additional intravesical thiotepa treatments indefinitely, their recurrence free interval increased to 41 months. Two patients developed leukopenia from systemic absorption.

The Medical Research Council (MRC) carried out a multicentre randomised clinical trial of either one or five installations of intravesical thiotepa (30mg) post-TURBT in the treatment of newly diagnosed superficial bladder cancer [184]. After transurethral resection, four hundred and seventeen patients were randomised to receive either: no thiotepa; one instillation of thiotepa at the time of resection or one instillation at the time of resection and then at 3-monthly intervals for one year (five instillations in total). The median follow-up for this study was 8 years and 9 months. This study failed to demonstrate any difference between the three groups with respect to time to first recurrence, recurrence rates or the failure-free interval rate. They concluded that thiotepa should not be used for patients with newly diagnosed superficial bladder cancer.

A later EORTC randomised trial, compared adjuvant intravesical thiotepa, doxorubicin and cisplatin in 356 patients with recurrent superficial TCC [185]. After transurethral resection of all visible tumour, patients were given their allocated intravesical chemotherapy weekly for 4 weeks and then monthly for 11 months. At a mean follow-up of 41 months, there were no significant differences between the treatments in terms of recurrence rate or disease free interval.

Ethoglucid 1% (Epodyl), another alkylating agent was investigated in the 1970's in view of its lower risk of systemic absorption due to its higher molecular weight of about 250.

One study reported the treatment of 44 patients with multifocal, superficial TCC with intravesical Epodyl [186]. Irritative cystitis occurred in 16 per cent of patients and they were withdrawn from the study. In those patients who were able to tolerate the treatment without side effects, complete or partial responses were observed in 66% (19 of 29).

Ethoglucid failed to gain widespread use, due to its main side effect of severe chemical cystitis which occurred in a significant proportion of patients.
Doxorubicin, an anthracycline antitumour antibiotic, was discovered 1969 [187] and was soon demonstrated to have potent antitumour activity [188]. This was the next drug to be evaluated as an intravesical agent.
A study from the EORTC compared the treatment of superficial TCC with transurethral resection alone or transurethral resection followed by intravesical chemotherapy with either doxorubicin or ethoglucid for 1 year [189]. 443 patients were randomised. The time to first recurrence was significantly longer for both intravesical chemotherapy groups. The recurrence rates per year were also significantly lower for both treatment arms compared to the resection only group (30% versus 68%). There were no differences in progression rates or death from bladder cancer between the groups.
The two most commonly used intravesical agents currently are epirubicin and Mitomycin C.
Epirubicin, a semi-synthetic epimer of doxorubicin, was first introduced into clinical use in the 1970s [190]. It was first evaluated as intravesical treatment for superficial bladder cancer in the 1980s [191], where a complete or partial response rate was demonstrated in 55% of patients.
Mitomcyin C was discovered in the 1960s [192] and its first intravesical use was in 1980 [193]. In this initial study, sixty-three patients with superficial TCC were given intravesical mitomycin C 20-60mg once a week for 8 weeks. The overall response rate was 67%, with a 45% complete remission rate. There were no systemic side effects and local side effects occurred infrequently.
Mitomycin was later subjected to a head-to-head trial with thiotepa by the National Bladder Cancer Group [194]. They reported the results of a prospective randomized clinical trial comparing Thiotepa and Mitomycin C in the treatment of residual superficial TCC of the bladder. Eight weekly instillations were given followed by cystoscopy 4 weeks after the treatment was stopped. Mitomycin C had a higher complete response rate than Thiotepa, 39 versus 26 percent. When partial responses were included the

overall response rate increased to 63 percent for mitomycin C and 53 percent for thiotepa.

Mitomycin C is the most commonly used intravesical cytotoxic agent in the UK currently.

Intravesical chemotherapy: Randomised controlled trials and meta-analyses

Although earlier randomised controlled trials had demonstrated a clear benefit from intravesical chemotherapy following TURBT, it was only in the 1990s following the publication of a large EORTC trial using epirubicin and an MRC study using mitomycin C, that intravesical chemotherapy came to be used routinely following TURBT.

EORTC trial of intravesical epirubicin:

In 1993 the results of a prospective EORTC trial comparing transurethral resection followed by a single intravesical instillation of epirubicin or water for solitary Ta / T1 papillary bladder carcinoma were reported [111].

This randomised multicentre trial included 431 eligible patients with solitary, primary or recurrent, Ta-T1, G1-3 bladder tumours. Patients with carcinoma in situ were excluded. The patients underwent standard transurethral resection of their tumours and were then randomised to receive a single dose of either epirubicin 80mg in 50ml of physiological solution or 50ml of sterile water, given within 6 hrs of resection for a period of 60 minutes. All patients were followed up with cystoscopic surveillance, 3 monthly for the first year, 4 monthly for the second year and 6 monthly thereafter. They were evaluated by several criteria of disease recurrence, including disease free interval (the interval between initial TURBT and date of first tumour positive bladder biopsy), recurrence rate per year (the total number of positive cystoscopic studies divided by total years of follow-up from initial TURBT to the time of the last cystoscopic examination) and the tumour rate per year (the total number of tumours observed during all positive cystoscopic studies divided by the total years of follow-up from initial TURBT to the time of the last cystoscopic examination).

The disease-free interval was significantly longer in the epirubicin group ($p=0.02$). The recurrence rates per year in the epirubicin group and water group respectively were 0.17 and 0.32, which was a highly statistically

significant difference ($p < 0.0001$). The tumour rates per year were 0.31 and 0.56 in the epirubicin and water groups respectively, again showing a statistically significant difference in favour of the epirubicin group ($p = 0.01$). Similar reductions in recurrence rates were noted in favour of the epirubicin group, in all subgroups examined as defined by T stage and grade.
This study therefore concluded that a single intravesical instillation of epirubicin 80mg post-TURBT reduced the recurrence rate by nearly 50% compared to water at a mean follow-up of 2 years in single Ta-T1, G1-3 transitional cell carcinomas of the bladder.

MRC trial of intravesical Mitomycin C:

In 1996, the results of an MRC randomised controlled trial looking at the effect of Mitomycin C on recurrence rates in newly diagnosed superficial bladder cancer were reported [110]. This study included 452 eligible patients with newly diagnosed Ta / T1, solitary or multifocal superficial TCC. Patients with carcinoma in situ were excluded. Following transurethral resection of their tumour(s) they were randomised into 3 groups: a control group who had no further treatment, Mitomycin C Group 1 who had a single instillation of Mitomycin C 40mg immediately after TURBT (MMC Group 1) and Mitomycin C Group 2 who had an instillation of Mitomycin C 40mg immediately after TURBT and 4 further instillations at 3-month intervals over the next 12 months (total 5 instillations) (MMC Group 2). The initial instillations were all given within 24 hrs of TURBT (median time from TURBT to instillation was 1 hour) for 60 minutes duration. The patients then underwent cystoscopic surveillance 3 monthly for year 1, 6 monthly for year 2 and annually thereafter. The median follow-up was 7 years at the time of analysis. The principal end points they used to assess the efficacy of Mitomycin C were the recurrence-free interval (interval to first recurrence from randomisation) and the recurrence rate during the initial 2 years (the number of positive cystoscopies divided by the total follow-up interval for 2 years). Secondary end points were progression to invasive disease, progression to metastases and death from bladder cancer. These 3 secondary end points were combined to define the progression free interval for each of the 3 groups. Overall survival was also documented for each group.

Pairwise comparison of recurrence-free intervals showed hazard ratios for MMC Group 1 versus controls of 0.66 and for MMC Group 2 versus controls of 0.50 representing a decrease in subsequent risk of recurrence by an estimated 34% in MMC Group 1 and 50% in MMC Group 2.
Pairwise comparison of annual recurrence rates in the first 2 years for the control group (recurrence rate 0.82), MMC Group 1 (recurrence rate 0.42) and MMC Group 2 (recurrence rate 0.31) are shown in the table 6 below.

Comparison	MMC Group 1 versus Control	MMC Group 2 versus Control	MMC Group 2 versus MMC Group 1
Ratio of recurrences*	0.52	0.38	0.73
95% Confidence Interval	0.34 – 073	0.26 – 0.53	0.48 – 1.11
P value	0.001	<0.001	0.14

Table 6: Data from MRC trial of intravesical mitomycin C in superficial bladder cancer: Pairwise comparison of annual recurrence rates in first 2 years

*Ratio of 1 indicates equivalence of groups being compared. Ratio <1 indicates annual recurrence rate in first 2 years was in favour of first group listed in the comparison

Both of the Mitomycin C groups had significantly lower annual recurrence rates than controls, with an estimated decrease in recurrence rates per year of 48% MMC group 1 and 62% in MMC group 2.
Although the results for 5 instillations (MMC group 2) were better than for a single post-operative instillation (MMC group 1) across the board, the difference between these two groups failed to reach statistical significance.
This study also failed to demonstrate any significant difference in progression free interval or overall survival between the 3 groups, possibly because so few patients developed progressive disease or died.
The MRC study group therefore concluded that intravesical mitomycin C,

either using single or multiple instillations, reduces the number of subsequent recurrences and increased the recurrence-free interval, but failed to demonstrate any benefit in terms of disease progression.

Meta-analyses of intravesical chemotherapy trials:

Several meta-analyses of the results of intravesical chemotherapy following transurethral resection have also been published. These have all come out in favour of intravesical chemotherapy but have sought to answer specific questions about its applicability in terms of timing and length of use and specific patient groups.

One meta-analysis looked at the question of early versus delayed instillations and short-term versus long-term treatment. It used results from 2 EORTC studies looking at intravesical Mitomycin C and Doxorubicin [112].

Early intravesical treatment, defined as instillation within 24 hours of TURBT, was found to be superior to delayed treatment, defined as instillation 7 – 15 days post-TURBT ($p = 0.01$).

Looking at the role of maintenance therapy, there appeared to be no benefit except in the delayed treatment group. The results were equivalent in the early instillation with maintenance, early instillation without maintenance and the delayed instillation with maintenance groups, all of which were significantly superior to the delayed instillation without maintenance group.

Another meta-analysis looked simply at adjuvant treatment versus no adjuvant treatment for superficial bladder cancer, with specific emphasis on its effect on disease-free interval and disease progression [104].

They used the results from 4 EORTC studies and 2 MRC trials and showed that adjuvant treatment was significantly better than no adjuvant treatment in terms of disease-free interval ($p<0.01$). However they failed to demonstrate a clear advantage of adjuvant treatment with respect to progression to invasive disease, time to metastases, duration of survival or progression-free survival. The trials included in this meta-analysis were heterogeneous in terms of the drug used, mode of administration, dose, duration of instillations, interval between instillations and duration of treatment, so no other conclusions were drawn.

A further meta-analysis looked more specifically at intravesical chemotherapy for primary superficial bladder cancer and the effect of the duration of treatment on recurrence rates [195].

It examined the results of 3703 patients from 11 randomized trials. Overall intravesical chemotherapy was found to reduce the 1 year recurrence rate by an average of 44%. They then examined the results by duration of treatment. Short-term protocols, where patients has a single instillation or multiple instillations for less than 2 months following TURBT, showed a reduction in 1 and 2 year tumour recurrence rates of 30% and 32% respectively. One-year protocols where patients received regular intravesical instillations for 1 year post-TURBT, demonstrated a reduction in 1 and 2 year tumour recurrence rates of 35% and 31% respectively. Two-year protocols where patients received intravesical instillations for 2 years following TURBT, showed a reduction in 1 and 2 year tumour recurrence rates of 80% and 73% respectively. This discrepancy between the results of 1 and 2 year protocols was curious. In the 2 year protocols instillations were often more frequent, with one study giving instillations every 2 weeks for the first year and then monthly for the second year, whereas some of the 1 year protocols only gave patients instillations every 3 months. This suggested that a dose response may account for the differences in the results of the 1 and 2 year protocols.

Another meta-analysis focused on the impact of intravesical chemotherapy on recurrence rates in recurrent superficial TCC [196].

Meta-analysis of results for 1609 patients from 8 randomised trials demonstrated a reduction in 1-year tumour recurrence rates of an average of 38% in those having adjuvant intravesical chemotherapy. Odds ratios for 2 and 3 year recurrence were 0.46 (95% CI 0.33-0.63; p=0.006) and 0.35 (95% CI 0.23-0.54; p<0.001) respectively, favouring TURBT with adjuvant chemotherapy over TURBT alone.

An additional meta-analysis examined the effect of a single immediate post-operative instillation of chemotherapy in reducing the risk of recurrence in patients with solitary or multifocal superficial bladder cancer [Sylvester RJ *et al*. 2004]. They reviewed the results of 1476 patients from 7 randomised trials. Chemotherapy reduced the risk of recurrence by 39% overall (p<0.0001), with a significant effect being seen for both single and multifocal

tumour patients. However, the overall recurrence rate for those with multiple tumours was 65.2% compared to 35.8% for single tumours, suggesting that a single instillation is insufficient treatment for those with multifocal disease.

Optimising intravesical chemotherapy: The variables

Timing of instillations:

Most of the trials reporting benefits from intravesical chemotherapy following TURBT have given a single dose within 6 hours of surgery. It is therefore recommended that where possible chemotherapy should be given within this time frame to achieve its maximum benefit.

Dosing of drugs:

Very few trials have been performed looking at optimising drug doses for intravesical chemotherapy. Logically one would assume that higher drug doses would be more effective, but this has to be balanced against side effects of chemical cystitis that may impact of the patients ability to retain the drugs for enough time to be effective.

Improving the pharmacokinetics of intravesical agents:

Several factors may affect the efficacy of intravesical chemotherapy including, drug dilution with residual urine or excessive urinary output during the exposure period, instability of chemotherapeutic drugs at low urinary pH, inadequate duration of exposure and limited penetration of the drug into the bladder wall. These factors can be optimised to improve the efficacy of the intravesical therapy.

Preventing drug dilution:

Elimination of residual urine from the bladder is desirable prior to instillation of the chemotherapy. Ensuring that the bladder has been adequately drained by repositioning the catheter or changing the position of the patient will help to avoid excessive residual volumes of urine.

Fasting patients for 6 – 8 hours prior to each instillation reduces urine output and hence dilution of the drug by up to 20% [197,198]. Administration of oral desmopressin 0.2mg 1 hour before each instillation is also effective, increasing mean intravesical drug concentration by up to 38% [198].

Alkalinisation of the urine:

Oral doses of 1.3g of sodium bicarbonate given the night before, morning of, and 30 minutes before intravesical chemotherapy with mitomycin C have

been shown to improve drug stability, cellular uptake and penetration into the deep muscle layers. An optimum pH of > 7 is achieved using this regimen. *In vitro* studies have also shown that alkalinisation improves the cellular uptake and cytotoxicity of epirubicin in bladder cancer cell lines [199]. Urinary alkalinisation may therefore be desirable for all types of chemotherapy, especially as urine is generally acidic.

Duration of each instillation:

The majority of the large trials of intravesical chemotherapy used instillation times of 1 hour. Prolonged exposure of the urothelium and exfoliated cells to intravesical chemotherapeutics seems likely to improve their cytotoxic action. Patients should be encouraged to retain the instillate as long as possible.

Optimising intravesical chemotherapy: Trial data

Whilst many studies have now demonstrated an improvement in terms of recurrence rates and disease free interval, they have been different in terms of the drugs used, doses and concentrations used, duration of instillations, timing of instillations, number of instillations and the period over which they are given. There are also issues about dilution of drug concentrations by urine production and the effects of urinary pH on drug stability. The effects of some of these variables have been addressed by some recent studies.

One study investigated the effect of drug concentration for intravesical epirubicin on recurrence of superficial bladder cancer [200]. Six hundred and fourteen patients with primary or recurrent, single or multifocal, Ta/T1, G1-2 bladder cancers were randomised to receive intravesical epirubicin at doses (concentrations) of 20mg/40ml (0.5mg/ml), 30mg/40ml (0.75mg/ml) or 40mg/40ml (1mg/ml).

Group A (N=205) received 17 instillations of 20mg/40ml over 12 months (total dose 340mg), Group B (N=204) received 12 instillations of 30mg/40ml over 7 months (total dose 360mg) and Group C (N=205) received 9 instillations of 40mg/40ml over 4 months (total dose 360mg). The best results were achieved with the highest dose (and concentration) administered over the shortest period of time. The 1-year recurrence free rates were 0.671, 0.730 and 0.739 for groups A, B and C respectively and the 2-year recurrence free rates were 0.487, 0.551 and 0.601 for groups A, B and C, respectively.

Another recent randomised phase III study looked to increase the efficacy of Mitomycin C with pharmacokinetic modification to increase the drug concentration and alkalinise the urine to aid drug stability [197]. Patients with TCC who were at high risk of recurrence were randomised to receive weekly instillations for 6 weeks in either the standard-treatment arm where they received Mitomycin C 20mg in 20mls of normal saline without pharmacokinetic manipulations or urine alkalinisation, or the optimised-treatment arm where they received mitomycin 40mg with pharmacokinetic manipulations to increase drug concentration by decreasing urine volume and urine alkalinisation to stabilise the drug. The modifications made to the administration of the chemotherapy in this group included increased drug dose (40mg versus 20mg), reduced dose volume (from normal 40ml to 20ml), minimising residual urine before instillation by adequate catheter drainage, voluntary dehydration for 8 hours before the chemotherapy was given and alkalinisation of the urine by administration of sodium bicarbonate 1.3g orally the night before, the morning of and 30 minutes before treatment. The instillations were retained in the bladder for 2 hours.

The results showed an increase in the median time to recurrence from 11.8 months in the standardised group to 29.1 months in the optimised group ($p = 0.005$). The recurrence free fraction at 5 years was 24.6% in the standard-treatment group compared to 41% in the optimised-treatment group.

It stands to reason that maintaining higher concentrations of cytotoxic drugs in the bladder for a longer period of time will lead to improved efficacy.

Increasing bladder wall drug penetration

Electromotive drug administration (EMDA), a technique based on iontophoresis and electro-osmotic phenomena, increases drug transport through biological membranes by 4 – 7 times and significantly enhances the efficacy of intravesical agents in comparison with passive administration [201,202].

Local microwave induced hyperthermia induced by an endovesical microwave applicator also enhances the effectiveness of intravesical drugs [201,203].

Electromotive administration of intravesical therapy:

Recently study data have been published for a new technique called electromotive drug administration (EMDA). This technique applies an electric

current across the urothelial surface which accelerates drug delivery into and across biological membranes, improving drug delivery to the urothelium.
A randomised study of electromotive Mitomycin C versus passive transport Mitomycin C for high risk superficial bladder cancer has recently been reported [202]. Patients with high risk superficial bladder cancer (108 patients with multifocal Cis, including 98 with T1 tumours) were randomised into 3 equal groups of 36 patients. Each of these groups received either electromotive Mitomycin C 40mg with a 20mA pulsed electric current applied for 30 minutes or for passive Mitomycin C 40mg for 60 minutes or intravesical BCG 81mg for 120 minutes. Treatments were given weekly for 6 weeks initially. Non-responders were given a further 6 weekly treatments and the responders were given monthly treatments for 10 months.
Treatment response was assessed by cystoscopy, biopsy and urine cytology. The primary end points were complete response rates at 3 and 6 months, as defined by negative biopsies and cytology.
Complete response rates at 3 months were 53%, 28% and 56% and at 6 months were 58%, 31% and 64% for electromotive Mitomycin C, passive Mitomycin C and BCG respectively, with the difference between Mitomycin groups being significant in favour of the electromotive group at 3 months ($p = 0.036$) and 6 months ($p = 0.012$). The median time to recurrence was also significantly longer in the electromotive MMC group, 35 months, compared to the passive MMC group, 19.5 months ($p = 0.013$). With BCG showing a median time to recurrence of 26 months.
EMDA increases bladder uptake of Mitomycin C, resulting in improved response rates in high risk superficial bladder cancer.

Combination intravesical chemotherapy:

Unlike systemic chemotherapy regimes, combination chemotherapy has not found widespread use in intravesical chemotherapy.
Some small trials have been performed using known MDR reversing agents in combination with chemotherapy in an attempt to improve efficacy.
Verapamil has been shown to reverse multidrug resistance in bladder cancer cell lines *in* vitro [199]. Its effects as part of a combination intravesical chemotherapy regime have been subject to several small scale studies, some

of which have yielded promising results, suggesting that larger scale studies may be warranted.

One randomised study looked at the effect of combining verapamil with epirubicin given intravesically following resection of recurrent superficial bladder carcinoma [204]. Intravesical instillations were performed 4 hours before surgery and then at weekly intervals for 1 month and then once a month until 2 years from initial resection. In the epirubicin and verapamil group only 37% developed recurrent tumours compared to 50% in the epirubicin group. The difference in recurrence rates between the two treatment arms did not reach statistical significance, but only 75 patients were included in this trial.

Verapamil has also been combined with doxorubicin for prophylactic intravesical instillation [205]. Following transurethral resection patients were randomised to receive Doxorubicin 30mg plus Verapamil 15mg or Doxorubicin 30mg alone for 19 instillations over 1 year. The overall 3-year non-recurrence rate was significantly higher in the doxorubicin and verapamil group than doxorubicin alone, being 78.4% and 64.5% respectively ($p = 0.0303$). There was no difference in the incidence or severity of side effects between the two groups.

Combined intravesical chemotherapy and immunotherapy regimes have gained some interest recently following the publication of a recent study combining BCG and Mitomycin C therapy. This compared sequential intravesical BCG and electromotive Mitomycin C versus BCG alone for high-risk superficial bladder cancer [206].

Two hundred and twelve patients with T1 bladder cancers were randomised into 2 groups. One group received 81mg of BCG intravesically for 120 minutes once a week for 6 weeks. Complete responders were then placed on maintenance therapy consisting of 81mg of BCG once a month for 10 months. The other group received 81mg of BCG intravesically for 120 minutes once a week for 2 weeks, followed by 40mg of mitomycin C with electromotive delivery with a 20mA electric current for 30 minutes once a week for 3 weeks. Complete responders went on to have further electromotive mitomycin C once a month for 2 months followed by 81mg of BCG once a month for 3 months.

The primary endpoint for this study was disease free survival with secondary endpoints being time to progression, overall survival and disease-specific survival.

The electromotive mitomycin C / BCG group had significantly longer disease-free interval (69 versus 21 months, p = 0.0012), a lower recurrence rate (41.9% versus 57.9%, p = 0.0012), a lower progression rate (9.3% versus 21.9%, p = 0.004), a reduced overall mortality (21.5% versus 32.4%, p = 0.045) and a reduction in disease-specific mortality (5.6% versus 16.2%, p = 0.01).

So intravesical sequential BCG and electromotive MMC leads to higher disease free interval, lower recurrence and progression and improved overall survival and disease-specific survival compared to BCG alone in high-risk superficial bladder cancer, suggesting a potential role in the future management of superficial bladder cancer.

The future

Newer agents are awaiting trial data to support their use in superficial bladder cancer.

Pirarubicin (tetrahydropyranyl-doxorubicin (THP)) is the only new agent that has proven effective in reducing recurrence rates after TURBT [207]. Other agents have been tested in phase I and II trials with promising results but phase 3 and 4 results are lacking.

Gemcitabine is a deoxycytidine analogue used systemically in the treatment of locally advanced or metastatic bladder cancer. Phase 1 studies have demonstrated its safety for intravesical administration [208] and phase 2 studies have shown its cytotoxic potential [209].

Meglumine γ-linolenic acid (MeGLA) is an essential fatty acid with cytotoxic activity which has shown to be effective both *in vitro* and *in vivo*. An initial phase 1 study looking at a single dose of intravesical MeGLA for recurrent superficial bladder cancer, showed a reduction in the size of marker lesions in 43% of patients [210]. Combination of MeGLA and epirubicin i*n vitro* has demonstrated a synergistic increase in cytotoxicity in human bladder cancer cell lines. It would seem logical therefore to subject this combination intravesical therapy to evaluation in randomised controlled clinical trials to see

if there are further benefits above and beyond standard chemotherapy regimens.

Suramin is an antitrypanosomal agent with antitumoural properties, that blocks epidermal growth factor (EGF) from accessing its receptor (EGFR). Phase 1 studies have shown its safety when administered intravesically, with negligible local toxicity and low systemic absorption [211,212]. Phase II trials are warranted to assess the efficacy of Suramin in the treatment of superficial bladder cancer.

Photosensitising agents have also been trialled in bladder cancer. These agents are selectively taken up by tumour cells when administered intravesically. When an intravesical light source is applied, the agent exerts its cytotoxic effect. This therapeutic option would therefore seem particularly attractive in patient where a "field change" has occurred within the urothelium such as multifocal TCC and Cis, allowing malignant cells throughout the entire urothelium to be treated selectively.

Photofrin was the first photosensitizing drug used in the treatment of superficial bladder cancer, but had significant local and systemic side effects [213]. Photodynamic therapy (PDT) with intravesical instillations of 5-aminolevulenic acid (5-ALA) has been used in superficial bladder tumours that could not be controlled by TURBT, in primary CIS and in BCG resistant tumours with good results and limited morbidity [214,215]. Porfimer sodium is another photosensitising agent that has been shown to be effective in BCG resistant CIS [216]. Hypericin [217] and more recently PAD-S31 [218] have been highly effective in destroying bladder tumours in animal models. Despite all the research that has gone into PDT as yet there are no randomised controlled trials to prove its efficacy over and above conventional treatments.

Chemosensitivity tests

It is possible that *in vitro* chemosensitivity assays could be performed to determine the sensitivity of a tumour to several drugs prior to instillation [219]. The drug regimen could then be tailored to the individual patient with the aim of improving response rate and reducing recurrences. To date there are no studies that have addressed the possibility of such a chemosensitivity assay in superficial bladder tumours.

Systemic Chemotherapy

Systemic therapy is reserved for muscle-invasive or metastatic bladder cancers and may be used in neoadjuvant or adjuvant settings. The role of systemic chemotherapy and available trial data has already been discussed in chapter 1.

The rationales for neoadjuvant and adjuvant systemic therapy are different. In neoadjuvant therapy the idea is to treat micrometastatic disease and downstage the primary tumour prior to surgery. It also has the advantages of being able to assess the chemotherapeutic response of the primary tumour and the benefit of an improved performance status in the patients pre-operatively meaning they are less likely to have complications. The disadvantages of neoadjuvant chemotherapy are that there is a delay in the definitive local treatment and that treatment is decided based on clinical staging meaning that some patients may receive unnecessary chemotherapy. Adjuvant chemotherapy is used to try and deal with residual disease and micrometastatic disease. The advantages of this approach to systemic therapy are that patients are treated on the basis of pathological staging (low-risk patients can be spared toxicity) and that immediate local treatment is not delayed in operable patients. Adjuvant chemotherapy is the strategy of choice in other chemo-sensitive cancers e.g. breast, colon. The problems with adjuvant therapy are that there is a lack of evidence for this approach with the trials conducted so far being small and of poor quality. One meta-analysis of adjuvant chemotherapy has been conducted suggesting a 3-year survival benefit of 9%, but its power is limited. The EORTC are running a study (EORTC 30994) of immediate versus deferred chemotherapy following cystectomy which may be the last chance to answer the question of whether immediate adjuvant chemotherapy confers a survival advantage in muscle-invasive bladder cancer.

1.3: Multidrug resistance in cancer

Different cancers vary in their response to cytotoxic drugs, with some being sensitive to treatment whilst others are resistant. Understanding the mechanisms of resistance may lead to the development of markers of resistance which can predict treatment outcomes and may also identify future therapeutic targets.

The term “multidrug resistance” (MDR) describes a phenomenon whereby cancer cells exposed to a single cytotoxic drug develop cross resistance to a number of other structurally unrelated cytotoxic compounds.

It was first described in 1970, when it was noted that Chinese hamster ovarian cancer cells exposed to actinomycin D developed cross-resistance to many other cytotoxic drugs, including the anthracyclines (daunomycin and doxorubicin), etoposide, colchicine and the vinca alkaloids (vincristine, vinblastine and vindesine) [220].

Cells exhibiting MDR were found to have much lower intracellular drug concentrations and this accumulation deficit was shown to be mediated by a 170 Kilodalton (KDa) transmembrane glycoprotein [221]. This glycoprotein was later named permeation-glycoprotein or P-glycoprotein (P-gp).

Subsequent studies suggested that the reduced intracellular levels of drug were as a result of increased drug efflux by an energy dependent process [222]. P-gp was found to be acting as an ATP-coupled drug efflux pump, removing cytotoxic compounds from MDR cells, thereby reducing their cytotoxic potential.

Since these early days many more mechanisms of multidrug resistance have been elucidated. It is accepted that tumours exhibiting MDR may have more than one of these mechanisms involved in their MDR status.

Some tumours exhibit intrinsic or natural resistance, meaning they do not respond to standard chemotherapy from the outset. Many other tumours appear responsive to chemotherapy initially and later develop resistance. This acquired resistance is likely to be due to either selection or induction of resistance, or both. Selection implies that tumours contain clones of cells that possess intrinsic MDR which are selected out by chemotherapy. Induction of resistance implies that chemotherapeutic exposure has stimulated

upregulation of the cellular MDR mechanisms of the tumour cells, rendering them resistant.

Clinically both of these scenarios would manifest as patients who respond well to chemotherapy initially, but then developing recurrent disease arising from these residual selected or induced MDR clone cells, that are insensitive to further courses of chemotherapy. This phenomenon is seen by oncologists relatively commonly, supporting these theories.

Selection and induction MDR theories are also supported by *in vitro* studies where MDR cell lines have been derived from sensitive parental cell lines either by low-dose chronic exposure to chemotherapy (induced MDR) or by high-dose pulsed chemotherapy (selected MDR).

Mechanisms of MDR:

P-glycoprotein (P-gp)

P-glycoproteins are members of the superfamily of ATP-binding cassette (ABC) transporter proteins. They are expressed in normal human tissues including gastrointestinal mucosal cells, biliary canalicular cells, adrenocortical cells, capillary endothelial cells (in brain and testis), renal tubular cells and placental trophoblastic cells. Here they are thought to act as a detoxification or cytoprotective mechanism by actively pumping toxins out of the cells.

P-glycoprotein otherwise known as P-gp or P170 is an energy dependant transmembrane glycoprotein efflux pump that is able to transport a variety of compounds that are structurally dissimilar. Most P-gp substrates are plant-derived or chemically-synthesised cytotoxic drugs or antibiotics, but are not limited to these substances.

Overexpression of P-gp is responsible for “classical” or “typical” MDR and occurs following amplification of the normal human gene, MDR-1.

Gene coding and product.

Two separate genes code for P-gp in humans, MDR-1 [223] and MDR-3 [224]. In humans MDR-1 codes for P-gp 1 and MDR-3 codes for P-gp 2 (in rodents three MDR genes have been identified hence this discrepancy in human nomenclature).

Both MDR-1 and MDR-3 genes are found on chromosome 7q21.1 [225]. There is a high degree of homology between the MDR-1 gene which is 4669

base pairs in length and the MDR-3 gene which is around 3900 base pairs long [226].

However, only MDR-1 expression resulting in functioning P-gp 1, has been associated with resistance to cytotoxic drugs. Cells with intrinsic MDR-1 expression or cells transfected with MDR-1 have been shown to develop the MDR phenotype [227], with levels of drug resistance increasing even with very low levels of MDR-1 expression [228].

The MDR-1 gene is regulated by two promoters, with the down stream promoter being more important in normal tissues and the upstream promoter in some MDR cell lines [229].

Structure

P-gp is a membrane glycoprotein with a molecular weight of 170KDa (hence P170). Each P-gp molecule is about 1280 amino acids long, consisting of two halves with very similar sequences, suggesting that it arose from the fusion of two closely related genes. It is composed of 12 hydrophobic transmembrane domains (TMDs) and 2 hydrophilic nucleotide-binding domains (NBD). Each half of the protein includes a short highly hydrophilic N-terminal segment. One NBD connects two TMDs with a hydrophilic NBD loop. Each NBD has an ATP-binding site where ATP is hydrolysed, liberating the energy necessary for the active transport process of this pump (Figure 7).

Cellular distribution and function

P-gp is predominantly distributed on the plasma membrane, but has also been located on other intracellular organelles such the luminal side of the golgi stack apparatus [230-232], lysosomes [233] and the nuclear membrane in MDR breast cancer cells [234].

The effects of P-gp on cellular accumulation of cytotoxic drugs have been mainly studied in relation to it role on the plasma membrane, where is acts as a drug efflux pump. The precise molecular mechanism whereby P-gp can transport such a wide variety of structurally diverse drugs have only been hypothesised and several models have been proposed.

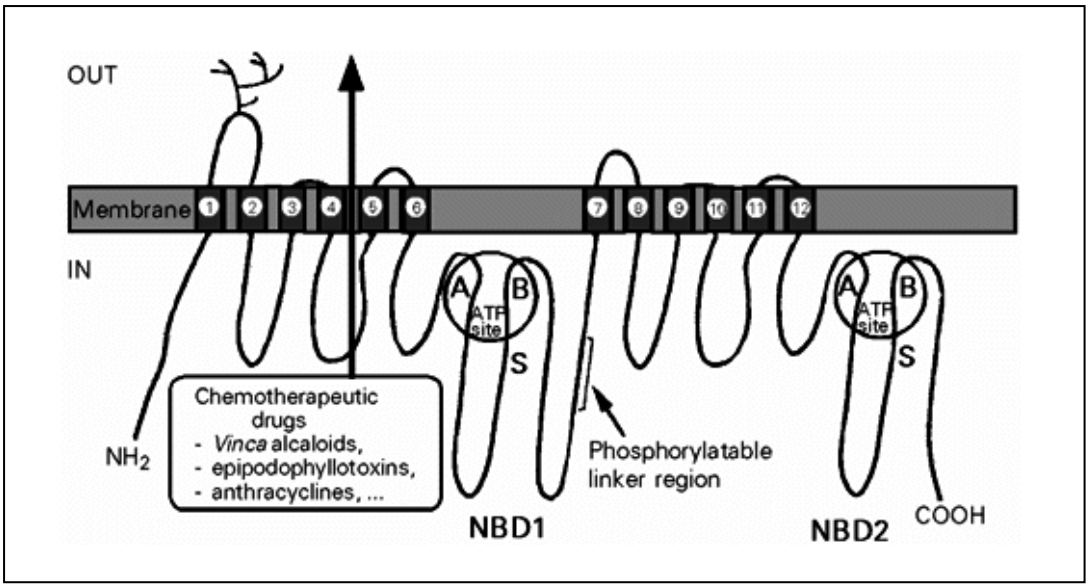

Figure 7: A membrane topology model of P-glycoprotein. (Reproduced with kind permission of BioMed Central Ltd)

The TMDs form channels for substrate drugs, determine the characteristics of the substrates to be transported and efflux substrate drugs. The NBDs are located in the interior of the cytoplasm and participate in ATP binding and hydrolysis [235]. P-gp undergoes conformational changes following binding of nucleotide to the NBDs [236-239]. This conformational change induced by nucleotide binding, involves a major reorganisation of the TMDs throughout the entire depth of the membrane. In the absence of nucleotide, the two TMDs form a single barrel 5 – 6 nm in diameter and about 5nm deep with a central pore that is open to the extracellular surface, spanning much of the depth of the membrane. Nucleotide binding induces reorganisation of the TMDs into three compact domains that are each 2 – 3nm in diameter and 5 – 6nm deep. This opens the central pore along its length, allowing access of hydrophobic drugs (transport substrates) directly from the lipid bilayer to the central pore of the transporter [238].

Inactivation of one of the two NBDs inhibits drug transport and ATP hydrolysis at the other NBD, indicating that the two NBDs function cooperatively and can not hydrolyse ATP independently [240].

Structural changes to the NBDs are also thought to occur as a result of drug binding to the TMD, resulting in a change in the distance between NBDs which affects their ATPase activity (Figure 8).

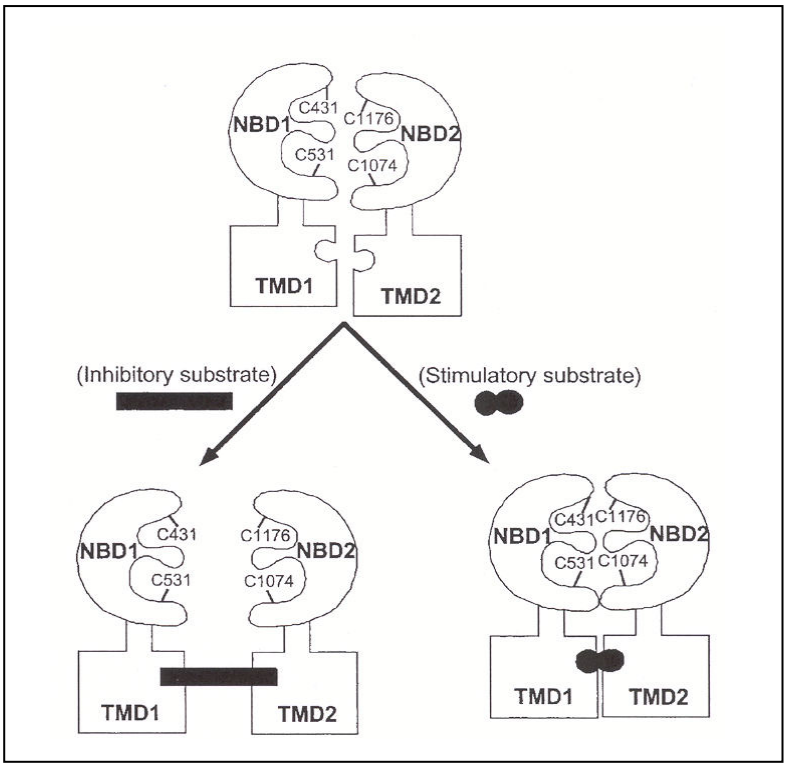

Figure 8: Model of NBD conformational change by drug binding to TMD (Reproduced with kind permission of BioMed Central Ltd).

Many suggest that P-gp acts as a transmembranous pore, binding drugs in the cytoplasm and expelling them into the extracellular space [241]. Others have suggested that P-gp binds substrates within the plasma membrane and pumps them out of the cell [242]. It has also been postulated that P-gp acts as a "flippase", flipping substrates from the intramembrane space to the outer leaflet promoting diffusion back into the extracellular matrix [243].

Certainly the function of P-gp involves an energy dependent process as it requires ATP to be effective, with studies showing that the effects of P-gp on drug efflux can be neutralised by reducing the temperature of cells or adding metabolic inhibitors such a sodium azide.

The discovery of P-gp at other cellular sites including Golgi apparatus and lysosomes suggests another pathway for drug expulsion may exist. It is possible that migrating membranous P-gp found on the prelysosomal sorting compartment (PLC] may actively pump drug into vesicles or the PLC [244]. Here the drug would remain trapped until released into the extracellular compartment by exocytosis.

Chemotherapeutic substrates transported by Pgp are shown in Table 7.

Drug
Anthracyclines Daunorubicin Doxorubicin Epirubicin
Vinca alkaloids Vincristine Vinblastine
Podophyllotoxins Etoposide Teniposide
Taxenes Paclitaxel Docetaxel
Mitomycin C
Mitoxantrone
Methotrexate (Only in carrier deficient cells)
Actinomycin D
Colchicine

Table 7: Cytotoxic substrates of P-glycoprotein

Multidrug resistance-associated protein (MRP)

It became apparent with time that P-gp was not the only mechanism involved in MDR, as many resistant cell lines did not exhibit P-gp overexpression. Multidrug resistance-associated protein (MRP) was discovered in 1992 [245], when a human small cell lung cancer cell line was found to be resistant to doxorubicin and vincristine, but did not express P-gp. Overexpression of MRP has been found in many, but not all non-P-gp expressing MDR cell lines. Normal tissues have also been shown to express MRP, including lung, spleen, thyroid, testis, bladder, adrenal and gall bladder [246], but the levels of MRP expression in tumour cells are much higher. Its distribution in these tissues may suggest a protective role against toxic compounds [247].

MRP overexpression has been demonstrated in the non-P-gp expressing MDR bladder cancer cell line, T24 [248]. MRP has also been identified in leukaemic cells [249] and in bladder tumours with no previous exposure to cytotoxic agents [250].

Whether MRP expression has any prognostic significance remains to be established.

Since the discovery of the first MRP (MRP1), numerous other MRPs have been identified and this “MRP family” now extends to nine members [251]. Their distribution in normal tissues is shown in table 8.

Gene coding and products:

The MRP1 gene is located on the short arm of chromosome 16 at band 13.1. The product of this gene, like P-gp, belongs to the ABC superfamily of transport molecules. The product of MRP1 is a 1531 amino acid phospho-glycoprotein with a molecular weight of 190KDa. It has more phosphorylated residues than P-gp and a cycle of dephosphorylation and rephosporylation occurs which may be important in its biological activity. Transfection of the MRP1 gene has been shown to confer the MDR phenotype [252].

The other MRP family gene loci have also been established (Table 8).

Name	Gene locus	Tissue distribution
MRP1	16p13.1	Lung, spleen, thyroid, testis, bladder, adrenal, gall bladder, brain
MRP2	10q24	Liver, gut, kidney, placenta
MRP3	17q21.3	Liver, gut, adrenal cortex, placenta, pancreas, gut
MRP4	13q32	Prostate, lung, muscle, pancreas, testis, ovary, bladder, gallbladder
MRP5	3q27	Ureter, urethra, placenta, heart, brain
MRP6	16p13.1	Liver, kidney
MRP7	6p12-21	Pancreas, liver, placenta, lung, kidney, brain, ovary, lymph node, spleen, heart, leukocytes, colon, skin, testis, stomach
MRP8	16q12.1	Breast, testis
MRP9	Unknown	Breast, testis

Table 8: Gene loci and tissue distribution of MRP molecules

A schematic representation of the primary protein structures of the products of the MRP1 – 9 genes are shown in Figure 9.

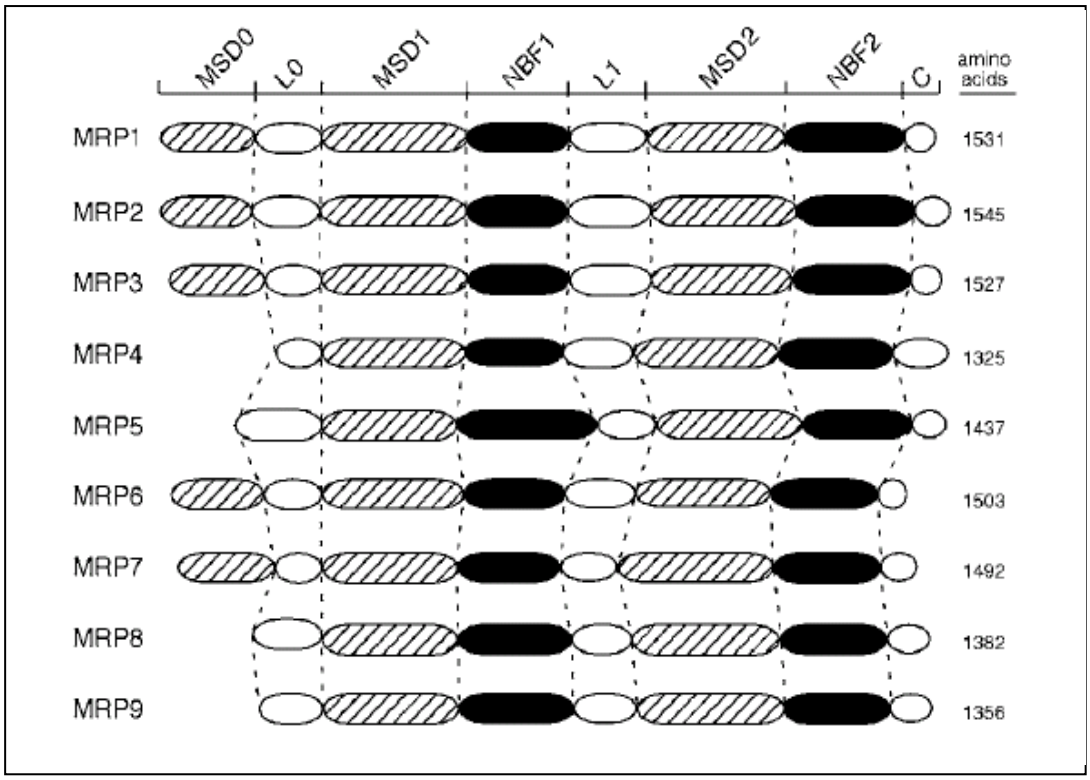

Figure 9: Schematic representation of the protein domains of MRP proteins 1 – 9. Stripes, membrane spanning domains; open, cytoplasmic loops located between MSD0 and MSD1, NBF1 and MSD2 and at the C terminus; black, nucleotide binding folds. (Reproduced with kind permission of Nature Publishing Group)

Structure

MRP1 is composed of a large "core" segment similar to P-glycoprotein, but in addition has an N-terminal region composed of a third membrane spanning domain (MSD0) made up of five transmembrane domains (TMD), an intracellular loop (L0) and an extracellular N-terminus (Figure 10). The core region is similar to P-gp in that it has two nucleotide binding domains (NBDs), two membrane spanning domains (MSDs) consisting of six transmembrane spanning helices and a linker segment (L1) located between NBD1 and MSD2. Not all of the MRPs possess MSD0 domains. MRP4, MRP5, MRP8 and MRP9 lack the third membrane spanning domain (MSD0), but possess the L0 domains. MRP2, MRP3, MRP6, MRP7 resemble MRP1 with a TMD0 domain (Figure 10).

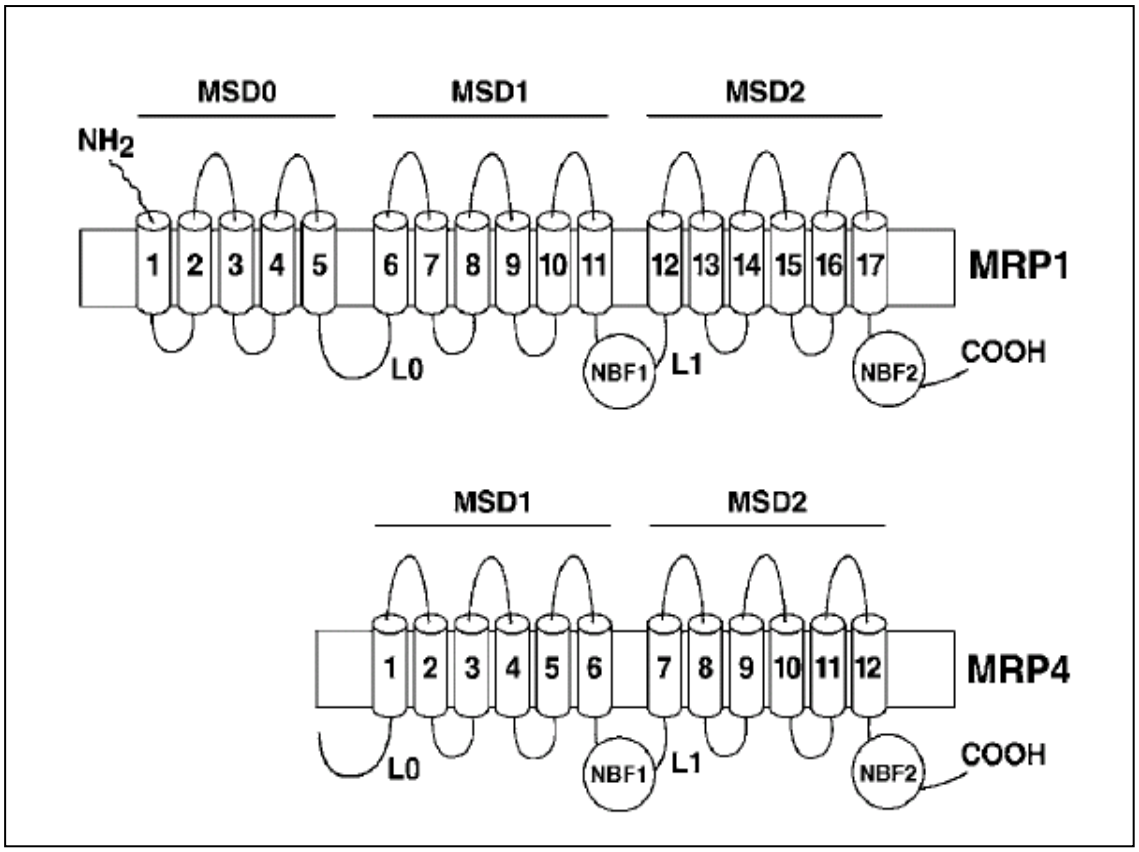

Figure 10: Topological model of MRP1 (similar to MRP2, MRP3, MRP6 and MRP7) and MRP4 (similar to MRP5, MRP8 and MRP9). NBF: nucleotide binding fold; MSD: membrane spanning domain (Reproduced with kind permission of Nature Publishing Group)

Cellular distibution and function

Unlike P-gp, MRP1 is mainly localised to the endoplasmic reticulum, but some monoclonal antibody studies have also demonstrated MRP on the plasma membrane [253].

Cells exhibiting MRP over-expression display resistance to a range of drugs similar to those excreted by P-gp, but may not have drug accumulation deficits as with P-gp mediated resistance. These drugs are generally either cationic or neutral and lipophilic. MRP expressing cells have reduced intracellular drug concentrations [254]. In addition to acting as a direct efflux pump, there is evidence that MRP packages drug within intracytoplasmic vesicles where the drugs are unable to act [255]. In non-P-gp MDR cells known to express MRP, drug has been shown to accumulate in a perinuclear localisation within the Golgi and lysosomes. This may represent a resistance

transport mechanism, where drug is transported away from the nucleus via the pre-lysosymal sorting compartment (PLC) to the outside of the cell [255]. MRP1 is one of the elusive glutathione-S-conjugate (GS-X) pumps, a transporter able to recognise and transport drugs conjugated to glutathione out of the cell [256] and also acts as a membrane bound ATP efflux pump ejecting hydrophobic drugs from the cell [257].

MRP1 appears to contribute to the inherent sensitivity of cancers in which it is expressed. However, there is no consensus with respect to its role in acquired resistance or its prognostic significance [251].

All of the characterised members of the MRP family are lipophilic anion pumps with the potential to confer resistance to anticancer drugs. Chemotherapeutic substrates transported by the MRP family of ABC transporters are shown in Table 9.

Name	Cytotoxic substrate
MRP1	Anthracyclines, cochicine, etoposide, heavy metals (arsenite, arsenate, antimonials), vincristine, vinblastine, paclitaxel
MRP2	Cisplatin, CPT-11, doxorubicin, etoposide, methotrexate, SN-38,vincristine, vinblastine
MRP3	Cisplatin, doxorubicin, etoposide, methotrexate, teniopside, vincristine
MRP4	Methotrexate, nucleotide analogs, PMEA
MRP5	Doxorubicin, methotrexate, nucleotide analogs, topotecan
MRP6	Doxorubicin, etoposide, teniposide
MRP7	Doxorubicin, vincristine, vinblastine, docetaxel, paclitaxel
MRP8	5'-Fluorouracil, 5'-fluoro-2'-deoxyuridine, 5'-fluoro-5'-deoxyuridine, PMEA
MRP9	Unknown

Table 9: Substrates of the multidrug resistance-associated protein (MRP) family of transporters

Breast Cancer Related Protein

Breast cancer resistance protein (BCRP) also known as mitoxantrone-resistance protein (MXR), was first described in a multi-drug resistant human breast cancer cell line which did not express Pgp or MRP [258]. Overexpression of BCRP is associated with high levels of resistance to a variety of anticancer agents, including mitoxantrone, anthracyclines, and the camptothecins, by enhancing drug efflux.

In normal tissues BCRP is thought to play an important role in drug disposition as it is prominently expressed in organs important for absorption (small intestine), distribution (placenta, blood-brain barrier), and elimination (liver and small intestine) of drugs.

BCRP overexpression has been detected in a variety of mitoxantrone-resistant cell lines, including those derived from human breast cancer (MCF-7), colon carcinoma (S1), gastric carcinoma (EPG85–257), and fibrosarcoma (EPF86–079). The expression of BCRP and/or mRNA has been detected in numerous types of human cancers, including haematological malignancies and solid tumours. BCRP expression was analysed in 150 untreated human solid tumours comprising 21 tumour types using a monoclonal antibody BXP-21. Moderate or strong expression of BCRP was seen in ~ 60% of the tumour samples examined [259]. BCRP expression was observed in all tumour types but was more frequently expressed in gastric carcinoma, hepatocellular carcinoma, endometrial carcinoma, colonic carcinoma, small cell lung carcinoma and malignant melanoma [259]. These results implicate BCRP as a mechanism of MDR in certain solid tumours.

BCRP expression in tumour samples from 42 patients with colorectal carcinoma, showed that BCRP mRNA expression in hepatic metastases after irinotecan-based chemotherapy were higher than those in irinotecan-naïve metastases. This suggests that upregulation of BCRP may be involved in the development of resistance to irinotecan in patients with colonic carcinoma [260].

Gene coding and product

Multidrug resistant human breast cancer cell lines expressing BCRP were found to overexpress a 2.4kb mRNA species by Northern blot analysis. This PCR product was radiolabelled and used as a probe to isolate a full length

cDNA from a lambda phage library derived from the same cell line [258]. The full length cDNA coded for a novel 655 amino-acid polypeptide with properties of a half-transporter, characteristic for members of the ABCG subfamily. The BRCP gene has subsequently been localised to locus 22 on chromosome 4, downstream from a TATA-less promoter [261].

Structure

BCRP is a 72 KDa half-transporter, consisting of a single nucleotide binding domain (NBD) and ABC signature motif within a relatively hydrophilic amino-terminal domain, and a relatively hydrophobic carboxyl-terminal domain containing a membrane spanning domain (MSD) with six putative transmembrane domains and four potential N-glycosylation sites (Figure 11) [258]. The BCRP sequences are similar to one-half of the Pgp or MRP1 molecule, except that in BCRP the nucleotide binding domain precedes the transmembrane domain (Figure 12). Current experimental evidence suggests BCRP may function as a homodimer or homotetramer.

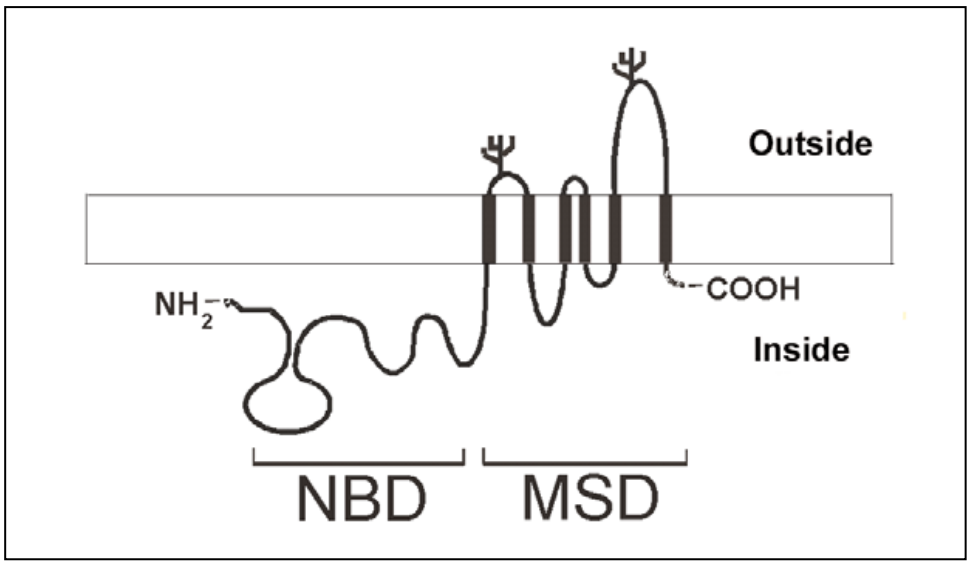

Figure 11: A membrane topology model of BCRP

Pgp / MRP1:	NH_2 – TMDs – NBD1 – TMDs – NBD2 – COOH
BCRP:	NH_2 – NBD – TMDs – COOH

Figure 12: Comparison of ABC transporter molecular configuration. TMD = Transmembrane domain; NBD = Nucleotide binding domain

Cellular distribution and function

BCRP has been localised to plasma membrane of drug-resistance cells overexpressing this transporter [262,263]. Recent evidence suggests that BCRP functions as a homodimer bridged by disulfide bonds. The fact that BCRP transfection directly confers MDR status suggests that BCRP is able to function by homodimerisation [258]. Co-transfection of BCRP with a mutant form of BCRP with an L554P alteration in the fifth transmembrane domain was found to partially inhibit BCRP function, again suggesting BCRP functions as a homodimer. Western blot protein analysis coupled with polyclonal antibodies directed against peptide epitopes of BCRP, after denaturation or treatment with cross-linking agents demonstrated a molecular mass shift from a 72KDa band to a 180KDa band, again suggesting the functional configuration of BCRP is through homodimerisation.

BCRP is a 72KDa member of the ABC superfamily of transporters which confers resistance to mitoxantrone, doxorubicin and daunorubicin, reduces daunorubicin accumulation and retention, and enhances efflux of rhodamine 123 in an ATP dependent fashion [258]. Most of the drug-selected cell lines exhibiting BCRP overexpression display strong resistance to mitoxantrone, suggesting that mitoxantrone is a high affinity substrate for BCRP [264]. Transport of anthracyclines is variable and appears to depend on the amino acid at position 482 in the BCRP molecule. If this amino acid is Threonine or Glycine then resistance to anthracyclines if conferred, but if it is an Arginine then anthracycline resistance is not conferred.

Chemotherapeutic substrates transported by BCRP are shown in Table 10.

Drug
Anthracyclines*
Daunorubicin
Doxorubicin
Epirubicin
Anthracenes
Mitoxantrone
Bisantrene
Aza-athrapyrazole (BBR 3390)
Camptothecin Derivatives
Topotecan
SN-38
9-amino-captothecin
Irinotecan
Diflomotecan
Polyglutamates*
Methotrexate
Methotrexate-Glu_2
Methotrexate-Glu_3

Table 10: Substrates of breast cancer resistance protein (BCRP) (*Transport of these substrates depends on the BCRP amino acid at position 482)

Lung resistance-related Protein (LRP) and vaults:

Lung resistance protein (LRP) was first described in 1993 in a non-small cell lung cancer non-P-gp MDR cell line [265]. LRP is widely expressed in normal tissues such as bronchial cells, intestinal epithelium, renal tubular cells, keratinocytes, adrenal gland and macrophages. All of these cells have an excretory or secretory function and are chronically exposed to xenobiotics and potentially toxic agents, suggesting that in normal cells LRP expression may play a protective role against toxic compounds.

LRP is overexpressed in several non-Pgp MDR cells lines of different histogenetic origin [265]. In a panel of 61 human cancer cell lines LRP and MRP were expressed in 78% and 87%, compared to just 24% for P-gp [266]. Of 174 clinical tumour specimens from 27 different tumour types, LRP was expressed in 63% [267]. LRP expression was found to be the greatest individual marker of *in vitro* resistance to a variety of MDR related drugs. LRP has also been identified as the human major vault protein [268-270].

Gene coding and product

The LRP gene is found on the short arm of chromosome 16, the same chromosome as the gene for MRP, which is located just next door. It codes for a 110KDa unglycosylated protein which is 896 amino acids long. Analysis of the LRP protein sequence has revealed that it is the human major vault protein (MVP) which forms the major component of vaults [268-270]. Most MDR cell lines expressing LRP also express MRP [253,266]. However most P-gp MDR cell lines are LRP negative [265].

Vaults

Vaults are barrel-like cytoplasmic ribonucleoprotein organelles which are probably associated with vesicles.

They are ovoid structures with dimensions of approximately 35 x 65nm and resemble a barrel with lobular walls and two centres of mass (Figure 13) [268,269]. This barrel structure can be split apart *in vitro*, and each half opens into a flower-like structure with eight petals surrounding a central ring [269]. Electron micrographs of vault particles at a resolution of 31 – 32 Å, have shown that the barrel structure is thin walled, solid structure which is hollow and has two protruding caps and an invaginated waist (Figure 13) [271].

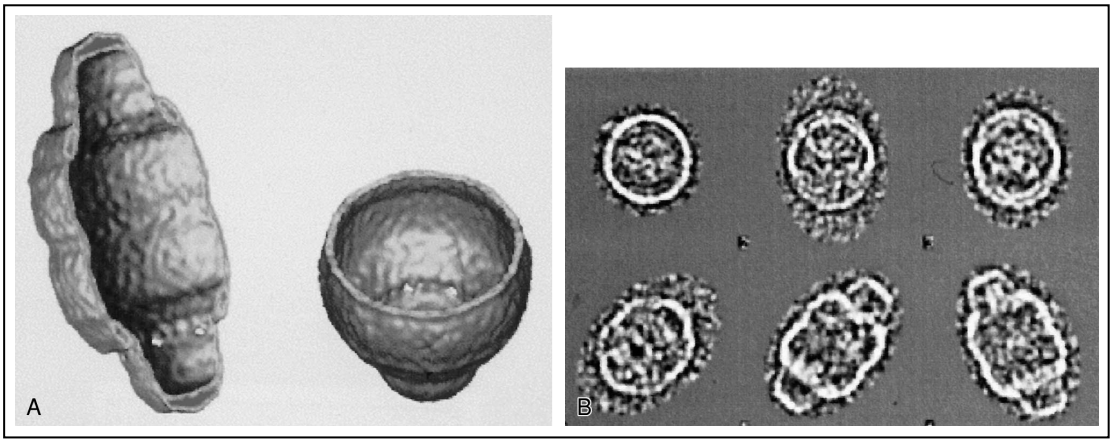

Figure 13: A: Three-dimensional reconstruction of rat vault structure from cryoelectron microscopy image at approximately 31 Å resolution B: Electron microscopy of negatively stained rat vaults (Reproduced with kind permission of Cambridge University Press)

Vaults have a mass of 13MDa and are the largest known ribonucleoprotein complexes. They are composed of multiple copies of three proteins, 240, 193 and 104KDa in size and small untranslated RNA molecules of 88 – 141 bases (Table 11).

Component	Name	Size	Copies per vault
Proteins			
Major Vault (Barrel protein)	MVP (LRP)	~ 104KDa	96
Minor Vault (Cap proteins)	p240 (TEP1)	~ 240KDa	2
	p193 (VPARP)	~ 193KDa	8
RNAs			
Vault RNA	hvg1	98 bases	Unknown
	hvg2	88 bases	Unknown
	hvg3	88 bases	Unknown
	hvg4	101 bases	Unknown

Table 11: Mammalian vault components

The 104KDa subunit (LRP) is termed the major vault protein, as it contributes more than 70% of the vaults mass. Two high molecular weight minor vault proteins have also been identified [272,273]. The p240 protein is identical to the telomerase-associated protein (TEP1) [273]. TEP1 is also present in the telomerase complex, another ribonucleoprotein complex, which helps to maintain the length of chromosomal telomeres in dividing cells [274].
The other high molecular weight minor vault protein, p193, is a poly (ADP-ribose) polymerase (PARP), called vault-PARP (VPARP) [272]. This protein ADP-ribosylates itself and the MVP in purified rat vaults. Proteins with PARP activity may play a role in differentiation, proliferation, tumour transformation and repair of damaged DNA [275-278].
Four species of vault RNA (vRNA) have been identified (hvg 1 – 4). The vRNA contributes less than 5% of the vault mass and exhibits species-specific length variation ranging from 88 – 141 bases. The vRNAs are not structural components of the vaults, but are likely to function in RNA-RNA recognition in

association with other cellular RNAs or proteins with the vault to facilitate localisation and / or transport.

Cellular distribution and function:

Vaults are present in high numbers, 10,000 – 100,000 copies per cell [279]. Most vaults appear to be located in the cell cytoplasm, as demonstrated by immunohistochemical staining with a monoclonal antibody to LRP (LRP-56) which demonstrated a coarsely granular, cytoplasmic distribution suggesting an association with cytoplasmic vesicles or lysosomal structures [265]. Vaults have also been shown to specifically associate with the nuclear membrane in tissue sections and with NPC's of isolated nuclei [280]. In mammalian cells, generally not more than 5% of the total vault fraction is found associated with the nucleus.

The cellular function of vaults has not been elucidated. Several studies have implicated vaults in nucleocytoplasmic trafficking and transport [281-284]. The hollow vault structure is consistent with a role in either compartmentalisation of macromolecular assemblies or in subcellular transport. The partial co-localisation of vaults with cytoskeletal elements has led to the hypothesis that vaults can be transported along cytoskeletal elements, in particular microtubules. Cytoskeletal-mediated transport would certainly allow vaults to shuttle cargo directionally to specific subcellular locations.

It has been postulated that vaults may control the bidirectional transport of a variety of substrates between the nucleus and cytoplasm [280]. Vault induced drug resistance may therefore be conferred through vesicular sequestration or nucleocytoplasmic transport of drugs [285].

There is some direct evidence that vaults play a role in nuclear efflux of anthracyclines from the nuclei of resistant cells [286-288]. A colorectal cancer cell line was treated with sodium butyrate which induced overexpression of MVP making the cells significantly less sensitive to doxorubicin, etoposide (VP-16), vincristine, paclitaxel and gramicidin D. Doxorubicin was shown to be effluxed from the nuclei of resistance cells more rapidly and was inhibited by anti-(MVP) antibodies and PAK-104P, a pyridine analogue specific inhibitor of vault-mediated drug efflux [287].

The minor vault proteins, TEP1 and VPARP, mass also play a role in protection of the genome contributing to drug resistance.
The proposed mechanisms of vault mediated MDR are shown in Figure 14.

Atypical MDR: Topoisomerase II mediated drug resistance

In the 1980s, a new form of non-P-gp related MDR was described in a leukaemia cell line that was found to have alterations in Topoisomerase II (TOPO II), a DNA repair enzyme [289]. Cell lines which exhibit drug resistance due to altered TOPO II are called at-MDR (altered TOPO II activity or atypical MDR). This type of MDR results in no alteration of drug accumulation, but is characterised by cross-resistance to anthracyclines and epipodophyllotoxins, but not vinca alkaloids.

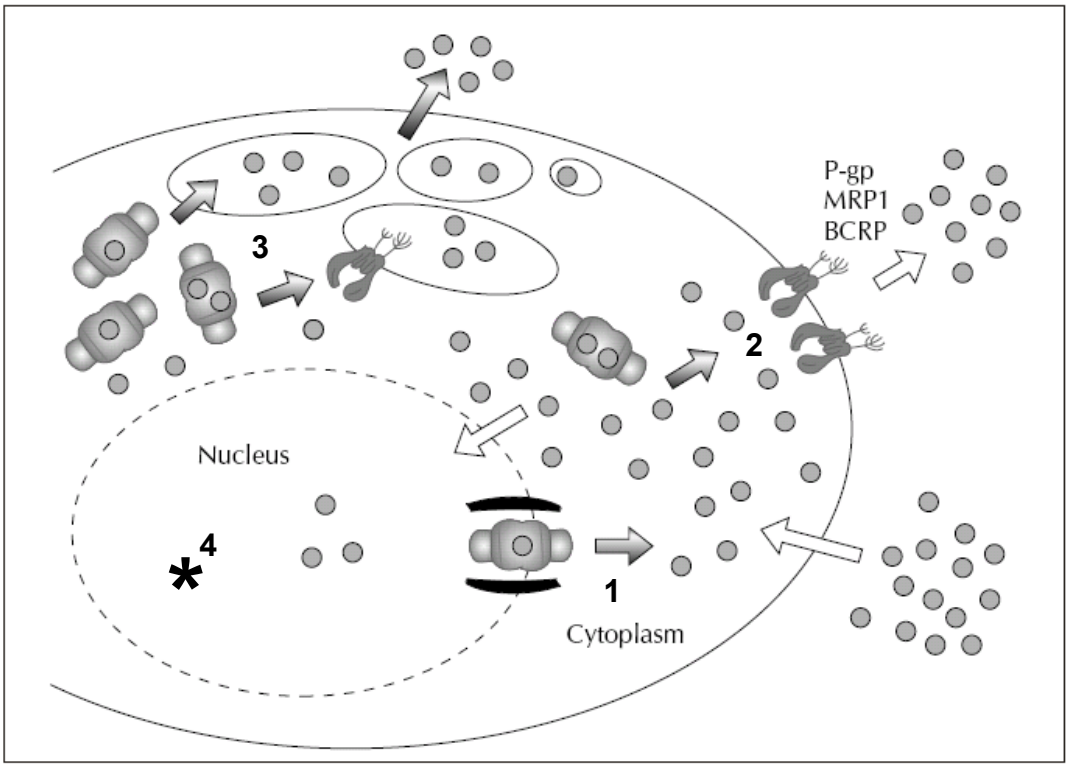

Figure 14: Hypothetical mechanisms of vault mediated multidrug resistance. Vaults may mediate multidrug resistance by transporting drugs away from their intracellular targets e.g. the nucleus (**1**) or by transporting them to efflux pumps (**2**) or exocytotic vesicles (**3**). Based on the characteristic of the minor vault proteins, vaults or vault components are possibly involved in DNA damage control (**4**). (Figure reproduced with kind permission of Lippincott Williams & Wilkins, Inc.)

Other at-MDR cell lines have also demonstrated this alteration in drug-induced DNA cleavable complex formation associated with reduced levels and activity of TOPO II.

Alterations in TOPO II drug activity are divided into two groups:

(1) Quantitative changes: e.g. decreased levels of TOPO II protein by downregulation of transcription, increased degradation or deletion of one allele; or (2) Qualitative changes: e.g. mutations resulting in altered drug-DNA-protein interaction or ATP binding, alterations in the ratio of isoenzymes, or altered enzymatic function by post-translational modification [289,290].

Most at-MDR cell lines have been selected by epipodophyllotoxin exposure, but at-MDR is also common in anthracycline selected cell lines. Most of these cell lines exhibit more than one mechanism of MDR. Thus, nuclear extracts from anthracycline-resistant PGP-positive murine P388 and Ehrlich ascites tumour cell lines demonstrated reduced amounts of TOPO II. [291,292].

Decreased levels of TOPO II have also been demonstrated in a DOX-resistant CHO cell line, despite unchanged DNA and mRNA content, suggesting that post-transcriptional events might lead to decreased enzyme levels [291].

Modulators of classical P-gp mediated MDR, such as verapamil, are unable to modify at-MDR. Other strategies may be effective in at-MDR, the most obvious being the use of non-TOPO II substrates. Some anthracycline analogs demonstrate equal cytotoxicity in at-MDR and drug-sensitive cells.

The efficacy of TOPO II inhibitors is dependent on the proliferation status of the cells. Hence manipulation of cellular proliferation could alter sensitivity to TOPO II inhibitors.

There is a lack of data correlating at-MDR status to clinical cancer chemoresistance and outcomes of therapy.

Glutethione-S-Transferases (GST)

Glutathione-S-Transferases (GSTs) are a family of phase II detoxification enzymes that catalyse the conjugation of glutathione (GSH) to a wide variety of endogenous and exogenous electrophilic compounds, rendering them inactive. GSTs are divided into two super-family members: the membrane-bound microsomal and cytosolic family members. Microsomal GSTs are involved in endogenous metabolism of leukotrienes and prostaglandins.

Human cytosolic GSTs are divided into 6 classes: α, μ, ω, π, θ, ζ. The π and μ classes of GSTs play a regulatory role in the mitogen-activated protein (MAP) kinase pathway that participates in cellular survival and death signals. GSTs have been implicated as a mechanism of multidrug resistance. It is possible that they do this through two pathways, either by direct detoxification or as an inhibitor of the MAP kinase pathway. They also possess intrinsic peroxidase activity leading to elimination of free-radicals induced by certain cytotoxic drugs [293].

A 45-fold increase in GST levels was initially described in a MDR subline of the MCF-7 (breast cancer cell line) [294], suggesting a role in MDR. High levels of GSTs have since been reported in many different tumour types [294]. A list of anticancer agents that have been shown to be subject to GST mediated multidrug resistance are shown in table 12.

Substrates of GST:
Chlorambucil Melphalan Nitrogen Mustard Phosphoramide mustard Acrolein Carmustine Hydroxyalkenals Ethacrynic acid Steroids
Not characterised as GST substrates:
Antimetabolites* Antimicrotubule drugs* Topoisomerase I & II inhibitors* Bleomycin Hepsulfam Mitomycin C* Doxorubicin* Cisplatin* Carboplatin

Table 12: Anticancer agents associated with resistance secondary to increased GST expression
* Require MAP kinase activation for cytotoxicity

Some of these are direct substrates of GSTs that are inactivated by catalytic conjugation to glutathione through thioether bond formation. Many others are metabolised to electrophilic species that are detoxified through glutathione metabolism or alternatively exert their apoptotic effects through the MAP kinase pathway, which is inhibited by elevated levels of GST.
In addition glutathione conjugates are effluxed by a 38KDa membrane protein, which has been implicated in efflux of cytotoxic drugs including daunomycin and daunorubicin [295]. Glutathione is also required specifically by MRP for the export of drugs from cells, suggesting a role in cytotoxic drug efflux [296].

Reversal of multidrug resistance

Multidrug resistance is one of the most important reasons for chemotherapeutic failure. There has been an extensive research effort in this area over the last 30 years or so, to find ways of reversing or inactivating the causes of multidrug resistance.

P-gp is widely recognised as the main mechanism of multidrug resistance. Much research has been done focusing on molecules that can inactivate this drug efflux pump, rendering MDR cells sensitive to chemotherapy. Research into the inactivation of the other MDR-related ABC transporter pumps, MRP and BCRP, has also been performed.

Many drugs have now been identified that can reverse MDR, making cells sensitive to chemotherapy again, so-called chemosensitisers. Some of these drugs are effective against one transporter, whilst others exert their effects at more than one site (Table 13).

Verapamil (a calcium channel antagonist) was the first reported chemosensitiser, restoring sensitivity to alkaloids and doxorubicin in MDR cells [297-299].

The mechanisms of MDR inactivation by each drug are different. Verapamil and Cyclosporin A inhibit resistance by functioning as competitive substrates of P-gp, which is thought to be through competition for the drug binding sites on P-gp.

The majority of these MDR reversing agents are unrelated, but share some structural similarities such a hydrophobicity and phenyl rings [300] and often have side chains containing a tertiary amine [301].

The first generation chemosensitizers were hampered by high levels of toxicity at resistance-inhibiting doses coupled with lower MDR reversing capabilities. Second generation chemosensitizers that have been developed specifically for their chemosensitizing effects have much lower toxicity, are more potent and have fewer drug interactions.

Most of the chemosensitizers act by binding with the TMD regions of the transporter molecules. Some newer chemosensitizers, e.g. steroid and flavanoid, inhibit the transporter molecules by binding to the NBD regions. The binding site of steroid on the NBD is near but not directly on the ATP binding site [302]. The flavanoids appear to bind to both the steroid binding

site and the ATP binding site [303]. It is believed that flavanoid chemosensitizers have a significant advantage with respect to their therapeutic index.

Name	Year	Chemosensitizer
Pgp	**2004**	**Benzyl-, phenethyl-, and alpha-naphthyl isothiocyanates***, diallyl sulfide, PK11195, small scFv recombinant, Pgp antibody fragment
	2003	Amooranin, etrandrine, fangchinoline, ginsenoside Rg(3), KR30031, methylenedioxyethylamphetamine, protopanaxatriol ginsenosides, saquinavir, siRNA of mdr1 gene, **tRA 98006**
	2002	3,5-dibenzoyl-1,4-dihydropyridines, PKC412, pyronaridine, sinensetin
	2001	**Agosterol A**, haloperidol and dihydrohaloperidol, SB203580, tropane alkaloid esters, SNF4435C and D, tea polyphenol, trans-N,N'-bis(3,4-dimethoxybenzyl)-N-solanesyl-1,2-diaminocyclo hexane (N-5228)
	2000	Astemizole, atorvastatin, 7-O-benzoylpyripyropene A, **5-O-benzoylated taxinine k,** clarithromycin and YM17K (3,4'-dideoxy mycaminosyl tylonolide hydrochloride), cyclopamine and tomatidine, 3,5-diacetyl-1,4-dihydropyridines, 7, 8-dihydroxy-3-benzazepine, **doxorubicin-gallium-transferrin conjugate**, macrolide antibiotics (josamycin, tamolarizine), nelfinavir, norverapamil, ontogen (ONT-093, formerly OC-144-093), R101933, taxuspine C, 2'-desacetoxyaustrospicatine and 2-desacetoxytaxinine, **V-104**
	1999	D-alpha-tocopheryl polyethylene glycol 1000 succinate, anti-MDR1 ribozymes, AR-2, carvedilol, **erythromycin**, ketoconazole, kopsiflorine, nomegestrol, PAK-200S, **pluronic block copolymer**, reversin, ritonarvir, rosemary extract, TTD, XR9576(2)
	1998	Ardeemins, AV200, 5-O-benzoylated taxuspine C, bromocriptine, **dipyridamole**, droloxifene, **imidazothiazole derivatives (N276-12, N276-14, N276-17)**, oxalyl bis(N-phenyl)hydroxamic acid, tetrandine and fangchinoline, tiamulin, XR9051
	1997	**Biricodar (VX-710; Incel)**, cyproheptadine
	1996	CL 329,753, indole-3-carbinol, **itraconazole**, LY335979, medroxyprogesterone, mefloquine, **mifepristone (RU-486)**, reserpine
	1995	Azelastine and flezelastine, B9209-005, dexniguldipine (B8509-035), dexverapamil, epidermal growth factor (EGF), insulin-like growth factor I (IGF-I), quercetin
	1994	**MS-209**, pentoxifylline, Ro11-2933 (DMDP), **RU486**
	1993	Dilantin, **GF120918**, meperidine, pentazocine, and methadone, Pgp monoclonal antibodies and antisense oligonucleotide, tamoxifen and toremifene
	1992	Staurosporine and NA-382
	1991	Biperidil, SDZ PSC 833
	1990	Cremophor EL
	1989	Cefoperazone, cetriaxone, phenothiazine, YM534
	1987	Diltiazem, cyclosporine A
	1986	Amiodarone
	1984	**Quinidine**
	1981	Verapamil
MRP	**2004**	**benzyl-, phenethyl-, and alpha-naphthyl isothiocyanates**
	2003	**tRA 98006**
	2001	**Agosterol A**
	2000	**5-O-benzoylated taxinine k**, 4-deacetoxyagosterol A, **doxorubicin-gallium-transferrin conjugate**, **V-104**, **pluronic block copolymer**, quinoline-based drugs (chloroquine, quinine, **quinidine**, and primaquine),
	1999	**dipyridamole**, **erythromycin and** ofloxacin, **mifepristone (RU-486)**, **MS-209**, rifampicin
	1998	**Biricodar (VX-710; Incel)**, **imidazothiazole derivatives (N276-12, N276-14, N276-17)**, NSAIDs (indomethacin, sulindac, tolmetin, acemetacin, zomepirac and mefenamic acid), ONO-1078, quercetin
	1997	Indomethacin, probenecid
	1996	Acrolein and chloroacetaldehyde, d,l-buthionine-(S,R)-sulfoximine, **itraconazol**, PAK-104P
	1995	Difloxacin, MK571
BCRP	**2004**	Chrysin and biochanin A, genistein and naligenin, Imatinib mesylate (Gleevec, STI571)
	2003	Estrone, diethylstilbestrol and TAG-139, **tRA 98006**
	2002	Ko143
	1999	**GF120918**
	1998	fumitremorgin C

Table 13: Chemosensitizers inhibiting P-gp, MRP and BCRP. *Boldface compounds indicate chemosensitizers inhibiting more than two transporters [304]

1.4: Bladder cancer and multidrug resistance

As with most MDR research, much of our understanding about the mechanisms of MDR involved in bladder cancer is derived from work using cancer cell lines rather than clinical tumour specimens. Cancer cell lines offer the advantages of being readily available, more easily cultured and of single cell type, allowing experiments to be repeated to ensure that results are reliable. They are useful to study certain facets of cancer cell biology and drug resistance, but may not provide a true representation of the multiclonal cancers they aim to model.

Clinical tumour samples by comparison are less user friendly, being difficult to obtain, of variable quality, requiring lengthy processing, having variability in cell populations and also finite viability. However, they do provide an accurate reflection of the tumour biology of "in vivo" cancers. Recent advances in molecular biological techniques have aided the study of MDR mechanisms in clinical tumour material.

Studies of MDR mechanisms in bladder cancer cell lines

In 1979, an *in vitro* assay allowing assessment of the sensitivities of several bladder cancer cell lines (MGH-U1, MGH-U2 and RT4) to cytotoxic drugs was described [305].

In 1985, another group reported testing a urothelial cancer cell line, RT-112, against a panel of twelve cytotoxic agents. The RT-112 cells were particularly susceptible to methotrexate, mitoxantrone, doxorubicin, mitomycin C and cisplatin, leading this group to suggest that such cytotoxicity assays could form the basis of a clinical tumour sensitivity assay [306].

Using the wild-type T24 bladder cancer cell line, another group demonstrated that the cytotoxic effects of doxorubicin and thiotepa were improved when combined with verapamil, despite verapamil having no independent cytotoxicity. This was the first reported use of verapamil as a chemosensitizer in bladder cancer cells, although it was suggested that verapamil exerted its effects through the "intracellular calcium environment", with no mention of MDR or P-glycoprotein mediated effects [307].

In 1988, McGovern *et al* established a doxorubicin resistant human bladder cancer cell line, MGH-U1R, by growing MGH-U1 (a subculture of T24) wild-type cells in increasing concentrations of the doxorubicin [308]. This group

also showed that reversal of doxorubicin resistance could be achieved by exposure to verapamil [309].

In 1990, Floyd *et al* confirmed the multidrug-resistant nature of the MGH-U1R cell line. Compared to MGH-U1, it was found to be 40 times more resistant to doxorubicin, 188 times more resistant to vinblastine and 13 times more resistant to etoposide, whilst remaining sensitive to bleomycin. They also reported that the observed multidrug resistance of MGH-U1R cells was due to overexpression of the MDR-1 gene [310]. In 1994, the MGH-U1R cell line was also shown to be resistant to epirubicin [311].

Several other doxorubicin resistant bladder cell lines have subsequently been established. Cell line KK47/ADM was established in 1992 [312] exhibiting cross-resistance to epirubicin, vinca alkaloids and etoposide, but not to cisplatin, carboplatin or mitomycin C. Cell line RT112/D21 was established in 1995 [313] and demonstrated cross-resistance to epirubicin and vinblastine. Sensitivity to methotrexate and mitomycin C were unchanged. Cell line BIU-87/ADMR was established in 1997 [314] and showed cross-resistance to epirubicin, daunorubicin, vincristine and etoposide, but not to cisplatin and mitomycin C. All of these cells lines demonstrated reversal of MDR following exposure to verapamil. Two of these cell lines were tested for P-gp expression with 70 – 75% of cells staining positive with monoclonal antibodies directed against P-gp [312,314].

In 1995, Hasegawa *et al* examined the expression of MDR-1, MRP and topoisomerase II in three doxorubicin resistant and one vincristine resistant bladder cancer cell lines which they had established. They demonstrated a concomitant induction of increased levels of MRP mRNA, decreased levels of topoisomerase II mRNA and decreased drug accumulation with variable MDR-1 expression within these MDR cell lines, suggesting that MDR is a multifactorial process [248].

Also in 1995, Naito *et al*, reported a doxourubicin resistant cell line without overexpression of MDR-1, which demonstrated decreased cellular levels of DNA Topo II, suggesting that *at*-MDR may also play a role in bladder cancer MDR [315].

Kim *et al,* reported further non-P-gp expressing MDR cell lines which appeared to achieve resistance status by a combination of overexpression of

MRP, reduced topo II activity, increased glutathione levels and glutathione-S-transferase activity [316].

Studies of MDR mechanisms in bladder cancer clinical tumour specimens

In 1993 Thomas *et al* published an immunohistochemical study of the expression of glutathione-S-transferase π in normal urothelium, 23 superficial bladder tumours and 26 invasive tumours (these invasive tumours had all received platinum-based chemotherapy). Cytoplasmic GSTπ staining was demonstrated in all specimens. Nuclear staining was seen in one superficial tumour and in 13/26 invasive tumours (p=0.003), although there was no association between nuclear staining and response to systemic chemotherapy in those patients with invasive disease. A possible association between GSTπ expression and disease progression was proposed [317].

In 1994, Park *et al* evaluated the expression of Pgp in 29 cystectomy specimens (from patients with no previous chemotherapeutic drug exposure) and bladder biopsies taken from 9 patients before treatment with intravesical doxorubicin and again at the time of recurrence. Pgp was expressed in 75% of the cystectomy specimens. There was no correlation between the level of P-gp expression and tumour pathological grade, stage or morphology.

Of the small series of superficial tumours examined (n = 9), five developed recurrences following intravesical doxorubicin and four remained recurrence free during follow up (15 – 60 months). Of the recurrent group, four had tumours that expressed P-gp before exposure to intravesical chemotherapy, whilst all five recurrences were P-gp positive. Of those with no recurrence, three tumours were P-gp positive before exposure to chemotherapy. The presence of P-gp overexpression in tumour cells before exposure to chemotherapy did not predict tumour sensitivity or recurrence in this series. They concluded that a significant proportion of bladder cancers exhibit P-gp overexpression without prior exposure to chemotherapeutic agents, and that the incidence of intrinsic MDR (as opposed to acquired) in bladder tumours was likely to be high [318].

In the same year, Petrylak *et al*, looked at P-gp expression in pre- and post-chemotherapy, primary and metastatic tumour tissue samples from patients

with TCCs treated with M-VAC (methotrexate, vinblastine, adriamycin and cisplatin). Untreated primary lesions were positive for P-gp in 13% compared to 38% post chemotherapy. None of the untreated metastases were positive, but 55% of the post-therapy specimens showed various degrees of P-gp positivity (p=0.002). The group with the highest percentage of cells staining positive for Pgp were those who had received 6 or more cycles of chemotherapy. They concluded that exposure to combination chemotherapy increased the proportion of cells exhibiting Pgp positivity [319].

In 1996, Pu *et al*, examined the expression of the MDR-1 gene in 14 bladder cancer cell lines (10 sensitive and 4 MDR) and in tumour/normal urothelium pairs from 88 patients, using reverse transcriptase-polymerase chain reaction (RT-PCR) and Southern blotting. They also assessed functional P-gp activity using a flow cytometric rhodamine-123 retention and efflux technique, an established P-gp model. They then examined the relationship between MDR-1 expression and response to systemic (n = 28) or intravesical (n = 60) chemotherapy. None of the 60 patients in the intravesical group, and only 5 in the systemic group had received prior intravesical chemotherapy.

Of the ten wild-type cell lines only two were MDR-1 positive, and only one exhibited functioning P-gp. In contrast, all four MDR lines had positive MDR-1 status and the two MDR lines that were produced by doxorubicin exposure also had functioning P-gp.

Of the 88 normal mucosa/tumour pairs, all 88 mucosal samples and 62 (75%) of the tumour samples expressed the MDR-1 gene. There appeared to be no correlation between MDR-1 positivity and subsequent response to chemotherapy (either systemic or intravesical) [320].

Expression of the MRP gene has been implicated in non-P-glycoprotein mediated MDR. In 1996, Clifford *et al* examined MRP and MDR-1 mRNA expression, using a sensitive RT-PCR-based technique, in a series of previously untreated TCCs (n = 24) and normal bladder samples (n = 5). MRP mRNA was detected in all samples analysed, but demonstrated up to 190-fold variation between tumour samples. Their results showed that MRP mRNA levels were significantly reduced in a higher proportion of high-grade (G3) bladder tumours (55%, 6/11) when compared to low- and moderate-grade (G1/2) bladder tumours (8%, 1/13) (P=0.018), suggesting that MRP

mRNA levels may be reduced as a result of tumour progression to advanced, poorly differentiated disease. There was no relationship between MRP mRNA levels and recurrence or progression risk, and no association with chemotherapy response. There was no correlation between MRP and MDR1 mRNA expression, suggesting that these two genes do not share common regulation or expression mechanisms [250].

Also in 1996, Kim *et al* examined the expression of the MDR-1, MRP, GSTπ and topo II genes in 44 patients with urothelial cancers, 14 of whom had received prior chemotherapy. Using a RT-PCR assay they examined 52 tumours samples and three normal urothelial samples and demonstrated that the mean expressions of MRP and GSTπ were higher than those for MDR-1 and topo II, and that the level of MRP expression correlated significantly with that of MDR-1 and GSTπ. They were unable to demonstrate any significant influence of chemotherapy on the induction of expression of MDR-1 or MRP, but established that the expression of GSTπ was significantly higher in those who did not receive chemotherapy. They concluded that the intrinsic and acquired resistance exhibited by urothelial cancers resulted from a multifactorial mechanism, and suggested that MRP and GSTπ expression activation occurred during tumorigenesis [321].

In 1996, Gan *et al*, looked at biological factors affecting doxorubicin sensitivity using primary cultures from seven superficial (Ta and T1) and nine invasive (T2 – T4) human bladder tumours. Firstly, they determined the sensitivities of each of these tumours, with IC50 values for the superficial tumours ranging from 0.14 to 5.2 micrometer and for the invasive tumours ranging from 1.4 to >100 micrometer. The difference in doxorubicin sensitivity between superficial and invasive tumours was more than 700-fold. Using previously acquired concentration-depth profiles (pharmacokinetic data predicting doxorubicin penetrance into normal bladder tissue) they compared predicted tissue concentrations with the IC50 and IC90 values of the tumour specimens. They predicted that the IC50 would be reached in all Ta tumours, 67 – 100% of T1 tumours, but only one out of nine invasive tumours. The IC90 was achieved in all Ta tumours, but none of the other tumours.

They then examined the relationship of chemosensitivity with pathological tumour variables and with expression of p-glycoprotein (P-gp) and p53 protein. The invasive, high-grade, highly proliferative, p53- and P-gp-positive tumours were more resistant than the superficial, lower-grade, p53- and P-gp-negative tumours. None of the tumours expressed bcl-2.
They concluded that the variability in response rates of superficial bladder cancer to intravesical doxorubicin therapy were due to a 35-fold variability in tumour sensitivity and, to a lesser extent, a 4-fold variability in tissue pharmacokinetics. The invasive tumours were less responsive to intravesical doxorubicin due to inadequate tissue concentrations in the deeper muscle layers and reduced sensitivity of more aggressive tumours. The most significant predictors of doxorubicin sensitivity appeared to be p53 expression and high stage, with P-gp expression being the least important factor in this study [322].
In 1997, Nakagawa *et al*, examined the prognostic significance of multi-drug resistance associated protein and P-glycoprotein in patients with bladder cancer. The expression of MRP and P-gp were investigated immunohistochemically using monoclonal antibodies, before and after chemotherapy. The correlation between expression of these MDR proteins and clinical outcome (tumour recurrence rate, cystectomy rate and 5-year survival rate) were assessed in 33 patients. MRP was expressed in 1 of 28 patients (4%) and P-gp was expressed in 22 of 33 (67%) of patients before chemotherapy. MRP expression was induced by chemotherapy in 6 of 28 patients (21%) compared to P-gp induction in 4 patients (14%). MRP induction appeared to be dose dependent, being more frequent in patient receiving high dose (more than 300mg) than low dose (less than 300mg) anthracyclines ($p < 0.01$). Co-expression of MRP and Pgp occurred in 5 of 28 patients (18%) post-chemotherapy. They concluded that MRP and P-gp expression can be induced by chemotherapy for bladder tumours, but that the presence of P-gp expression pre-chemotherapy did not predict their clinical outcome.
In 2001, Chen Z et al studied the expression MRP, P-gp, P53 and Bcl-2 proteins in 40 specimens of bladder transitional cell carcinoma. The overall expression rates for MRP, P-gp, P53 and Bcl-2 were 52.5%, 57.5%, 47.5%

and 62.5% respectively. When analysed by grade the positive rate of MRP, Pgp, P53 and Bcl-2 were 46.3%, 38.5%, 38.5%, 23.1% for grade I tumours, 52.9%, 39.8%, 47.1%, 76.4% for grade II tumours and 60.0%, 80.0%, 60.0%, 90.0% for grade III of tumours, respectively. In 24 primary tumour specimens the expression rates for MRP, P-gp, P53 and Bcl-2 were 37.5%, 41.7%, 33.3%, 45.8% compared to 75.0%, 81.3%, 68.8%, and 87.5% in 16 recurrent cases following chemotherapy. They concluded that the rates of MRP, P-gp, P53 and Bcl-2 expression increased with higher tumour grade and were also significantly increased in recurrent cases following chemotherapeutic exposure ($p < 0.05$), suggesting that these proteins play a role in chemotherapy failure [323].

In 2002, Tada Y *et al*, examined the relationship between MDR1, MRP1, MRP2 and MRP3 expression and clinical outcome and response to doxorubicin chemotherapy in 47 clinical bladder cancer samples. MDR protein expression was assessed using a combination of quantitative RT-PCR analysis and immunohistochemical staining using monoclonal antibodies to MDR1, MRP1, MRP2 and MRP3. The chemosensitivity of bladder tumour samples to doxorubicin was determined using the *in vitro* succinate dehydrogenase inhibition test. They confirmed a significant correlation of MDR1, MRP1 and MRP3 mRNA levels with resistance to doxorubicin and demonstrated that expression of MDR1, MRP1, MRP2 and MRP3 in recurrent and residual tumours following chemotherapeutic treatment was higher than that in untreated primary tumours. Levels of MDR1 expression in residual tumours were particularly high, being 5.7 times higher than in untreated primary tumours [324].

In 2003, Diestra *et al*, investigated the predictive value of expression of MDR related proteins P-gp, MRP1, breast cancer resistance protein (BCRP) and lung resistance related protein/major vault protein (LRP/MVP) in the response to neoadjuvant chemotherapy, bladder preservation and prognosis in locally advanced bladder cancer. Immunohistochemical methods were used to determine the expression of MDR proteins in tumours from 83 patients with locally advanced bladder cancer treated with neoadjuvant chemotherapy using a bladder sparing approach. P-gp, MRP1, BCRP and LRP/MVP showed high level expression in 53%, 59%, 28% and 70% of cases,

respectively. P-gp expression correlated with shorter progression-free survival ($p = 0.04$) but not with overall survival. Surprisingly MRP1 expression correlated with an improved response rate ($p = 0.005$) and an increased chance of bladder preservation following neoadjuvant chemotherapy ($p = 0.001$). BCRP had no impact on prognosis. High LRP/MVP expression was associated with a significantly worse response to neoadjuvant chemotherapy and a decreased probability of bladder preservation ($p = 0.035$). They concluded that MRP1 and LRP/MVP could potentially be of use in combination with other clinicopathological prognostic factors for selecting patients with locally advanced bladder cancer to be candidates for bladder preservation after neoadjuvant chemotherapy. Although larger prospective studies are warranted to confirm these results [325].

In 2004, Zhu *et al*, looked at the expression of lung resistance-related protein (LRP) in a group of 66 patients with newly diagnosed primary bladder cancer, without prior exposure to either radiotherapy or chemotherapy. Reverse transcriptase-polymerase chain reaction analysis was used to measure LRP, MDR1 and MRP1 mRNA expression. Expression of LRP, p53 and p63 proteins were also examined using immunohistochemistry. LRP demonstrated the highest levels of expression in primary bladder cancer being expressed by 63.6% of tumours. LRP mRNA levels were significantly higher in normal bladder tissue than in bladder cancer tissue ($P < 0.01$) and in superficial cancers than in invasive cancers ($P = 0.013$). LRP mRNA expression did not correlate with either MDR1 or MRP1 expression, but was closely related to the LRP levels ($P = 0.001$). LRP was expressed more frequently in low-grade ($P < 0.01$) and low-stage ($P < 0.05$) cancers, but bore no relation to the expression of tumour suppressor proteins, p53 or p63. The higher levels of expression in lower grade and stage-related bladder cancer, suggest that LRP may be an indicator of intrinsic MDR in early bladder cancer. Cytotoxic drugs that are not susceptible to LRP resistance may be more effective in early bladder cancers [326].

1.5: Anthracyclines in multidrug resistance

Anthracycline Antibiotics

Anthracyclines antibiotics are cytotoxic drugs that are used to treat a wide variety of malignancies, both haematological and visceral.

Daunorubicin, the first drug discovered in this class, was isolated from a strain of the soil fungus *Streptomyces peucetius*. It's activity on experimental tumours was first described in 1959 [327], indicating the anti-tumour potential of the anthracyclines. Daunorubicin demonstrated activity against various tumours including Ehrlich carcinoma, sarcoma 180, Yoshida hepatoma and a variety of human haematological tumours. Doxorubicin (formerly known as adriamycin) was the next anthracycline to be discovered being derived from a mutant strain of *Streptomyces peucetius*. Doxorubicin was a more potent cytotoxic agent than daunorubicin, but was hampered by its dose limiting cardiotoxicity. Since then numerous anthracycline derivatives have been synthesised in an attempt to increase their antitumour activity and eliminate their unwanted side effects, the most limiting being their cumulative cardiotoxicity. Most of the newer anthracyclines are produced by a combination of microbial synthesis and biochemical modification. They include epirubicin, idarubicin and pirarubicin.

The anthracyclines are characterised by a tetracycline group attached by a glycoside bond to one or several sugar groups (Figure 15).

Epirubicin (4'-Epi-doxorubicin; molecular weight 580) is a stereoisomer of doxorubicin, differing from its parent molecule, doxorubicin, by a different configuration of the hydroxyl group (-OH) on the C4 position of the amine sugar. This minor alteration has not affected its antitumour activity, but has reduced its cardiotoxicity [328].

Idarubicin (molecular weight 497) differs from daunorubicin by the absence of a methoxy group at the carbon-4 position. This alteration results in increased lipophilicity which increases the rate of intracellular uptake and enhances its cytotoxicity.

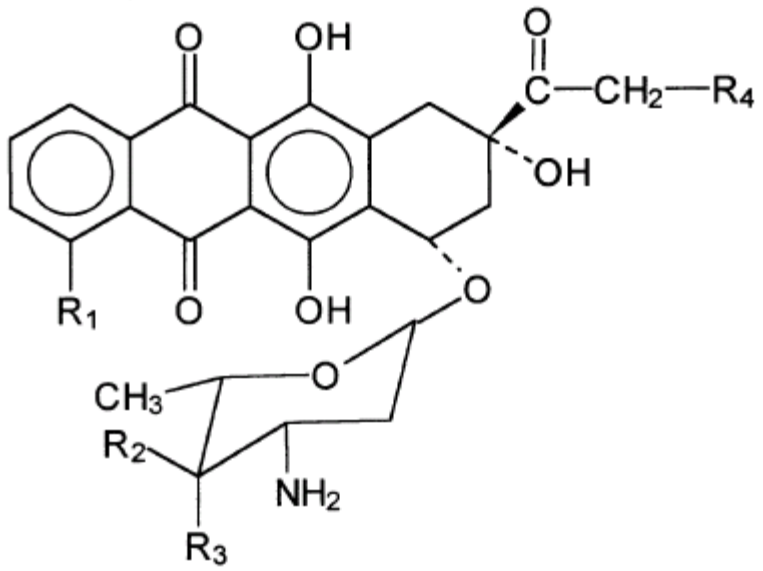

	R_1	R_2	R_3	R_4
Doxorubicin	OCH_3	H	OH	OH
Epirubicin	OCH_3	H	OH	OH
Idarubicin	H	H	OH	H

Figure 15: Biochemical structures of the anthracyclines: Doxorubicin, epirubicin and idarubicin

Anthracycline Autofluorescence

Anthracyclines possess the property of autofluorescence, which allows their study by a variety of fluorescence based techniques, including confocal microscopy and flow cytometry. These techniques have aided the study of intracellular accumulation and distribution of the anthracyclines in sensitive and MDR cancer cell line models.

This autofluorescence is attributed to the aromatic ring structure of doxorubicin, epirubicin and idarubicin (Figure 16). It is this four ring tetracene group which has a diffuse cloud layer of “Pi” electrons floating above and below it. These “Pi” electrons are easily excited into higher energy states by laser light of certain wavelengths. When these electrons fall back to their original unexcited energy state they liberate energy as photons of light, otherwise known as autofluorescence.

Doxorubicin, epirubicin and idarubicin have almost identical excitation and emission spectra as shown in Figure 16. Their peak excitation is achieved using a laser with a wavelength of 490nm (range 400 – 560nm). This yields a peak emission of 590 – 600nm wavelength (range 510 – 700nm).

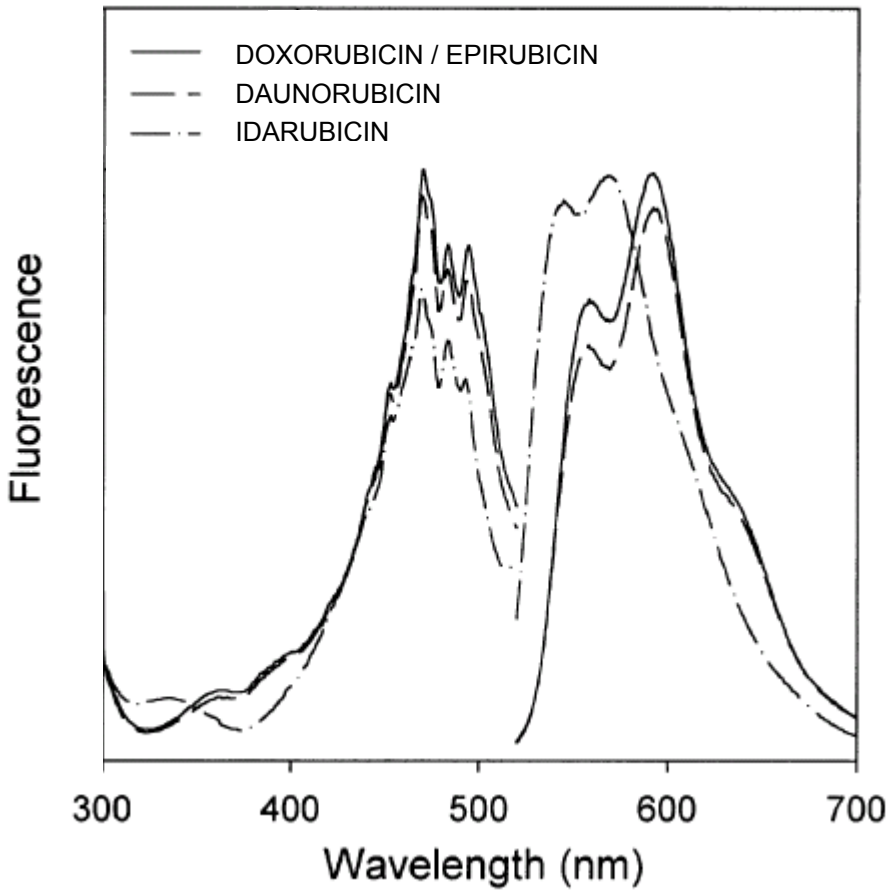

Figure 16: Excitation and emission spectra of the anthracyclines: Doxorubicin, epirubicin, daunorubicin and idarubicin.

Anthracyclines: Mechanisms of action

Major research efforts have been directed towards elucidating the mechanism of action and clinical pharmacology of known anthracycline compounds.
At present there are four major groups of action that have been postulated.

1. DNA intercalation

There is high affinity binding of the anthracyclines to cellular DNA through intercalation, with consequent blockade of the replication and transcription of the DNA [329-331]. This intercalation of anthracycline and DNA has several consequences; local relaxation with the DNA helix unwinding by 15 degrees and disruption of the ability of nucleic acid to act as a template for

polymerases leading to inhibition of DNA synthesis and repair, and fragmentation of DNA.

2. Membrane binding

Anthracyclines are able to bind onto membranes altering their fluidity, ion transport and interfering with membrane based signalling systems [332]. It has been suggested that the primary cytotoxic effect of the anthracyclines on non-dividing cells, may arise from their tendency to disrupt the electrolyte balance of the cell, by increasing the sodium permeability and altering the calcium handling of the cells [333].

3. Free radical formation

Many of the anthracyclines can be reduced through cytochrome P450 mediated reductive processes to generate semiquinone free radicals. These free radicals can further reduce molecular oxygen to the superoxide ion, which causes damage to DNA, cell membranes and mitochondria through perioxidation of membrane lipids [334,335]. This action may also be responsible for cardiac toxicity through oxygen radical-mediated damage to the membranes, as heart muscle cells lack the enzyme catalase which inactivates oxygen free radicals [332].

4. Topoisomerases

Another important cytotoxic action of the anthracyclines takes place in the nucleus of the cell and appears to be mediated, at least partly, through an effect on *topoisomerase II* (a DNA gyrase), the activity of which is markedly increased in proliferating cells. The topoisomerases catalyse the interconversion of topoisomers in DNA. The significance of these enzymes lies in the fact that during replication of the DNA helix in mammalian cells, reversible swivelling needs to take place around the replication fork in order to prevent daughter DNA molecules becoming inextricably entangled during mitotic segregation. This swivelling is produced by a three step process:

1. Cleavage of one (topoisomerase I) or both strands (topoisomerase II) of DNA,
2. Passage of a segment of DNA through this break, and
3. Resealing of the break (topoisomerase II).

Cleavage of DNA by topoisomerase II is stimulated by, but not dependent upon, ATP. The anthracyclines are thought to act on topoisomerase II

stimulating formation of cleavable complexes with topoisomerase *in vitro* and inducing protein-linked DNA breaks *in vitro* and *in vivo*. The mechanism of DNA breakage induced by the anthracyclines is most likely due to the drug stabilisation of a cleavable complex formed between topoisomerase II and DNA, resulting in both double- and single-strand DNA breaks [336-339].

Anthracyclines: Mechanisms of resistance

Most information regarding mechanisms of resistance to anthracyclines is derived from *in vitro* models, where cells can be exposed to doses of drugs that cannot be achieved clinically. There are multiple mechanisms of resistance to anthracyclines and resistance is often multifactorial. The main mechanisms of action are outline below:

1. Classical P-glycoprotein mediated MDR

Anthracyclines are susceptible to classic P-gp mediated multidrug resistance. Active drug efflux by P-gp leads to reduced intracellular accumulation and efficacy of anthracyclines.

2. Non-Pgp mediated MDR

Anthracyclines are also subject to efflux by other plasma membrane pumps including MRP and BCRP.

3. Changes in the intracellular distribution of the drug

In both classic and non-P-gp mediated MDR, the subcellular localisation of anthracyclines has been shown to alter from mainly nuclear in wild-type cells to mainly cytoplasmic, with more free drug present in acidic vesicles or bound to the membranes of vesicles in MDR cells [340,341]. This compartmentalisation of the anthracyclines away from their nuclear target is an additional mechanism of resistance in both P-gp and non-P-gp mediated MDR.

4. Glutathione-S-transferases (GSTs) and detoxification mechanisms

These enzymes conjugate glutathione to chemically reactive groups and have been found to be overexpressed in several doxorubicin resistant cell lines. Direct evidence of GST activity in anthracycline resistance is missing. However, elevated levels of GSTs may indirectly lead to anthracycline resistance by inhibition of the MAP kinase apoptotic pathway.

5. Alterations in TOPO II (at-MDR)

Low levels of expression or alterations in TOPO II may contribute to anthracycline resistance, as one of their modes of action is via interaction with TOPO II in dividing cells.

6. Increased DNA repair

In several cell lines, increased levels of DNA repair have been associated with resistance to doxorubicin [342].

Anthracyclines in the study of MDR

The anthracyclines are substrates for several of the ABC transporters including P-gp, MRP1 and BCRP and are also susceptible to other mechanisms of MDR. They also possess the property of autofluorescence which allows their study by a variety of fluorescence based techniques including confocal microscopy and flow cytometry. For these reasons the anthracyclines have been used extensively in the study of MDR mechanisms in cell line models. These studies have principally looked at drug uptake and localisation within cells, as well as some dynamic variables such as efflux. Initial studies were able to demonstrate reductions in anthracycline uptake in MDR cells. Cellular localisation of drug could also be studied. MDR cells have altered cellular distribution of anthracyclines with predominantly cytoplasmic drug localisation, where it appears to be sequestered within vesicles. This gives the so-called nuclear sparing appearance which is characteristic of MDR drug uptake.

Flow cytometric experiments:

In 1979, Krishan *et al*, described how intracellular levels of anthracyclines could be detected and quantified using laser flow cytometry. Krishan used two methods, an indirect method based on the interference of the anthracyclines with nuclear DNA binding of propidium iodide and therefore reducing fluorescence levels and a direct method where intracellular anthracycline fluorescence was excited and detected [343].

In 1980, Krishan *et al*, demonstrated how laser flow cytometry could be used to examine the pharmacokinetics of intracellular anthracycline uptake. They were able to examine dose responses and rates of drug uptake for several anthracyclines including adriamycin (doxorubicin) and daunomycin (daunorubicin). Drug fluorescence was also detectable in tumour and spleen

samples from animals that were injected with adriamycin (4 mg/kg) and sacrificed 3 hours later [344].

In 1982, the same group demonstrated how flow cytometry could be used to rapidly compare and quantitate cellular Adriamycin (ADR) fluorescence in ADR-sensitive P388 leukemia (P388/S) and ADR-resistant P388 leukemia (p388/R) cells. Drug levels in resistant cells were two to fourfold lower that levels in sensitive cells exposed to the same concentration of adriamycin (1 – 10 µg/ml) [345]

Confocal microscopy experiments

In 1991, Gervasoni *et al*, first described the use of Laser-assisted Confocal Microscopy to look at the subcellular distribution of anthracyclines in cancer cell lines. They examined the difference in cellular localisation of daunorubicin in four well defined MDR cell lines (HL-60/AR, P388/ADR, KBV-1 and MCF-7/ADR) and their drug sensitive counterparts (HL-60/S, P388/S, KB3-1 and MCF-7/S). Both resistant and sensitive cells showed rapid distribution of drug from the plasma membrane to the perinuclear region within 2 minutes. From 2 – 10 minutes, in the drug sensitive HL-60/S, P388/S, and MCF-7/S cells drug was redistributed throughout the cytoplasm and into the nucleus in a diffuse pattern. In contrast, drug-resistant HL-60/AR, P388/ADR, and MCF-7/ADR cells redistributed drug away from the nucleus into cytoplasmic vesicles, seen as a "punctate" cytoplasmic pattern of drug fluorescence. The redistribution of daunorubicin away from the nucleus in MDR cells was inhibited by glucose deprivation and by lowering the temperature of the medium below 18^{o}C, suggesting that this was an energy dependent phenomenon. The differences in distribution between sensitive and resistant cells did not appear to be related to the levels of intracellular Daunorubicin or as a result of cell death. Drug-sensitive KB3-1 and -resistant KBV-1 cells demonstrated an intermediate intracellular distribution of Daunorubicin with both "punctate" and nuclear/cytoplasmic uptake, sometimes in the same cell. The nuclear sparing of Daunorubicin uptake in resistant cells was felt to represent another mechanism of drug resistance independent of P-glycoprotein overexpression, presumably by protecting cellular DNA against drug toxicity [244].

In 1993, Coley et al, used laser scanning confocal microscopy to study the intracellular distribution of anthracyclines in two pairs of parental and multidrug resistant (MDR) cell lines. They used mouse mammary tumour cells lines EMT6/P (parental) and EMT6/AR1.0 (resistant)) and a human large cell lung cancer line COR-L23/P (parental) and the COR-L23/R (resistant). Sensitive cell lines demonstrated predominantly nuclear and cytoplasmic drug fluorescence. Whilst in the resistant cell lines intracellular fluorescence levels were much lower, with comparatively more loss of nuclear fluorescence than cytoplasmic fluorescence. The COR-L23/R cell line additionally showed an area of intense perinuclear staining consistent with drug localised in the Golgi apparatus. The addition of verapamil during anthracycline exposure led to increased levels of fluorescence in the MDR lines, particularly in the nucleus. Verapamil exerted minimal effects in parental lines.

They summarised that confocal microscopy is a useful tool for examining the subcellular distribution of anthracyclines in parent and MDR cell lines, which may provide useful insights into the mechanisms of MDR and suggest strategies to circumvent MDR [340].

Anthracyclines in the study of MDR in bladder cancer

Anthracyclines have also been used to investigate mechanisms of MDR in bladder cancer. Here their use is particularly pertinent as doxorubicin and epirubicin are agents that are in regular use as intravesical cytotoxic agents. In 1996, Duffy *et al*, published two papers comparing epirubicin uptake and distribution in a sensitive (MGH-U1) and a MDR (MGH-U1R) bladder cancer cell line, using flow cytometry in one and confocal microscopy in the other. The flow cytometric analysis looked at the detection of intracellular levels of epirubicin using autofluorescence in both sensitive and resistant bladder cancer cell lines *in vitro* [346]. This study also examined the effects of verapamil, a known MDR reversing agent on epirubicin accumulation within these cells. They found a reliable, highly significant and consistent difference in intracellular epirubicin uptake between the resistant and sensitive bladder tumour cells. The resistant cell lines demonstrated significantly lower levels of epirubicin fluorescence. Over the range of epirubicin concentrations between 1 to 40μg/ml there was a consistent eightfold difference in epirubicin uptake

between sensitive and resistant cell lines. They demonstrated that verapamil increased the levels of epirubicin uptake in MDR cell lines to almost the same levels as in sensitive cell lines. It was suggested that such an assay of epirubicin uptake could be applied to clinical tumour specimens allowing targeted treatment of sensitive tumours. They also suggested that verapamil in combination with epirubicin may improve the efficacy of treatment in patients whose tumors exhibit MDR.

The confocal microscopy paper looked at the intracellular distribution of epirubicin in sensitive and resistant bladder cancer cell lines, in particular looking at the effects of temperature, viability and verapamil [347]. They demonstrated a striking and consistent difference in the intracellular distribution of the drug between resistant and sensitive cells. Sensitive cells demonstrated greater overall levels of epirubicin fluorescence, predominantly accumulating in the nucleus. In contrast epirubicin fluorescence in resistant cells was cytoplasmic with a granular appearance, with characteristic sparing of uptake from the nucleus. When incubated at $0^{o}C$, both cell lines showed an absence of nuclear uptake, resembling the nuclear sparing pattern of resistant cells at $37^{o}C$. Dead cells developed brightly fluorescent nuclei of sensitive phenotype very rapidly, highlighting the need to assess cell viability before making any claims about reversal of the nuclear uptake pattern by pharmacological means. Addition of the MDR-reversing agent verapamil changed resistant cells to the sensitive phenotype, which were subsequently proven viable by Trypan blue exclusion. They concluded that sensitive and resistant cells could be differentiated reliably by confocal microscopy and pointed to another mechanism of resistance to epirubicin, namely the nuclear exclusion of drug. The technique described in this study could be applied to clinical tumours specimens to detect tumours containing resistant cells that could potentially benefit from MDR-reversing agents such as verapamil as part of a combination chemotherapy regime.

Another study from the same research group used confocal microscopy to examine cellular uptake and localisation of epirubicin and mitozantrone (a cytotoxic drug from the anthraquinone group also demonstrating autofluorescence) in combination with gammalinolenic acid (an essential fatty acid) or verapamil in sensitive (MGH-U1) and resistant (MGH-U1R) cell lines.

Mitozantrone exhibited similar differences in terms of cellular drug localisation with sensitive cells having a predominantly nuclear uptake and resistant cells sparing drug from the nucleus. At a mitozantrone dose of 20µg/ml, the ratio of sensitive to resistant nuclear uptake was 10:1, which with the addition of GLA decreased to 6:1. For epirubicin similar patterns of drug localisation to those described by Duffy *et al*, were reported, with reversal of the MDR cells to a nuclear uptake pattern with the addition of verapamil [348].

The demonstration of nuclear exclusion of another class of cytotoxic drug, suggests that this "nuclear sparing phenomenon" may be a common mechanism of resistance to many different cytotoxic agents with nuclear modes of action.

In another study from the same group, primary cells cultured from bladder cancer explants also demonstrated heterogeneity in their nuclear uptake of epirubicin, with many demonstrating the MDR phenotype [349].

Multidrug resistance in bladder cancer: Does the nuclear membrane play a role?

Like MDR, nuclear sparing has been demonstrated in MDR cell lines from numerous organs, appearing to transcend tissue type. It has also been shown in viable clinical tumour material. It seems likely therefore that this mechanism is an important reason for chemotherapeutic failure in tumours exhibiting MDR, as many cytotoxic drugs have their main mode of action within the nucleus.

Nuclear sparing has also been demonstrated using other fluorescent chemotherapeutics such as the anthraquinones, which include Mitozantrone [348,350,351]. Difficulties in visualising the cellular distribution of non-fluorescent chemotherapeutic agents makes it impossible to prove that in MDR cells, nuclear sparing limits the efficacy of all MDR-affected anticancer agents and not just those possessing autofluorescence.

Previous investigators have questioned whether the nuclear sparing phenomenon is merely a reflection of low levels of drug accumulation in MDR cells, due to drug efflux by P-glycoprotein, or whether the nuclear membrane is also playing a role [234,244,340,347,352]

Previous work looking at the role of the nuclear membrane in adriamycin uptake in isolated sensitive and MDR nuclei, from a lymphoblastic tumour cell line [352], showed that in isolated nuclei, nuclear transport of adriamycin (doxorubicin) was reduced in MDR cells compared to sensitive cells. Blockade of active nuclear transport by Wheat Germ Agglutinin (WGA; Triticum vulgaris lectin) reduced sensitive nuclear uptake of adriamycin to approximately the level of MDR nuclear uptake, but had no effect on adriamycin accumulation in MDR nuclei. These results suggested that there are two mechanisms of drug uptake at play in sensitive cells, namely passive diffusion and active transport.

The role of the nuclear membrane in this nuclear sparing phenomenon in MDR cancer cells has not been clearly established, but clearly warrants further investigation.

Nuclear sparing of anthacycline uptake in bladder cell lines: The enigma of idarubicin

Idarubicin is somewhat of an enigma in terms of its uptake and subcellular distribution in MDR cancer cell lines. Idarubicin demonstrates high levels of intracellular drug fluorescence, but unlike the other anthracyclines there is clear nuclear sparing pattern of subcellular localisation in both sensitive and MDR cell lines [350,353]. Most cells demonstrate high levels of cytoplasmic drug fluorescence with an area of intense peri-nuclear staining, probably representing drug within the Golgi apparatus. The addition of verapamil results in no change in the cellular distribution of idarubicin, but does result in increased cytotoxicity presumably as a result of increased intracellular drug levels [353]. This suggests that substantial nuclear drug fluorescence may not be required for all anthracyclines to exert their cytotoxic effects.

1.6: The nuclear membrane and nuclear pore complexes

Molecular trafficking of ions, small molecules and macromolecules, between nucleus and cytoplasm occurs via nuclear pore complexes (NPCs). These large (~125 MDa) supramolecular assemblies are an integral part of the double-membraned nuclear envelope. The nuclear membrane of a proliferating human cell has approximately 3000–5000 NPCs. NPCs allow passage of molecules by two mechanisms: passive diffusion and facilitated translocation.

In eukaryotic cells the spatial separation of transcription and translation is a powerful mechanism for controlling gene expression, but requires selective transport between the nuclear and cytoplasmic compartments to maintain the distinctive composition of each. Consequently, it is vital that both proteins and RNA are transported across the nuclear membrane in a regulated manner. NPCs have been implicated in carcinogenesis and have also been suggested as a possible mechanism of nuclear MDR [352].

The nuclear membrane:

In eukaryotic cells during interphase, the nucleus is separated from the cytoplasm by the nuclear envelope (NE), consisting of a double membrane enclosing a lumen or “perinuclear space”. The outer membrane faces the cytoplasm and is in continuity with the endoplasmic reticulum (ER), so that the perinuclear space communicates with the lumen of the ER. This outer cytoplasmic leaf is often studded with ribosomes forming the rough ER. The inner nuclear membrane faces the nucleoplasm and its inner surface is lined by the nuclear lamina, a polymer of intermediate filament-like proteins, the nuclear lamins. The nuclear lamina provides a general framework for NE structure and provides an anchoring site for interphase chromatin. At irregular intervals the inner and outer nuclear membranes are fused to form the “pore membrane”, sites at which the NPCs traverse the nuclear envelope.

Nuclear pore complexes (NPCs)

NPCs are sites of bidirectional exchange of material between the nucleus and the cytoplasm. They allow passive diffusion of ions and small molecules, but molecules above 9nm in diameter do not freely cross the NPC. Macromolecules greater than ~ 40Kda are transported actively across the nuclear envelope through NPCs using soluble transport factors or carrier

molecules that cycle between the cytoplasm and nucleus [354-357]. These larger molecules are selectively imported by a signal-requiring and ATP-dependent mechanism. Macromolecular assemblies such as ribonucleoprotein (RNP) particles containing mRNA also undergo selective nuclear export.

Nuclear pore complexes: Structure

Nuclear membrane pores in vertebrates are huge macromolecular protein structures approximately 1200 Å in diameter with a depth of about 700 Å, where they cross the nuclear envelope [358,359]. NPCs are constructed from multiple copies of about 30 different proteins, collectively known as nucleoporins [360-362]. NPCs in vertebrates have a tripartite architecture with a molecular weight of around 125MDa [363]. The central framework for the NPC is a ~ 55 MDa ring-like assembly built of eight multidomain spokes each consisting of two roughly identical halves [358,363].

This central framework is sandwiched between a ~ 32 MDa cytoplasmic ring and a ~ 21 MDa nucleoplasmic ring. The cytoplasmic ring radiates eight short, kinky fibrils, whereas the nuclear ring anchors a basket-like structure (or fishtrap), assembled from eight thin 50nm long filaments joined distally by a 30–50nm diameter ring [364]. The central framework of the NPC has a central channel, about 40 nm [365] in diameter, through which molecules diffuse or are transported. This central channel of the NPC is often plugged with a distinct particle of variable appearance, called the central plug or transporter [366].

A schematic diagram of the nuclear pore substructures is shown in Figure 17.

Nuclear pore complex: Function

Nuclear pores form aqueous channels through which all nuclear – cytoplasmic transport of molecules proceeds, either by passive diffusion or facilitated transport.

Passive diffusion through NPCs

The passive diffusion channel of the NPC has functional diameter of approximately 9nm [367]. Passive diffusion is relatively fast for small molecules < 20–30KDa, but becomes very inefficient as the size of the molecule approaches the 9nm limit, which translates to a molecular weight of around 40KDa.

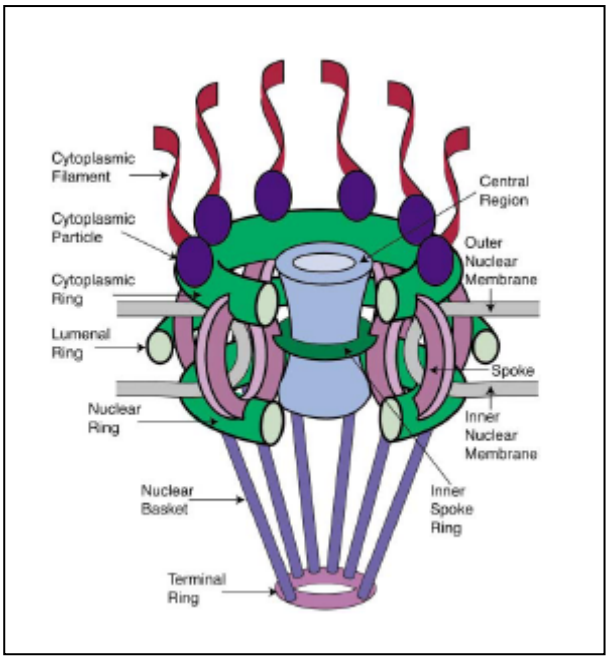

Figure 17: Schematic diagram of nuclear pore complex substructures (Figure reproduced with kind permission of Cell Press)

Facilitated transport through NPCs

In contrast, facilitated transport permits the translocation of much larger objects, often against a gradient of chemical activity [354]. Particles with molecular weights of several megadaltons can be transported by this process, such as ribosomal subunits (1.4 and 2.8 MDa) or Balbiani ring particles (>10MDa). Facilitated transport is an energy dependent process which requires specific interactions between the translocating molecule and the NPC, making the process very selective.

There are several nuclear transport pathways, each transporting a specific range of macromolecules into or out of the nucleus. Most pathways use a homologous family of carrier molecules collectively called β-karyopherins, with import carriers called importins and export carriers called exportins.

Many proteins are imported to the nucleus using importin-β, often using importin-α as an adaptor. Other proteins are transported by other importins, such as transportin. Nuclear export of proteins is mediated in many cases by the export carrier CRM1. Various exportins facilitate nuclear export of RNA, for example pre-micro-RNA is exported by exportin-5 and t-RNA is exported by exportin-t, both of which are importin-β analogues. In contrast, mRNA is exported by the NXF1:NXT1 heterodimer which is unrelated to karyopherins.

Nuclear protein import occurs by different pathways many of which share common features based on a concerted series of protein:protein interactions allowing cargo recognition in the cytoplasm, translocation through NPCs and release into the nucleus. In each pathway, cargo proteins are targetted for nuclear import by short sequences of amino acids know as nuclear localisation sequences (NLS). Each of the different import pathways requires a specific NLS.

The classic nuclear protein import pathway is the best characterised nuclear transport cycle, transporting a wide range of cargo proteins using importin-β as a carrier. This pathway has been studied in substantial detail and all of its components have been identified.

The classic nuclear protein import cycle

The classic nuclear protein import cycle is driven by a series of protein:protein interactions and generates transport rates of ~ 100 – 1,000 cargoes per minute per NPC [365].

The nuclear protein import cycle can be conveniently divided into four steps: assembly of the cargo:carrier import complex in the cytoplasm; translocation through NPCs; import-complex disassembly in the nucleus; and importin recycling (Figure 18a).

In the cytoplasm, proteins containing a classic NLS are imported by importin-β, which binds them through the adaptor protein importin-α, forming an import complex, importin-α:β heterodimer, which facilitates movement through NPCs. In the nucleus, RanGTP binds to importin-β, which dissociates importin-β from importin-α. The NLS carrying cargo protein is then released by importin-α. Importin-β complexed with RanGTP is recycled to the cytoplasm, whereas importin-α is exported complexed with its nuclear export factor, β-karyopherin CAS and RanGTP. Finally, in the cytoplasm RanGAP (Ran GTPase activating protein) stimulates GTP hydrolysis by Ran GTPase, generating RanGDP, which then dissociates from the importins, releasing them for another import cycle.

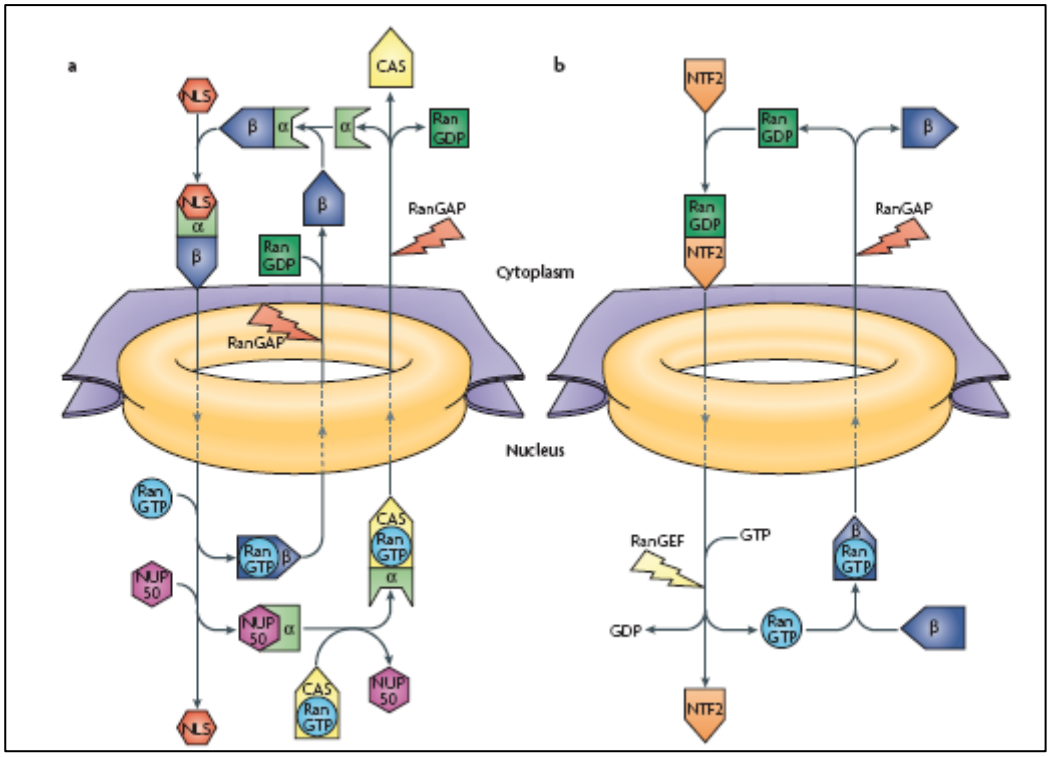

Figure 18a: Overview of classic nuclear protein import cycle.
Figure 18b: RanGTP/GDP cycle associated with nuclear protein import. (Reproduced with kind permission of Nature Publishing Group)

Interactions between cargoes and carriers are coordinated by the nucleotide state of Ran, which cycles between GTP- and GDP-bound states (Figure 18b). The state of the Ran nucleotide is controlled by its guanine nucleotide-exchange factor (RanGEF), which catalyses recharging of RanGDP with GTP, and RanGAP, which stimulates GTP hydrolysis. RanGEF is nuclear and RanGAP is cytoplasmic, and so nuclear Ran is in the GTP-bound state, whereas cytoplasmic Ran is GDP bound. RanGTP is exported from the nucleus bound to β-karyopherin carriers and, after RanGAP-mediated GTP hydrolysis, cytoplasmic RanGDP is transported to the nucleus by its specific carrier, nuclear transport factor-2 (NTF2) [368,369], for recharging with GTP. The conformation of key structural loops in Ran (the switch I and II loops) changes markedly with nucleotide state. This structural change determines the way in which importin-β family transport factors interact with cargoes, and so ultimately, the Ran GTPase provides the energy for nuclear transport.

Nuclear pore complexes and cancer

The targeting of a tumour suppressor, transcription factor or oncoprotein to its intracellular site of action is regulated at multiple points. Such regulatory steps include upstream cell-signalling events, protein modification and the ability of nuclear transport proteins to recognise and bind nuclear transport signals. Transport signals can be masked by the binding of another protein or folding of an inhibitory domain, making the signal inaccessible to nuclear transport receptors. Any of these processes can be altered, resulting in subcellular mislocalisation, which could result in uncontrolled cell growth.

Cell cycle regulatory proteins

Cyclin B1 is a cell cycle regulator that requires nuclear localization to be biologically active [370]. During the S and G2 phases of the cell cycle, cyclin B1 accumulates in the cytoplasm following which at the beginning of mitosis, it rapidly relocates to the nucleus. This relocalisation is the result of regulated nuclear export [371,372], suggesting that deregulation of this process can alter the mitotic process and could lead to cancer. Several other mitotic inducers have been identified and shown to rely on nuclear transport to exert their effects, such as Cdc 25, cyclin D1 and $p27^{kip1}$ [373,374]. Cyclin D1 is overexpressed in many different tumours and decreased expression of $p27^{kip1}$ correlates with a poorer prognosis in breast and colon cancer.

Inactivation of p53

P53 is a well described tumour suppressor gene and over half of all human cancers contain mutations in p53 that result in its inactivation [375]. Interestingly, p53 inactivation can also occur from mutation-independent mechanisms, such as sequestration of p53 in the cytoplasm [375,376]. The function of p53 depends on nuclear localisation, so its nuclear-cytoplasmic transport is tightly regulated. Increased nuclear levels of p53 are required during times of cell stress, such as DNA damage, where p53 activates transcription of its target genes. The regulation of p53 by nuclear transport has only recently been studied and characterised [377,378]. P53 contains 3 nuclear localisation signals (NLS) [379] and one nuclear export signal (NES). Functional cytoplasmic p53 has been discovered in many different types of human cancers. The mechanism by which p53 is sequestered in the cytoplasm of tumour cells is unknown. It may be a result of increased export,

due to expression of a hyperactive form of MDM2. Nuclear exclusion could also result from binding to a cytoplasmic anchor protein, such as the glucocorticoid receptor or the parkin-like ubiquitin ligase (PARC)

Cellular Apoptosis

Apoptosis, or programmed cell death, is necessary to maintain homeostasis in normal tissues. Failure of apoptosis is now recognised as an important factor in carcinogenesis. Apoptotic signals are transmitted through a common pathway that involves the death-driving ICE-family proteases and anti-cell death protein Bcl-2 in the cytoplasm. These signals must be transported from the cytoplasm to the nucleus. Blockade of active nuclear pore transport with WGA prevented Fas-induced apoptotic nuclear changes, such as chromatin condensation, nuclear fragmentation and the formation of apoptotic bodies [380]. Caspases, the major execution system in apoptosis, also alter nucleocytoplasmic transport by degradation of nucleoporins [381].

Alterations in nucleoporins

Several cancer-associated fusion proteins have been identified that involve nucleoporins. Many of these involve NUP98 fusions, most of which appear to be associated with haematogenous cancers, such as myeloid and lymphoid malignancies [382]. Another fusion involving the nucleoporin CAN or NUP214 and the nuclear binding protein DEK has also been associated with acute myeloid leukaemia [383]. These fusion proteins retain the FXFG repeat region that is characteristic of several nucleoporins and helps to regulate the nuclear-cytoplasmic transport of proteins and RNAs as well as functioning as docking sites for importins. These FXFG repeat regions are also required for cell transformation and transactivation and act as transcriptional activators.

1.7: Summary of study hypotheses, aims and objectives:

The main object of this study was to investigate and further define the role of the nuclear membrane in the nuclear sparing of anthracycline uptake associated with the multidrug resistance phenomenon.

Hypothesis 1:

The nuclear membrane is responsible for nuclear sparing of epirubicin uptake in MDR bladder cancer cells.

Aims and Objectives:

1. To establish sensitive and MDR nuclear epirubicin uptake phenotypes in bladder cancer cell lines using confocal microscopy.
2. To establish the nuclear epirubicin uptake characteristics of cell fusion products arising from fusion of sensitive and MDR cells.
3. To establish the chromosomal epirubicin staining patterns of sensitive and MDR bladder cancer cells during metaphase arrest.
4. To determine the nuclear epirubicin uptake characteristics of sensitive and MDR bladder cancer cell lines following cytoplasmic microinjection of epirubicin.

Hypothesis 2:

An active efflux mechanism is responsible for nuclear sparing of epirubicin in MDR bladder cancer cells.

Aims and Objectives:

1. To determine the effects of incubation temperature and cell death on nuclear uptake of anthracyclines in sensitive and MDR bladder cancer cells using confocal microscopy.
2. To assess anthracycline uptake in nuclear isolates exposed to epirubicin pre- and post-nuclear fractionation using confocal microscopy.
3. To determine the size of molecules that can diffuse through nuclear pores of live cells using various sized FITC-labelled dextrans.
4. To demonstrate peri-nuclear localisation of Wheat Germ Agglutinin and establish whether WGA nuclear pore blockade affects nuclear uptake of FITC-dextrans or epirubicin.
5. To determine the effect of temperature on nuclear uptake characteristics of sensitive and MDR bladder cancer cells following cytoplasmic microinjection of epirubicin.

6. To establish whether P-glycoprotein is expressed on the nuclear membrane of MDR bladder cancer cells using a monoclonal FITC-labelled anti-Pgp antibody with confocal microscopy and flow cytometric analysis.
7. To determine the effect of verapamil on cytoplasmic and nuclear epirubicin uptake in sensitive and MDR cells using time series confocal microscopy and flow cytometric studies.

In addition we sought to clarify some other questions that have been raised by previous researchers from our group.

Hypothesis 3:

The nuclear membrane is not responsible for nuclear exclusion of idarubicin in sensitive and MDR bladder cancer cells.

Aims and Objectives:

1. To establish sensitive and MDR nuclear idarubicin uptake phenotypes in bladder cancer cell lines using confocal microscopy.
2. To assess idarubicin uptake in nuclear isolates exposed pre- and post-nuclear fractionation using confocal microscopy.
3. To establish the chromosomal idarubicin staining patterns of sensitive and MDR bladder cancer cells during metaphase arrest.

Hypothesis 4:

Mitomycin C fluorescence can be detected using direct or indirect fluorescence methods, allowing us to study its cellular uptake and localisation.

Aims and Objectives:

1. To assess whether Mitomycin C fluorescence could be detected in sensitive and MDR cells using confocal microscopy (including time series uptake studies) and flow cytometric analysis.
2. To assess cellular Mitomycin C uptake in sensitive and MDR cells indirectly by exclusion of acridine orange DNA staining, using confocal microscopy and flow cytometric analysis.

Hypothesis 5:

GFP fluorescence can be used as a viability stain in cell lines.

Aims and Objectives:

1. To assess loss of GFP fluorescence as a marker of cell death following cell killing using confocal microscopy and time series confocal studies.

Hypothesis 6:

Changes in the localisation of epirubicin in MDR bladder cancer cells following cell death are due to leakiness of the cell and nuclear membranes.

Aims and Objectives:

1. To determine the effects of cell death on nuclear uptake of anthracyclines in sensitive and MDR bladder cancer cells using confocal microscopy.
2. To establish the cellular and nuclear uptake pattern of a 77KDa FITC-labelled dextran in dead cells using confocal microscopy.

Overall design of experiments to address our main hypotheses:

Rationale for experiments to address hypothesis 1:

"The nuclear membrane is responsible for nuclear sparing of epirubicin uptake in MDR bladder cancer cells."

1. Nuclear epirubicin uptake characteristics of sensitive and MDR cells to be confirmed with incubation studies.

2. Cell fusion experiments: Attempting to fuse sensitive and resistant cells followed by examination of the nuclear epirubicin uptake characteristics of these "mixed" cell fusion products. Demonstration of phenotypically different nuclei in the same cell environment would provide strong evidence that the nuclear membrane is responsible for the nuclear sparing phenomenon in MDR cells.

3. Metaphase arrest experiments: During metaphase the nuclear membrane is absent. Chromosomal epirubicin staining in MDR cells arrested in metaphase would implicate the nuclear membrane in the nuclear sparing phenomenon.

4. Microinjection studies: Direct microinjection of MDR cells with epirubicin overcomes the cell membrane P-gp pump which is a major mechanism of drug resistance. If cells continue to demonstrate nuclear sparing following direct injection of drug into the cytoplasm, this would implicate the nuclear membrane in this phenomenon.

Rationale for experiments to address hypothesis 2:

"An active efflux mechanism is responsible for nuclear sparing of epirubicin in MDR bladder cancer cells."

1. Active cell processes are abolished by cell cooling and by cell death. Studying the effects of these factors on nuclear epirubicin uptake in sensitive and MDR bladder cancer cells gives insight into the effects of the energy dependent processes involved in MDR.
2. The assessment of epirubicin uptake in nuclear isolates exposed to epirubicin pre- and post-nuclear fractionation gives insight into nuclear drug uptake when active cellular processes are at play when compared to “non-viable” extracted nuclei.
3. Nuclear pore sizing using various sized FITC-dextrans in conjunction with scrape-loading and microinjection techniques allows assessment of the size of molecules that are able to freely diffuse across the nuclear membrane, which should gain entry to the nucleus.
4. Wheat Germ Agglutinin is known to block nuclear pores by reducing their functional diameter and abolishing active transport processes. Following WGA nuclear pore blockade, we assessed whether diffusion of a 19.5KDa FITC-dextran across the nuclear membrane was affected and also assessed whether there were any changes in the nuclear uptake of epirubicin using confocal microscopy and flow cytometric analysis of cellular and nuclear uptake.
5. Direct microinjection of cells that were cooled on ice, allowed us to determine whether any energy dependent processes are involved in the nuclear exclusion of epirubicin from MDR nuclei.
6. The MDR cell lines used in this study were known to express P-glycoprotein. We performed experiments using a FITC-labelled anti-Pgp antibody to determine whether P-gp is expressed on the nuclear membrane of these MDR cell lines, which might account for the nuclear exclusion of epirubicin.
7. Verapamil is known to increase nuclear uptake of epirubicin in MDR cells. We assessed the effects of verapamil on the uptake of epirubicin in the cytoplasmic and nuclear cell compartments to determine whether its action was likely to be at the cell membrane or the nuclear membrane. We also assessed the affects of incubation time on MDR reversal by verapamil using flow cytometric time series.

Chapter 2: Materials and Methods

2.1: General Procedures

The following section describes general procedures undertaken throughout the research period. Any modification to these procedures is described in more detail in the relevant section.

Cytotoxic drug storage

Both epirubicin (Pharmacia, UK) supplied in solution (2mg/ml) and idarubicin (Pharmacia, UK) supplied as dry powder were diluted with sterile water to 1mg/ml stock concentrations. Stock solutions were divided into 1ml aliquots and stored at -20^{o}C to maintain drug stability. They were reconstituted in fresh culture medium supplemented with 1:100 HEPES buffering solution (Sigma, UK) at the time of use.

Mitomycin C was diluted with sterile water to a 1mg/ml stock solution and diluted further in culture medium and used immediately. Any remaining stock solution was discarded, as mitomycin C is highly unstable once solubilised.

Fluorescein Diacetate (FDA)

A stock solution of fluorescein diacetate (FDA) (Sigma, UK) 500µg/ml in acetone was prepared. This was stored at -20^{o}C to prevent drug deterioration and diluted at the time of use to a concentration of 500ng/ml in phosphate buffered saline (PBS).

Acridine Orange (AO)

Acridine Orange (AO) (Sigma, UK) stock solution was prepared by dissolving 15mg AO in 1ml of 95% ethanol followed by further dilution in 49mls of distilled water. The stock solution was divided into 1ml aliquots and stored at -20^{o}C. At the time of use the stock solution was diluted 1:100 with PBS to make a final concentration of 3µg/ml. This working concentration was stored at 4^{o}C and used for up to one month, after which it was discarded.

Ethidium Bromide (EB)

Ethidium Bromide (EB) (Sigma, UK) stock solution was prepared by dissolving 50mg EB in 1ml 95% ethanol followed by further dilution in 49mls of distilled water. The stock solution was divided into 1ml aliquots and stored at -20^{o}C. At the time of use the stock solution was diluted 1:100 in PBS to make a final concentration of 10µg/ml. Working concentrations were stored at 4^{o}C and used for up to one month, after which it was disposed of.

Cell lines

The derivation and sourcing of cell lines used in this research are shown below.

1. Sensitive bladder transitional cancer cell lines:

MGH-U1 (Human, female, superficial TCC cell line (T1 G3), donated by Professor John Masters, UCL) [384].

RT112 (Human, female, TCC cell line (G2), purchased from Deutsche Sammlung von Mikroorganismen und Zellkulturen (DSMZ); catalogue Number: ACC 418).

MGH-U1-GFP (Green fluorescent protein (GFP) expressing subline of MGH-U1, produced in house by transfection with GFP [385].

2. Multidrug resistant (MDR) bladder transitional cancer cell lines

MGH-U1R (MDR subline of MGH-U1, produced by continuous low-dose exposure to Doxorubicin [308], donated by Professor John Masters, UCL).

MGHU-MMC (MDR subline of MGH-U1, produced in house by continuous low-dose exposure to mitomycin C [386].

MGH-U1R-GFP (GFP expressing subline of MGH-U1R, produced in house by transfection with GFP [385].

Cell culture

Cell lines were cultured in 25 – 75cm^2 culture flasks. All cell lines were cultured in Dulbecco's Modified Eagle's Medium (DMEM) (Sigma, UK) supplemented with 10% foetal calf serum (FCS) and 2mM L-glutamine, and 100µg/ml of both penicillin / streptomycin solution (Both: Sigma, UK). Cultures were maintained in a humidified incubator with 5% CO_2 at 37^{o}C. Cells were passaged when 85% confluent. For passage, culture medium was tipped off and cells were washed twice with PBS. For 25 cm^2 flasks, ten drops of EDTA (Sigma, UK) and 3-4 drops of 1% trypsin-EDTA (Sigma, UK) were added to release cells. Release was hastened by incubation at 37^{o}C for 3-4 minutes. Ten millilitres of supplemented culture medium was added to neutralise trypsin activity. Cells were then aliquotted into new flasks containing 6.5mls of fresh culture medium. The number of flasks and the thickness of the passage was adjusted according to experimental requirements. Generally cells were passaged twice a week, for which 0.4 – 0.6mls of cell suspension were seeded into each new flask.

For confocal microscopy experiments adherent cells were sub-cultured in 40mm diameter culture grade polystyrene Petri dishes, before assay application (Nunc, UK for normal experiments and Orange Scientific, UK for microinjection experiments (shallower sides)).

Cell suspensions for flow cytometry experiments were achieved using the same technique as for cell passage, applied after cell exposure to the various drug regimes. Cells were then centrifuged in a Heraeus Labofuge® 400 at 438g (1500rpm) for 3 minutes, supernatant was poured off and the cells were resuspended in fresh culture medium, transferred to flow cytometry test tubes and placed on ice.

2.2: A guide to fluorescent probes

Various fluorescent probes or fluophores were used throughout this research.

Anthracyclines:

Epirubicin and idarubicin belong to the anthracycline antibiotic group of chemotherapeutic agents. They possess the property of autofluorescence which allows us to study their cellular uptake and distribution using a variety of fluorescence based techniques. These two drugs have similar excitation and emission spectra (see chapter 1.4), being excited maximally by laser light of 480nm wavelength resulting in maximal emission at a wavelength of 595nm (red).

Fluorescein Isothiocyanate (FITC)

FITC is a fluorescent molecule that can be attached to many different molecules to allow their study. During our research we used several FITC labelled molecules including dextrans, wheat germ agglutinin (WGA) and an antibody directed at P-gp. FITC is excited maximally by light of 495nm wavelength and has maximal emission at a wavelength of 520nm.

Fluorescein Diacetate (FDA):

FDA is a fluorescein probe and a viability stain. In viable cells, FDA undergoes hydrolysis by intracellular esterases in an ATP dependent reaction to form fluorescein, which fluoresces green. Fluorescein is excited maximally by laser light of 501nm wavelength, with maximal emission detected at a wavelength of 525nm.

Acridine Orange (AO):

AO is amongst other things, a marker of cell viability, staining the nuclei of viable cells green by complexing with DNA [387]. It has similar excitation characteristics to FITC, but its emissions are detected over a wider range of wavelengths extending into the orange-red spectrum. Maximal excitation is achieved by a laser of 502nm wavelength with maximal emission at a wavelength of 525nm.

Ethidium Bromide (EB):

EB is a DNA stain which can be used as quantitative DNA stain for analysis of cell cycle populations and also acts indirectly as a viability stain, where it stains the nuclei of dead cells orange [388]. EB fluorescence is excited

maximally by laser light of 520nm wavelength, with maximal emission detected at a wavelength of 604nm.

Propidium Iodide (PI):

PI is a DNA stain which again can be used for analysis of cell cycle populations and is also an indirect viability stain, staining the nuclei of dead cells red. Cell membrane integrity stops PI from staining viable and apoptotic cells. PI is excited maximally with laser light of 533nm wavelength, with maximal emission detected as a wavelength of 620nm.

2.3: Principles of confocal microscopy

Confocal microscopy differs from conventional light microscopy and fluorescence microscopy, in that it allows the collection of light exclusively from a single plane within the subject being studied.

A point light source produces a small, well-defined light spot in the focal plane. Emitted fluorescent light from the focal plane is collected by the objective lens and sent back through a beam splitter (Dichroic mirror), which directs it into a photomultiplier tube detector. A pinhole sitting parallel to the focal plane only allows light through to the detector from that particular plane, with light that is reflected or emitted from any other planes being kept from the detector (Figure 19).

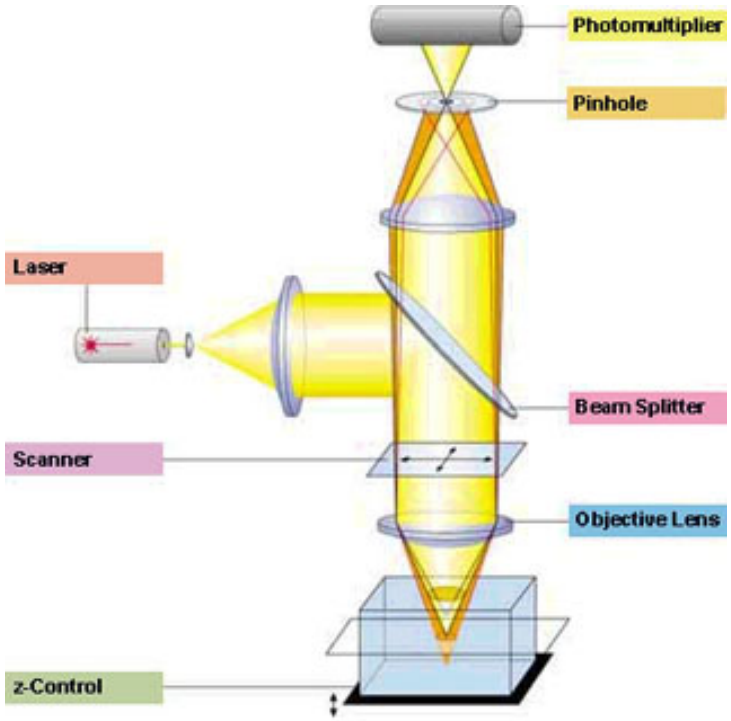

Figure 19: Schematic picture of confocal microscope showing how fluorescence is detected only from the plane that is focused through the confocal pinhole (Figure reproduced with the kind permission of Carl Zeiss)

Confocal microscopy is therefore able to produce optical sections of the specimen being studied that are always in focus. The thickness of the optical image slice is affected by the numerical aperture of the objective lens, the detector pinhole diameter and the excitation wavelength of the light used, with

thicker slices resulting in a less focused image akin to that produced by conventional fluorescence microscopy.

The laser scanning microscope scans the sample sequentially point by point and line by line and assembles the pixel information to form a single image. This allows optical slices of the specimen to be imaged with high contrast and high resolution in x, y and z axes. A pixel based image is displayed on a high resolution computer screen for the purposes of fluorescence intensity analysis and photographic image capture.

By moving the focal plane, single images or optical slices can be taken through the specimen, called a z-stack. These images can be digitally processed afterwards to create three dimensional images of the specimen.

Origin of fluorescence

Fluorescent molecules are called fluorochromes or fluophores. When these molecules are excited by laser light of a wavelength (Lex), certain electrons are excited to higher energy levels. During a very short dwell time these electrons lose some of their energy dropping back to their original level whilst emitting light of a longer wavelength (Lem). The emitted light always has a longer wavelength that the excitatory light wavelength (Lem > Lex), the difference between these wavelengths is known as the Stokes shift. In multiphoton excitation, the energies of several photons with n times the excitation wavelength add together to raise the electrons to the higher energy level (Figure 20).

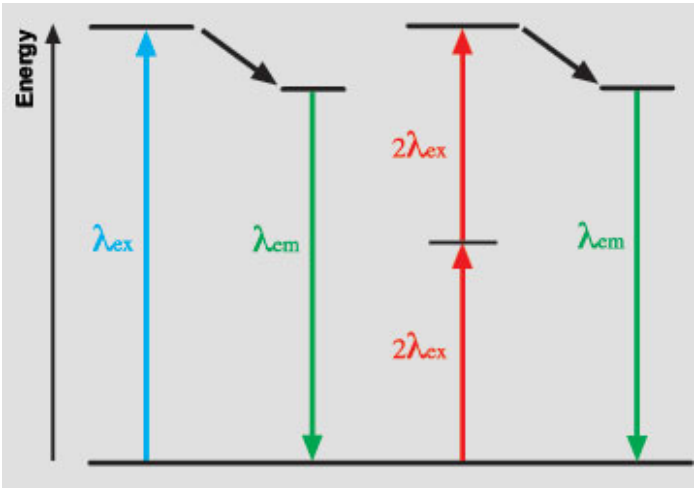

Figure 20: The origin of fluorescence (Figure reproduced with the kind permission of Carl Zeiss)

Fluorescence Spectra

A fluorescent molecule can be irradiated with different wavelengths within its excitation spectrum and, accordingly, will emit light with a characteristic emission spectrum. Its amplitude is determined by the intensity of radiation and the excitation efficiency, which is a function of the excitation wavelength (Figure 21).

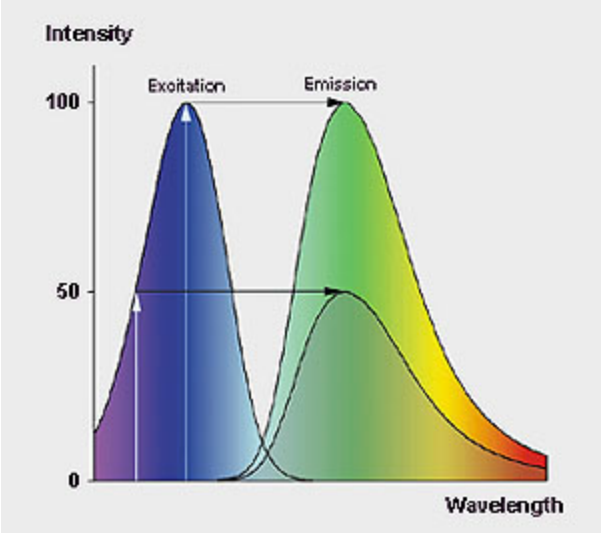

Figure 21: Fluorescence spectra (Figure reproduced with the kind permission of Carl Zeiss)

Zeiss LSM 510 Confocal Microscope

The Zeiss LSM 510 confocal microscope was used for visualisation of cells and nuclei in all confocal experiments

This microscope allows direct visualisation of cellular or nuclear fluorescence via a mercury vapour lamp fluorescence microscope, allowing detection of blue, green and red fluorescence. Once cells or nuclei exhibiting fluorescence have been identified they can then be viewed by confocal microscopy. Confocal microscopy allows direct imaging of the uptake and distribution of the various fluophores within the studied cells and nuclei with images being captured in digital format.

Lens Selection

The microscope has a selection of lenses, of which the x20 dry and x40 water immersion lens were most frequently used during image capture for our experiments. The x20 dry lens was used for experiments in which cells or nuclei were coverslipped, with the x40 water immersion lens being used for

visualisation of live cells. Using the immersion lens, cells can be visualised in various media from PBS to culture medium.

Time Series Function

The Zeiss LSM 510 confocal microscope also has a time series function which used in combination with the water immersion lens and culture medium containing HEPES buffering solution and our drug(s) of choice, allowed time series of drug uptake to be performed. This allows the study drug uptake and localisation in real time.

Image Optimisation

Confocal images were enhanced by optimising a number of factors that contribute to better images. Firstly the image was brought into sharp focus by focusing the specimen whilst in scanning mode. Whilst still in scanning mode the differential interference contrast (DIC) image was also focused to give a sharp image of the cells ultrastructural characteristics. The fluorescence gain and background were then finely tuned whilst in scanning mode to reduce all background interference and optimise the fluorescence gain to allow better definition of the fluophore localisation. Increasing the scanning time means that more time is spent scanning each pixel of the image, resulting in more detailed images. The image was then sharpened further by increasing the number of averages to either 8 or 16, meaning that each pixel was scanned 8 – 16 times and the average pixel count was included in the final image. The Zeiss LSM 510 also features digital zoom function allowing you to magnify a certain area of the cell or nucleus for a more detailed look. At the higher range of the digital zoom the image begins to pixelate slightly.

Laser Excitation Wavelegths

The Zeiss LSM confocal microscope features 3 different lasers, one Argon laser and two Helium-Neon (HeNe) lasers, each exciting different wavelengths. The Argon Laser is able to excite at 458, 488, 505 and 514nm. The HeNe1 laser excites at 543nm and the HeNe2 laser excites at 633nm. The laser used obviously depends on the excitation wavelength of the fluophore being used, although many fluophores can be excited by lasers of different wavelengths depending on their excitation spectra.

Emission Detection

Fluorescence emitted at the focal plane and at planes above and below is directed via an XY scanner onto a main dichroic beam splitter, which separates the emissions from the excitation light. The fluorescences are separated from each other by a series of dichroic beam splitters and directed to individual photomultipliers.

Up to four simultaneous image acquisition channels, usable for reflection or fluorescence, and an additional transmitted-light channel can be used for the investigation of specimens stained with multiple fluophores.

The emission filters can be changed for each of these four acquisitions channels. A variety of filters can be used to optimise fluorescence detection for the fluophore being used. Long pass (LP) filters will allow detection of all fluorescence above a certain wavelength (e.g. LP 560nm, means all fluorescence with a wavelength longer than 560nm will be collected) whilst band pass (BP) filters detect fluorescence between two wavelength values (e.g. BP 505 – 530nm, means fluorescence between 505nm and 530nm will be filtered exclusively).

Where samples stained with multiple fluophores are examined, identical optical sections are obtained for each confocal channel. This allows comparison of the cellular distribution of each fluophore within the same optical slice.

The microscope's transmitted-light channel is also equipped with a photomultiplier, allowing multiple fluorescence images to be superimposed on a brightfield, differential interference or phase image.

The laser excitation and emission wavelengths and filter settings for the various fluophores used in our experiments are listed below (Table 14).

Multitrack Mode

The multitrack scanning mode was used where more than one fluophore was being used. This mode excites one fluophore at a time by scanning the specimen with one excitation laser at a time. This reduces cross interference in the fluorescent signals of the fluophores resulting in clearer definition of the cellular localisation of the individual fluophores.

Fluophore	Excitation Wavelength (nm)	Emission Wavelength (nm)	Detection Filter Set used
Epirubicin	488 or 543	> 560	Rhodamine /Texas Red LP 560
Idarubicin	488 or 543	> 560	Rhodamine / Texas Red LP 560
Fluorescein-Isothiocyanate (FITC)	488	> 505	FITC LP 505 or BP 505 – 530
Fluorescein Diacetate (FDA)	488	> 505	FITC LP 505 or BP 505 – 530
Acridine Orange (AO)	488	> 505	FITC / Rhodamine / Texas Red LP 505 or BP 505 – 530
Ethidium Bromide (EB)	488 or 543	> 560	Rhodamine / Texas Red LP 560
Propidium Iodide (PI)	488 or 543	> 560	Rhodamine / Texas Red LP 560

Table 14: Confocal microscopy: Fluophore laser excitation wavelengths, fluorescence emission wavelengths and detection filter sets

Data analysis

Confocal microscopy was predominantly used to visualise the cellular or nuclear localisation of various fluophores within the specimens being studied. However, the Zeiss LSM 510 also allows semi-quantitative analysis of drug and fluophore uptake via its region of interest mode (ROI). This allows you to draw around a region of interest and the analysis software will then generate data on the area size and the fluorescence average per unit of area, for the area of interest.

It is important when capturing images of different samples that you wish to compare that you ensure that all image capture settings are the same including the laser wavelength used, laser power settings, fluorescence gain, scanning time, averages and zoom settings. Any difference in these settings will produce inaccurate results, meaning that direct comparisons between samples cannot be made. Within each sample, variation in the levels of fluorescence between optical slices can be marked. Comparisons between samples may also be biased by this interslice variation. Bleaching of

fluorescence levels can also occur with prolonged scan times, which may introduce further inter-sample variation. This is why confocal microscopy can only be regarded as semi-quantitative.

The ROI mode can also be used for time series data analysis allowing us to plot a graph of drug uptake in certain areas of the cell over time. Time series utilise cells as their own control comparing drug fluorescence with their baseline fluorescence without drug, which obviously gives a more accurate picture of the rate of drug uptake within certain cellular compartments. During time series experiments the samples are scanned many times which may result in some bleaching of the samples. This may account for some fluctuations in the fluorescence levels detected. Also, during time series cells do move around slightly so accurate placement of the ROI allowing for this movement is necessary. Some hyper-mobile cells are thus excluded from this type of analysis. This movement artefact may also account for some of the fluctuations in fluorescence levels throughout the time series. The ROI time series data once generated can be exported into an Excel database allowing more detailed analysis.

2.4: Principles of flow cytometry

Flow cytometry is a technique which permits rapid analysis of particles (cells, nuclei, chromosomes etc) in suspension. These particles are forced to flow in single file within a fluid sheath by a suitable hydrodynamic system. They are delivered to a fixed point where they intersect a beam of monochromatic laser light, when several optical parameters can be measured.

Measurement of Physical Characteristics of Cells

The light scattered by the particle in the forward direction (2-19^{o})(Forward scatter (FSC)) travels to the forward angle scatter detector and gives direct information about the size of the particle, increased scatter indicating increased size. Light that is scattered sideways (Side scatter (SSC)) due to collision with particular contents is detected at 90^{o} to the laser and provides a measure of the granularity, increased scatter indicating increased granularity. These two parameters can give us an idea of the morphology of the particles we are looking at. Using these parameters and adjusting the forward and side scatter detectors we are able spread our particle population on scatter plots (Figure 22).

Gating of live cell populations

For experiment purposes it is important to only examine drug uptake or fluorescence within a population of viable individual cells, as clumps of cell with more fluorescence or debris particles with less fluorescence would skew our results.

Using FDA fluorescence as a marker of viability, we were able to determine the FSC – SSC dot plot characteristics of our viable individual cell population for each cell type. We could then gate out the viable individual cell population for each cell type for subsequent fluorescence data collection and analysis. In addition we set the FSC threshold at 200 to exclude any smaller particles of debris from fluorescence detection (Figure 22).

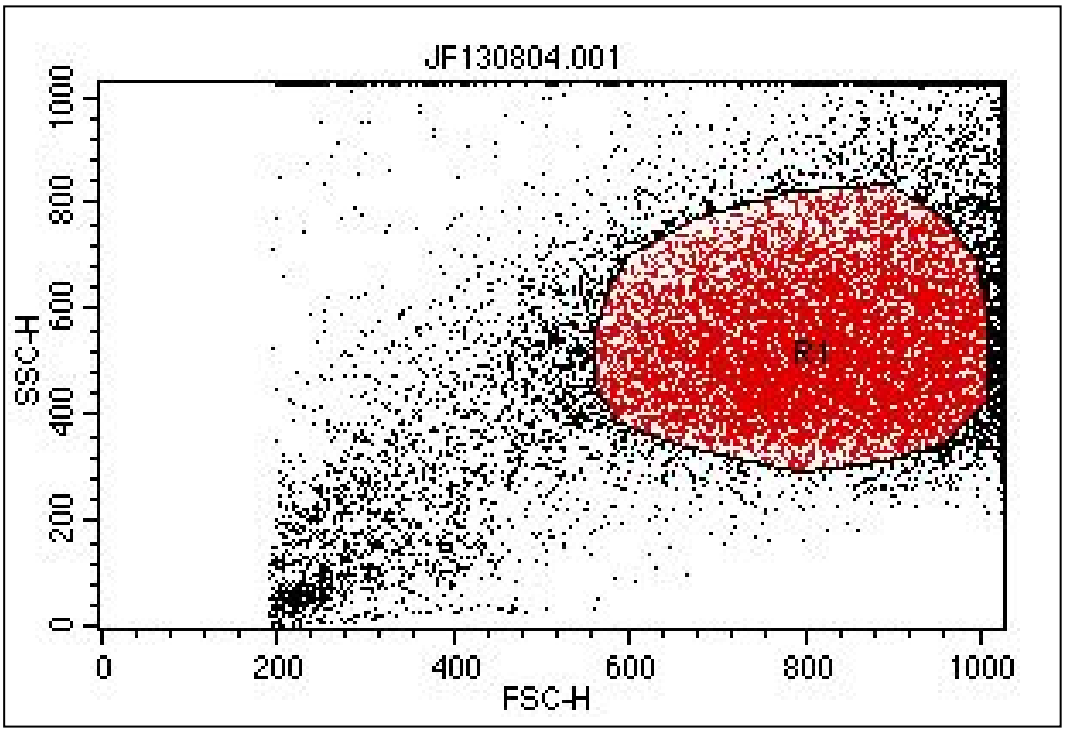

Figure 22: A scatter plot showing cells plotted according to their side scatter (SSC) and forward scatter (FSC) characteristics. Live cells have been gated in region1 (R1) (Red)

Measurement of Fluorescent Events

Three other photomultiplier detectors are also present within the system. These are used to detect fluorescent emissions. Each detector works within a specified range; FL-1 (530nm +/- 15), FL-2 (585nm +/- 15) and FL-3 (>650nm). Different wavelengths of emitted light from particles that are carrying more than one type of fluorescent molecule (acting as a marker or probe) can be detected simultaneously (Figure 23).

FL-1 detects light in the green part of the visual spectrum (515 – 545nm), FL-2 detects light in the orange – near red part of the visual spectrum (570 – 600nm) and FL-3 detect light in the far red part of the spectrum (>650nm). Fluorescent signals and scattered light signals pass through lenses and are focused onto photomultiplier detectors. The photomultipliers convert the signals into electric signals which vary according to the amount of fluorescence or scatter detected.

The measurements that take place are performed on each separate particle within the suspension and are not just an average value for the whole population.

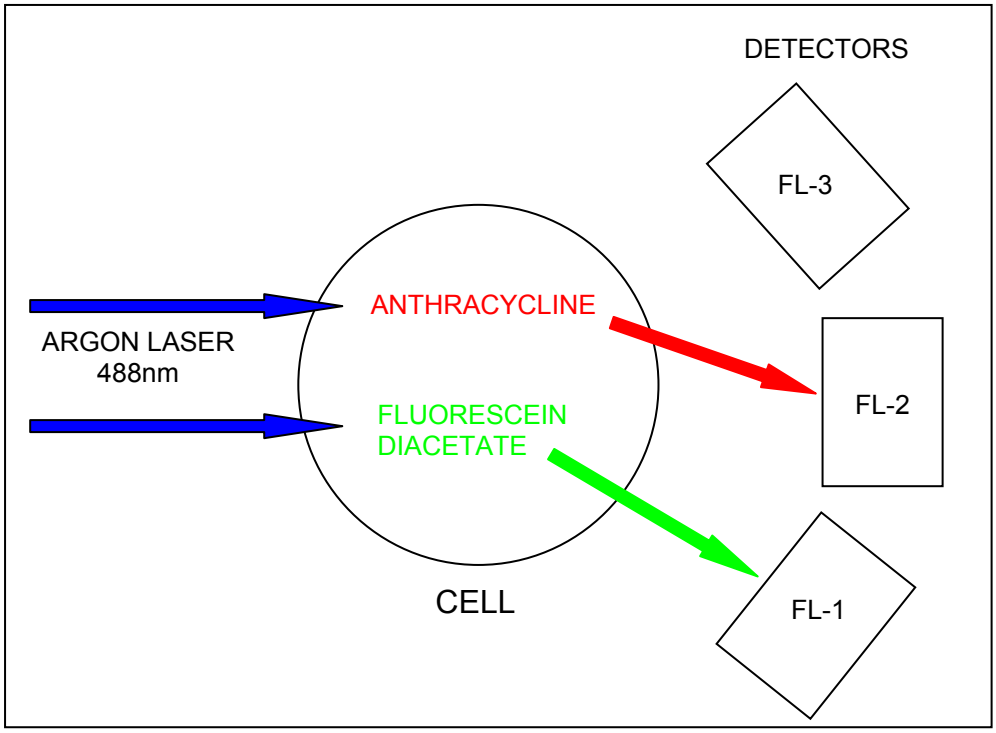

Figure 23: Measurement of simultaneous fluorescent events

Flow cytometry allows large numbers of particles to be assessed very rapidly, with typical sample sizes being between 10,000 and 20,000 cells.

The applications of flow cytometry are numerous. A wide range of fluorescent probes are available for direct estimation of cellular parameters such as nucleic acid content, enzyme activity, calcium flux, membrane potential and pH. Conjugation of fluorescent dyes to ligands and to mono- and polyclonal antibodies has enabled the density and distribution of cell surface and cytoplasmic determinants and receptors to be studied and functional subpopulations of cells to be identified.

Flow cytometry has many advantages over older techniques since it is capable of analysing enormous numbers of cells very quickly; it is also able to monitor drug retention in individual cells allowing it to demonstrate the concept of heterogeneity, meaning, some cells may take up and concentrate more of the drug than other cells within the same tumour. One problem of flow cytometry is that some anthracyclines quench their fluorescence on binding to DNA or other target molecules, so-called drug quenching.

The laser excitation and emission wavelengths and filter settings for the various fluophores used in our flow cytometry experiments are listed below (Table 15).

Fluophore	**Excitation Wavelength (nm)**	**Emission Detector (Wavelength (nm))**
Epirubicin	488	FL-2 (585 +/- 15)
Idarubicin	488	FL-2 (585 +/- 15)
Fluorescein-Isothiocyanate (FITC)	488	FL-1 (530 +/- 15)
Fluorescein Diacetate (FDA)	488	FL-1 (530 +/- 15)
Acridine Orange (AO)	488	FL-1 (530 +/- 15)
Ethidium Bromide (EB)	488	FL-2 (585 +/- 15)
Propidium Iodide (PI)	88	FL-2 (585 +/- 15)

Table 15: Flow cytometry: Fluophore laser excitation wavelengths, fluorescence emission wavelengths and detection filter sets

Explanation of Data Display and Analysis

The electrical pulses generated by all of the photomultiplier detectors are then amplified, measured, computerised and displayed. The display data is a record of the photon signal emitted translated as a voltage signal.

The result of analogue to digital conversion is a steam of numbers which can be printed or held in computer memory or on mass storage devices.

The most common and useful forms of data display are the frequency histogram and the dual parameter dot plot.

The frequency histogram is a direct graphical representation of the number of events occurring for each channel or number of events plotted against fluorescence intensity (on a logarithmic scale) (Figure 24).

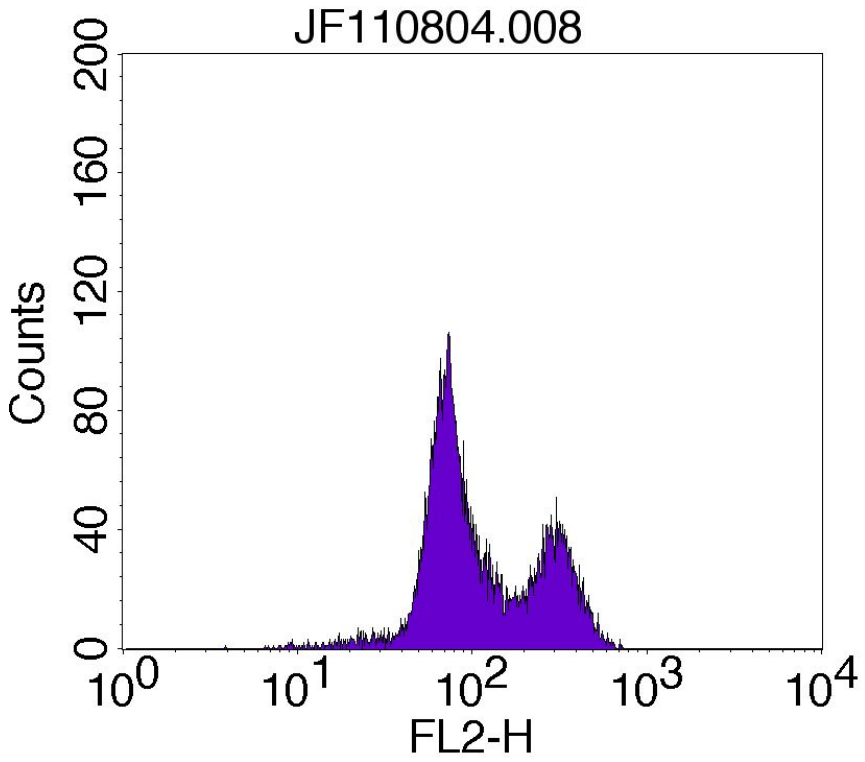

Figure 24: A frequency histogram, plotting number of events against FL-2 fluorescence intensity (logarithmic scale)

The dot plot is a two-dimensional extension of the frequency histogram. In this case, the channels of one detector are correlated against another, for example, side scatter against forward scatter. This produces a plot where each cell is represented at the coordinates appropriate to the measured values (Figure 22).

Gating can be undertaken on any of these plots to examine sub-populations of interest in more detail.

Statistics are also generated for each sample run including mean, geomean and median fluorescence, standard deviations, peak fluorescence and peak channel of fluorescence. As such large numbers of particles are analysed any difference between samples treated in the same way is likely to be significant.

The flow cytometer we used for our experiments was a Becton Dickinson FACScaliber flow cytometer.

2.5: Principles of microinjection

Microinjection allows direct injection of substances, whether they be drugs, fluophores or labelled-antibodies, either into the cell cytoplasm or nucleus. Many of these substances have difficulties in overcoming the plasma membrane barrier due to their size or their lipophobicity or because their molecular charges exclude them. Multidrug resistant cancer cells also exclude many cytotoxic drugs because they express a plasma membrane glycoprotein efflux pump, P-glycoprotein, that actively effluxes these drugs. Microinjection provides a novel technique for studying the intracellular localisation of many of the above mentioned molecules, as direct microinjection into cell cytoplasm overcomes the plasma membrane barrier in all instances.

Equipment for Microinjection

Microinjection was performed using an Eppendorf InjectMan® NI 2 micromanipulator combined with an Eppendorf Femtojet microinjector. The micromanipulator is mounted on a Zeiss Axiovert 200 microscope. Pre-drawn capillaries with a tip diameter of 0.5µm were used for microinjection (Femtotip®/Femtotip®II, Eppendorf). The Femtojet system allows the pressure of injection (150KPa), time of injection (0.5 sec) and background pressure (50KPa - to counteract capillarity) to be set, in order to control the amount injected. There are variations in how well the capillaries breach the cell membrane, hence the amount of drug injected cannot be accurately quantified and can vary significantly between cells.

The injection buffer used was 48mM K_2HPO_4, 4.5mM KH_2PO_4, 14mM NaH_2PO_4, pH 7.2 (Eppendorf - personal communication). All injection fluids were mixed in eppendorf tubes and then centrifuged at 16000g (13000rpm) for 3 minutes in a Heraeus Biofuge *pico* centrifuge, before transfer into capillaries, to ensure that any particles were separated from the injection liquid. Injection fluid was pipetted into capillaries using Eppendorf Microloaders, taking care not to stir up any precipitate.

Technique for microinjection of cells

Cells were cultured in 40mm low-sided Petri dishes (Orange scientific, UK) for 2 – 3 days to allow cells to become fully adherent. Cell culture media was changed prior to microinjection to HEPES buffered culture medium (1:25

HEPES buffer solution) (Sigma, UK), to keep cells adequately buffered whilst out of the incubator. Cells were microinjected at ambient temperature (18 – 20^{o}C). Cells were placed on the microscope mounting stage and viewed using the x40 objective lens. The focus was then altered to bring the loaded microinjection capillary into view. The capillary was then lowered under direct visualisation until the cells were also in focus. The capillary was then lowered onto a cell until an indentation in the plasma membrane could be clearly seen. This indentation of the plasma membrane was usually accompanied by a slight swelling of the cell, associated with membrane breach and some leakage of the capillary into the cell, as a result of the back pressure against capillary action. The depth of injection was then fixed at this depth. The capillary could then be moved around the Petri using a joystick to control the mechanically driven capillary holder. The capillary was moved until it lay over individual cells and then the microinjection button (Joystick mounted) was depressed to deliver a single, semi-automatic intracytoplasmic injection under direct visualisation. The cell can be seen to swell during injection. This process was repeated until a sufficient number of cells had been injected. The cells were then placed into an incubator to recover before visualisation under a confocal microscope.

2.6: Principles of Cytotoxicity Assay

The differences in cellular and nuclear uptake of cytotoxic drugs are meaningless without evidence linking these to differences in cellular cytotoxicity. It is therefore important to study not only drug uptake and localisation within cells, but also to measure drug cytotoxicity directly by means of cytotoxicity assay. Cytotoxicity assays also allow *in vitro* testing of potential MDR reversing agents.

The MTT (3-(4,5-dimethylthlazol-2-yl)-2,5-diphenyltetrazolium) assay is a widely used cytotoxicity assay [389]. It is a colorimetric dye assay based on the ability of viable cells to reduce MTT to a purple formazan dye.

Cells are exposed to various drugs or drug combinations in 96-well plates. Following a period of cell recovery and when control wells have reached 90 percent confluence, MTT is added to each well and the plates are cultured for a further 3 – 4 hours. Viable cells will then metabolise MTT into purple formazan dye crystals. These crystals are dissolved by the addition of dimethyl sulphoxide (DMSO), forming a purple liquid. The optical density of this purple liquid can then be analysed on a photometric well-plate reader, which correlates directly with the residual viable biomass of each well.

Data can be transferred from the well-plate reader to a spreadsheet allowing the mean percentage viable cellular biomass to be calculated for each drug dilution compared to control wells. Cytotoxicity curves can then be plotted to include 95% confidence intervals. The IC50 value which is the concentration of the drug required to inhibit cell growth by 50%, can then be calculated from the cytotoxicity curve.

2.7: Specific experiments

2.71: Confocal Experiments

Anthracycline incubation studies: Establishing cell phenotypes

Epirubicin and Idarubicin uptake at 37°C:

Cells were cultured in 40mm Petri dishes until 75 – 100% confluent. Cells were then exposed to either epirubicin or idarubicin at a concentration of 10µg/ml in HEPES buffered medium (1:100 HEPES) for 2 hours at 37°C. Culture medium was then pipetted off and replaced with PBS. Fluorescein diacetate (FDA), a viability stain, was added to the PBS to a final concentration of 500ng/ml. Cells were then viewed on the con-focal microscope to assess the drug uptake and accumulation characteristics of viable cells.

Epirubicin and Idarubicin uptake at 0 – 4°C:

Cells were cultured in 40mm Petri dishes until 75-100% confluent. Cells were then exposed to either epirubicin or idarubicin at a concentration of 10µg/ml in HEPES buffered medium (1:100 HEPES) for 60 minutes and placed on ice in a fridge (0 – 4°C). Culture medium was then pipetted off and replaced with ice-cold PBS. FDA, a viability stain, was added to the PBS to a final concentration of 500ng/ml. Cells were then viewed on the con-focal microscope to assess the drug uptake and accumulation characteristics of viable cells.

Epirubicin and Idarubicin uptake in dead cells at 37°C:

Cells were cultured in 40mm Petri dishes until 75-100% confluent. Cells were then killed by microwaving them in a 650W oven for 10 seconds on 100% power. Cells were then exposed to either epirubicin or idarubicin at a concentration of 10µg/ml in HEPES buffered medium (1:100 HEPES) for 60 minutes at 37°C. Culture medium was then pipetted off and replaced with PBS. Cells were then viewed on the con-focal microscope to assess the drug uptake and accumulation characteristics of non-viable cells. Viability stains were then added, either FDA to a concentration of 500ng/ml or ethidium bromide (EB) to a final concentration of 10µg/ml. Cell death was confirmed by lack of FDA fluorescence or the presence of EB nuclear staining.

Anthracycline incubation studies: Uptake in isolated nuclei

Epirubicin and Idarubicin uptake at 37°C:

Nuclear epirubicin and idarubicin uptake was assessed in nuclei harvested from whole cells that had been pre-exposed to these drugs and prepared nuclei that were exposed to drug immediately following extraction from cells. For pre-exposed cell nuclei, cells were cultured to confluence and then incubated with epirubicin 10µg/ml or idarubicin 20µg/ml for 2 hours at 37°C. Nuclear preparations were then prepared according to an established protocol [390] (Appendix 1). Nuclei were re-suspended in PBS containing protease- and phosphatase-inhibitors (PBSI), dropped onto microscope slides and cover-slipped. They were then visualised on the confocal microscope.

For experiments looking at direct nuclear exposure to drug, nuclear preparations were performed according to a standardised protocol (Appendix 1). Nuclei were then exposed to either epirubicin 10µg/ml or idarubicin 20µg/ml in cultured medium for 10 minutes at 37°C. Nuclei were centrifuged at 800g for 5 minutes and the drug was then pipetted off and replaced with PBSI. Nuclei were resuspended, dropped onto microscope slides and cover-slipped. Con-focal microscopy was then used to assess drug uptake in these nuclei.

Mitomycin C fluorescence

Several attempts were made to see if we could elicit fluorescence from Mitomycin C. Mitomycin C is a similar molecule to the anthracyclines, with a three ring structure, suggesting that it might fluoresce.

MGH-U1 and MGH-U1R cells were cultured in 40mm Petri dishes until 75-100% confluent and then used for the following experiments.

Direct fluorescence experiments:

Dose response:

Cells were then either exposed to mitomycin C at various concentrations from 100, 250 and 1000µg/ml in HEPES buffered medium (1:100 HEPES) for 60 minutes at 37°C. Culture medium was then pipetted off and replaced with PBS. Cells were then viewed on the con-focal microscope in an attempt to assess the drug uptake and accumulation characteristics of viable cells compared to unexposed control cells. Laser excitation was performed using

458, 488, 505, 514, 543, 633nm wavelengths with appropriate filter and detector settings.

Time series:

For time series experiments culture medium was replaced with HEPES buffered medium (1:100 HEPES). Cells were then viewed on the confocal microscope and baseline fluorescence was assessed. As soon as the time series had been started mitomycin C was added to a concentration of 250mcg/ml. Time series was performed looking at FITC fluorescence in response to excitation at 488nm. The gain setting was fixed at 900.

Indirect fluorescence experiments:

Cells were then either exposed to mitomycin C at concentrations of 250 and 1000µg/ml in HEPES buffered medium (1:100 HEPES) for 60 minutes at 37^{o}C. Culture medium was then pipetted off and replaced with PBS. Acridine orange was then added to a final concentration of 3µg/ml. Mitomycin C is said to bind to the same DNA sites as acridine orange, meaning that any reduction in nuclear uptake of AO can be assessed by con-focal microscopy as an indirect measure of nuclear mitomycin uptake, by comparing unexposed cells with mitomycin C exposed cells. The FITC confocal filter settings were used to detect nuclear uptake of AO. Analysis was then undertaken by measuring nuclear fluorescence using a region of interest function for all evaluable nuclei within each sample to prevent any selection bias.

Wheat Germ Agglutinin (WGA) nuclear pore binding studies

FITC-WGA cellular localisation studies:

The cytotoxicity of WGA (Triticum Vulgaris Lectin) (Sigma, UK) was assessed using a standard MTT assay (See cytotoxicity experiments). A dose of 0.4µg/ml was found to be minimally cytotoxic to cells in its own right. Cells were cultured in 40mm Petri dishes until 50% confluent. Cells were then incubated with FITC-WGA (Sigma) 0.4µg/ml in culture medium at 37^{o}C for exposures of 1 hour or 24 hours continuous exposure. Following 1 hour exposures the culture medium was changed to fresh medium and cells were then incubated for various times in order to establish the optimum time of WGA localisation to the nuclear membrane. The time intervals assessed in this experiment were 30 minutes, 1, 2, 4, 8, 16, 24, 48 hours. After incubation

culture medium was discarded and replaced by PBS and the cellular localisation of FITC-WGA was visualised using con-focal microscopy.

FITC-WGA nuclear localisation studies:

Nuclear pore binding was assessed using nuclear preparations produced by a proven method (Appendix 1). Nuclear preparations were then incubated with FITC-WGA (Sigma) 0.4µg/ml in culture medium at 37^{o}C for 10 minutes. Nuclei were then centrifuged at 800g (2000rpm) for five minutes and the FITC-WGA containing medium was removed. Nuclei were then covered with 0.5ml PBSI and resuspended. The nuclear suspension was then dropped onto a slide and coverslipped. Nuclei were viewed on the confocal microscope to visualise FITC-WGA localisation.

Nuclear pore sizing using FITC-dextrans and the effects of WGA nuclear pore blockade:

MGH-U1 and MGH-U1R cells were cultured in 25cm^2 flasks until 90% confluent. One flask of each cell type had been pre-incubated with WGA 0.4µg/ml in culture medium at 37^{o}C for 24 hours. Scrape-loading of cells with various sized FITC-dextrans was then performed according to an established protocol [391] (Appendix 2). The sizes of FITC-dextrans used were 4.4, 19.5, 42 and 77 kilodaltons (KDa) (Sigma, UK). The pre-exposed WGA cells were scrape-loaded with 19.5KDa FITC-dextran. Once scape-loaded cells were centrifuged at 438g (1500rpm) for 3 minutes and the medium was pipetted off. Cells were re-suspended in fresh medium and plated out in 40mm Petri dishes. Cellular localisation of the various sized FITC-dextrans was visualised using confocal microscopy. Cells were viewed at several different time points to allow cells to become adherent, as well as to assess any changes in cellular localisation over time. The time points at which cells were visualised were 6, 18, 24, 48 and 72 hours.

The effects of WGA pre-incubation on nuclear uptake of epirubicin

Whole cells

MGH-U1 and MGH-U1-R cells were cultured in 40mm Petri dishes and allowed to settle for 24 hours. Cells were then incubated with 0.2µg/ml WGA for 1 hour at 37^{o}C. Cells were then incubated for a further 23 hours to allow WGA to redistribute to the nuclear membrane and then incubated with

epirubicin 10µg/ml for 1 hour at 37^{o}C. Cells were covered with PBS and viewed by confocal microscopy.

Nuclei

MGH-U1 and MGH-U1-R cells were cultured in 25cm^2 flasks until 75-80% confluent. Cells were then cultured in 0.4µg/ml WGA for 24 hours at 37^{o}C. Cells were then either exposed to epirubicin 10µg/ml for 2 hours at 37^{o}C followed by nuclear fractionation or nuclear fractionation was performed and cells were then exposed to epirubicin 10µg/ml for 10 minutes at 37^{o}C. Nuclear preparations were then suspended in PBSI, dropped onto slides, coverslipped and viewed by confocal microscopy using a x20 lens, to assess nuclear uptake of epirubicin post-WGA exposure.

Cell fusion experiments using polyethylene glycol (PEG):

Fusion of cells in suspension using polyethylene glycol (PEG) has previously been described, enabling production of larger multinucleate cells [392]. We modified and optimised this technique to allow fusion of adherent cells (Appendix 3).

For cell fusion experiments, MGH-U1 and MGH-U1-R cells were harvested and cell density was adjusted to 5 x 10^4 cells/ml. Cells were then seeded into 40mm Petri dishes (Nunc, UK), either as single cell cultures, 1.5mls per Petri dish, or as mixed cultures, 0.75ml of each cell type per Petri dish. In an attempt to determine whether any mixed fusions had taken place, in some experiments either the MGH-U1 or MGH-U1-R cells were grown as a single cell culture (0.75ml with 0.75ml culture medium added) and after 24hrs were exposed to FITC-Wheat Germ Agglutinin (FITC-WGA) (Sigma, UK) 0.4µg/ml in culture medium for 24 hours in normal culture conditions. The FITC-WGA was then removed, cells were washed with PBS and 1.5mls of 5 x 10^4 cells/ml of the opposite cell type were added and incubated for a further 24 hours. Wheat germ agglutinin (WGA) is a lectin from *triticum vulgaris*, that binds selectively to nuclear membrane pores. It allows us to identify one type of nucleus and hence recognise any mixed cell fusions with phenotypically different FITC-WGA staining nuclei, more easily.

Cells were grown to confluence (approximately 48-72 hours in total) and then cell fusion using polyethylene glycol 50% w/v (Sigma, UK) was performed.

Protocol for cell fusion using polyethylene glycol (PEG)

The optimal method for cell fusion was as follows. Culture medium was pipetted off the cells and they were covered with 0.5mls of polyethylene glycol (PEG) 50%w/v (Sigma). The cells were exposed to PEG for 5 minutes, with gentle agitation of the Petri dishes. PEG was then serially diluted off using fresh culture medium over 1 minute. This medium was then discarded and the cells were re-covered with 1.5mls of fresh medium. Cell fusions were then incubated for 2 hours in normal culture conditions to allow the fusions to complete and recover.

Cells were then exposed to epirubicin 10µg/ml in culture medium at 37^{o}C for 60 minutes. Epirubicin was pipetted off and cells were covered with PBS. FDA was added to a concentration of 500ng/ml after initial visualisation, in order to assess cell fusion viability.

Metaphase arrest experiments

Cells were plated out in 40mm Petri dishes, 1.5mls of 1 x 10^5 cells/ml cell suspension per dish. Cells were cultured for 24 hours, allowing them to get established and commence log-phase cell growth. They were then subjected to the following metaphase arrest protocol.

Protocol for metaphase arrest

Culture medium was changed to include demecolcine 0.05µg/ml and cells were incubated overnight to allow metaphase arrest to occur (Approximately 16-24 hours).

Once this time had passed we exposed our metaphase arrested cells to either epirubicin or idarubicin at a concentration of 10 – 20 µg/ml in culture medium for 60 minutes at 37^{o}C. In later experiments higher concentrations of epirubicin were used (20 – 80µg/ml) to see if this would have any effect on chromosome staining.

The drug was then pipetted off and cells were covered with 4mls of phosphate buffered saline (PBS). Cell metaphases were then identified by direct fluorescence microscopy followed by confocal microscopy. In our initial experiments fluorescein diacetate (FDA) was added to a final concentration of 500ng/ml, to assess cell viability. In later experiments cells were visualised and then acridine orange was added to a final concentration of 3µg/ml, in

order to visualise chromosomes in metaphase cells not stained by epirubicin or idarubicin.

Confocal Time Series Experiments

Confocal time series experiments were performed using drug-sensitive MGH-U1 and RT112 cell lines and multidrug resistant (MDR) variants MGH-U1R and MGHU-MMC. For confocal time series experiments, cells were harvested using trypsin-EDTA (Sigma, UK) and cell density was adjusted to 1×10^5 cells/ml. Cells were sub-cultured in 40mm Petri dishes (Nunc, UK). Cells were grown to 90-95% confluence (approximately 48 hours) and then used for time series incubation experiments.

For time series the culture medium was changed to DMEM HEPES modification (containing 25mM HEPES buffering solution, Cat No. D6171, Sigma, UK). This HEPES containing medium buffers the cells whilst incubated on the heated stage and also controls the pH of the medium as this has been shown to affect epirubicin uptake [199].

Cells were placed on the Zeiss LSM 510 confocal microscope and incubated on the heated stage at 37^{o}C throughout each time series. Samples were allowed 15 minutes to acclimatise before time series were started. Cells were then visualised through a x40 water immersion lens. Using the differential interference contrast (DIC) image in scanning mode, a Z-stack was set up to take 6 image slices through each cell sample. As there is no cellular fluorescence initially, taking slices at 6 levels through our cells gave the best chance of capturing cell fluorescence during our time series, the level of maximum fluorescence capture was then used for subsequent analysis. The time series was set to take images every 2 minutes for 120 minutes.

Cell samples were exposed to various drug regimes as set out below. Drug concentrations represent their final concentrations in the HEPES medium.

1. Epirubicin 10μg/ml
2. Epirubicin 10μg/ml combined with verapamil 100μg/ml

The time series was commenced and the drugs were then added, meaning that baseline fluorescence for each cell was recorded, so they acted as their own controls. Experiments were repeated twice for each cell type.

Epirubicin fluorescence was excited by the 543nm HeNe laser and emission of wavelengths of 560nm and greater (red) were detected. The laser power

was fixed at 50.5% and gain setting was fixed at 1250 throughout all time series. Standardisation of all fluorescence excitation characteristics meant that we could directly compare the fluorescence – time curves of the different cell lines for samples with and without verapamil.
Fluorescein diacetate (FDA) was added at the end of the time series to confirm viability in our cell samples.

Confocal Time Series Data Analysis

Analysis of epirubicin uptake during our confocal time series was performed using the region of interest (ROI) mode. Regions of interest were drawn within the nuclei and cytoplasm of 20 cells from each sample and fluorescence uptake measurements were generated. During time series some cells were quite mobile, so care was taken to place the ROIs over areas of the cells that were static for the duration of the time series. The data from the ROIs were exported and analysed using Microsoft Excel, producing graphs of mean fluorescence over time with 95% confidence intervals, for each cell type. The differences in epirubicin uptake between cell lines incubated with and without verapamil were then analysed.

Cellular staining of P-gp using a FITC conjugated Anti-P-gp antibody (17F9, BD Biosciences):

MGH-U1, RT112, MGH-U1R and MGHU-MMC cells were grown in 40mm Petri dishes until confluent. Cells were then exposed to either Hanks Balanced Salt Solution (HBSS) with 1% Bovine Serum Albumin (BSA) or HBSS with 1% BSA and 20µl/ml of FITC labeled anti-P-gp antibody, 17F9 (BD Biosciences, UK) for 20 minutes at room temperature in a dark room.
The medium was then pipetted off and cells were recovered with PBS and placed on ice. Cells were then viewed on the confocal microscope using FITC laser and filter settings.

Nuclear P-gp staining with a FITC conjugated Anti-P-gp antibody (17F9, BD Biosciences):

MGH-U1 and MGH-U1R cells were grown in 25cm^2 flasks until confluent. Nuclear fractionation was then performed as per standardised protocol (Appendix 1). Nuclei were then exposed to HBSS with 1% BSA and 20µl/ml of FITC labeled anti-P-gp antibody, 17F9 (BD, Biosciences) for 20 minutes at room temperature in a dark room. Nuclei were then dropped onto a slide and

coverslipped. They were then viewed by confocal microscopy using FITC laser and filter settings.

Membrane Leakiness Studies using FITC-dextrans:

MGH-U1 and MGH-U1R cells cultured in 40mm Petri dishes until confluent. Cells then killed by microwaving them in a 650W oven for 10 seconds on 100% power. Cells then exposed to 77KDa FITC-dextrans in PBS for 30 minutes at 37^{o}C. Cells then viewed by confocal microscopy to establish the cellular localisation of FITC-dextrans in dead cells.

Green Fluorescent Protein cell line experiments:

Two Green fluorescent protein (GFP) cell lines had previously been established in our research unit. We assessed the purity of frozen cultures (Appendix 7) and the MDR characteristics of these cells after being frozen at -180^{o}C. We also assessed the potential of using GFP as a viability marker.

GFP cells – epirubicin uptake characteristics:

MGH-U1-GFP and MGH-U1R-GFP cells were cultured in 40mm Petri dishes until 75 – 100% confluent. Cells were then exposed to epirubicin at a concentration of 10µg/ml in HEPES buffered medium (1:100 HEPES) for 2 hours at 37^{o}C. Culture medium was then pipetted off and replaced with PBS. Cells were then viewed on the con-focal microscope to assess the drug uptake and accumulation characteristics of viable cells.

Assessment of GFP as viability marker using time-lapse confocal microscopy:

MGH-U1-GFP and MGH-U1R-GFP cells were cultured in 40mm Petri dishes until 75 – 100% confluent.

Cell media was changed to DMEM HEPES buffered culture medium (containing 25mM HEPES buffer solution (Sigma, UK)). Cells were then placed on the heated stage of the confocal microscope at 37^{o}C. Cells exhibiting GFP fluorescence were visualised and confocal images were taken. Propidium iodide (PI) 50µg/ml was added to the medium to confirm cell viability (excluded from nuclei of viable cells). A time series was then commenced at 1 minute intervals looking at both green (GFP) and Red (PI) fluorescence. Several drops of glutaraldehyde were then added to kill the cells. Time series were continued until cell death was confirmed by nuclear PI

uptake. It was necessary to perform a z-stack time series as the level of maximum GFP fluorescence was different to the level of nuclear PI fluorescence.

A control time series experiment was performed looking at viable MGH-U1-GFP cells to confirm that any reduction in GFP fluorescence over time was not caused by fluorescence bleaching.

2.72: Flow cytometry experiments

Epirubicin Dose Response:

MGH-U1 and MGH-U1R cells were grown in 25cm^2 flasks until confluent. Cells were then exposed to various concentrations of epirubicin in culture medium supplemented with 1:100 HEPES medium at 37^{o}C for 120 minutes. The concentrations used were 1, 2.5, 5, 10, 20, 40 and 80µg/ml. A control sample was also performed for each cell type. Following incubation drug was immediately tipped off and cells were washed 3 times with ice-cold PBS. Cells were then harvested using trypsin-EDTA and transferred into centrifuge tubes. They were then centrifuged at 438g (1500rpm) for 3 minutes and the supernatant was discarded. The cell pellet was resuspended in 1ml of ice-cold HEPES buffered medium and the cells were placed on ice. Cells were then transferred into flow tubes and analysed on a FACScaliber flow cytometer (Becton Dickinson). Epirubicin fluorescence was excited using the Argon 488nm laser and emissions were detected with the FL-2 detector (585nm +/- 15). Experiments were repeated twice to confirm results.

Idarubicin Dose Response:

MGH-U1 and MGH-U1R cells were grown in 25cm^2 flasks until confluent. Cells were then exposed to various concentrations of idarubicin in culture medium supplemented with 1:100 HEPES medium at 37^{o}C for 120 minutes. The concentrations used were 1, 2.5, 5, 10, 20, 40 and 80µg/ml. A control sample was also performed for each cell type. Following incubation drug was immediately tipped off and cells were washed 3 times with ice-cold PBS. Cells were then harvested using trypsin-EDTA and transferred into centrifuge tubes. They were then centrifuged at 438g (1500rpm) for 3 minutes and the supernatant was discarded. The cell pellet was resuspended in 1ml of ice-cold HEPES buffered medium and the cells were placed on ice. Cells were then transferred into flow tubes and analysed on a FACScaliber flow

cytometer (Becton Dickinson). Idarubicin fluorescence was excited using the Argon 488nm laser and emissions were detected with the FL-2 detector (585nm +/- 15). Experiments were repeated twice to confirm results.

Effects of WGA pre-incubation on Cellular Epirubicin Dose Response:

MGH-U1 and MGH-U1R cells were grown in 25cm^2 flasks until 75-80% confluent. Cells for WGA pre-incubation were then exposed to WGA 0.2µg/ml for 24 hours at 37^{o}C. Control cells (no WGA pre-incubation) were left in standard CM. Cells were then exposed to various concentrations of epirubicin in culture medium supplemented with 1:100 HEPES medium at 37^{o}C for 120 minutes. The concentrations used were 1, 2.5, 5, 10, 20, 40 and 80µg/ml. A control sample was also performed for each cell type. Following incubation drug was immediately tipped off and cells were washed 3 times with ice-cold PBS. Cells were then harvested using trypsin-EDTA and transferred into centrifuge tubes. They were then centrifuged at 438g (1500rpm) for 3 minutes and the supernatant was discarded. The cell pellet was resuspended in 1ml of ice-cold HEPES buffered medium and the cells were placed on ice. Cells were then transferred into flow tubes and analysed on a FACScaliber flow cytometer (Becton Dickinson). Epirubicin fluorescence was excited using the Argon 488nm laser and emissions were detected with the FL-2 detector (585nm +/- 15).

Effects of WGA pre-incubation on Nuclear Epirubicin Dose Response:

MGH-U1 and MGH-U1R cells were grown in 60mm Petri dishes until 75-80% confluent. Cells for WGA pre-incubation were then exposed to WGA 0.2µg/ml for 24 hours at 37^{o}C. Control cells (no WGA pre-incubation) were left in standard CM. Cells were then exposed to various concentrations of epirubicin in culture medium supplemented with 1:100 HEPES medium at 37^{o}C for 120 minutes. The concentrations used were 1, 2.5, 5, 10, 20, 40 and 80µg/ml. A control sample was also performed for each cell type. Following incubation drug was immediately tipped off and cells were washed 3 times with ice-cold PBSI. Nuclear fractionation was then performed as per protocol (Appendix 1). The nuclear pellet was resuspended in 0.5ml of ice-cold PBSI and placed on ice. Nuclei were then transferred into flow tubes and analysed on a FACScaliber flow cytometer (Becton Dickinson).

Mitomycin C dose response:

MGH-U1 and MGH-U1R cells were grown in 25cm^2 flasks until confluent. Cells were then exposed to various concentrations of mitomycin C in culture medium supplemented with 1:100 HEPES medium at 37^{o}C for 120 minutes. The concentrations used were 125, 250, 500 and 1000µg/ml. A control sample was also performed for each cell type. Following incubation drug was immediately tipped off and cells were washed 3 times with ice-cold PBS. Cells were then harvested using trypsin-EDTA and transferred into centrifuge tubes. They were then centrifuged at 438g (1500rpm) for 3 minutes and the supernatant was discarded. The cell pellet was resuspended in 1ml of ice-colds HEPES buffered medium and the cells were placed on ice. Cells were then transferred into flow tubes and analysed on a FACScaliber flow cytometer (Becton Dickinson). The 488nm Argon laser was used for excitation and detection was performed using all three fluorescence detectors, FL-1 (530nm +/-15), Fl-2 (585nm +/- 15) and Fl-3 detectors (>650nm).

Assessing mitomycin C dose response by reduction acridine orange fluorescence:

Previous studies have assessed mitomycin C uptake by a reduction in acridine orange fluorescence presumably due to similarities in binding sites of these two molecules [393]. MGH-U1 and MGH-U1R cells were grown in 25cm^2 flasks until confluent. Cells were then exposed to various concentrations of mitomycin C in culture medium supplemented with 1:100 HEPES medium at 37^{o}C for 120 minutes. The concentrations used were 125, 250, 500 and 1000µg/ml. Two control samples were also performed for each cell type one with and one without acridine orange exposure. Following incubation drug was immediately tipped off and cells were washed 3 times with ice-cold PBS. Cells were then harvested using trypsin-EDTA and transferred into centrifuge tubes. They were then centrifuged at 438g (1500rpm) for 3 minutes and the supernatant was discarded. The cell pellet was resuspended in 0.5ml of acridine orange 4µM/L for 10 minutes at 37^{o}C. Cells were then centrifuged at 438g (1500rpm) for 3 minutes and acridine orange was discarded and cells were resuspended in 0.5ml of ice-cold PBS and placed on ice. Cells were then transferred into flow tubes and analysed on a FACScaliber flow cytometer (Becton Dickinson). The 488nm Argon laser

was used for excitation and detection was performed using FL-1 (530nm +/- 15) and FL-2 (585nm +/- 15) detectors.

Effects of verapamil on epirubicin dose response:

Cells for flow cytometric studies were grown to near confluence in 25cm^2 flasks. Cells were exposed to epirubicin and/or verapamil diluted in culture medium supplemented with 1:100 HEPES buffering medium as follows.

1. Control – No epirubicin and no verapamil
2. Verapamil only for 120 minutes
3. Epirubicin 10µg/ml for 60 minutes
4. Epirubicin 10µg/ml and Verapamil 100µg/ml for 60 minutes
5. Verapamil 100µg/ml for 60 minutes then Epirubicin 10µg/ml for 60 minutes
6. Verapamil 100µg/ml for 60 minutes then Epirubicin 10µg/ml and Verapamil 100µg/ml for 60 minutes
7. Epirubicin10µg/ml for 120 minutes
8. Epirubicin 10µg/ml and Verapamil 100µg/ml for 120 minutes
9. Verapamil 100µg/ml for 60 minutes then Epirubicin 10µg/ml for 120 minutes
10. Verapamil 100µg/ml for 60 minutes then Epirubicin 10µg/ml and Verapamil 100µg/ml for 120 minutes

During drug exposure cells were maintained in a humidified incubator with 5% CO_2 at 37^{o}C. After exposure, cells were trypsinised into suspension and 10mls of culture medium was added to neutralize the trypsin-EDTA. Cells were then centrifuged at 438g (1500rpm) for 3 minutes. The supernatant was discarded and cells were resuspended in 1ml of ice-cold culture medium and placed on ice. Samples were then run on the flow cytometer.

Analysis of cellular drug uptake was performed using a Becton Dickinson FACScaliber flow cytometer. Cellular drug fluorescence was excited using the 488nm Argon laser and epirubicin fluorescence (red) was detected using the FL-2 detector (585nm +/- 15).

Flow cytometric time series data analysis:

We collected fluorescence data for 5,000 – 10,000 gated cells in each sample. All experiments were repeated to confirm results. Results were plotted as histograms with number of fluorescent events on the x-axis against fluorescence intensity units on a logarithmic scale on the y-axis. Histogram statistics were generated for each cell sample. Comparisons were made between different cell types and the various exposure regimens using geomean fluorescence values. Given the number of cells sampled, any differences between cell samples were significant. Experiments were repeated to confirm results.

Effect of verapamil pre-exposure on epirubicin uptake in isolated nuclei:

MGH-U1 and MGH-U1R cells were cultured in 25cm^2 flasks until confluent. Cells were then either exposed to 100µg/ml verapamil in culture medium for 120 minutes at 37^{o}C or kept in normal culture medium. Nuclei were then extracted by a standardised protocol (Appendix 1) followed by exposure to epirubicin 10µg/ml for 10 minutes at 37^{o}C. Nuclei were centrifuged at 800g (2000rpm) for 5 minutes and the epirubicin containing supernatant was discarded. The nuclei were then re-suspended in 0.5ml of PBSI and placed on ice. The samples were then transferred into flow tubes and run on the flow cytometer.

Cellular P-gp staining with a FITC conjugated Anti-P-gp antibody (17F9, BD Biosciences):

MGH-U1, RT112, MGH-U1R and MGHU-MMC cells were grown in 25 cm^2 flasks until confluent. Cells were then trypsinised into suspension. Cells were counted using a haemocytometer and 5 x 10^5 cells were placed into each centrifuge tube. They were then centrifuged at 438g (1500rpm) for 3 minutes and the supernatant was discarded. Cells were then re-suspended in 0.5mls of their allocated fluid. Controls were re-suspended in HBBS (Sigma, UK) containing 1% Bovine Serum Albumin (BSA) (Sigma, UK). FITC-controls were re-suspended in HBSS containing 1% BSA and 20µl/ml of FITC labelled IgG (Sigma, UK). FITC-anti-P-gp cells were re-suspended in HBSS containing 1% BSA and 20µl/ml of FITC-anti-P-gp (17F9, BD Biosciences, UK). Cells were then incubated at room temperature for 20 minutes. Cells were then transferred to flow tubes, placed on ice and analysed on the flow cytometer.

Nuclear P-gp staining with a FITC conjugated Anti-P-gp antibody (17F9, BD Biosciences):

MGH-U1, RT112, MGH-U1R and MGHU-MMC cells were grown in 25cm^2 flasks until confluent. Nuclei were then isolated as per standardised protocol (Appendix 1). Nuclei were counted using a haemocytometer and 5 x 10^5 nuclei were placed into each centrifuge tube. They were then centrifuged at 800g (2000rpm) for 5 minutes and the supernatant was discarded. Nuclei were then re-suspended in 0.5mls of their allocated fluid. Controls were re-suspended in HBSS (Sigma, UK) containing 1% Bovine Serum Albumin (BSA) (Sigma, UK). FITC-controls were re-suspended in HBSS containing 1% BSA and 20µl/ml of FITC labeled IgG (Sigma, UK). FITC-anti-P-gp nuclei were re-suspended in HBSS containing 1% BSA and 20µl/ml of FITC-anti-P-gp (17F9, BD Biosciences, UK). The samples were then incubated at room temperature for 20 minutes. They were then transferred to flow tubes, placed on ice and analysed on the flow cytometer.

2.73: Microinjection experiments:

Microinjection of cytotoxic drugs into MDR cells provides a novel means of studying MDR status and mechanisms of MDR. Microinjection of epirubicin into the cytoplasm of MDR cells, bypasses the plasma membrane P-gp efflux pump. If MDR cells microinjected with epirubicin still exhibit their characteristic nuclear sparing, this would provide direct evidence of the nuclear membrane's role and establish another mechanism of MDR in bladder cancer. Microinjection also allows molecules that would not normally cross the plasma membrane to be injected into cells, e.g. FITC-dextrans.

Cytoplasmic microinjection with epirubicin at 37^{o}C:

MGH-U1, RT112, MGH-U1R and MGHU-MMC cells were cultured in low-sided 40mm Petri dishes (Orange Scientific, UK) until 50 – 75% confluent. Cell culture medium was changed to HEPES buffered medium (1:100 HEPES). Epirubicin (0.5mg/ml) was co-injected with a 77KDa FITC-dextran (0.5mg/ml) into the cytoplasm of adherent cells. The FITC-dextran allowed us to clearly identify our injected cell population. FITC-dextrans of 77KDa are ordinarily excluded from cells and cell nuclei, as they are too large to passively diffuse across these membranes. The injection buffer used was 48mM K_2HPO_4, 4.5mM KH_2PO_4, 14mM NaH_2PO_4, pH 7.2 (Eppendorf -

personal communication). Once microinjected, cells were incubated for 60 minutes in normal culture conditions to allow cell recovery and time for epirubicin to distribute itself within the cells.

Microinjected cells were then viewed by confocal microscopy. Injected cells were easily identified by their green FITC-dextran fluorescence, on direct fluorescence microscopy. Confocal microscopy allowed direct visualisation of the distribution of the various fluophores within the microinjected cells. Epirubicin fluorescence was excited by a 543nm HeNe laser and emission of wavelengths of 560nm and greater (red) were detected. FITC-dextran fluorescence was excited by a 488nm Argon laser and emission wavelengths between 505 and 530nm (green) were detected. The multitrack scanning mode on the confocal microscope was used to reduce cross interference in the fluorescent signals of these two fluophores.

Acridine orange (3µg/ml) stains the nuclei of viable cells green and was added after initial image capture in order to confirm cell viability. Acridine orange has similar fluorescence properties to FITC and was detected with the same filter settings.

Cytoplasmic microinjection with epirubicin on ice:

By placing cells on ice, energy dependant cellular processes are abolished. MGH-U1 and MGH-U1R cells were cultured in low-sided 40mm Petri dishes (Orange Scientific, UK) until 50 – 75% confluent. Cell culture medium was changed to ice-cold HEPES buffered medium (1:100 HEPES) and the cells were placed on ice to cool for 20 – 30 minutes. The injection fluids and the microscope stage were also placed on ice. The injection fluid was then centrifuged at 16000g (13000rpm) for 3 minutes at 4^{o}C in a Heraeus Biofuge *Fresco* centrifuge. Epirubicin (0.5mg/ml) was co-injected with a 77KDa FITC-dextran (0.5mg/ml) into the cytoplasm of adherent cells. The injection buffer used was 48mM K_2HPO_4, 4.5mM KH_2PO_4, 14mM NaH_2PO_4, pH 7.2 (Eppendorf - personal communication). Once microinjected, cells were visualised by confocal microscopy as soon as possible. Our injected cell population was identified by its FITC-dextran fluorescence. Confocal microscopy allowed direct visualisation of the distribution of the various fluophores within the microinjected cells. The same confocal settings were used as in the previous experiment protocol.

Acridine orange (3µg/ml) was again used to assess cell viability.

Nuclear pore sizing by cytoplasmic microinjection of various sized FITC-dextrans:

Microinjection of various FITC-dextrans into the cytoplasm of cells allows us to size nuclear membrane pores depending on which FITC-dextrans are able to cross the nuclear membrane. Microinjection had significant advantages over our previous attempts at nuclear pore sizing using a scrape-loading technique. The scrape-loading technique wasted large quantities of dextrans and was frequently unsuccessful, with a low yield of cells that took up dextrans.

MGH-U1 and MGH-U1R cells were cultured in low-sided 40mm Petri dishes (Orange Scientific, UK) until 50 – 75% confluent. Cell culture medium was changed to HEPES buffered medium (1:100 HEPES).

Cells were then microinjected with 1mg/ml FITC-dextrans of various sizes in injection buffer. FITC-dextran sizes used were 4.4KDa, 19.5KDa, 42KDa and 77KDa (Sigma). Once microinjected, cells were incubated for 60 minutes at 37°C to allow cell recovery and distribution of the FITC-dextran to occur. Cells were the visualised using confocal microscopy.

2.74: Cytotoxicity experiments:

Cytotoxicity experiments were performed using the MTT (3-[4,5-dimethylthiazol-2-yl]-2,5-diphenyltetrazolium bromide; thiazolyl blue) assay.

Plating Method

Cells lines were trypsinised into suspension in culture medium as described previously. Cell density was adjusted to 2 x 10^4 cells/ml. One hundred microlitres of cell suspension was seeded into each well of 96-well culture-grade microtitre plates (Nunc, UK), giving an initial plating cell concentration of 2 x 10^3 $well^{-1}$ (Figure 25). Cells were allowed to settle for 24 hours in normal culture conditions.

Cells were exposed to the following agents and incubated at 37°C for one hour. Drug-containing medium was then removed, and the cells were cultured in drug free culture medium until control wells achieved 90% confluence.

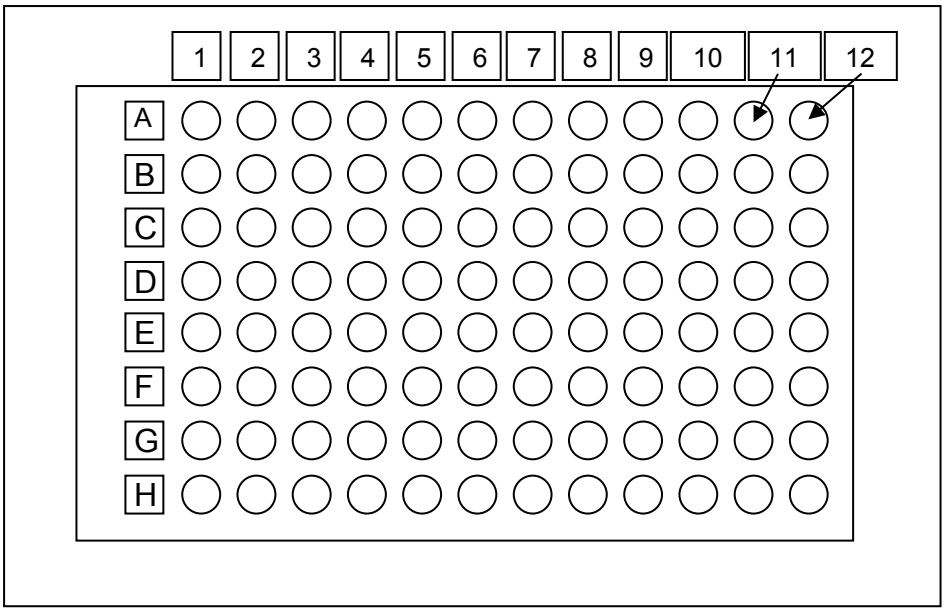

Figure 25: Diagram of a 96-well microtitre plate with 8 rows (A-H) and 12 columns (1 – 12)

Specific drug cytotoxicity experiments

Cytotoxic drugs

Dilutions of epirubicin, idarubicin and mitomycin C were made up from stock solutions, diluted in culture medium supplemented with 1:100 HEPES buffer solution (Sigma, UK).

Epirubicin:

Epirubicin was diluted to a concentration of 640µg/ml and serially diluted across two 96-well plates giving final assay concentrations of 320, 160, 80, 40, 20, 10, 5, 2.5, 1.25, 0.63, 0.31, 0.16, 0.08, 0.04, 0.02, 0.01, 0.005, 0.0025 µg/ml.

Idarubicin:

Idarubicin was diluted to a concentration of 20µg/ml and serially diluted across each 96-well plate giving final assay concentrations of 10, 5, 2.5, 1.25, 0.63, 0.31, 0.16, 0.08, 0.04µg/ml.

Mitomycin C

Mitomycin C was diluted to a concentration of 1mg/ml and serially diluted across each 96-well plate giving final assay concentrations of 500, 250, 125, 62.5, 31.25, 15.63, 7.81, 3.91, 1.95, 0.98µg/ml.

Wheat Germ Agglutinin (WGA) (Triticum *vulgaris* Lectin)

WGA was diluted to a concentration of 25.6µg/ml and serially diluted across each 96-well plate giving final assay concentrations of 12.8, 6.4, 3.2, 1.6, 0.8, 0.4, 0.2, 0.1, 0.05, 0.025 µg/ml.

Drug Combinations

Epirubicin and WGA:

Cells were pre-incubated with 0.2µg/ml WGA for 60 minutes at 37^{o}C. After exposure cells WGA tipped off and cells were recovered with fresh culture medium and re-incubated for a further 23 hours. Cells were then exposed to epirubicin for 1 hour which was serially diluted across each 96-well plate giving final assay concentrations of 160, 80, 40, 20, 10, 5, 2.5, 1.25, 0.63 and 0.31µg/ml.

Epirubicin and Demecolcine

Cells were pre-incubated with demecolcine at various concentrations for 24 hours across the rows A – H of the well plates. The final concentrations of demecolcine were 0.5, 0.25, 0.125, 0.06, 0.03, 0.016µg/ml. After 24 hours the cells were then exposed to epirubicin for 1 hours which was serially diluted across the columns of the well plates, giving final assay concentrations of 40, 20, 10, 5, 2.5, 1.25, 0.063, 0.031, 0.016, 0.008µg/ml.

MTT Method

Subsequently 50µl of 1mg/ml MTT diluted in culture medium was added to each well and the plates were incubated for a further 3 – 4 hours. Medium containing MTT was then removed and the resultant formazan crystals were solubilised by the addition of 150µl of dimethyl sulphoxide (DMSO, 100%) per well. The optical density (representing residual viable cell biomass) was determined on a Wallac microplate reader set to detect at 570nm. Data was transferred from the well-plate reader to a spreadsheet. Spreadsheet analysis allowed the mean residual viable biomass to be calculated for each drug dilution as a percentage of the control well mean residual viable biomass. The external cells were excluded for analysis purposes as they are subject to drying and inaccurate results. Cytotoxicity graphs were then plotted to include 95% confidence intervals. The IC50 value (concentration of the drug required to inhibit cell growth by 50%) was calculated for each drug or drug combination.

Chapter 3: Results: Specific techniques and experiments

3.1: Confocal experiments

Anthracycline incubation studies: Establishing cell phenotypes

Epirubicin uptake at 37°C

At 37°C, the sensitive bladder cancer cell lines, MGH-U1 and RT112 both exhibited the "sensitive phenotype" with a clear nuclear uptake pattern of epirubicin. Comparatively, levels of epirubicin fluorescence in the cytoplasm were much lower (Figures 26a and b). Fluorescein diacetate confirmed cell viability, with strong green fluorescence being demonstrated by all cells.

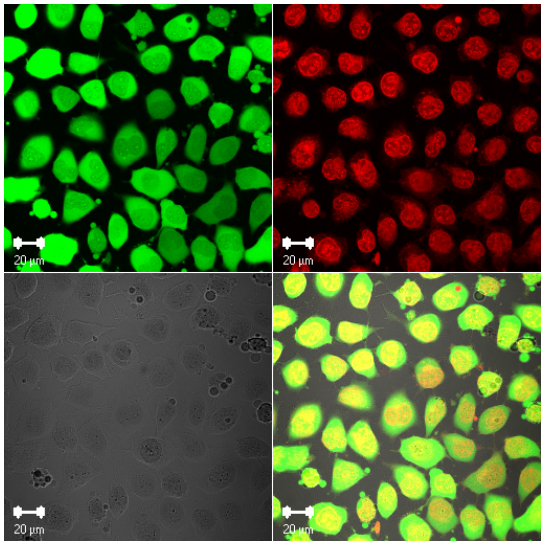

Figure 26a: MGH-U1 cells (x40 Lens; Digital Zoom x1; Epirubicin Gain 700). Top Left: Fluorescein Diacetate (FDA) fluorescence (Green); Top Right: Epirubicin Fluorescence (Red); Bottom Left: Differential Interference Contrast Image (DIC); Bottom Right: Overlay image

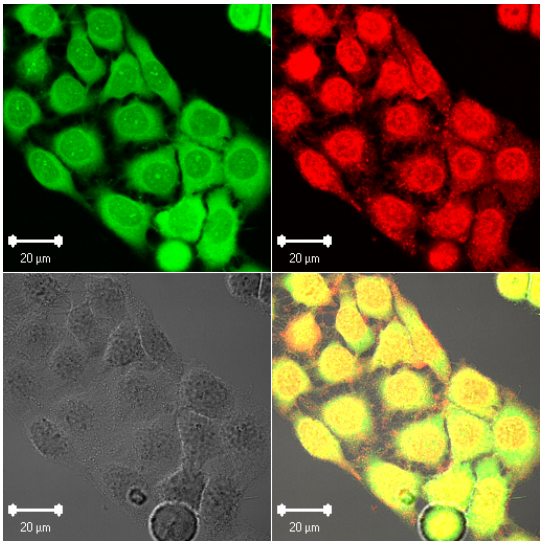

Figure 26b: RT112 cells (x40 Lens; Digital Zoom x2; Epirubicin Gain 700). Top Left: Fluorescein Diacetate (FDA) fluorescence (Green); Top Right: Epirubicin Fluorescence (Red); Bottom Left: Differential Interference Contrast Image (DIC); Bottom Right: Overlay image

In contrast, the MDR cell lines, MGH-U1R and MGHU-MMC, both demonstrated the "resistant phenotype", with nuclear sparing of epirubicin uptake when incubated with drug at 37°C. The drug within MDR cells is mainly cytoplasmic and appears to be packaged in cytoplasmic vesicles. Some cells also exhibit a rim of drug around their periphery, which may represent drug being effluxed or ejected from these vesicles by exocytosis (Figures 26c and d). Fluorescein diacetate again confirmed cell viability with cells fluorescing bright green.

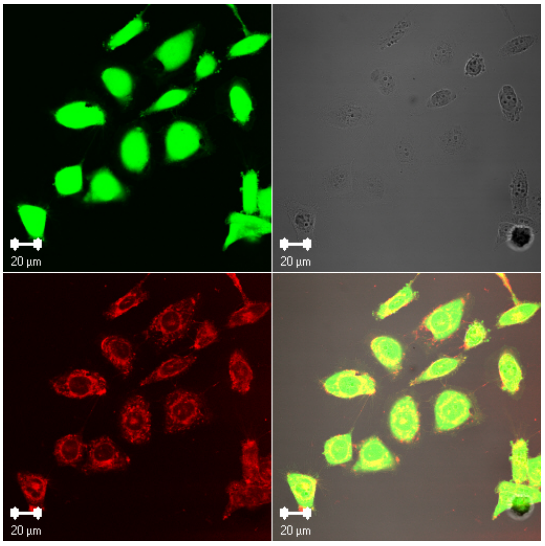

Figure 26c: MGH-U1R cells (x40 Lens; Digital Zoom x1; Epirubicin Gain 1025). Top Left: Fluorescein Diacetate (FDA) fluorescence (Green); Top Right: Differential Interference Contrast Image (DIC); Bottom Left: Epirubicin Fluorescence (Red); Bottom Right: Overlay

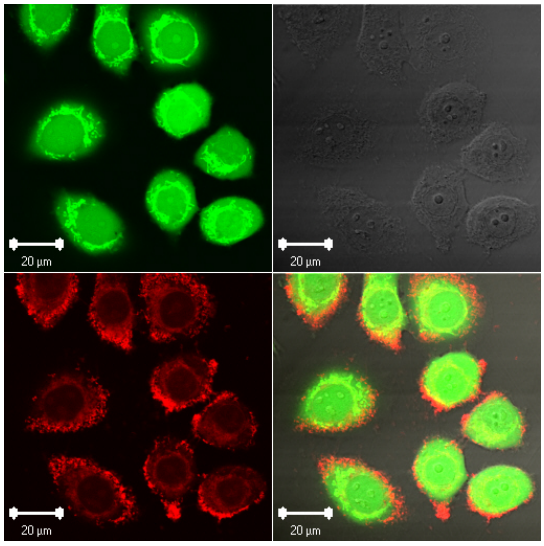

Figure 26d: MGHU-MMC cells (x40 Lens; Digital Zoom x2; Epirubicin Gain 900). Top Left: Fluorescein Diacetate (FDA) fluorescence (Green); Top Right: Differential Interference Contrast Image (DIC); Bottom Left: Epirubicin Fluorescence (Red); Bottom Right: Overlay image

Idarubicin uptake at 37°C

In contrast to epirubicin, all cell lines demonstrated nuclear sparing of idarubicin at 37°C (Figures 27a – d). This is the only anthracycline that has been shown to be excluded from the nuclei of both sensitive and resistant cells and remains something of an enigma.

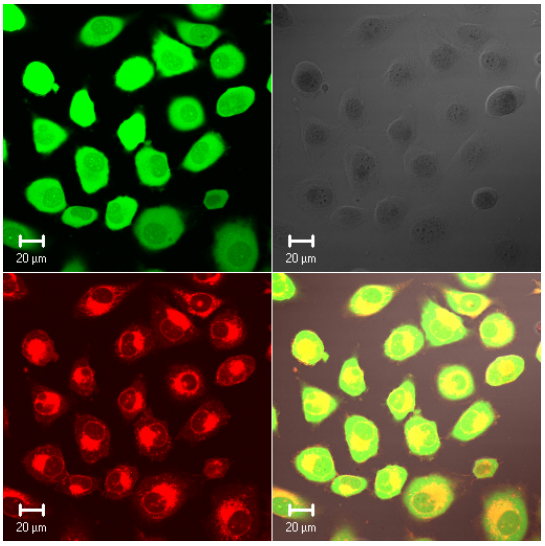

Figure 27a: MGH-U1 cells (x40 Lens; Digital Zoom x1; Gain 750) Top Left: Fluorescein Diacetate (FDA) fluorescence (Green); Top Right: Differential Interference Contrast Image (DIC); Bottom Left: Idarubicin Fluorescence (Red); Bottom Right: Overlay image

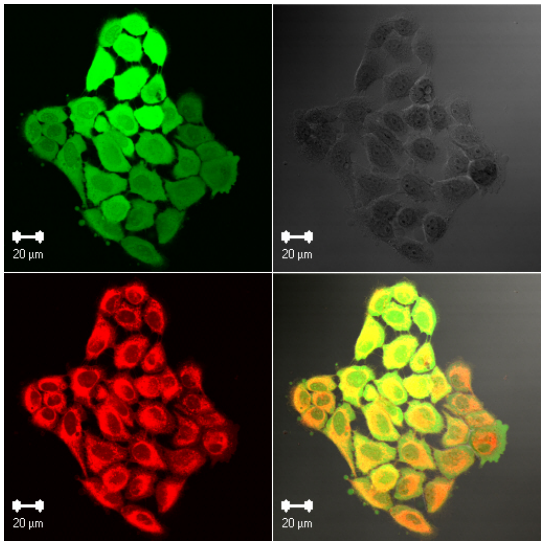

Figure 27b: RT112 cells (x40 Lens; Digital Zoom x1; Gain 725) Top Left: Fluorescein Diacetate (FDA) fluorescence (Green); Top Right: Differential Interference Contrast Image (DIC); Bottom Left: Idarubicin Fluorescence (Red); Bottom Right: Overlay image

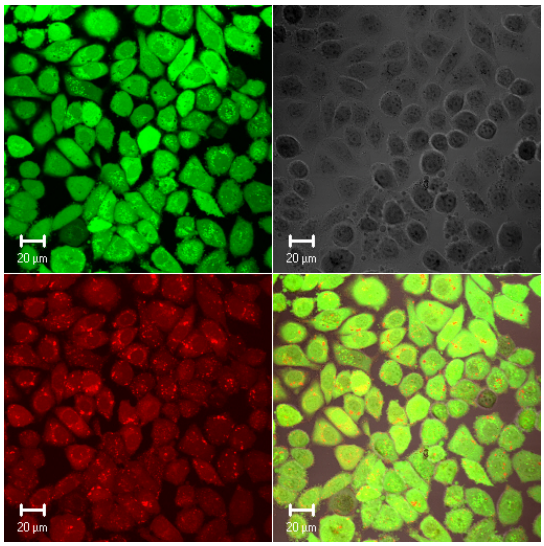

Figure 27c: MGH-U1R cells (x40 Lens; Digital Zoom x1; Gain 750) Top Left: Fluorescein Diacetate (FDA) fluorescence (Green); Top Right: Differential Interference Contrast Image (DIC); Bottom Left: Idarubicin Fluorescence (Red); Bottom Right: Overlay image

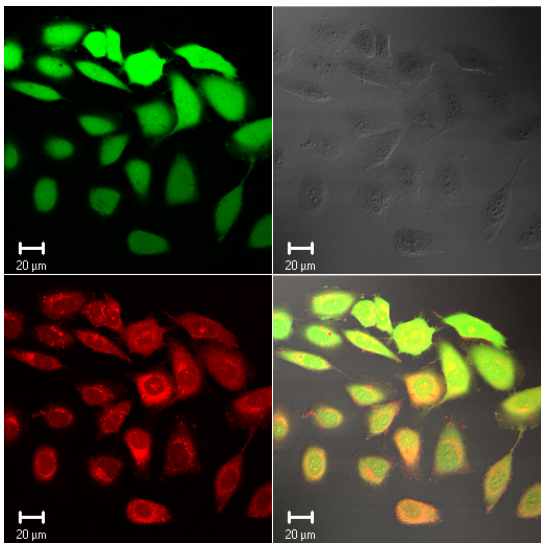

Figure 27d: MGHU-MMC cells (x40 Lens; Digital Zoom x1; Gain 800) Top Left: Fluorescein Diacetate (FDA) fluorescence (Green); Top Right: Differential Interference Contrast Image (DIC); Bottom Left: Idarubicin Fluorescence (Red); Bottom Right: Overlay image

In sensitive cells the idarubicin appears to be concentrated in an area just outside the nucleus, which with further magnification appears to be the golgi apparatus (Figs 28a and b). In resistant cells idarubicin is present to a lesser extent in the golgi, but also appears to be packaged in cytoplasmic vesicles (Figs 28c and d). It is conceivable that drug is taken up by the golgi and packaged into vesicles ready for export from the cell by exocytosis. It is also possible that this process occurs more rapidly in MDR cells as evidenced by the presence of more cytoplasmic vesicles.

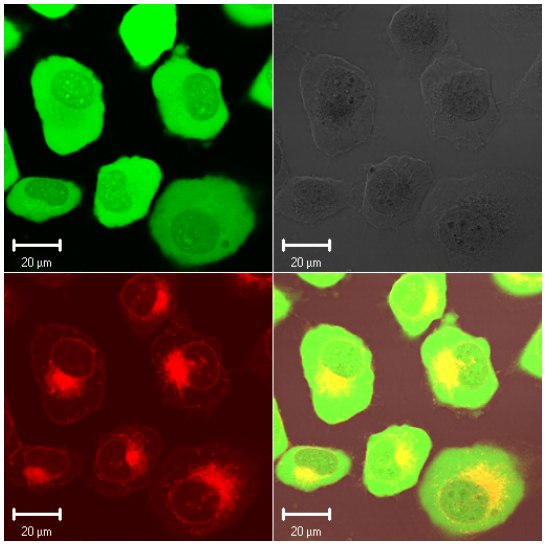

Figure 28a: MGH-U1 cells (x40 Lens; Digital Zoom x2; Gain 680) Top Left: Fluorescein Diacetate (FDA) fluorescence (Green); Top Right: Differential Interference Contrast Image (DIC); Bottom Left: Idarubicin Fluorescence (Red); Bottom Right: Overlay image

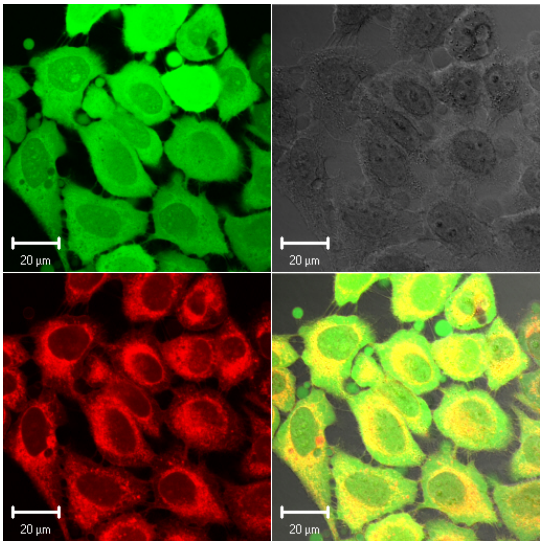

Figure 28b: RT112 cells (x40 Lens; Digital Zoom x2; Gain 725) Top Left: Fluorescein Diacetate (FDA) fluorescence (Green); Top Right: Differential Interference Contrast Image (DIC); Bottom Left: Idarubicin Fluorescence (Red); Bottom Right: Overlay image

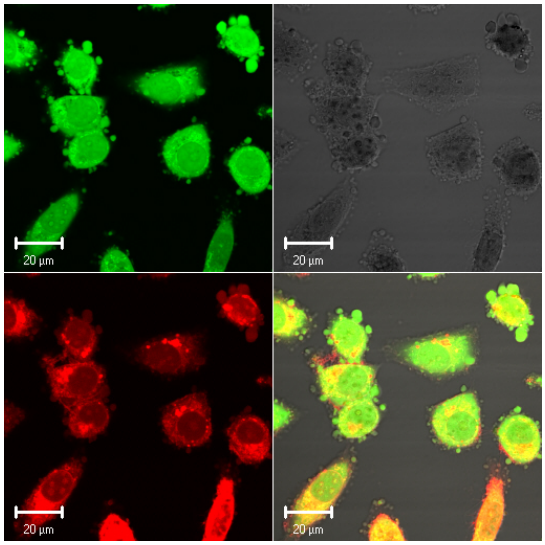

Figure 28c: MGH-U1R cells (x40 Lens; Digital Zoom x2; Gain 865) Top Left: Fluorescein Diacetate (FDA) fluorescence (Green); Top Right: Differential Interference Contrast Image (DIC); Bottom Left: Idarubicin Fluorescence (Red); Bottom Right: Overlay image

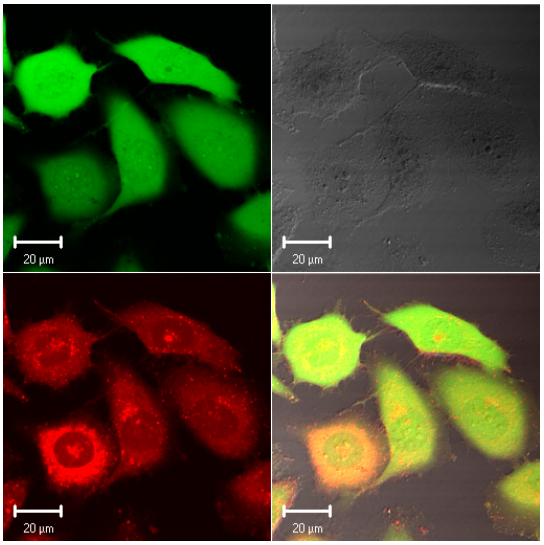

Figure 28d: MGHU-MMC cells (x40 Lens; Digital Zoom x2; Gain 785) Top Left: Fluorescein Diacetate (FDA) fluorescence (Green); Top Right: Differential Interference Contrast Image (DIC); Bottom Left: Idarubicin Fluorescence (Red); Bottom Right: Overlay image

Epirubicin uptake at 0 – 4°C

The sensitive cell lines, MGH-U1 and RT112, demonstrate very low levels of epirubicin uptake when incubated on ice. They also reverse their normal uptake pattern to a pattern of nuclear drug exclusion (Figures 29a and b).

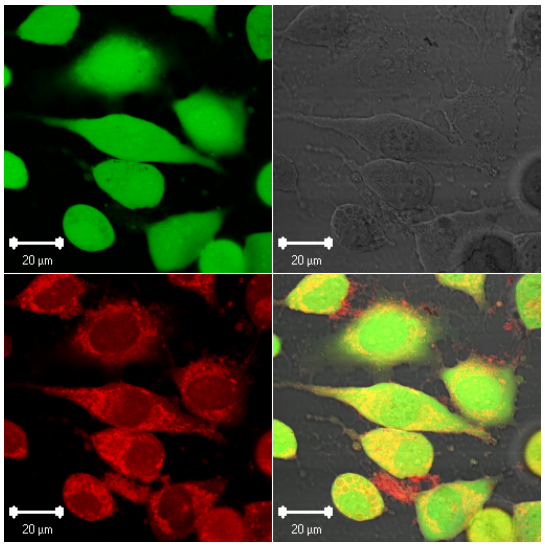

Figure 29a: MGHU-1 cells (x40 Lens; Digital Zoom x2; Gain 1000); Top Left: Fluorescein Diacetate (FDA) fluorescence (Green); Top Right: Epirubicin Fluorescence (Red); Bottom Left: Differential Interference Contrast Image (DIC); Bottom Right: Overlay image

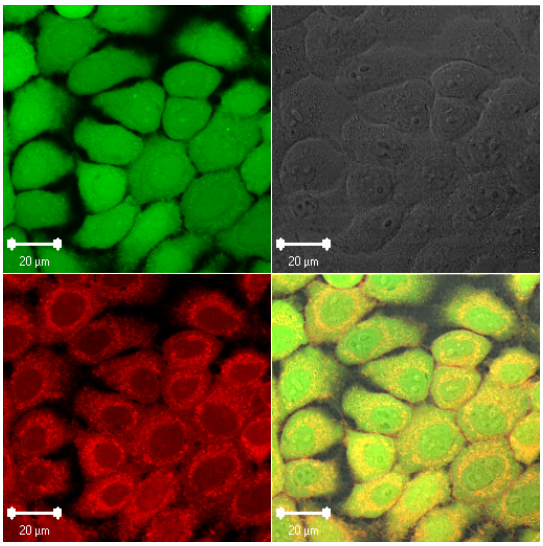

Figure 29b: RT112 cells (x40 Lens; Digital Zoom x2; Gain 1000); Top Left: Fluorescein Diacetate (FDA) fluorescence (Green); Top Right: Epirubicin Fluorescence (Red); Bottom Left: Differential Interference Contrast Image (DIC); Bottom Right: Overlay image

The resistant cell lines, MGH-U1R and MGHU-MMC, also exhibit very low levels of drug uptake at 0 – 4°C, which were comparable to sensitive cell drug levels at the same temperature. The MDR cells maintained their normal nuclear sparing pattern of drug uptake and had similar levels of drug uptake to MDR cells incubated at 37°C (Figures 29c and d).

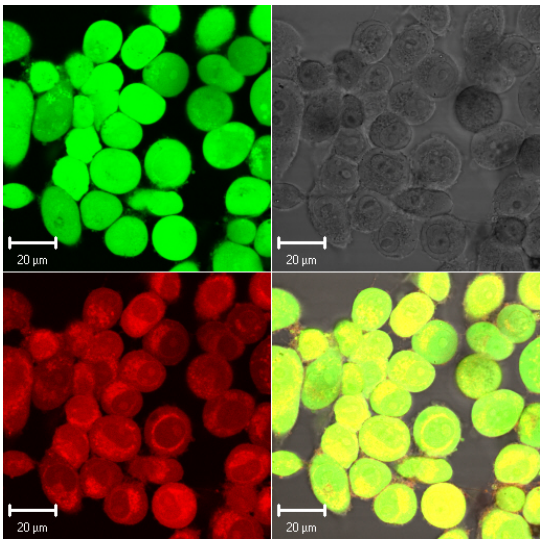

Figure 29c: MGH-U1R cells (x40 Lens; Digital Zoom x2; Gain 950); Top Left: Fluorescein Diacetate (FDA) fluorescence (Green); Top Right: Epirubicin Fluorescence (Red); Bottom Left: Differential Interference Contrast Image (DIC); Bottom Right: Overlay image

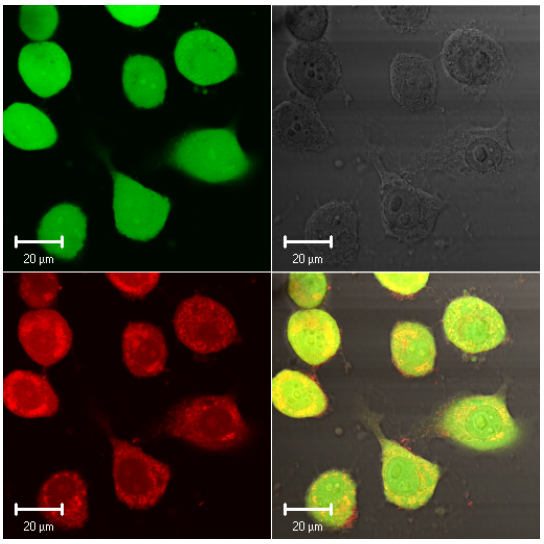

Figure 29d: MGHU-MMC cells (x40 Lens; Digital Zoom x2; Gain 950); Top Left: Fluorescein Diacetate (FDA) fluorescence (Green); Top Right: Epirubicin Fluorescence (Red); Bottom Left: Differential Interference Contrast Image (DIC); Bottom Right: Overlay image

All cell lines were viable after incubation with epirubicin on ice, as demonstrated by green fluorescence on FDA staining.

Idarubicin uptake at 0 – 4°C

All cell lines showed a similar nuclear sparing pattern of idarubicin uptake when incubated on ice (Figures 30a – d). They also demonstrated clear viability with FDA staining.

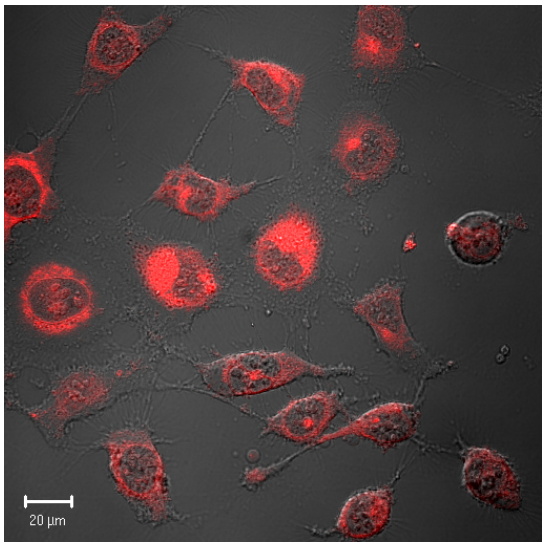

Figure 30a: MGH-U1 cells (x40 lens; Digital Zoom x1; Gain setting 756) Idarubicin fluorescence (Red) overlayed on DIC image

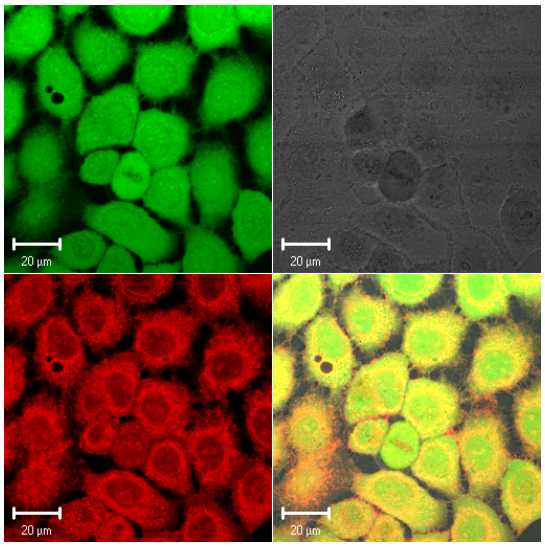

Figure 30b: RT112 cells (x40 lens; Digital Zoom x2; Gain setting 950) Top Left: Fluorescein Diacetate (FDA) fluorescence (Green); Top Right: Differential Interference Contrast Image (DIC); Bottom Left: Idarubicin Fluorescence (Red); Bottom Right: Overlay image

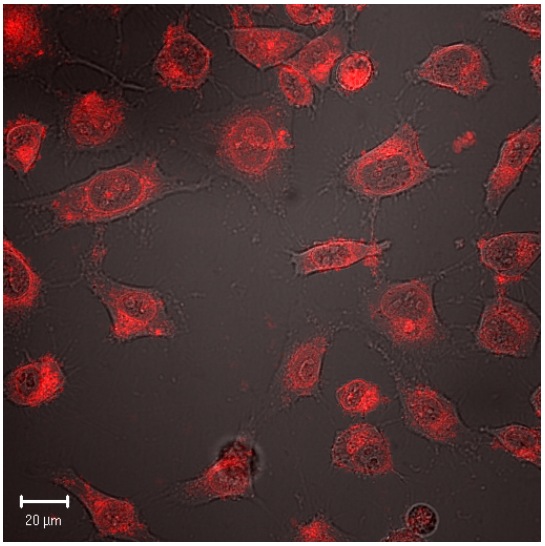

Figure 30c: MGH-U1R cells (x40 lens; Digital Zoom x1; Gain setting 812) Idarubicin fluorescence (Red) overlayed on DIC image

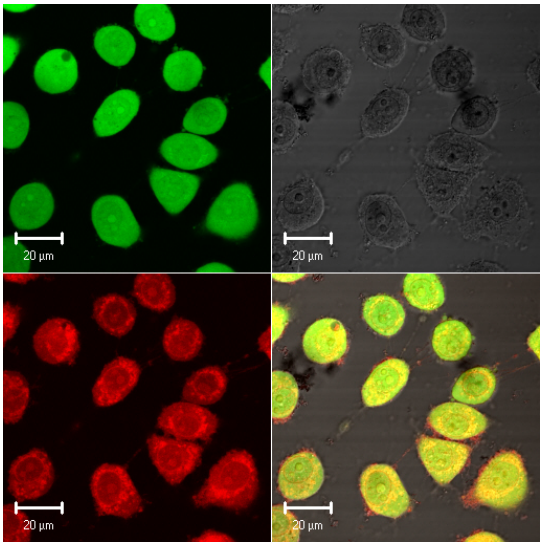

Figure 30d: MGHU-MMC cells (x40 lens; Digital Zoom x2; Gain setting 950) Top Left: Fluorescein Diacetate (FDA) fluorescence (Green); Top Right: Differential Interference Contrast Image (DIC); Bottom Left: Idarubicin Fluorescence (Red); Bottom Right: Overlay image

Epirubicin uptake in dead cells at 37°C

Following cell killing, all cell types showed strong nuclear staining with epirubicin when incubated at 37°C (Figure 31a – d). Absence of FDA staining confirmed death in all cells after microwaving them in a 650W oven for 10 seconds on 100% power. Sensitive cells showed no change in their pattern of drug uptake with cell death, whereas dead MDR cells altered their epirubicin uptake pattern to a strong nuclear staining pattern. This result clearly demonstrates the need to confirm cell viability when MDR cells are

changed to a sensitive nuclear epirubicin uptake pattern by whatever pharmacological means, to ensure that MDR reversal is not simply due to cell death.

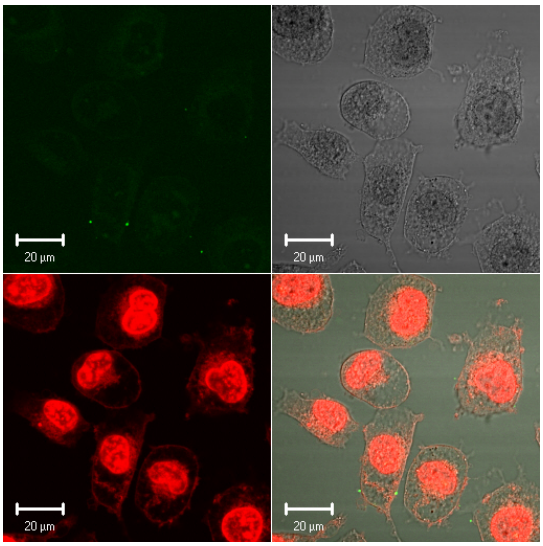

Figure 31a: Dead MGH-U1 cells (x40 lens; Digital Zoom x2; Gain setting 825) Top Left: Fluorescein Diacetate (FDA) fluorescence (Green); Top Right: Differential Interference Contrast Image (DIC); Bottom Left: Epirubicin Fluorescence (Red); Bottom Right: Overlay image

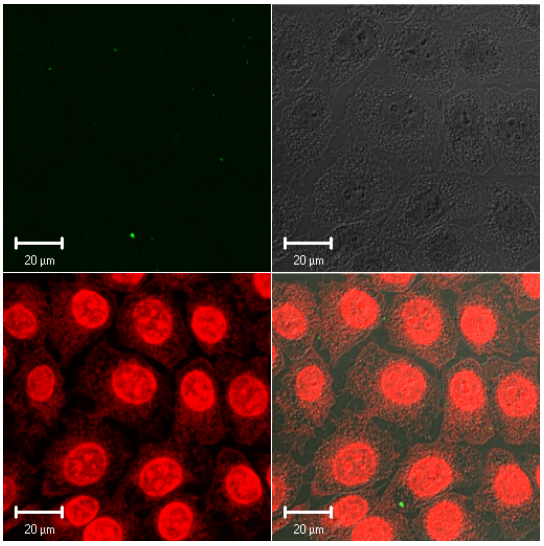

Figure 31b: Dead RT112 cells (x40 lens; Digital Zoom x2; Gain setting 825) Top Left: Fluorescein Diacetate (FDA) fluorescence (Green); Top Right: Differential Interference Contrast Image (DIC); Bottom Left: Epirubicin Fluorescence (Red); Bottom Right: Overlay image

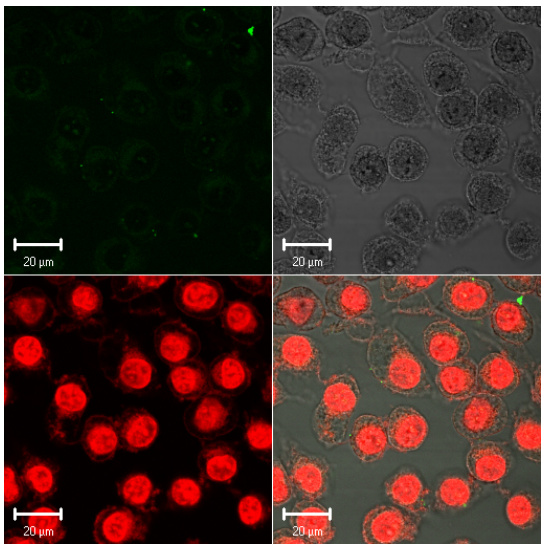

Figure 31c: Dead MGH-U1R cells (x40 lens; Digital Zoom x2; Gain setting 800) Top Left: Fluorescein Diacetate (FDA) fluorescence (Green); Top Right: Differential Interference Contrast Image (DIC); Bottom Left: Epirubicin Fluorescence (Red); Bottom Right: Overlay image

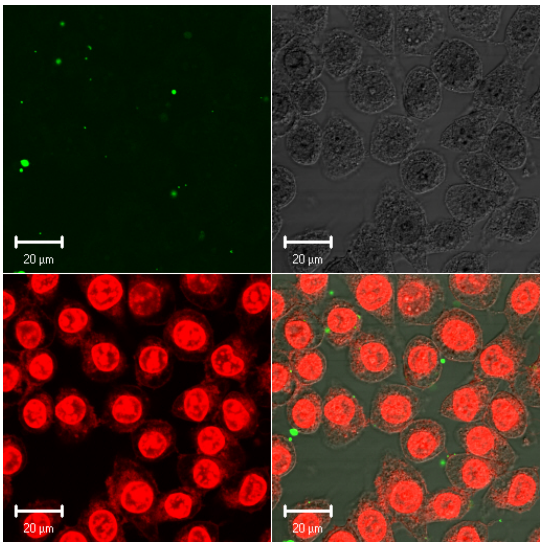

Figure 31d: Dead MGHU-MMC cells (x40 lens; Digital Zoom x2; Gain setting 800) Top Left: Fluorescein Diacetate (FDA) fluorescence (Green); Top Right: Differential Interference Contrast Image (DIC); Bottom Left: Epirubicin Fluorescence (Red); Bottom Right: Overlay image

Idarubicin uptake in dead cells at 37°C

After cell killing, all cell types showed no changes in their uptake pattern of idarubicin, all demonstrating a nuclear sparing pattern similar to that of viable cells (Figures 32a – d). Again, much of the drug appears to be sequestered in

the Golgi apparatus as with viable cells. Cell death was confirmed by the absence of green fluorescence when stained with FDA.

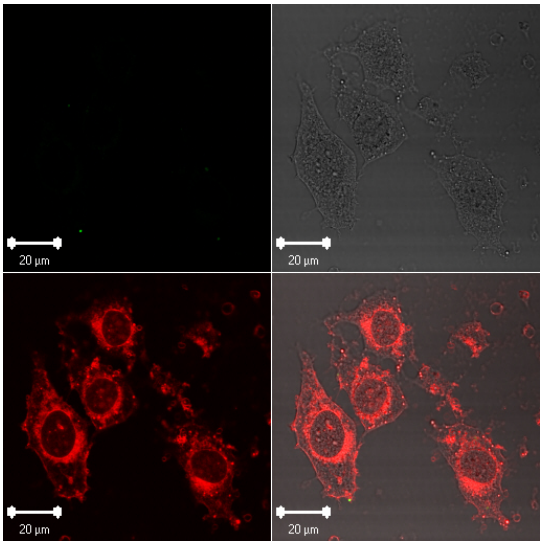

Figure 32a: Dead MGH-U1 cells (x40 lens; Digital Zoom x2; Gain setting 900) Top Left: Fluorescein Diacetate (FDA) fluorescence (Green); Top Right: Differential Interference Contrast Image (DIC); Bottom Left: Idarubicin Fluorescence (Red); Bottom Right: Overlay image

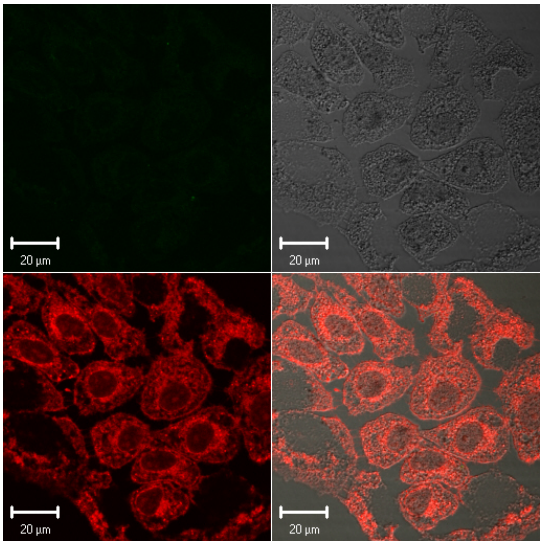

Figure 32b: Dead RT112 cells (x40 lens; Digital Zoom x2; Gain setting 900) Top Left: Fluorescein Diacetate (FDA) fluorescence (Green); Top Right: Differential Interference Contrast Image (DIC); Bottom Left: Idarubicin Fluorescence (Red); Bottom Right: Overlay image

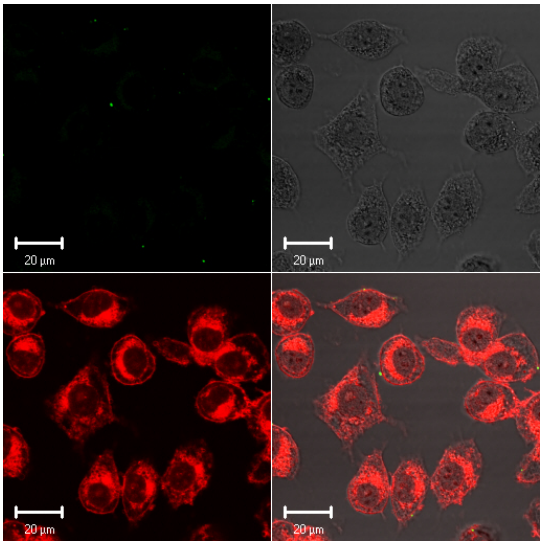

Figure 32c: Dead MGH-U1R cells (x40 lens; Digital Zoom x2; Gain setting 900) Top Left: Fluorescein Diacetate (FDA) fluorescence (Green); Top Right: Differential Interference Contrast Image (DIC); Bottom Left: Idarubicin Fluorescence (Red); Bottom Right: Overlay image

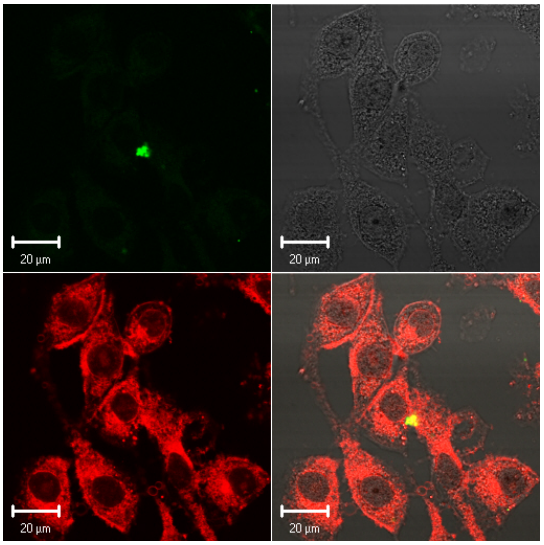

Figure 32d: Dead MGHU-MMC cells (x40 lens; Digital Zoom x2; Gain setting 900) Top Left: Fluorescein Diacetate (FDA) fluorescence (Green); Top Right: Differential Interference Contrast Image (DIC); Bottom Left: Idarubicin Fluorescence (Red); Bottom Right: Overlay image

Anthracycline incubation studies: Uptake in isolated nuclei

Epirubicin uptake at 37°C

Epirubicin uptake in nuclear extracts from cells that were pre-exposed to epirubicin showed dramatic differences in nuclear uptake between MGH-U1 (sensitive) and MGH-U1R (MDR) nuclei. Figures 33a and b show the

epirubicin staining characteristics of MGH-U1 and MGH-U1R nuclei with the confocal gain setting for epirubicin fluorescence set at 825. Figure 33d shows MGH-U1R nuclei (fluorescence only image) at a gain setting of 1000, now demonstrating weak epirubicin fluorescence. There is significantly less nuclear fluorescence when compared to MGH-U1 cells (fluorescence only image) at a much lower gain setting of 825 (Figure 33c). Nuclei tend to clump together when extracted from cells, making analysis of individual nuclear fluorescence counts using the confocal analysis software unfeasible.

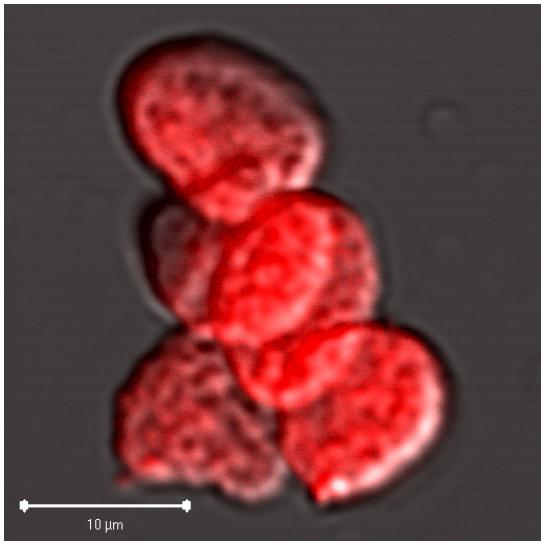

Figure 33a: MGH-U1 nuclei extracted after exposure of cells to epirubicin 10µg/ml for 2 hours (x40 Lens; Gain 825; Zoom x14)
Epirubicin fluorescence overlaid on DIC image

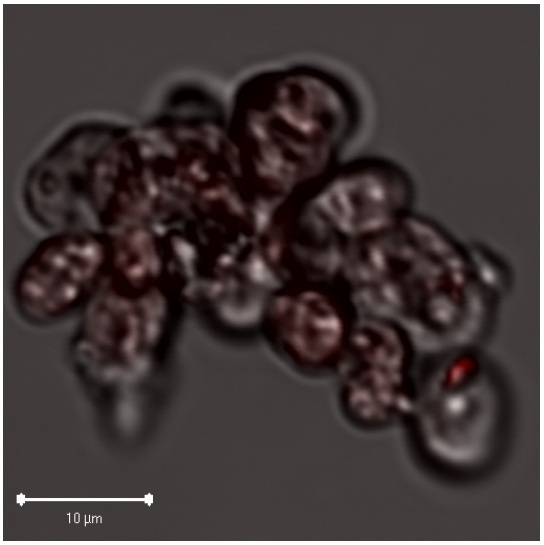

Figure 33b: MGH-U1R nuclei extracted after exposure of cells to epirubicin 10µg/ml for 2 hours (x40 Lens; Gain 825; Zoom x11)
Epirubicin fluorescence overlaid on DIC image

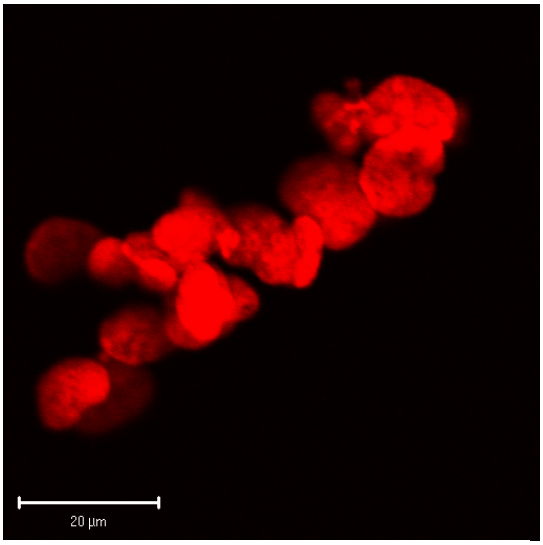

Figure 33c: MGH-U1 nuclei extracted after exposure of cells to epirubicin 10µg/ml for 2 hours (x40 Lens; Gain 825; Zoom x6)
Epirubicin fluorescence only

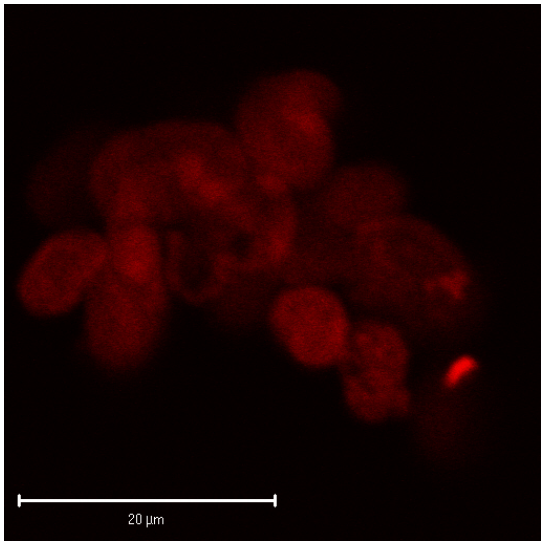

Figure 33d: MGH-U1R nuclei extracted after exposure of cells to epirubicin 10µg/ml for 2 hours (x40 Lens; Gain 1000; Zoom x11)
Epirubicin fluorescence only

Direct exposure of nuclei to epirubicin after nuclear fractionation showed that levels of drug uptake in MGH-U1 and MGH-U1R nuclei were very similar. Figures 34a and c show the epirubicin staining characteristics of MGH-U1 and MGH-U1R nuclei with the same confocal gain setting of 825. Figures 34b and d show the same nuclei at a lower gain setting of 735 allowing a clearer visualisation of epirubicin uptake in the isolated nuclei.

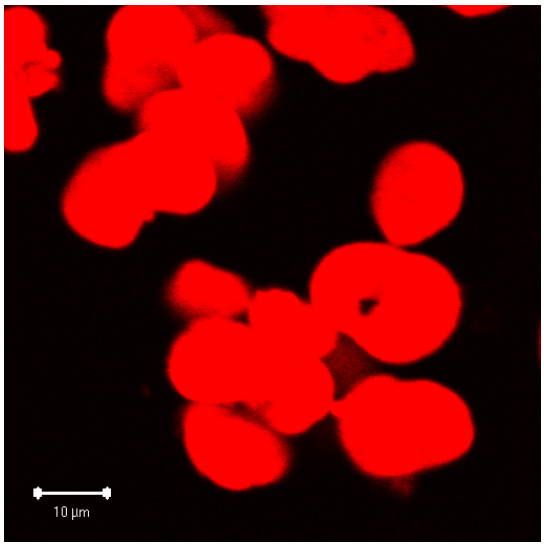

Figure 34a: MGH-U1 nuclei exposed to epirubicin 10µg/ml for 10 minutes after nuclear fractionation (x40 Lens; Gain 825; Zoom x6)
Epirubicin fluorescence only

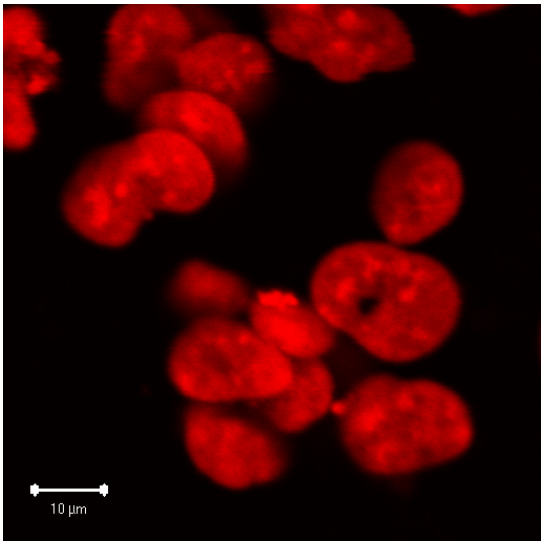

Figure 34b: MGH-U1 nuclei exposed to epirubicin 10µg/ml for 10 minutes after nuclear fractionation (x40 Lens; Gain 735; Zoom x6)
Epirubicin fluorescence only

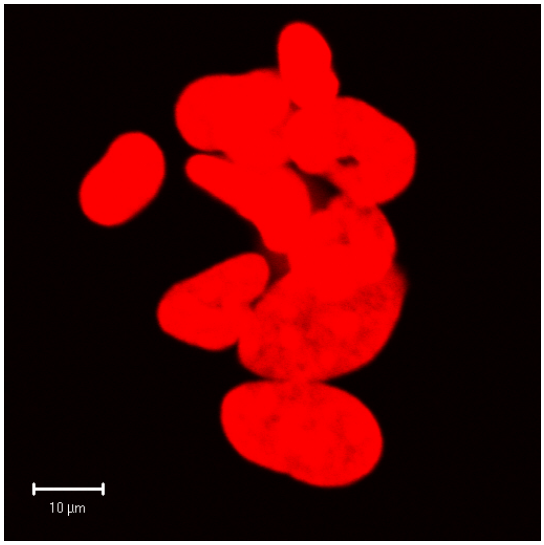

Figure 34c: MGH-U1R nuclei exposed to epirubicin 10µg/ml for 10 minutes after nuclear fractionation (x40 Lens; Gain 825; Zoom x6)
Epirubicin fluorescence only

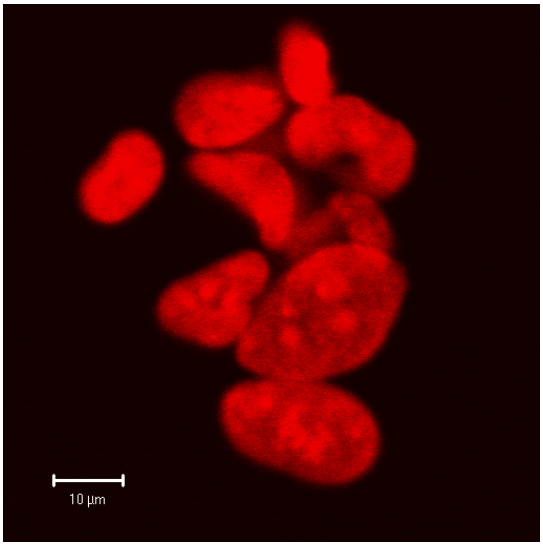

Figure 34d: MGH-U1R nuclei exposed to epirubicin 10µg/ml for 10 minutes after nuclear fractionation (x40 Lens; Gain 735; Zoom x6)
Epirubicin fluorescence only

Comparing nuclei that have been pre-exposed to epirubicin rather than exposed post nuclear fractionation shows that pre-exposed nuclei of both cell types take up much less epirubicin. This difference is most noticeable in the

MGH-U1R nuclei, but also exists in the MGH-U1 nuclei when images at similar gain settings of 825 are compared (Figure 33c and 34c).

Idarubicin uptake at 37^{o}C

The nuclear uptake of idarubicin is very similar in MGH-U1 and MGH-U1R nuclei extracted from cells pre-exposed to idarubicin. This is shown in figures 35a and b where the nuclear idarubicin staining of MGH-U1 and MGH-U1R nuclei can be compared, with the confocal gain set at 850.

MGH-U1 and MGH-U1R nuclei exposed to idarubicin after nuclear fractionation showed very similar levels of drug uptake, at a confocal gain setting of 850, as demonstrated in figures 36a and b.

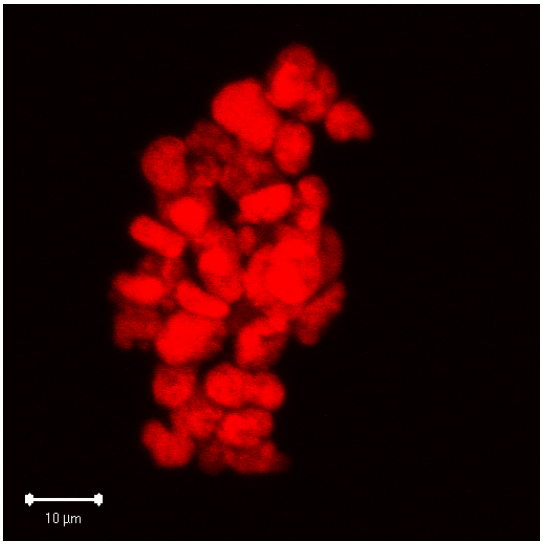

Figure 35a: MGH-U1 nuclei extracted after exposure of cells to idarubicin 20µg/ml for 2 hours (x40 Lens; Gain 850; Zoom x6)
Idarubicin fluorescence only

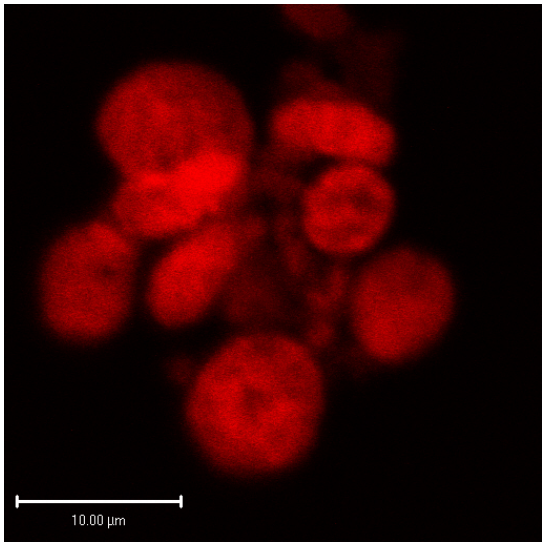

Figure 35b: MGH-U1R nuclei extracted after exposure of cells to idarubicin 20µg/ml for 2 hours (x40 Lens; Gain 850; Zoom x14)
Idarubicin fluorescence only

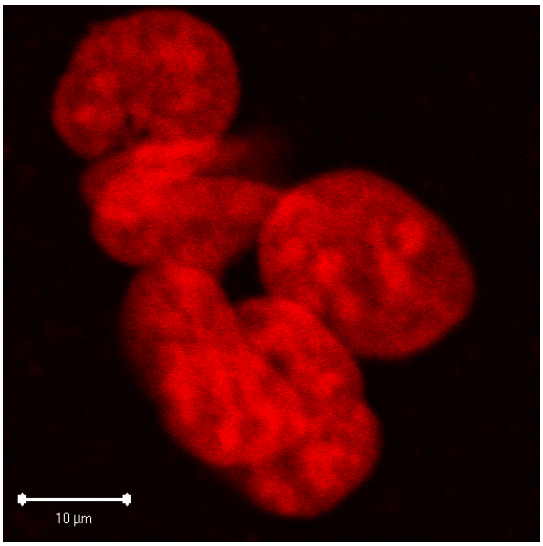

Figure 36a: MGH-U1 nuclei exposed to idarubicin 20µg/ml for 10 minutes after nuclear fractionation (x40 Lens; Gain 850; Zoom x9)
Idarubicin fluorescence only

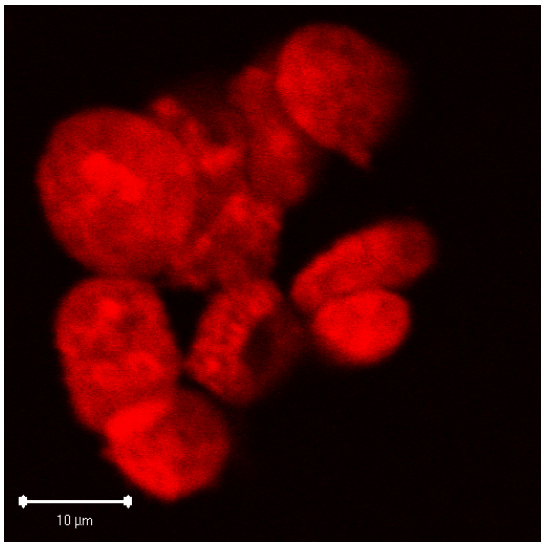

Figure 36b: MGH-U1R nuclei exposed to idarubicin 20µg/ml for 10 minutes after nuclear fractionation (x40 Lens; Gain 850; Zoom x9)
Idarubicin fluorescence only

There doesn't appear to be much difference in idarubicin uptake between pre and post- nuclear fractionation exposure. This suggests nuclear drug uptake is not affected by being in the cells and suggest that there is something preventing nuclear uptake in both sensitive and resistant nuclei that is a nuclear uptake problem rather that a cellular uptake problem.
This highlights a common problem with confocal imaging, in that the fluorescence gain for your image is set based on the area with the highest levels of drug uptake. If the fluophore is most concentrated in an area other than the nucleus, then it may appear that there is no nuclear uptake when in fact there could be low level nuclear uptake.
In comparison to nuclei exposed to epirubicin, there are lower levels of nuclear fluorescence in nuclei exposed to idarubicin post-fractionation, despite using a higher concentration of drug (20µg/ml). This again suggests that some nuclear factor contributes to idarubicin exclusion. Perhaps idarubicin does not bind to DNA as avidly as epirubicin or when it does its fluorescence is quenched in some way.

Mitomycin C fluorescence

Direct fluorescence experiments:

Dose response:

Fluorescence was only detected with FITC detection settings using a 488nm laser to excite emissions and a long pass 505nm filter to detect fluorescence (Figures 37a – f).
Whilst some cells demonstrated nice fluorescence, others did not. The reasons for this are unclear. Mitomycin C is quite an unstable drug, so it is possible that in some experiments the mitomycin C was degraded to a non-fluorescent molecule.

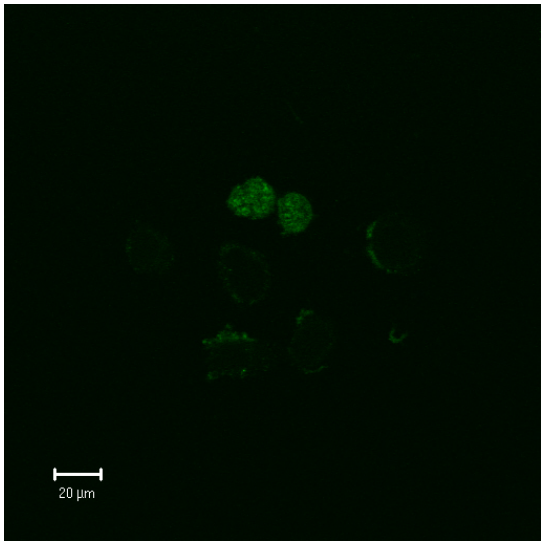

Figure 37a : MGH-U1 cells – control (No mitomycin C) (x40 lens; Gain setting 900) Baseline FITC fluorescence only

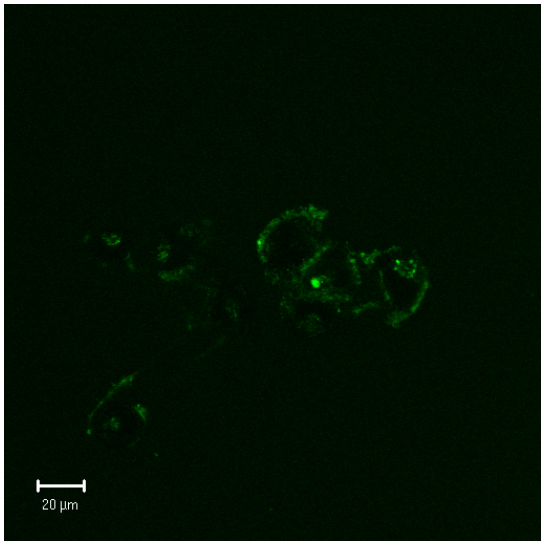

Figure 37b : MGH-U1R cells – control (No mitomycin C) (x40 lens; Gain setting 900) Baseline FITC fluorescence only

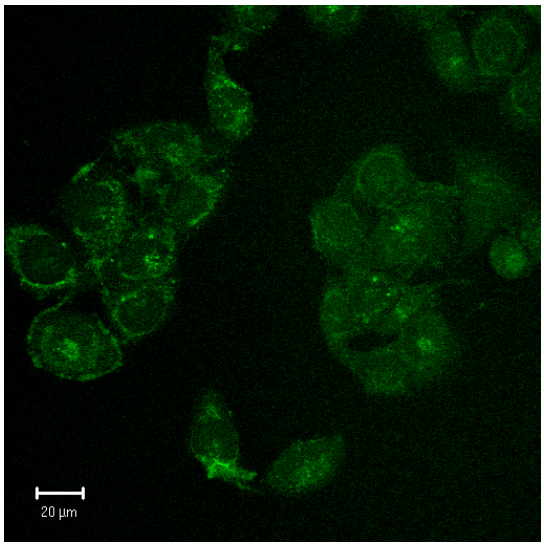

Figure 37c : MGH-U1 cells – 250µg/ml mitomycin C (x40 lens; Gain setting 900) FITC fluorescence only

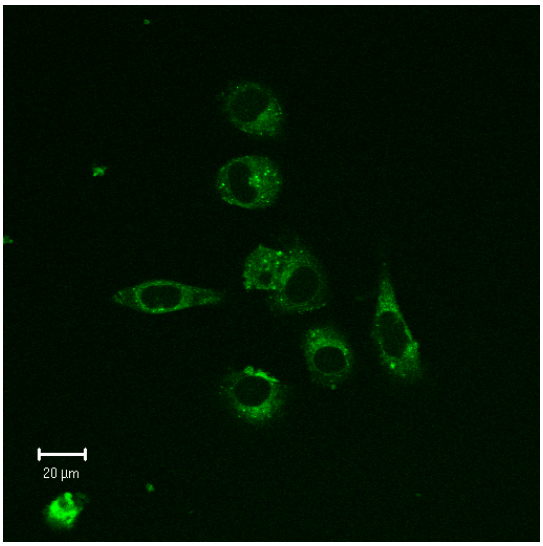

Figure 37d : MGH-U1R cells – 250µg/ml mitomycin C (x40 lens; Gain setting 900) FITC fluorescence only

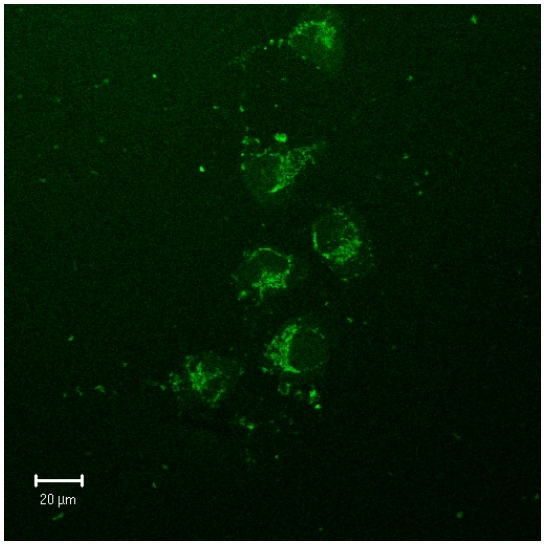

Figure 37e : MGH-U1 cells – 1000µg/ml mitomycin C (x40 lens; Gain setting 900) FITC fluorescence only

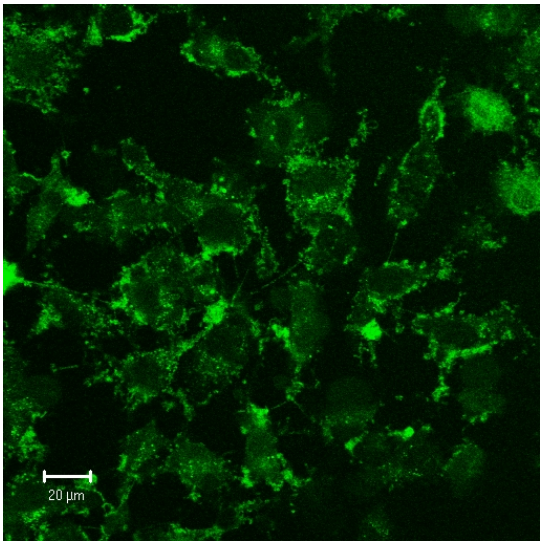

Figure 37f : MGH-U1R cells – 1000µg/ml mitomycin C (x40 lens; Gain setting 900) FITC fluorescence only

Time series:

Time series experiments were performed looking at FITC fluorescence, comparing baseline cell fluorescence to fluorescence levels over 50 minutes once mitomycin C 250µg/ml was added to the culture medium. The FITC detector gain was set at 900. Cellular fluorescence levels over time were assessed using a region of interest (ROI) function, allowing us to plot graphs of fluorescence over time for MGH-U1 and MGH-U1R cells as shown below (Figure 38). For MGH-U1, 18 cells were analysed, whereas for MGH-U1R only 5 cells were evaluable. Confidence intervals (95%) for MGH-U1 cells were all ≤0.044 and for MGH-U1R cells were all ≤0.39.

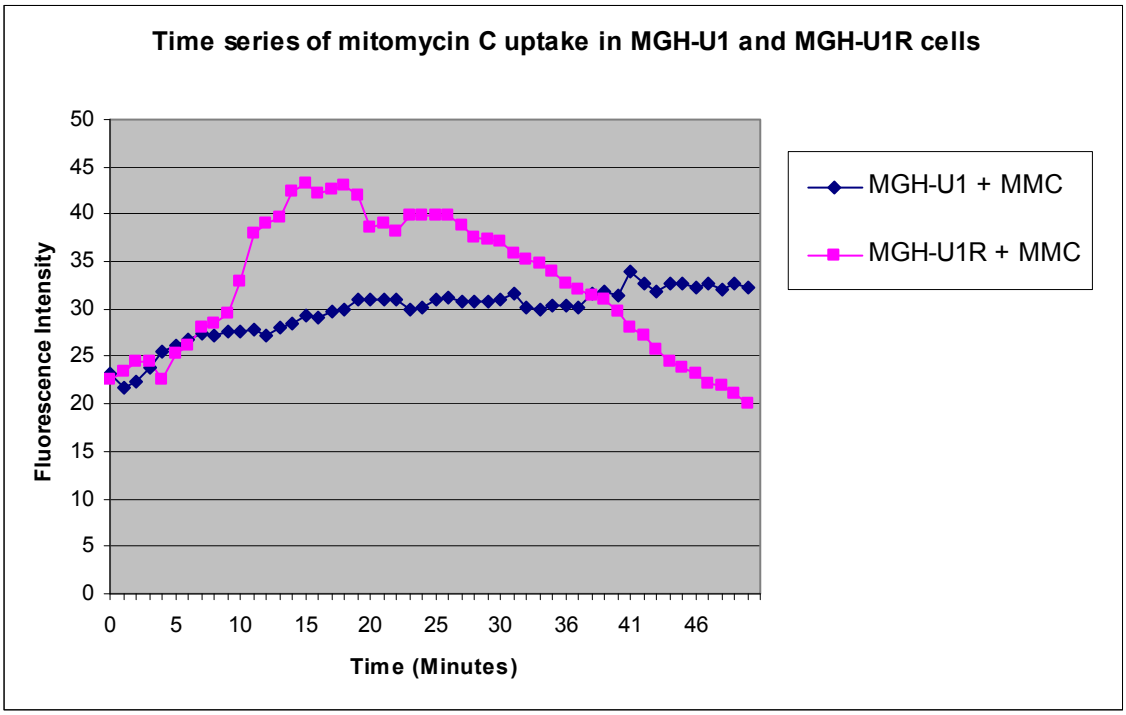

Figure 38: Graph of mitomycin C uptake over time in MGH-U1 and MGH-U1R cells incubated with 250µg/ml of mitomycin C for 50 minutes.

Overall these experiments did not convincingly prove that we could detect mitomycin C fluorescence. The MGH-U1 cells showed a small increase in fluorescence levels over time, suggesting that we may be able to detect low level mitomycin C fluorescence. The MGH-U1R cells demonstrated peak fluorescence levels after 20 minutes. From there fluorescence levels declined, again suggesting the presence of some low level mitomycin C fluorescence. These falling levels of fluorescence may indicate that

mitomycin C is being removed from the cells by an MDR mechanism such as P-gp related drug efflux or could possibly represent degradation of mitomycin C to non-fluorescent derivatives.

Indirect fluorescence experiments:

A comparison of control cells (incubated with acridine orange (AO) only) with cells incubated with either 250 or 1000µg/ml of mitomycin C followed by incubation with AO, are shown below for MGH-U1 and MGH-U1R cells (Table 16).

Cell Type / MMC Dose	Number of Nuclei	Area μm^2	Mean Fluorescence	Standard Deviation	Maximum Frequency Intensity (Min – Max)
MGH-U1:					
Control	40	6274.5	102	32	107 (4 – 239)
250 MMC	48	7600.6	78	31	65 (5 – 214)
1000 MMC	33	4883.4	68	29	61 (4 – 200)
MGH-U1R:					
Control	51	5948.2	103	39	86 (7 – 254)
250 MMC	58	7477.5	94	42	87 (5 – 251)
1000 MMC	24	2064.8	76	47	39 (7 – 212)

Table 16: Acridine orange fluorescence after exposure of MGH-U1 and MGH-U1R cells to mitomycin C

These results show that in sensitive cells nuclear AO fluorescence is reduced by incubation with mitomycin C with evidence of a dose response. In the resistant cells, acridine orange fluorescence is also reduced by mitomycin C exposure, but to a lesser degree as one would expect. The results for the MDR cells incubated with 1000µg/ml of mitomycin C may be slightly spurious as only 24 nuclei were evaluable.

Wheat Germ Agglutinin (WGA) nuclear pore binding studies

FITC-WGA cellular localisation studies

This experiment looked at the optimum time for localisation of FITC-WGA to the nuclear membrane. Confocal images are shown below for MGH-U1 and MGH-U1R cells after incubation times of 30 minutes, 1, 2, 4, 8, 16, 24 and 48 hours following exposure to 0.4µg/ml of FITC-WGA for 1 hour at 37^{o}C (Figures 39a – r).

MGH-U1 cells:

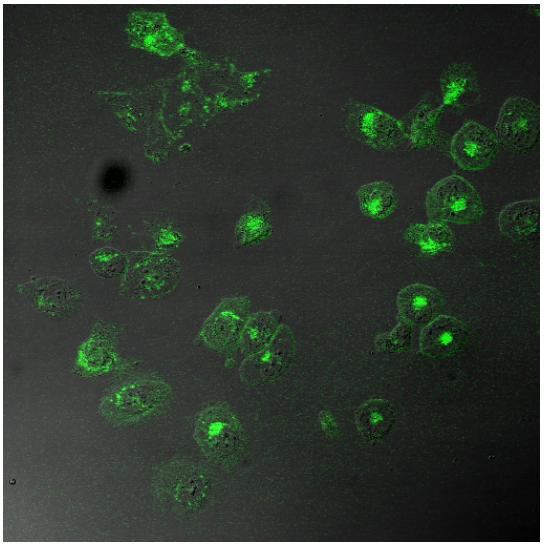

Figure 39a: MGH-U1 cells: 30 minutes post FITC-WGA exposure; FITC fluorescence only

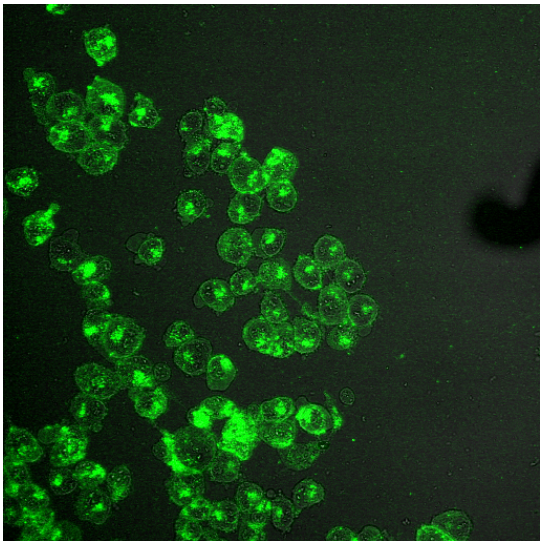

Figure 39b: MGH-U1 cells: 1 hour post FITC-WGA exposure; FITC fluorescence only

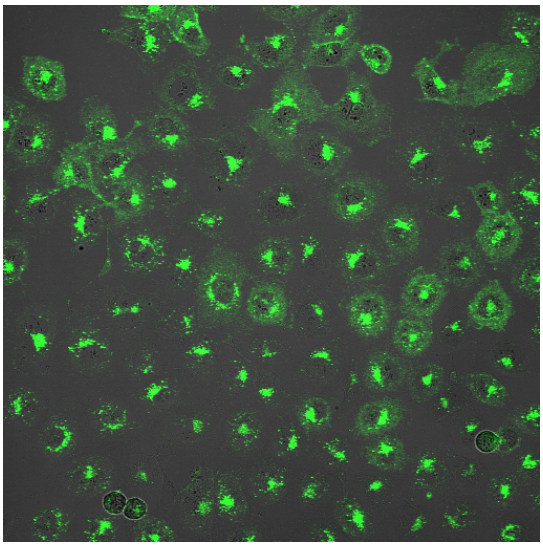

Figure 39c: MGH-U1 cells: 2 hours post FITC-WGA exposure; FITC fluorescence only

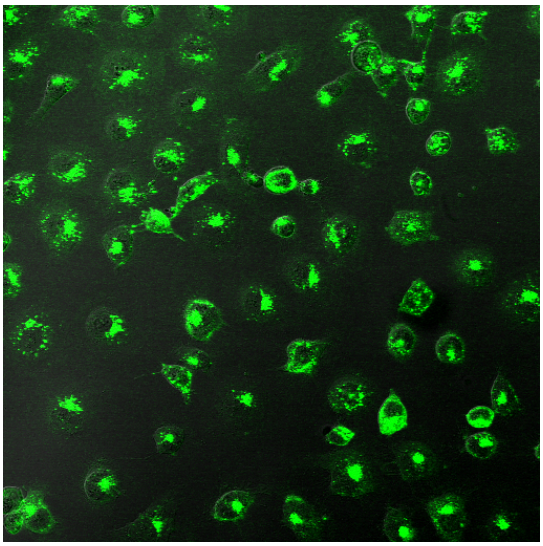

Figure 39d: MGH-U1 cells: 4 hours post FITC-WGA exposure; FITC fluorescence only

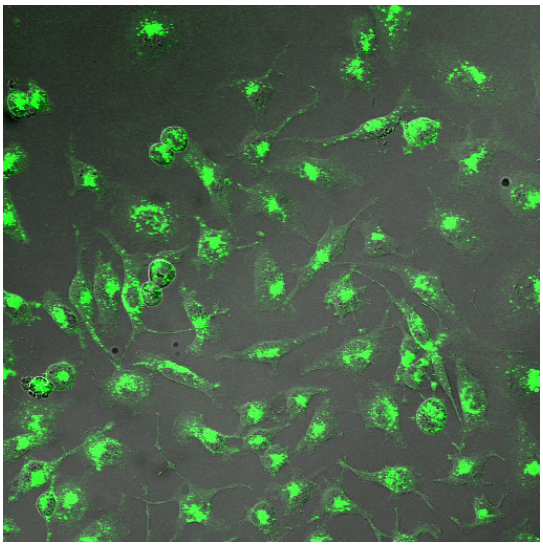

Figure 39e: MGH-U1 cells: 8 hours post FITC-WGA exposure; FITC fluorescence only

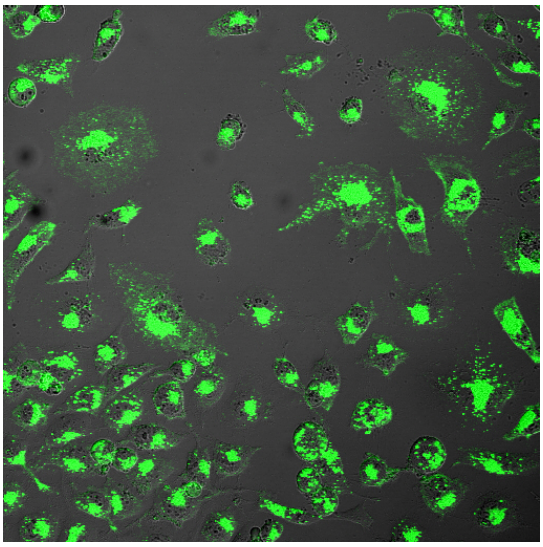

Figure 39f: MGH-U1 cells: 16 hours post FITC-WGA exposure; FITC fluorescence only

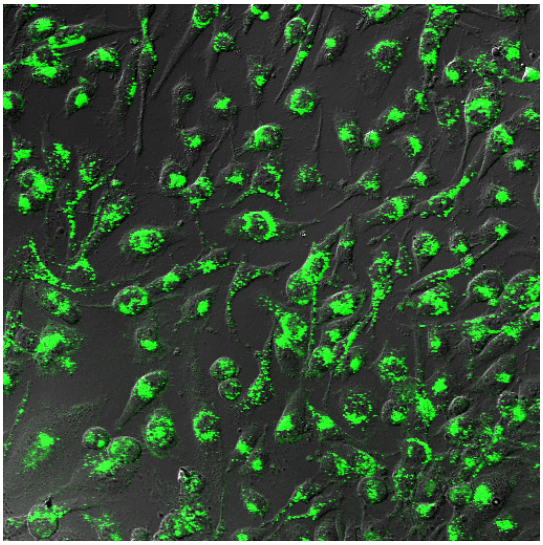

Figure 39g: MGH-U1 cells: 24 hours post FITC-WGA exposure; FITC fluorescence only

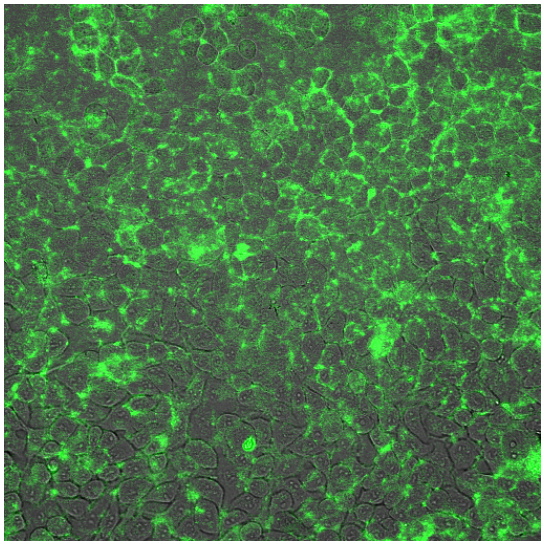

Figure 39b: MGH-U1 cells: 48 hours post FITC-WGA exposure; FITC fluorescence only

MGH-U-1R cells:

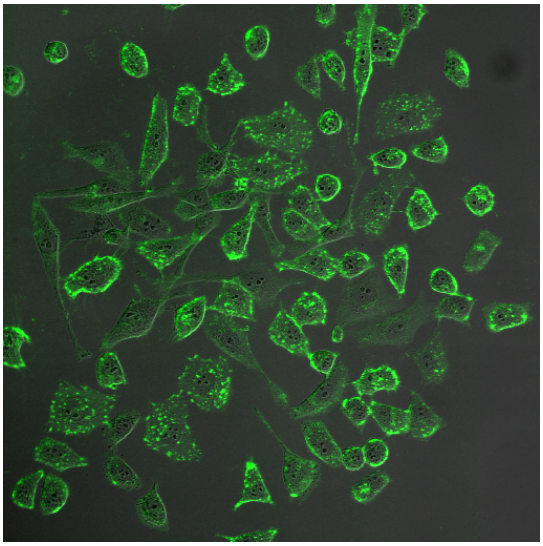

Figure 39i: MGH-U1R cells: 30 minutes post FITC-WGA exposure; FITC fluorescence only

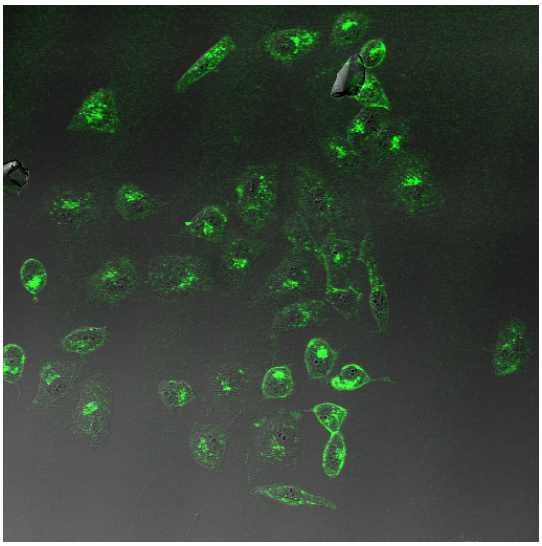

Figure 39j: MGH-U1R cells: 1 hour post FITC-WGA exposure; FITC fluorescence only

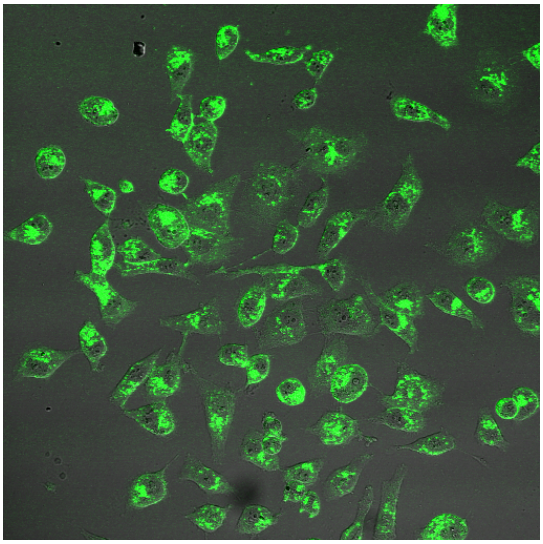

Figure 39k: MGH-U1R cells: 2 hours post FITC-WGA exposure; FITC fluorescence only

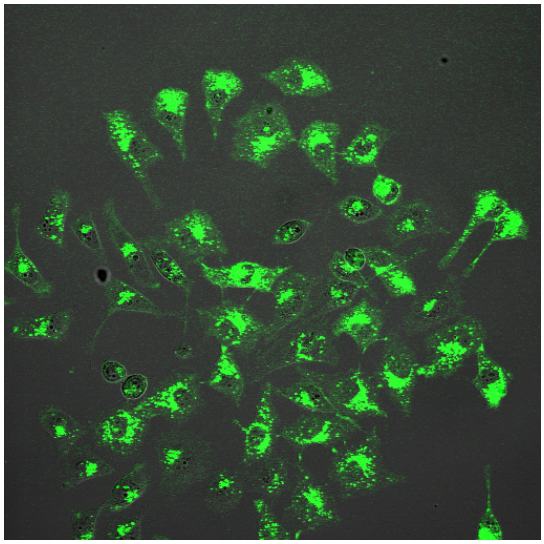

Figure 39l: MGH-U1R cells: 4 hours post FITC-WGA exposure; FITC fluorescence only

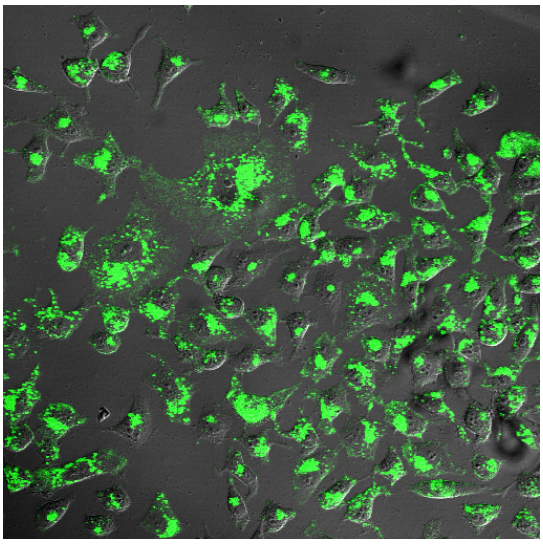

Figure 39m: MGH-U1R cells: 8 hours post FITC-WGA exposure; FITC fluorescence only

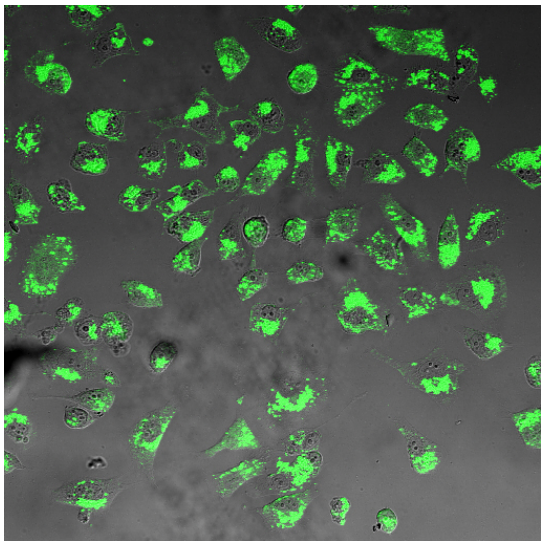

Figure 39n: MGH-U1R cells: 16 hours post FITC-WGA exposure; FITC fluorescence only

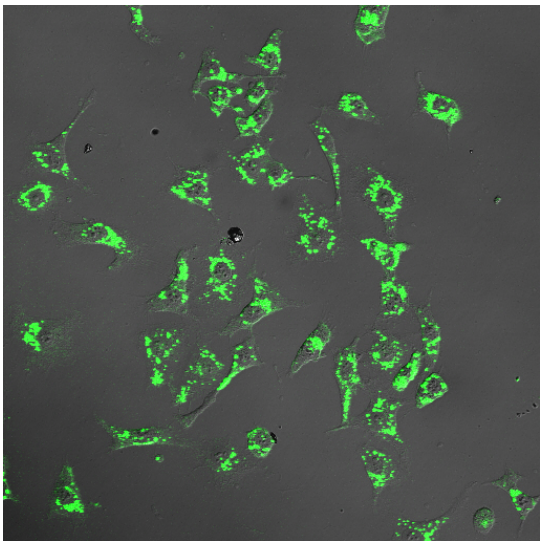

Figure 39o: MGH-U1R cells: 24 hours post FITC-WGA exposure; FITC fluorescence only

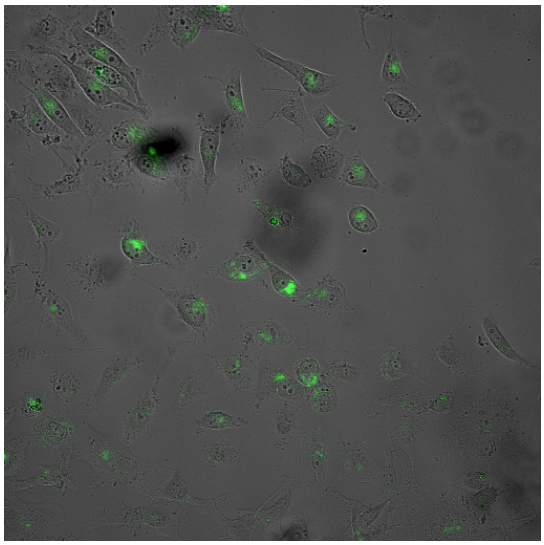

Figure 39p: MGH-U1R cells: 48 hours post FITC-WGA exposure; FITC fluorescence only

We also exposed cells to FITC-WGA 0.4µg/ml for 24 hours continuously.

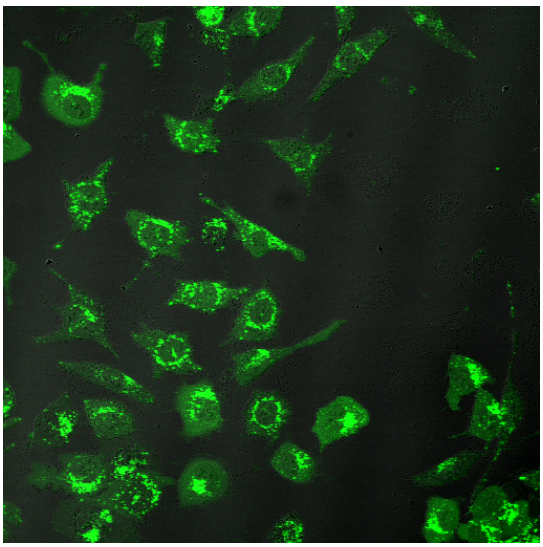

Figure 39q: MGH-U1 cells: Continuous exposure to FITC-WGA for 24 hours; FITC fluorescence only

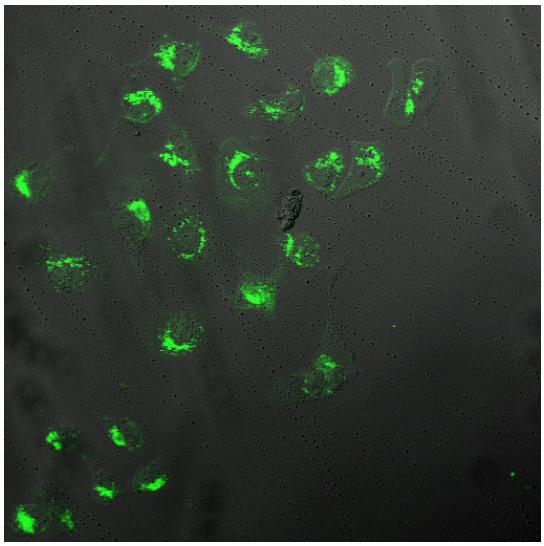

Figure 39r: MGH-U1R cells: Continuous exposure to FITC-WGA for 24 hours; FITC fluorescence only

This experiment showed that FITC-WGA accumulates around the nuclear membrane almost immediately with 30 minute samples showing some peri-nuclear staining. Peri-nuclear staining increases with time reaching a plateau at about 4 hours which persists up to 24 hours. Continuous exposure gives a similar pattern of peri-nuclear staining at 24 hours. Levels of peri-nuclear staining at 48 hours are much lower, presumably due to dilution as a result of cell division.

FITC-WGA nuclear localisation studies

Nuclear preparations exposed to FITC-WGA again showed strong perinuclear staining suggesting active binding to nuclear pore complexes (Figures 40a–d).

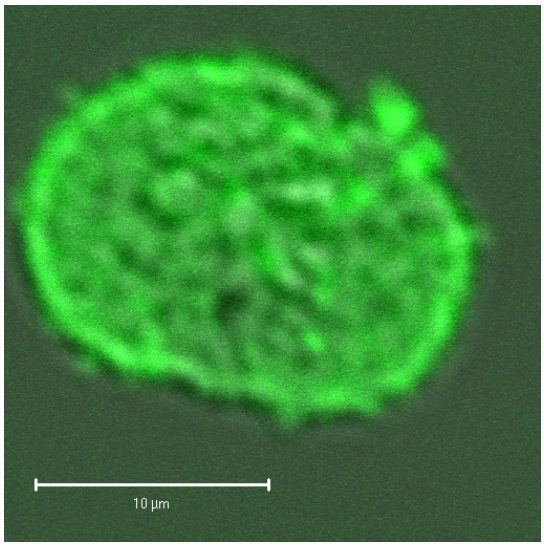

Figure 40a: Single MGH-U1 nucleus: exposed to FITC-WGA 0.4µg/ml for 10 minutes after nuclear fractionation (x20 Lens; Gain 1047; Zoom x20) FITC fluorescence overlaid on DIC image

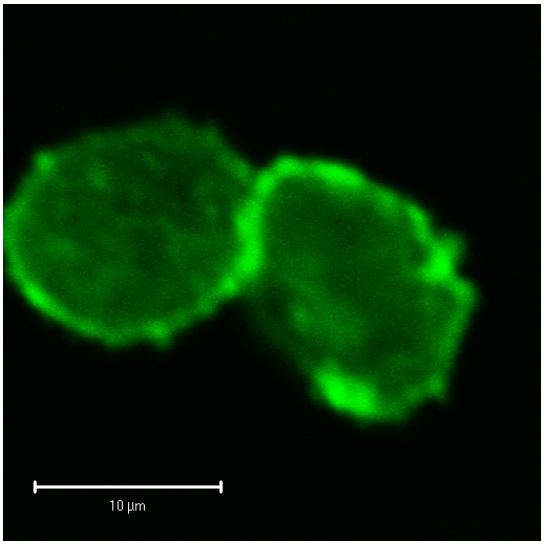

Figure 40b: Two MGH-U1R nuclei: exposed to FITC-WGA 0.4µg/ml for 10 minutes after nuclear fractionation (x20 Lens; Gain 827; Zoom x9) FITC fluorescence only

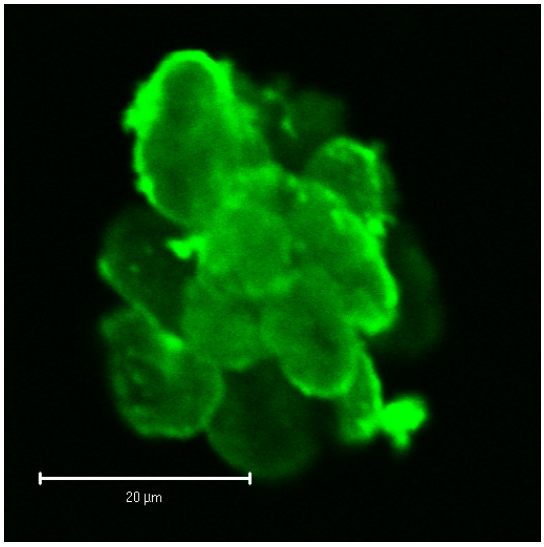

Figure 40c: Cluster of MGH-U1 nuclei: exposed to FITC-WGA 0.4µg/ml for 10 minutes after nuclear fractionation (x20 Lens; Gain 852; Zoom x16) FITC fluorescence only

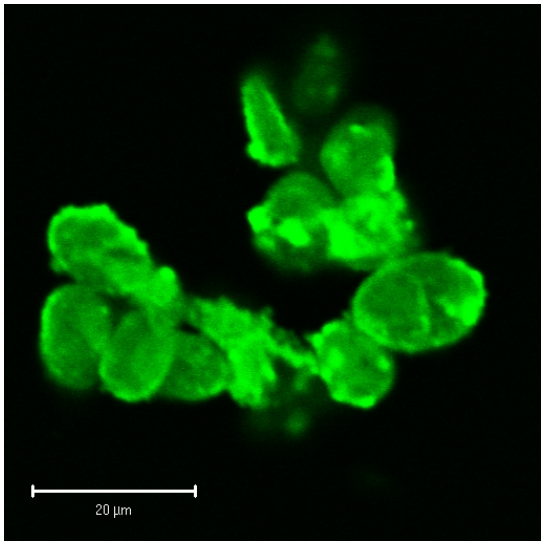

Figure 40d: Cluster of MGH-U1R nuclei: exposed to FITC-WGA 0.4µg/ml for 10 minutes after nuclear fractionation (x20 Lens; Gain 831; Zoom x7) FITC fluorescence only

Nuclear pore sizing using FITC-dextrans and the effects of WGA nuclear pore blockade

Scrape-loading of cells with various sized FITC-dextrans was a slightly hit or miss procedure with cells being heterogeneous as to the amount of dextrans taken up. This heterogeneity relates to the fact that FITC-dextran uptake is dependent on the small breaches made in the plasma membrane of cells during the scrape loading process, so was not unexpected.

Cells were viewed at several different time points to assess any changes in cellular localisation over time. The time points at which cells were visualised were 6, 18, 24, 48 and 72 hours.

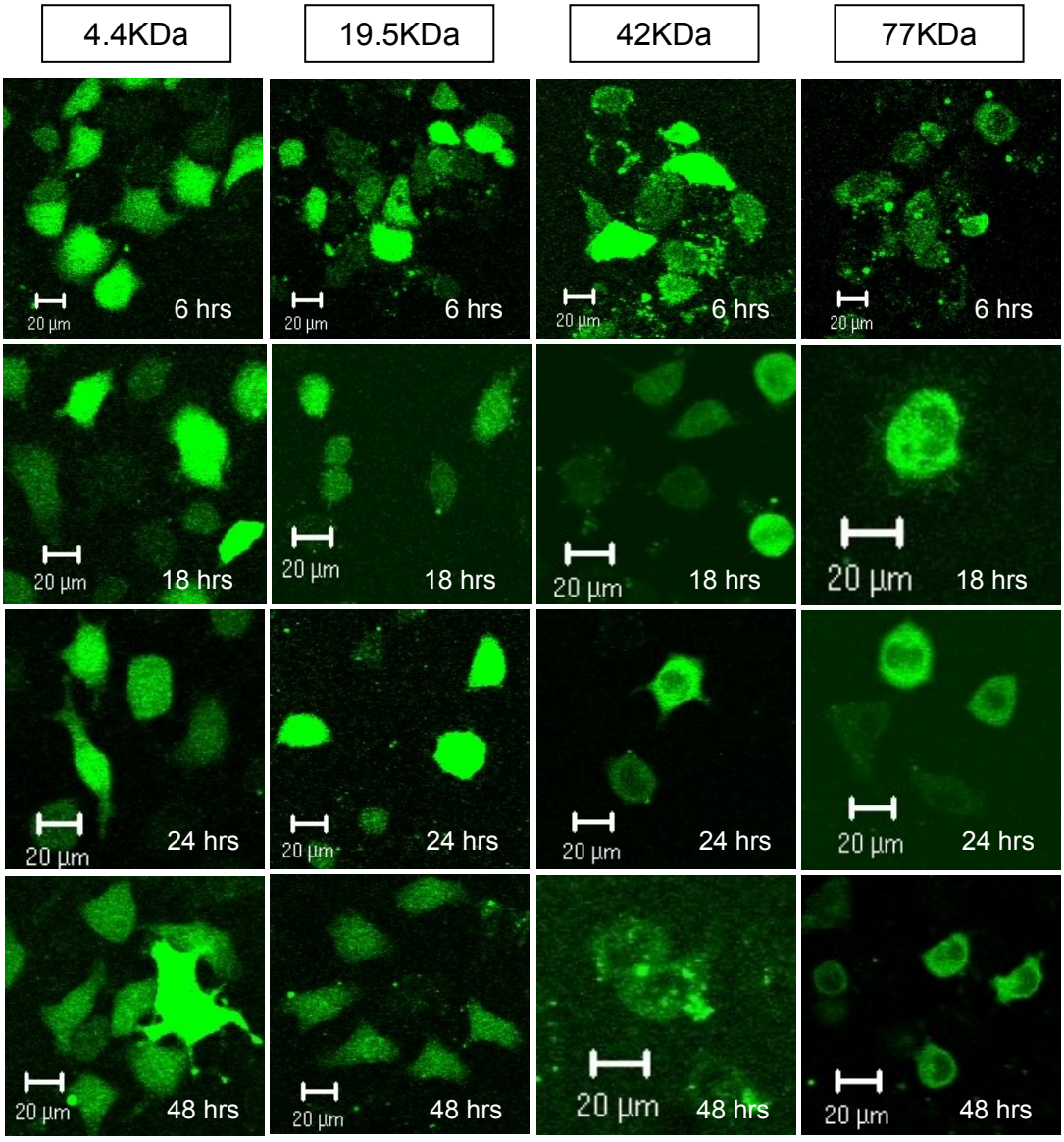

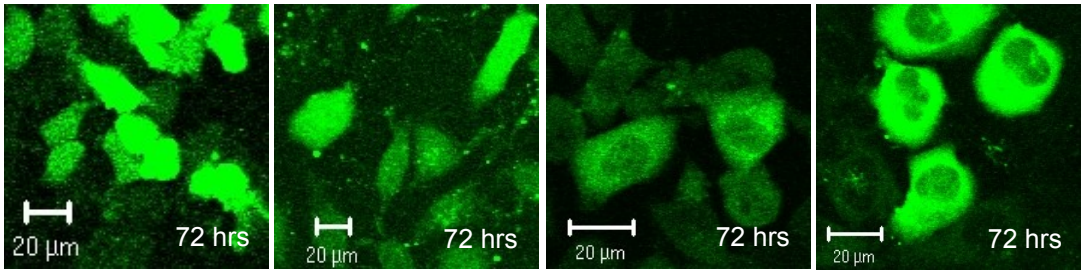

Figure 41: MGH-U1 cells scrape-loaded with FITC-dextrans

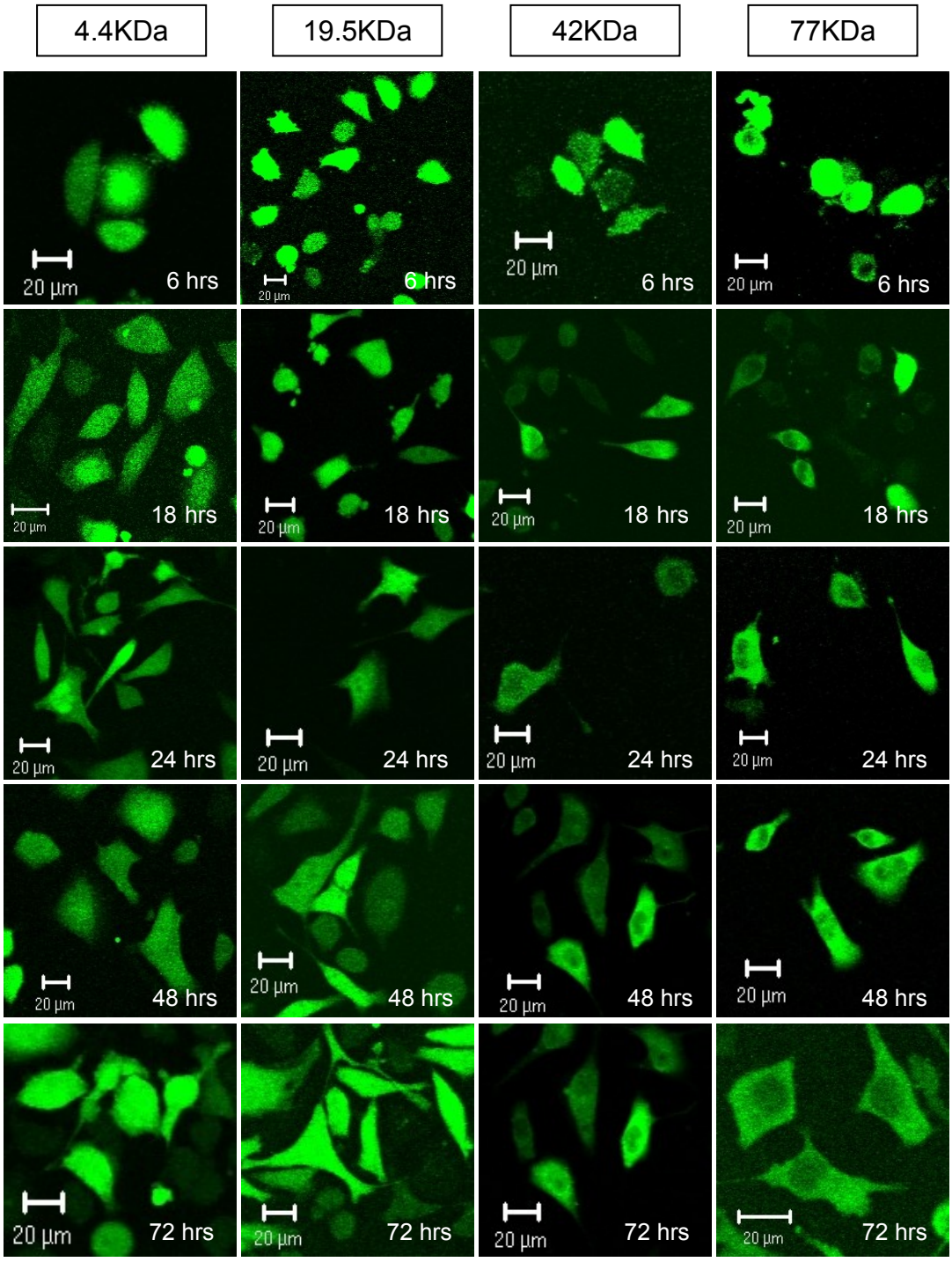

Figure 42: MGH-U1R cells scrape-loaded with FITC-dextrans

These experiments showed that FITC-dextrans larger that 42KDa were excluded from the nuclei of MGH-U1 (sensitive) and MGH-U1R (MDR) cells. FITC-dextrans smaller than 19.5KDa gained entry to the nuclei of MGH-U1 (sensitive) and MGH-U1R (MDR) cells. There were no changes in the distribution of the FITC-dextrans over time, suggesting that the FITC-dextrans enter the nucleus by passive diffusion through nuclear membrane pores and not by active transport, otherwise we would have expected increases in nuclear uptake with time (Figures 41 and 42).

We assessed the ability of wheat germ agglutinin (WGA) to reduce the functional diameter of nuclear pores by first pre-incubating cells with WGA for 24 hrs followed by scrape loading with the 19.5KDa FITC-dextran. We reviewed the cells 24 hours later (Figures 43a and b).

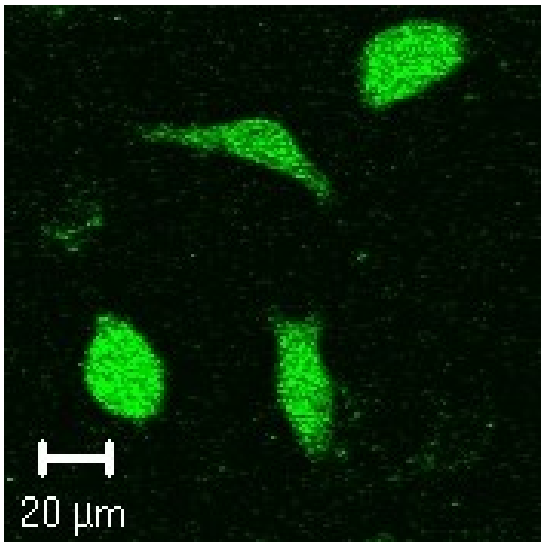

Figure 43a: MGH-U1 cells incubated with WGA and then scrape-loaded with 19.5KDa FITC-dextran; FITC fluorescence only

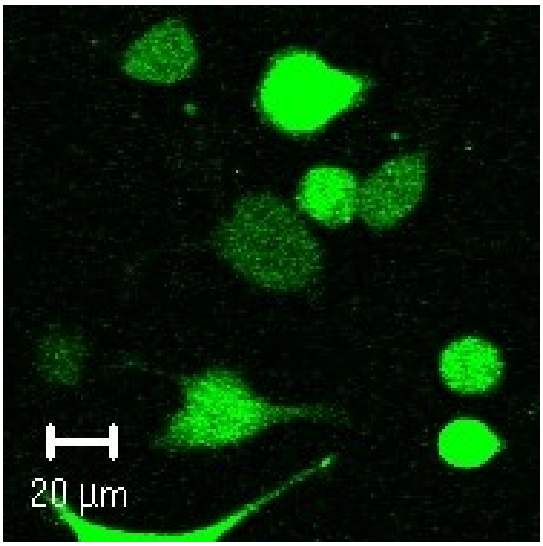

Figure 43b: MGH-U1R cells incubated with WGA and then scrape-loaded with 19.5KDa FITC-dextran; FITC fluorescence only

This study showed that WGA did not preclude entry of a 19.5KDa FITC-dextran into the nuclei of MGH-U1 (sensitive) or MGH-U1R (MDR) cells. This does not mean that the functional diameter of the nuclear pores is not reduced by WGA, just that our experiment was too insensitive to detect a change in the functional diameter. This experiment suggests that if epirubicin is permitted entry to the nucleus by passive diffusion, WGA should not affect this process, as epirubicin is only 0.58KDa in size.

The effects of WGA pre-incubation on nuclear uptake of epirubicin

Whole cells:

The results of incubating MGH-U1 and MGH-U1R cells with epirubicin with or without pre-incubation with WGA, on the phenotypic uptake of epirubicin are shown below (Figure 44a – d).

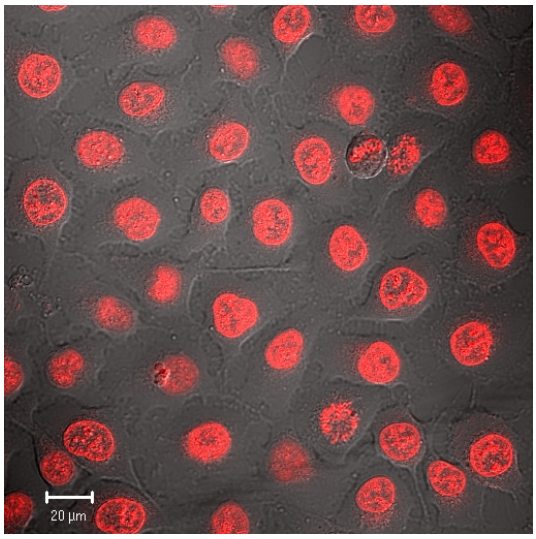

Figure 44a: MGH-U1 cells incubated with epirubicin alone. Epirubicin fluorescence overlaid on DIC image (Gain 800)

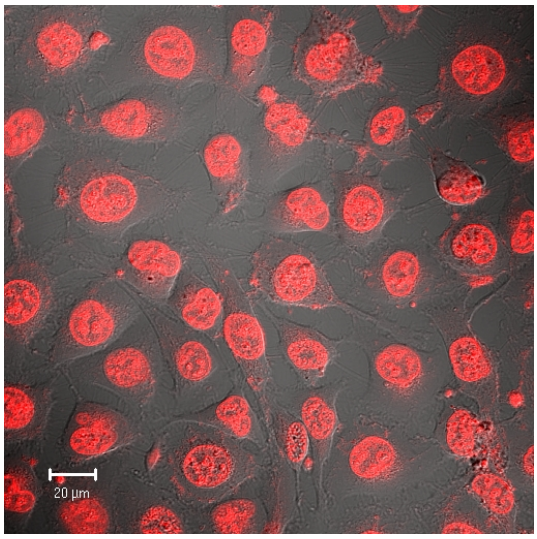

Figure 44b: MGH-U1 cells pre-incubated with WGA and then incubated with epirubicin. Epirubicin fluorescence overlaid on DIC image (Gain 800).

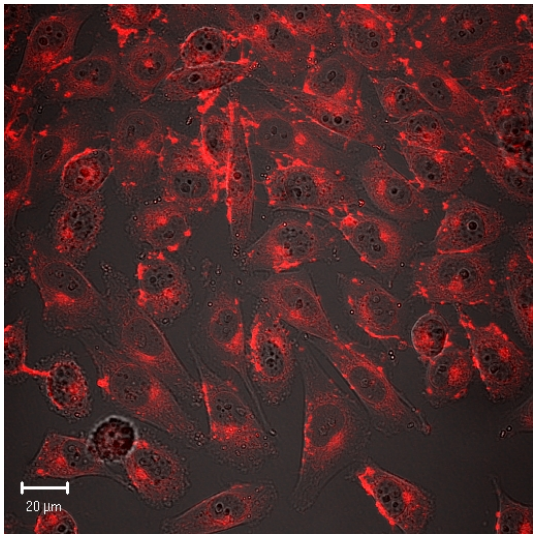

Figure 44c: MGH-U1R cells incubated with epirubicin alone. Epirubicin fluorescence overlaid on DIC image (Gain 1050)

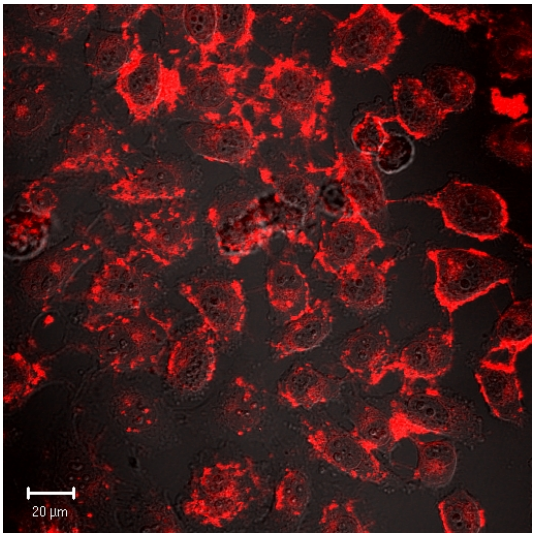

Figure 44d: MGH-U1R cells pre-incubated with WGA and then incubated with epirubicin. Epirubicin fluorescence overlaid on DIC image (Gain 1050)

No change in the cellular distribution of epirubicin after exposure to WGA was demonstrated. Sensitive cells maintained their sensitive nuclear uptake pattern and resistant cells exhibited their characteristic nuclear sparing of epirubicin uptake. These results were confirmed on multiple occasions.

Analysis was undertaken using a region of interest (ROI) function on the confocal microscope. Gain settings for all analysis images were set at 1050. As we were primarily interested in the nuclear uptake of epirubicin, nuclear fluorescence was analysed in 20 cells from each sample. To avoid any bias between samples, all nuclei were drawn around using the DIC image with no fluorescence. The fluorescence image was then reinstated and analysis undertaken. Data from this experiment are displayed below (Table 17). Confocal microscopy is only a semi-quantitative means of measuring fluorescence and given the small differences between samples, these are not significant. Flow cytometric experiments were performed to accurately analyse differences in cellular drug uptake attributable to WGA.

Experiment n = 20	Total Area μm^2	Mean Fluorescence (SD)	Maximum Frequency / Intensity	Range of Fluorescence
MGH-U1 + Epirubicin alone	4778.6	249 (25)	20733 at 255 (Max)	9 – 255
MGH-U1 + WGA + Epirubicin	4658.6	248 (27)	20214 at 255 (Max)	8 – 255
MGH-U1R + Epirubicin alone	4003.2	41 (32)	790 at 126	43 - 255
MGH-U1R + WGA + Epirubicin	4016.6	46 (35)	628 at 140	22 – 255

Table 17: Confocal microscopy ROI data for nuclear epirubicin uptake cells pre-incubated with WGA

Nuclei

Results for MGH-U1 and MGH-U1R nuclear preparations pre-exposed to WGA are shown below. Nuclei that were exposed to epirubicin for 2 hours prior to nuclear fraction preparation are shown first (Figures 45a – d).
The figures following these show the results of epirubicin uptake post-nuclear fractionation in control cells and cells that were pre-exposed to WGA (Figures 46a – d).

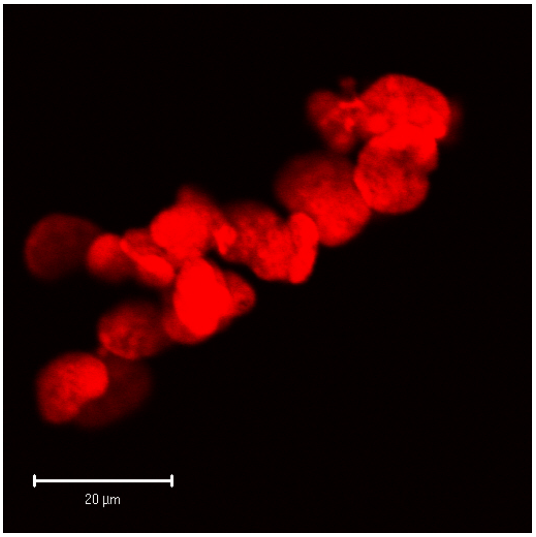

Figure 45a: MGH-U1 nuclei exposed to epirubicin for 2 hours before nuclear preparation. Fluorescence only image. Zoom x6. Gain 825.

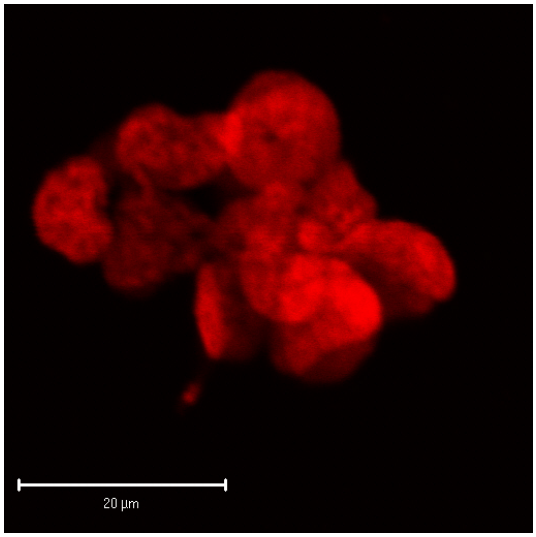

Figure 45b: MGH-U1 nuclei exposed to WGA and then epirubicin for 2 hours before nuclear preparation. Fluorescence only image. Zoom x9. Gain 825.

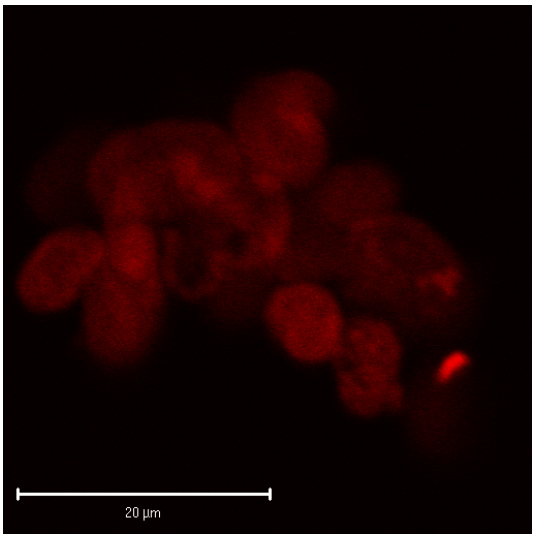

Figure 45c: MGH-U1R nuclei exposed to epirubicin for 2 hours before nuclear preparation. Fluorescence only image. Zoom x6. Gain 1000.

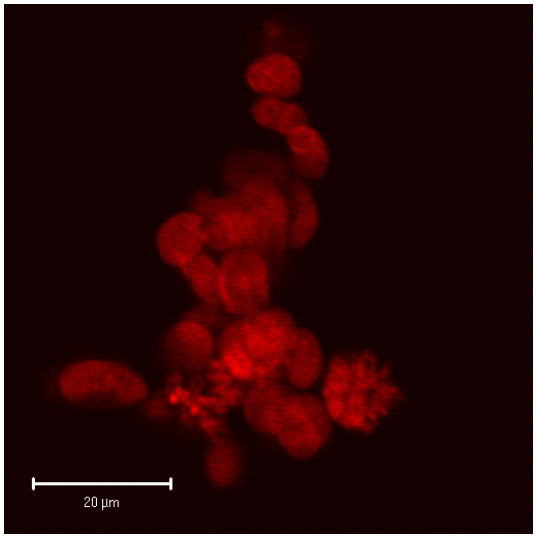

Figure 45d: MGH-U1R nuclei exposed to WGA and then epirubicin for 2 hours before nuclear preparation. Fluorescence only image. Zoom x6. Gain 1000.

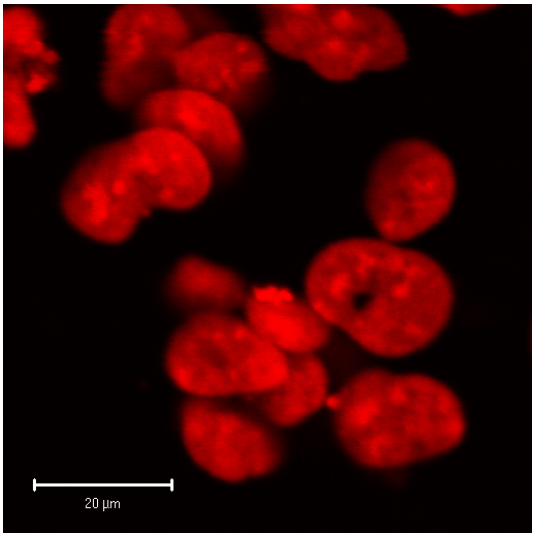

Figure 46a: MGH-U1 nuclei exposed to epirubicin for 10 minutes after nuclear preparation. Fluorescence only image. Zoom x6. Gain 735.

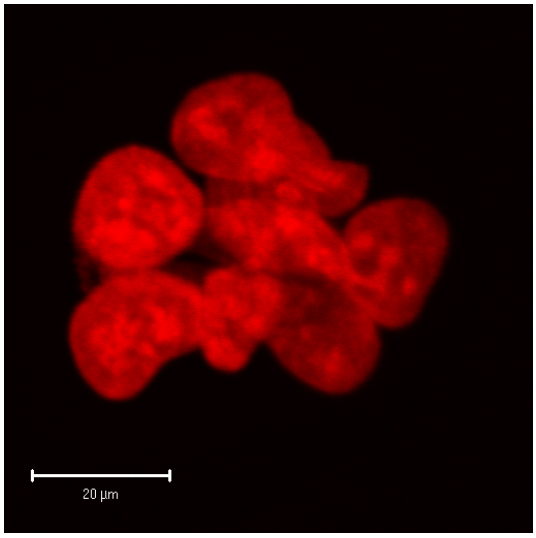

Figure 46b: MGH-U1 nuclei exposed to WGA and then to epirubicin for 10 minutes after nuclear preparation. Fluorescence only image. Zoom x6. Gain 735.

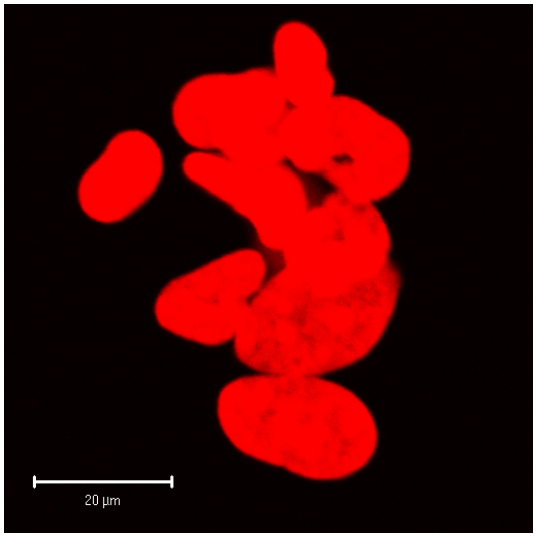

Figure 46c: MGH-U1R nuclei exposed to epirubicin for 10 minutes after nuclear preparation. Fluorescence only image. Zoom x6. Gain 825.

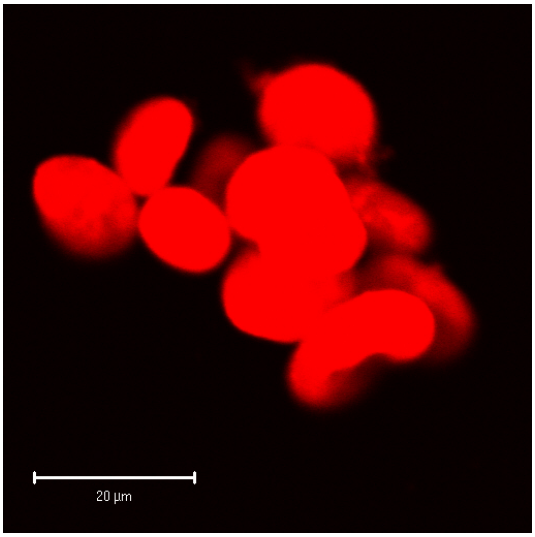

Figure 46d: MGH-U1R nuclei exposed to WGA and then to epirubicin for 10 minutes after nuclear preparation. Fluorescence only image. Zoom x7. Gain 825.

Analysis of nuclear fluorescence by confocal microscopy was impossible due to the clustering and random orientation of nuclei. Generally though, WGA did not seem to exert any effect on the nuclear accumulation of epirubicin in sensitive or MDR cells.

Flow cytometric analysis was later used to assess the impact of WGA on nuclear epirubicin fluorescence more accurately.

Cell fusion experiments using polyethylene glycol (PEG):

Fusion of cells offered a simple way to try and establish that the nuclear membrane plays a role in the MDR nuclear sparing phenotype.

Demonstration of a mixed cell fusion with a phenotypically sensitive nucleus and a phenotypically resistant nucleus in the same cell environment, would have provided clear evidence that the nuclear membrane is involved in this phenomenon.

The results of our non-mixed cell culture fusions showed that when sensitive cells fused together their normal pattern of epirubicin uptake was preserved with characteristic nuclear staining of both nuclei (Figure 47a). Resistant cell fusions also showed preservation of their characteristic pattern of epirubicin uptake with nuclear sparing in both nuclei (Figure 47b). Both cell fusion types were viable demonstrating strong green FDA fluorescence (Figures 47a – b).

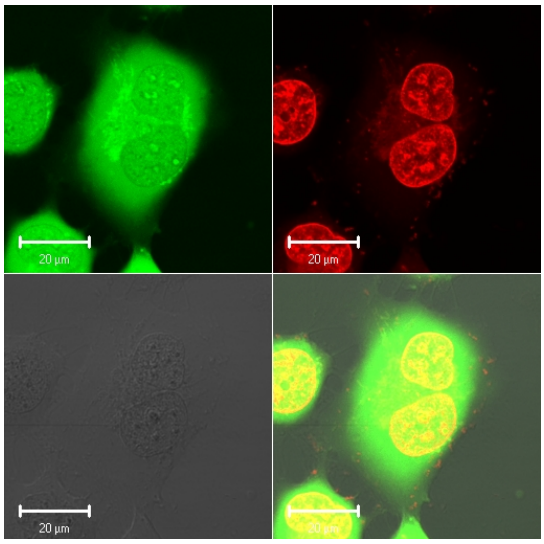

Figure 47a: Unmixed cell culture fusions: Sensitive-Sensitive cell fusion: Top Left: FDA fluorescence (Green); Top Right: Epirubicin fluorescence (Red); Bottom Left: DIC Image; Bottom Right: Overlay image

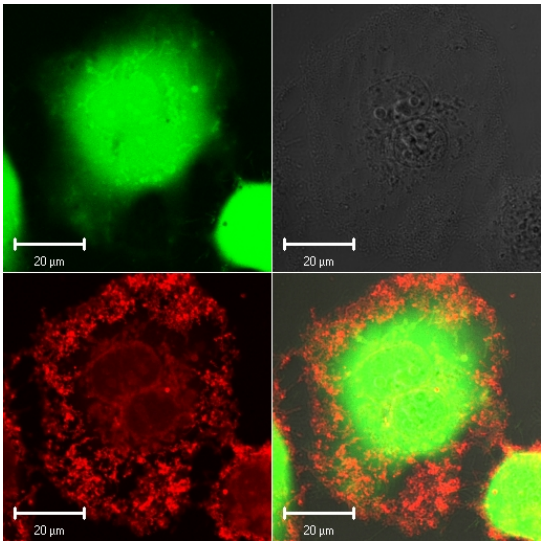

Figure 47b: Unmixed cell culture fusions: Resistant-Resistant cell fusion: Top Left: FDA fluorescence (Green); Top Right: DIC Image; Bottom Left: Epirubicin fluorescence (Red); Bottom Right: Overlay image

Not infrequently, multinucleate cell fusion products are seen, all of which maintain their characteristic nuclear phenotype (Figures 47c – f).

In mixed cell cultures we did not demonstrate any mixed cell fusions. Again we saw multiple cell fusions with phenotypically similar nuclei from bi-nucleate to multi-nucleate cells (Figures 47g – j). Again all fusion products appeared viable on staining with FDA.

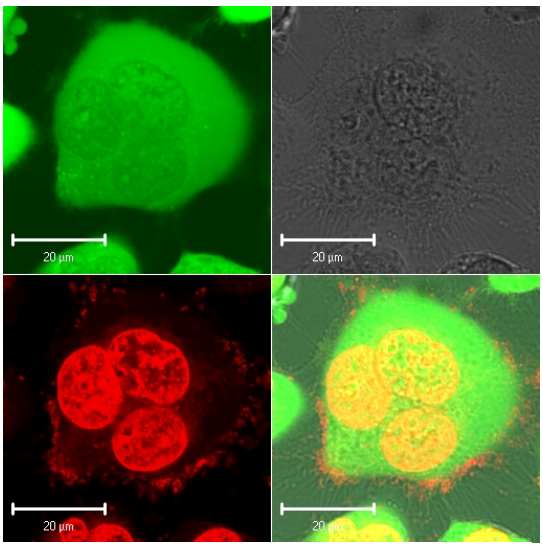

Figure 47c: Unmixed cell culture fusions: Sensitive tri-nucleate cell fusion: Top Left: FDA fluorescence (Green); Top Right: DIC Image; Bottom Left: Epirubicin fluorescence (Red); Bottom Right: Overlay image

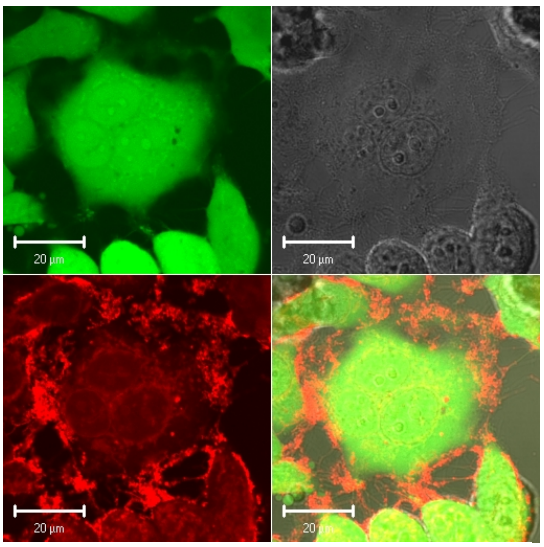

Figure 47d: Unmixed cell culture fusions: Resistant tri-nucleate cell fusion: Top Left: FDA fluorescence (Green); Top Right: DIC Image; Bottom Left: Epirubicin fluorescence (Red); Bottom Right: Overlay image

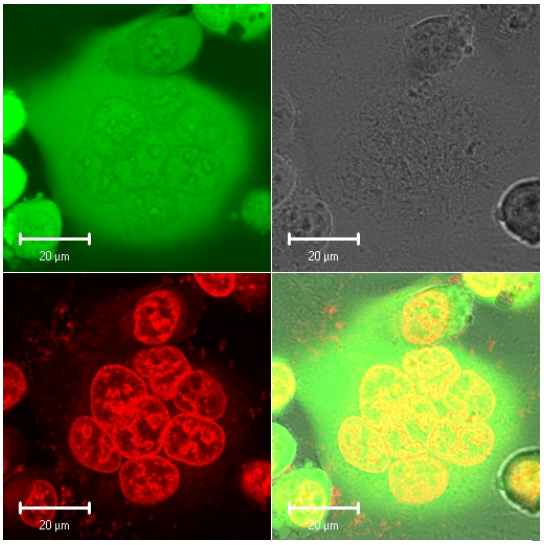

Figure 47e: Unmixed cell culture fusions: Sensitive multi-nucleate cell fusion: Top Left: FDA fluorescence (Green); Top Right: DIC Image; Bottom Left: Epirubicin fluorescence (Red); Bottom Right: Overlay image

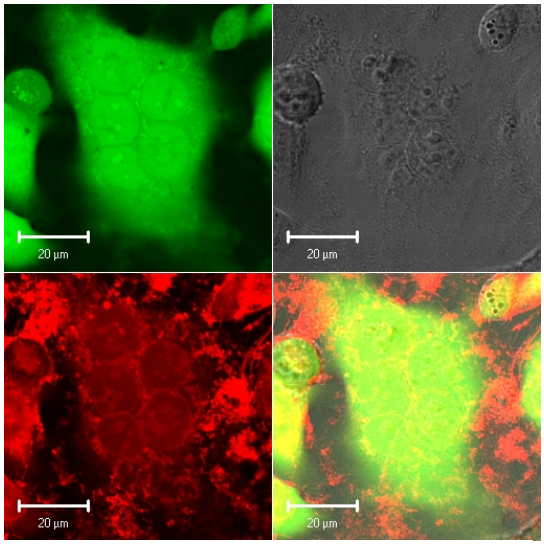

Figure 47f: Unmixed cell culture fusions: Resistant multi-nucleate cell fusion: Top Left: FDA fluorescence (Green); Top Right: DIC Image; Bottom Left: Epirubicin fluorescence (Red); Bottom Right: Overlay image

Despite numerous attempts we were unable to demonstrate a mixed cell fusion. There are several potential explanations for this, it could be that we have failed to fuse a sensitive and resistant cell, or it is possible that by fusing the different cell types together one of the nuclei changes to the opposite phenotype, either the resistant nucleus becoming sensitive or vice versa. This would indicate that either there is some cytoplasmic-nuclear membrane interaction at play or that by fusing cells together the resultant alteration of the level of P-glycoprotein on the plasma membrane, results in a change of nuclear phenotype.

It is the author's impression that resistant-resistant fusions were much less common than sensitive-sensitive fusions. A simple counting technique may have formed a stronger basis for this statement. If true, this would suggest that the resistant nucleus changes to a sensitive phenotype. This would suggest dilution in plasma membrane P-glycoprotein resulting in higher intracellular levels of epirubicin with increased nuclear uptake or that some cytoplasmic factor from the sensitive cell allows epirubicin to gain nuclear entry.

As we could not exclude the presence of mixed cell fusion based on nuclear uptake characteristics with certainty, we looked for another method of demonstrating mixed cell fusions.

This method involved pre-incubating either MGH-U1 or MGH-U1R cells with FITC-WGA prior to cell fusion to stain the nuclei with FITC fluorescence, making the sensitive and resistant nuclei distinguishable from one another.

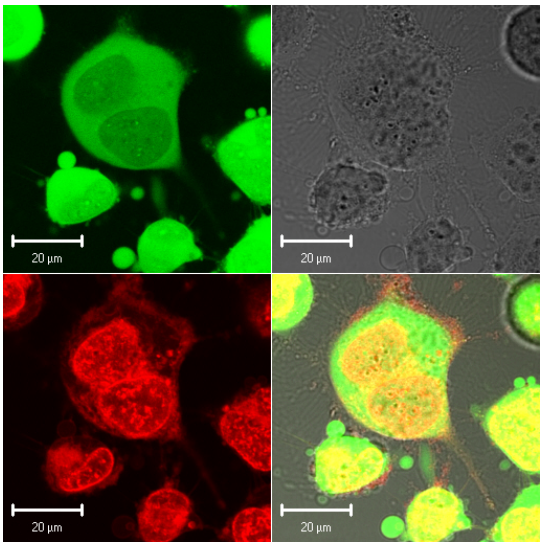

Figure 47g: Mixed cell culture fusions: Sensitive-Sensitive cell fusion: Top Left: FDA fluorescence (Green); Top Right: DIC Image; Bottom Left: Epirubicin fluorescence (Red); Bottom Right: Overlay image

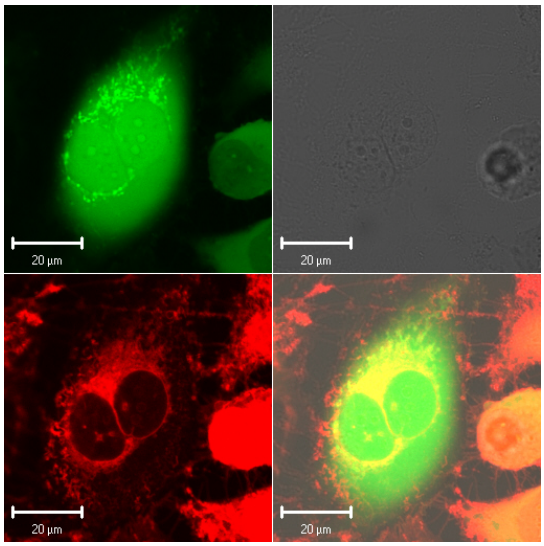

Figure 47h: Mixed cell culture fusions: Resistant-Resistant cell fusion: Top Left: FDA fluorescence (Green); Top Right: DIC Image; Bottom Left: Epirubicin fluorescence (Red); Bottom Right: Overlay image

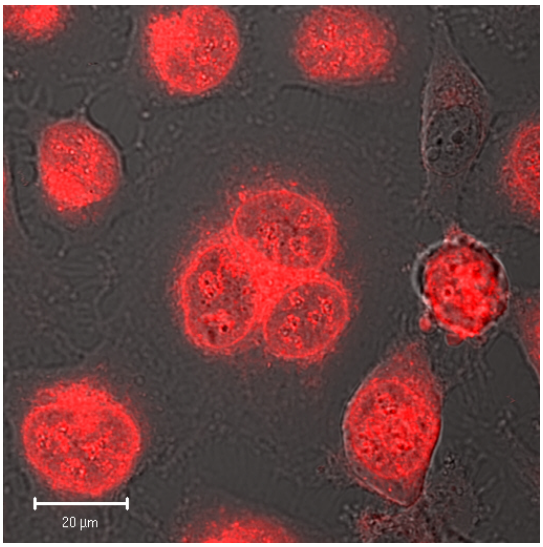

Figure 47i: Mixed cell culture fusions: Sensitive tri-nucleate cell fusion: Epirubicin fluorescence (Red) overlaid on DIC image.

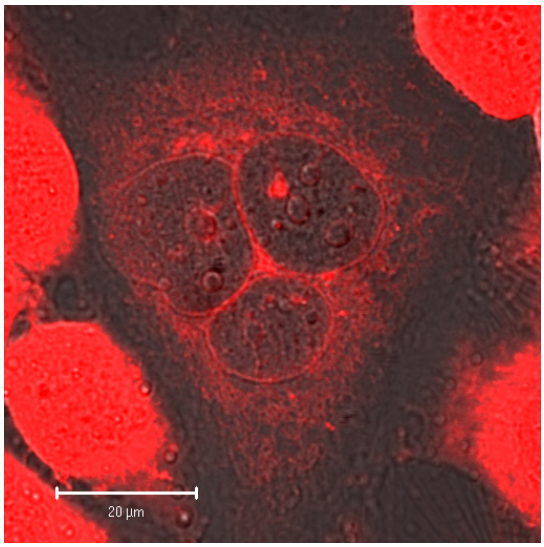

Figure 47j: Mixed cell culture fusions: Resistant tri-nucleate cell fusion: Epirubicin fluorescence (Red) overlaid on DIC image.

Only a couple of possible mixed fusions resulted from these experiments. Figures 47k – m show a possible mixed cell fusion with FITC staining of the sensitive nucleus and a non-FITC staining resistant nucleus. The epirubicin uptake characteristics of both nuclei are of sensitive phenotype, suggesting that the resistant nucleus has changed to a sensitive phenotype as a result of cell fusion. We performed several 3D reconstructions of this cell fusion to be

certain that the cells had fused. However, viability staining with FDA showed that this cell fusion was non-viable meaning that the nuclear epirubicin uptake could just be as a result of cell death and not cell fusion as originally thought (Figure 47n).

The second of our possible mixed cell fusions is shown in figure 47o. In this experiment the resistant nuclei were stained with FITC-WGA. There is a resistant-resistant cell fusion on the right side of this picture, with both nuclei demonstrating FITC-WGA staining and very low levels of epirubicin fluorescence. The fusion on the left side shows FITC-WGA staining of one or both nuclei and yet both nuclei are of sensitive phenotype. Of note there is also another cell demonstrating FITC-WGA staining with a sensitive epirubicin uptake phenotype. This may suggest that this cell fusion and cell are in fact non-viable and that is why their nuclear uptake characteristics have changed. We did not perform FDA analysis of cell viability on this sample so cannot be sure.

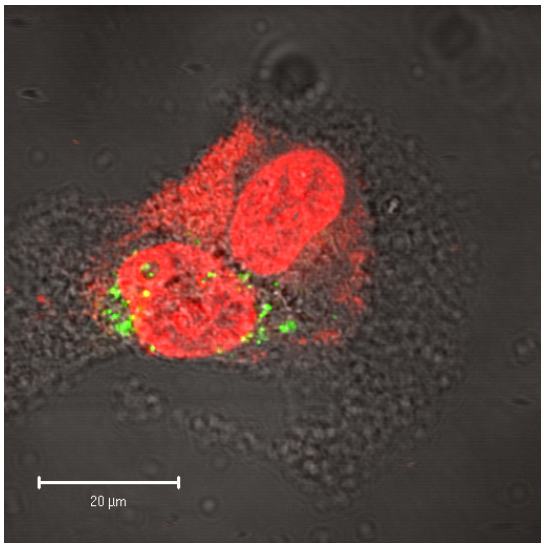

Figure 47k: Mixed cell culture fusions: MGH-U1cells pre-incubated with FITC-WGA. Appears to show a FITC-WGA stained sensitive nucleus and a non-FITC stained resistant nucleus

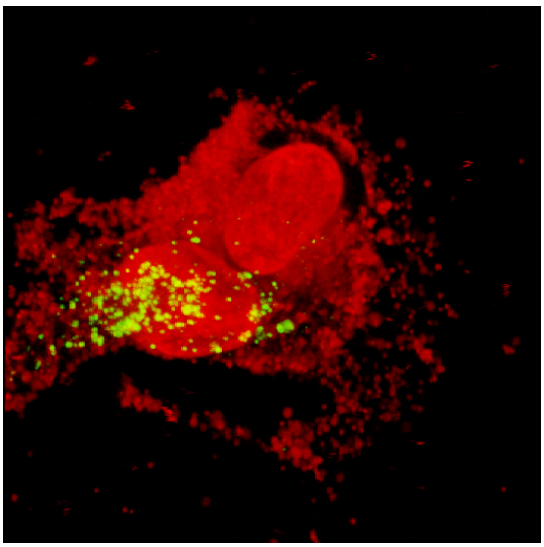

Figure 47l: 3D reconstruction of mixed cell fusion shown in figure Xc. Fluorescence only image.

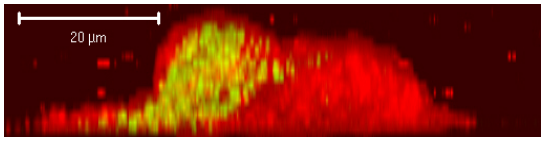

Figure 47m: Lateral view of 3D reconstruction of mixed cell fusion shown in figure 19l. Fluorescence only image.

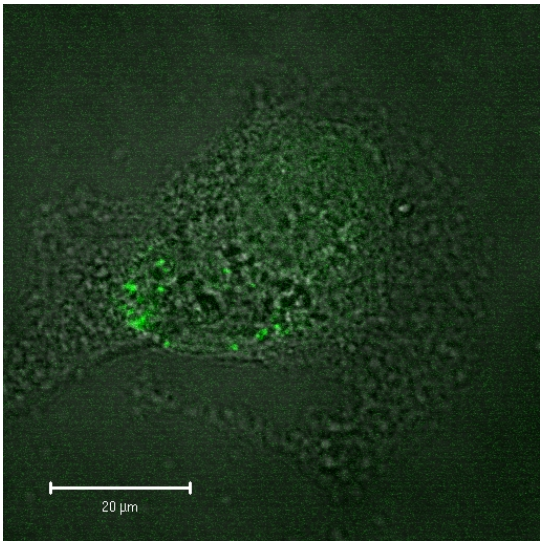

Figure 47n: Mixed cell fusion from figure 19 k – m showing no FDA fluorescence suggesting the cell fusion is not viable. Some FITC- WGA fluorescence is seen.

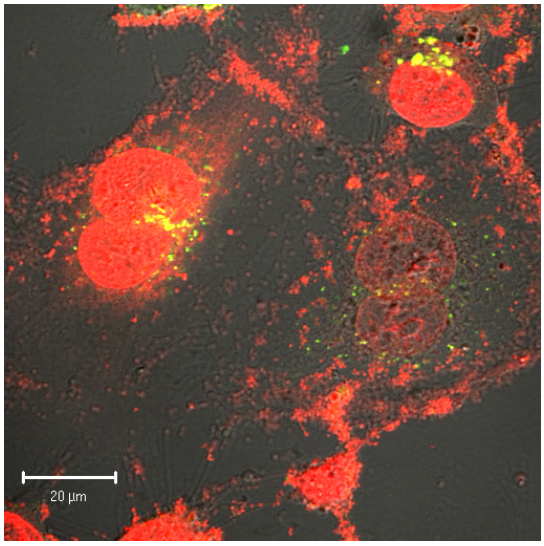

Figure 47o: Mixed culture cell fusion: Right side of picture: resistant- resistant cell fusion with FITC-fluorescence and minimal nuclear epirubicin fluorescence; Left side of picture cell fusion of uncertain origin.

Metaphase arrest experiments

During metaphase the nuclear membrane is absent and the cell's chromosomes are free within the cytoplasm. We incubated metaphase arrested cells with epirubicin, based on the rationale that if the chromosomes stained with epirubicin in both sensitive and resistant cells this would implicate the nuclear membrane in the nuclear sparing of epirubicin uptake in MDR cells. Idarubicin experiments were performed in order to characterise the effects of metaphase on chromosomal staining with idarubicin, to see it the lack of a nuclear membrane had any effect on DNA staining.

Epirubicin

Sensitive cells showed strong chromosomal staining with epirubicin during metaphase. FDA staining proved that these cells were viable (Figure 48a). There appeared to be very few resistant metaphase cells showing chromosomal epirubicin staining. Furthermore on FDA staining, these

resistant cells showing chromosome staining were clearly non-viable (Figure 48b).

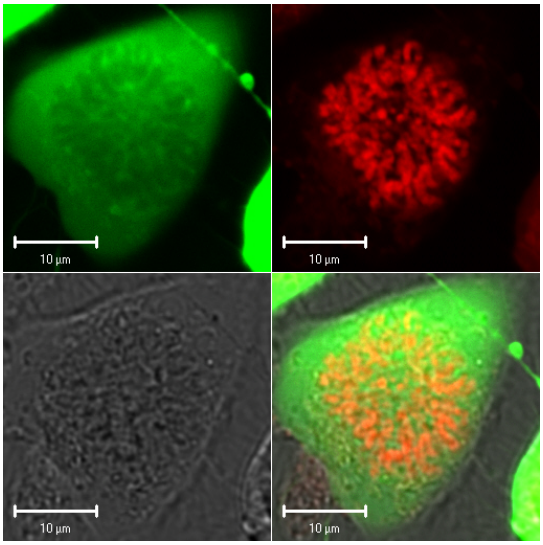

Figure 48a: MGH-U1 Metaphase cell: Top Left: FDA fluorescence (Green); Top Right: Epirubicin fluorescence (Red); Bottom Left: DIC Image; Bottom Right: Overlay image

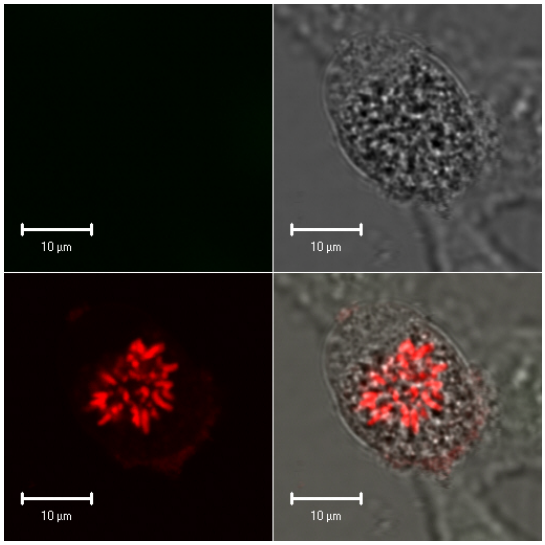

Figure 48b: MGH-U1R Metaphase cell: Top Left: FDA fluorescence (Green); Top Right: DIC Image; Bottom Left: Epirubicin fluorescence (Red); Bottom Right: Overlay image

Because there was such a large discrepancy between the numbers of sensitive and resistant metaphase cells seen with epirubicin chromosome staining, we tried staining chromosomes with acridine orange. This showed that there were in fact a large number of resistant cells in metaphase, but that their chromosomes had not stained with epirubicin.

On imaging at higher digital magnification, there appeared to be filling defects in the cellular uptake of epirubicin at lower doses (Figures 48c and e). These were shown to correspond to chromosomes that had not stained with epirubicin, by the subsequent addition of acridine orange, which clearly stained the chromosomes green (Figures 48d and f). Cells in metaphase were generally rounded up and detached from the Petri dish making them quite mobile, so there was some cell movement following addition of the acridine orange.

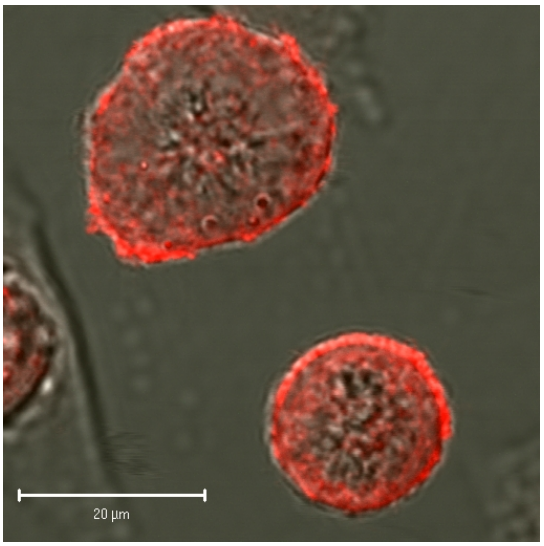

Figure 48c: MGH-U1R cells showing filling defects in cytoplasmic epirubicin fluorescence. Epirubicin fluorescence combined with DIC image.

Figure 48d: MGH-U1R cell from figure 48c with acridine orange staining of chromosomes corresponding to filling defects in cytoplasmic epirubicin fluorescence. Acridine orange fluorescence combined with DIC image.

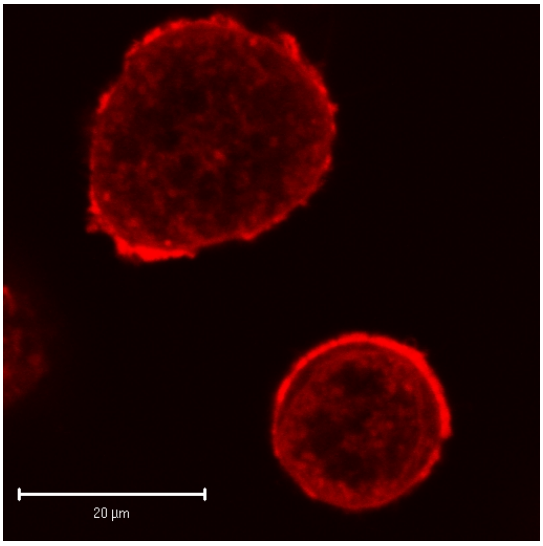

Figure 48e: MGH-U1R cells from figure 48c and d showing filling defects in cytoplasmic epirubicin fluorescence. Epirubicin fluorescence only.

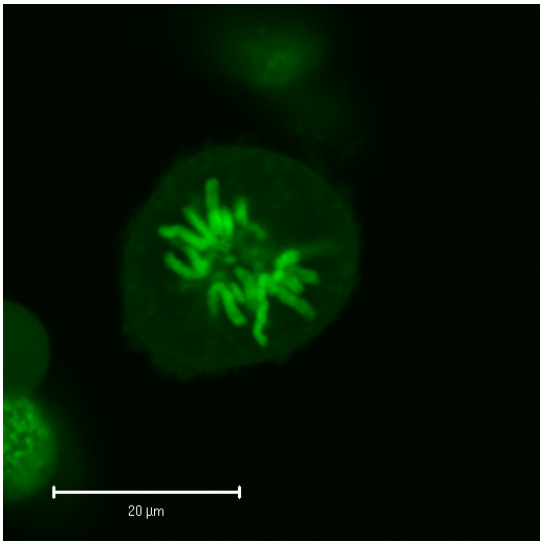

Figure 48f: MGH-U1R cell from figures 48c – e with acridine orange staining of chromosomes corresponding to filling defects in cytoplasmic epirubicin fluorescence. Acridine orange fluorescence only.

Incubation with epirubicin at higher doses causes some low level chromosomal staining in viable MGH-U1R cells (Figure 48g). These central structures were again confirmed to be chromosomes by the addition of acridine orange (Figure 48h). These results suggest that perhaps a combination of lower levels of intracellular epirubicin and the nuclear membrane both play some role in the exclusion of epirubicin from MDR nuclei.

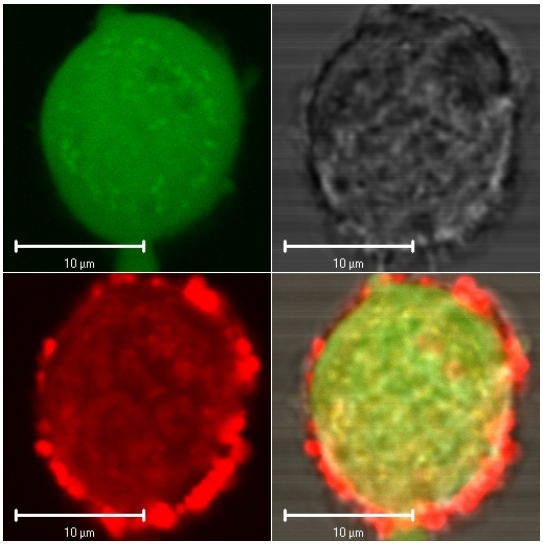

Figure 48g: MGH-U1R Metaphase cell: Top Left: FDA fluorescence (Green); Top Right: DIC Image; Bottom Left: Epirubicin fluorescence (Red); Bottom Right: Overlay image.

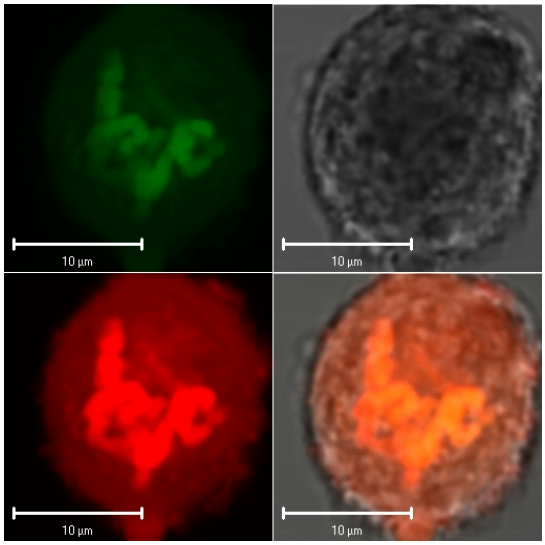

Figure 48h: MGH-U1R Metaphase cell (same cell as 48g): Top Left: Acridine orange fluorescence (Green); Top Right: DIC Image; Bottom Left: Acridine Orange fluorescence (Red); Bottom Right:

Idarubicin

Idarubicin failed to stain the chromosomes of any metaphase cells, sensitive or resistant, despite gaining reasonable levels of cellular fluorescence. Instead numerous rounded up cells with no distinct nuclei, had odd centrally situated filling defects. When stained with propidium iodide after cell killing these filling defects were shown to be chromosomes (Figures 49a – f). These experiments showed that despite the absence of a nuclear membrane in metaphase cells there was no chromosomal staining with idarubicin. We used higher doses of idarubicin in some of these experiments, but the samples were relatively acellular with no cells in metaphase. This presumably related to cell killing at higher idarubicin levels with cells becoming non-adherent and being lost during sample preparation. We are unable to comment on whether chromosomes would have stained at higher drug levels, although this seems unlikely given the high cytoplasmic drug levels in the lower dose samples.

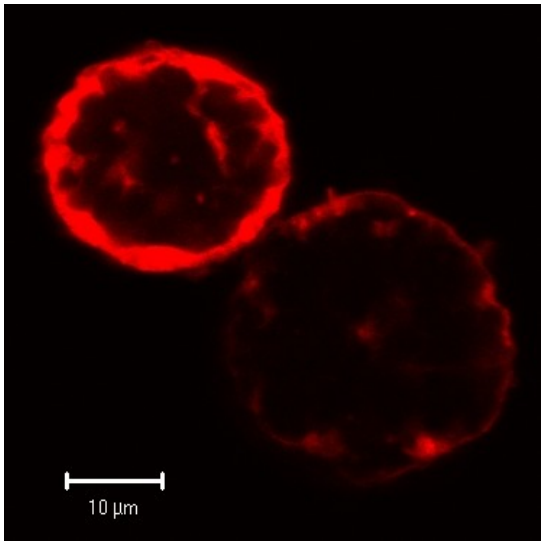

Figure 49a: MGH-U1 metaphase arrested cells incubated with idarubicin. Fluorescence only images showing negative chromosome staining.

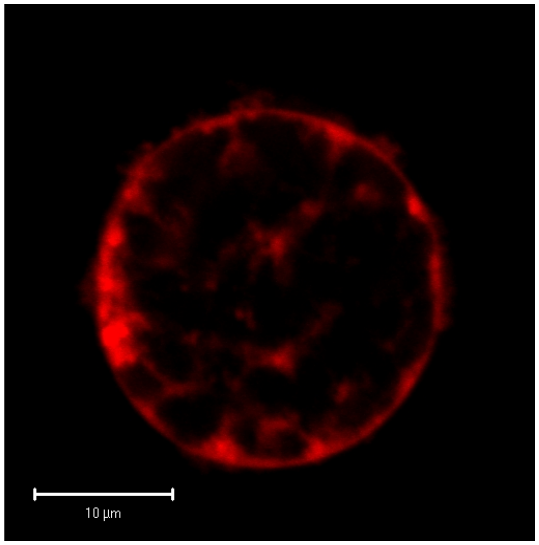

Figure 49b: MGH-U1 metaphase arrested cell incubated with idarubicin. Fluorescence only images showing negative chromosome staining.

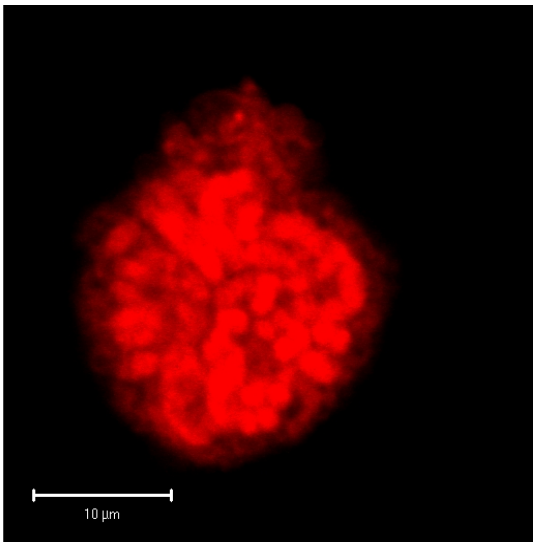

Figure 49c: Same metaphase cell as in 49b, killed with glutaraldehyde and stained with propidium iodide showing chromosomal staining in place of negative idarubicin staining (cell shrank with cell killing).

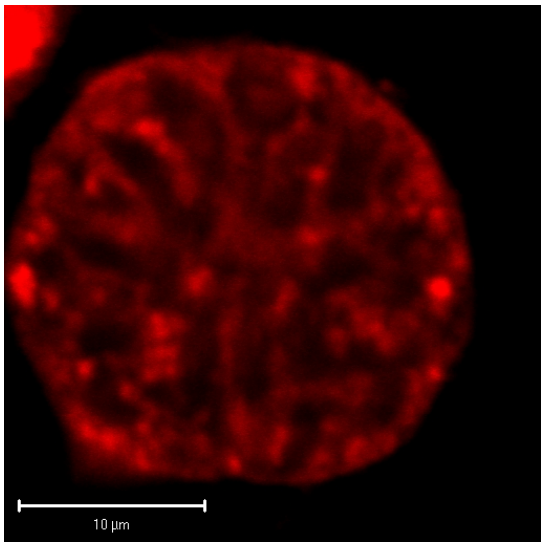

Figure 49d: MGH-U1R metaphase arrested cell stained with Idarubicin. Fluorescence only image showing negative chromosome staining

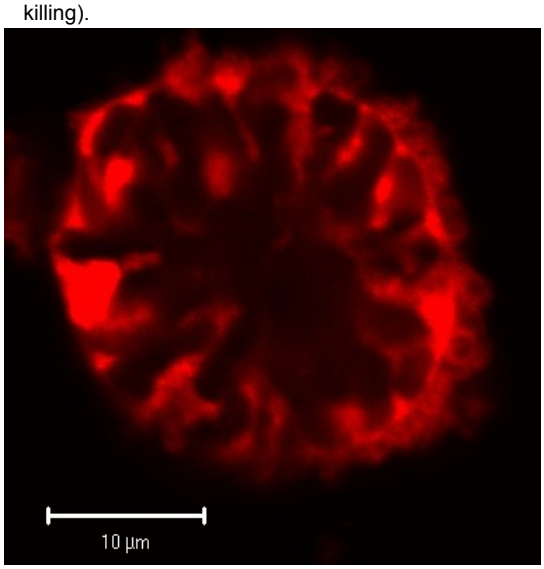

Figure 49e: MGH-U1R metaphase arrested cell stained with Idarubicin. Fluorescence only image showing negative chromosome staining

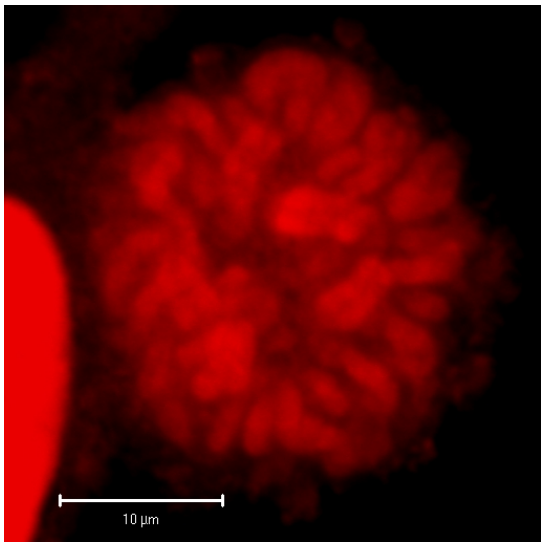

Figure 49f: MGH-U1R metaphase arrested cell stained initially with idarubicin – then killed and chromosomes stained with propidium iodide. Fluorescence only image showing cells staining negatively with idarubicin are in metaphase.

Confocal time series experiments

Confocal time series experiments were performed using drug-sensitive MGH-U1 and RT112 cell lines and multidrug resistant (MDR) variants, MGH-U1R and MGHU-MMC. The time series results for each of the cell lines are shown in Figures 50a – d.

These graphs show nuclear and cytoplasmic epirubicin uptake over time i.e. the rate of epirubicin uptake in these cellular compartments, with and without verapamil.

We used the same confocal gain and laser settings for all experiments and the same fluorescence scale for all experiment graphs, allowing us to directly compare the differences in rates and levels of drug uptake between the cell lines.

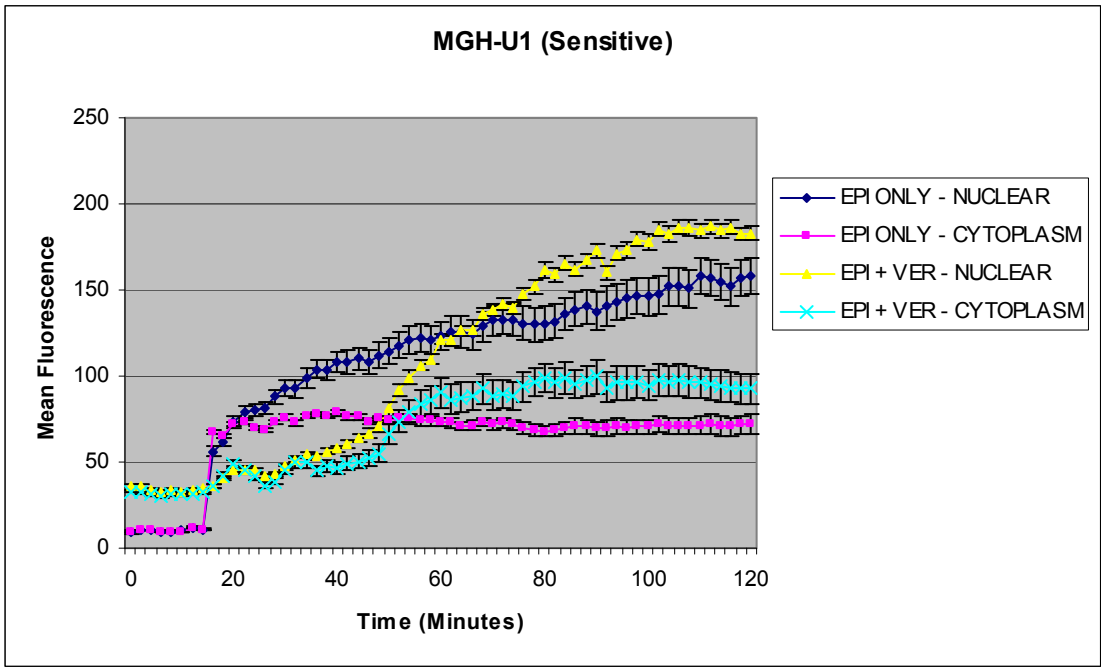

Figure 50a: MGH-U1 confocal time series showing nuclear and cytoplasmic epirubicin uptake with and without verapamil (with 95% confidence intervals)

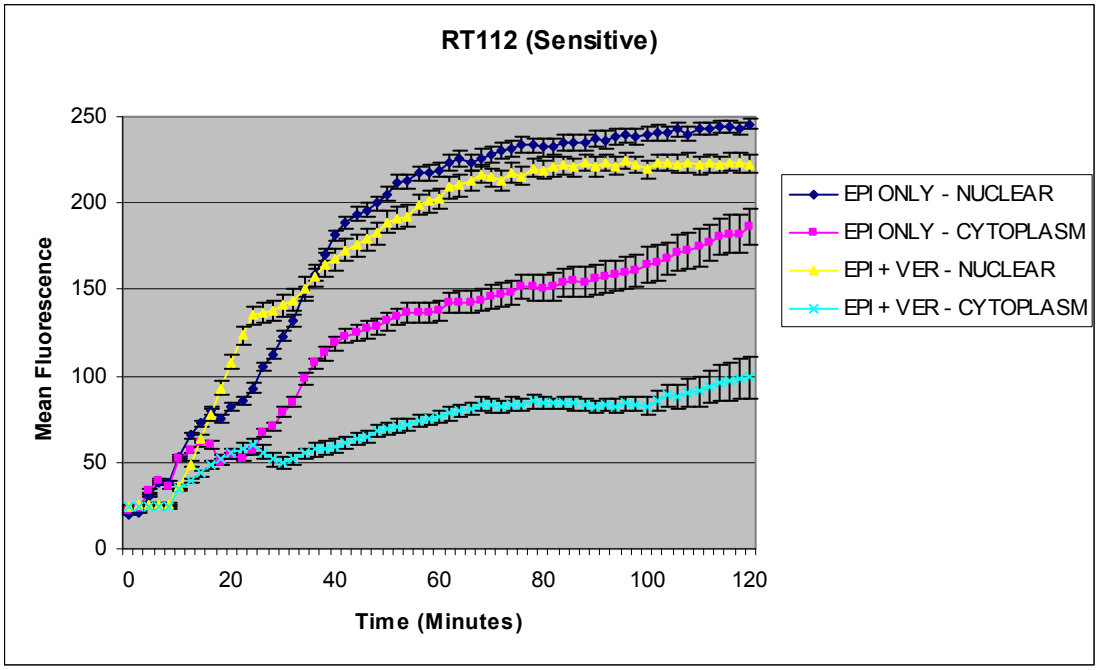

Figure 50b: RT112 confocal time series showing nuclear and cytoplasmic epirubicin uptake with and without verapamil (with 95% confidence intervals)

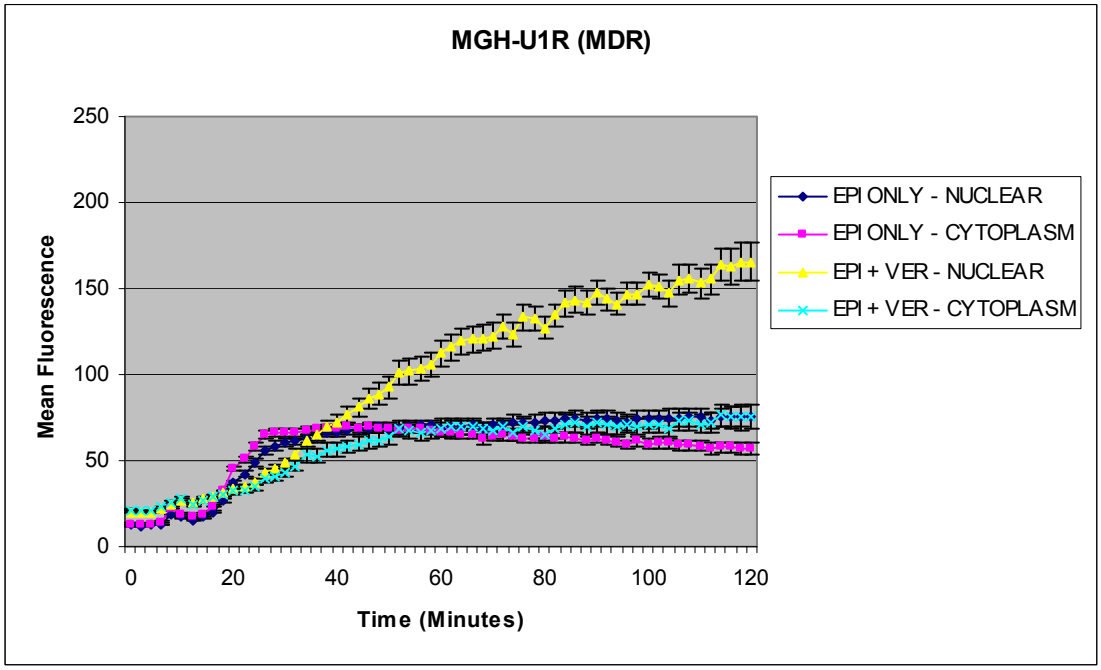

Figure 50c: MGH-U1R confocal time series showing nuclear and cytoplasmic epirubicin uptake with and without verapamil (with 95% confidence intervals)

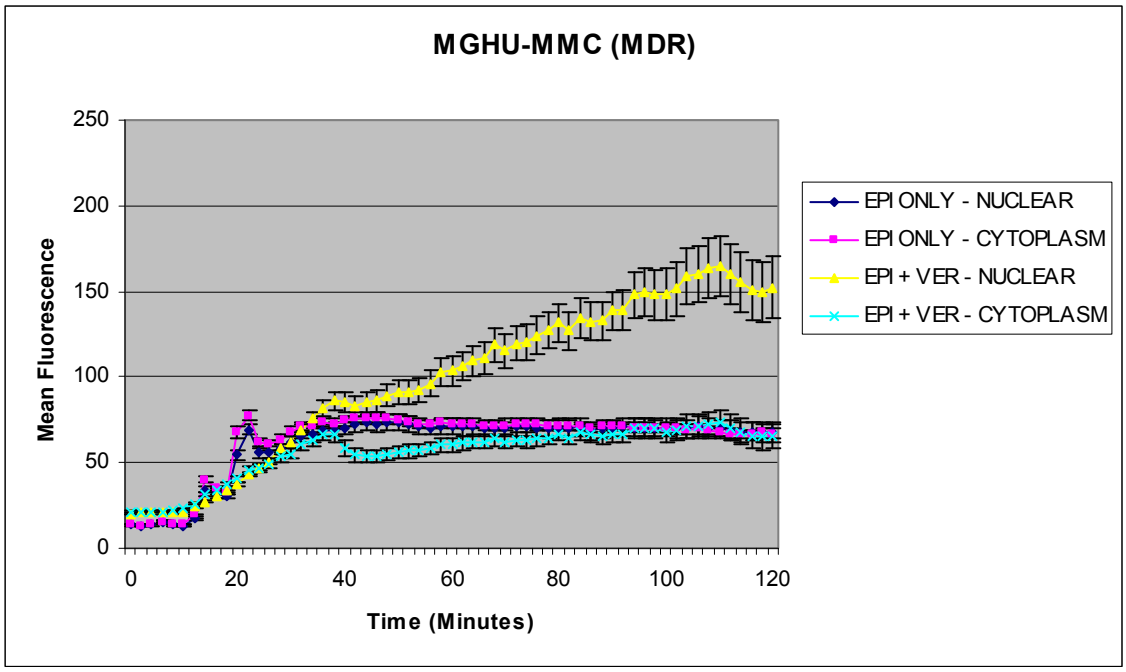

Figure 50d: MGHU-MMC confocal time series showing nuclear and cytoplasmic epirubicin uptake with and without verapamil (with 95% confidence intervals)

Confocal time series analysis showed that in MGH-U1R and MGHU-MMC cells incubated with epirubicin alone, nuclear uptake only reached 48% and 42.6% respectively, of sensitive MGH-U1 levels at 2 hours. Verapamil increased the rate and 2-hour accumulation levels of epirubicin to 104.8% in MGH-U1R nuclei and 96.4% in MGHU-MMC nuclei when compared to MGH-U1 incubated with epirubicin alone.

Comparison of nuclear epirubicin uptake curves for the MDR cell lines incubated with epirubicin and verapamil to the sensitive cell lines incubated with epirubicin alone are shown in figure 50e. This clearly demonstrates that verapamil changes the uptake characteristics back to a sensitive phenotype with very similar final nuclear drug levels, although the sensitive cells had a faster initial drug uptake. The RT112 cell line appeared much more sensitive in terms of drug uptake than the parental MGH-U1 cell line.

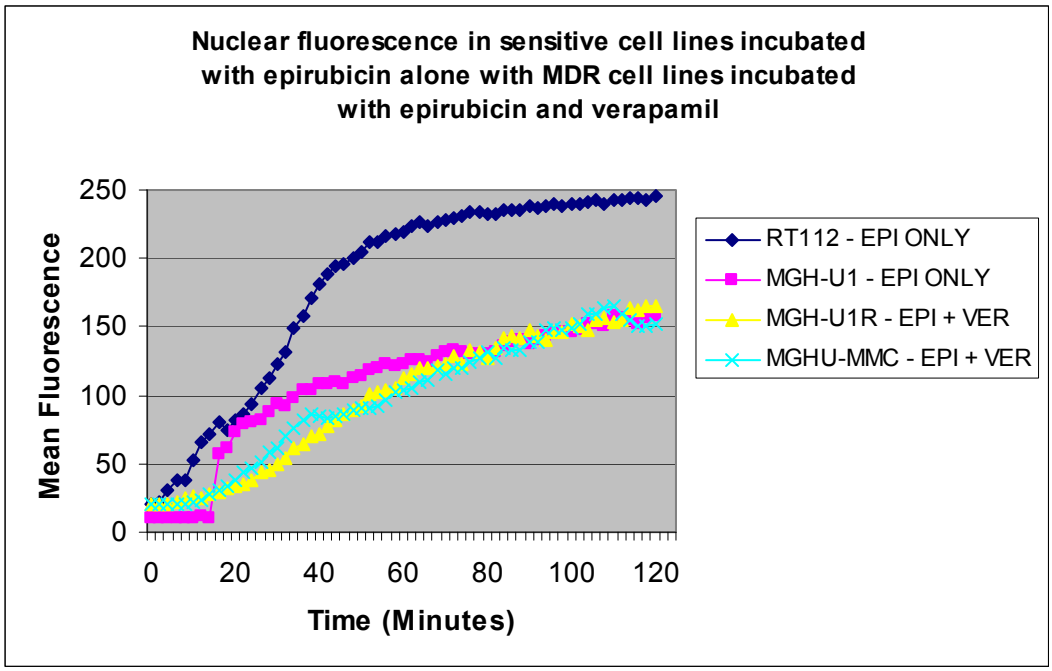

Figure 50e: Comparison of nuclear epirubicin uptake in sensitive cells incubated with epirubicin alone and MDR cells incubated with epirubicin and verapamil (95% confidence intervals for clarity).

However, comparison of cytoplasmic uptake curves shows that there is very little difference in epirubicin uptake between the MGH-U1, MGH-U1R and MGHU-MMC cell lines incubated with epirubicin alone. The cytoplasmic uptake of RT112 cells is much greater in comparison and fits with their higher overall drug uptake levels (Figure 50f).

The addition of verapamil appears to slow initial drug uptake levels in all cell lines. In the RT112 it appears to reduce the nuclear and cytoplasmic uptake significantly. The MGH-U1 cells ultimately have higher cytoplasmic levels than when incubated with epirubicin alone. MDR cell lines have slower initial cytoplasmic drug uptake, but their final concentration is very similar when comparing epirubicin alone to epirubicin and verapamil (Figure 50g).

The nuclear uptake of epirubicin in combination with verapamil continues to rise throughout the incubation period in all cell lines. This suggests that epirubicin uptake levels may increase with exposure times longer than 2 hours. It takes about 80 minutes for nuclear drug levels in the MDR cell lines to reach that of MGH-U1 cells incubated with epirubicin alone.

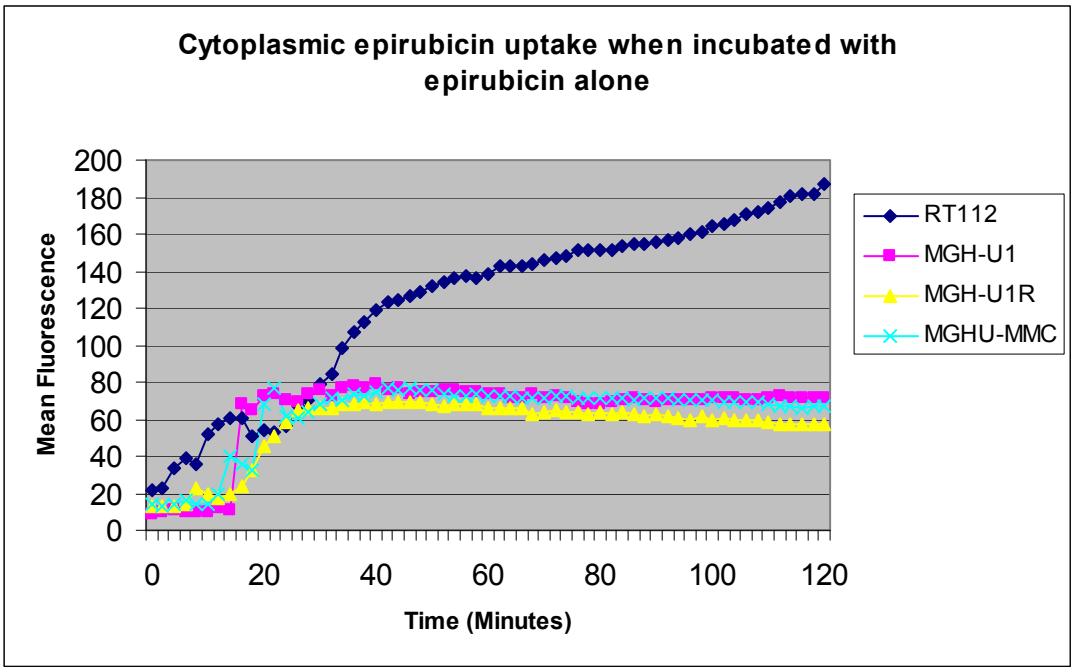

Figure 50f: Comparison of cytoplasmic epirubicin uptake in sensitive and MDR cells incubated with epirubicin alone (95% confidence intervals removed for clarity)

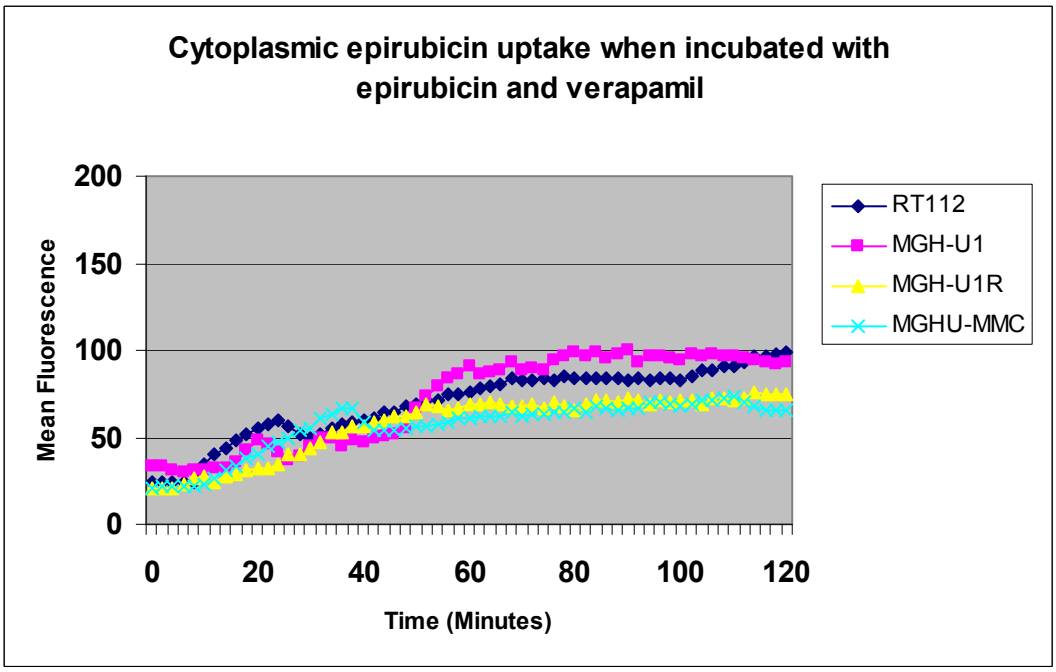

Figure 50g: Comparison of cytoplasmic epirubicin uptake in sensitive and MDR cells incubated with epirubicin and verapamil (95% confidence intervals removed for clarity).

Combination therapy with verapamil appears to achieve increased nuclear drug uptake from about 40 minutes in both the MGH-U1R and MGHU-MMC

cells. In the MGH-U1R cells at 60 minutes, there is a 63% increase in nuclear uptake whilst at 2 hours this rises to 119% compared to epirubicin alone. For the MGHU-MMC cell line at 60 minutes, there is a 46% increase in nuclear uptake whilst at 2 hours this rises to 126% compared to epirubicin alone. This suggests that whilst a 1 hour combination intravesical instillation should have benefit over epirubicin alone, combination instillations for longer periods up to 2 hours may bring improved benefits in terms of nuclear drug uptake and cytotoxicity.

Cytoplasmic epirubicin uptake in the MGH-U1R and MGHU-MMC cell lines reaches a maximum level at 46 minutes and then the curves decline to 2hrs. With verapamil, the cytoplasmic uptake in these cells increases to maximum at 114 and 110 minutes respectively. These results may be demonstrating p-glycoprotein mediated drug efflux, which is abolished by the addition of verapamil.

In the absence of verapamil, cytoplasmic drug fluorescence in MDR cells is equal to nuclear drug fluorescence. This suggests that either there is free diffusion across the nuclear membrane which equilibrates or that the amount of drug entering the nucleus reaches a steady state with an equal amount being effluxed from the nucleus. It is interesting that verapamil only causes a minimal increase in cytoplasmic drug levels, but causes a dramatic increase in nuclear fluorescence levels, suggesting that it may also have some action at the nuclear membrane.

Regimen / Cell line	Maximum level of drug fluorescence (Time reached)	Level of drug fluorescence at 120 minutes
Epirubicin alone – Nuclear uptake		
RT112	**245.6 (120 minutes)**	**245.6**
MGH-U1	**158.1 (110 minutes)**	**158**
MGH-U1R	**75.8 (116 minutes)**	**75.8**
MGHU-MMC	**73.8 (50 minutes)**	**67.3**
Epirubicin + Verapamil – Nuclear uptake		
RT112	**223.7 (116 minutes)**	**222.8**
MGH-U1	**186.4 (106 minutes)**	**182.9**
MGH-U1R	**165.6 (120 minutes)**	**165.6**
MGHU-MMC	**164.7 (110 minutes)**	**152.3**
Epirubicin alone – Cytoplasmic uptake		
RT112	**186.7 (120 minutes)**	**186.7**
MGH-U1	**78.6 (40 minutes)**	**71.8**
MGH-U1R	**69.4 (46 minutes)**	**57**
MGHU-MMC	**76.5 (46 minutes)**	**66.7**
Epirubicin + Verapamil – Cytoplasmic uptake		
RT112	**99.3 (120 minutes)**	**99.3**
MGH-U1	**99.8 (90 minutes)**	**92.6**
MGH-U1R	**76.2 (114 minutes)**	**75.1**
MGHU-MMC	**73.1 (110 minutes)**	**65.8**

Table 18: Comparison of maximum drug fluorescence levels and levels of drug fluorescence at 2 hours in the nuclear and cytoplasmic compartments for each cell line

	RT112 EPI ALONE	MGH-U1 EPI ALONE	RT112 EPI + VER	MGH-U1 EPI + VER
EPI ALONE NUCLEAR (%)				
MGH-U1R				
Max	**30.9**	**47.9**	**33.8**	**40.6**
2-hour	**30.9**	**48**	**34**	**41.4**
MGHU-MMC				
Max	**30**	**46.6**	**32.9**	**39.5**
2-hour	**27.4**	**42.6**	**30.2**	**32.9**
EPI + VER NUCLEAR (%)				
MGH-U1R				
Max	**67.4**	**104.7**	**74**	**88.8**
2-hour	**67.4**	**104.8**	**74.3**	**90.5**
MGHU-MMC				
Max	**67.1**	**104.2**	**73.6**	**88.4**
2-hour	**62**	**96.4**	**68.4**	**83.3**
EPI ALONE CYTOPLASM (%)				
MGH-U1R				
Max	**37.2**	**88.3**	**69.9**	**69.5**
2-hour	**30.5**	**79.4**	**57.4**	**61.6**
MGHU-MMC				
Max	**41**	**97.3**	**77**	**76.8**
2-hour	**35.7**	**92.9**	**67.2**	**72**
EPI + VER CYTOPLASM (%)				
MGH-U1R				
Max	**40.8**	**96.9**	**76.7**	**76.3**
2-hour	**40.2**	**104.6**	**75.6**	**81.1**
MGHU-MMC				
Max	**39.2**	**93**	**73.6**	**73.2**
2-hour	**35.2**	**91.6**	**66.2**	**71.1**

Table 19: Comparison of drug fluorescence levels in MGH-U1R and MGHU–MMC cells expressed as a percentage of RT112 / MGH-U1 drug uptake levels

Cellular staining of P-gp using a FITC conjugated Anti-P-gp antibody (17F9, BD Biosciences)

Cellular fluorescence related to FITC labelled anti-P-gp antibody, 17F9 (BD, Biosciences) was not readily detectable by confocal means (Figures 51a – g).

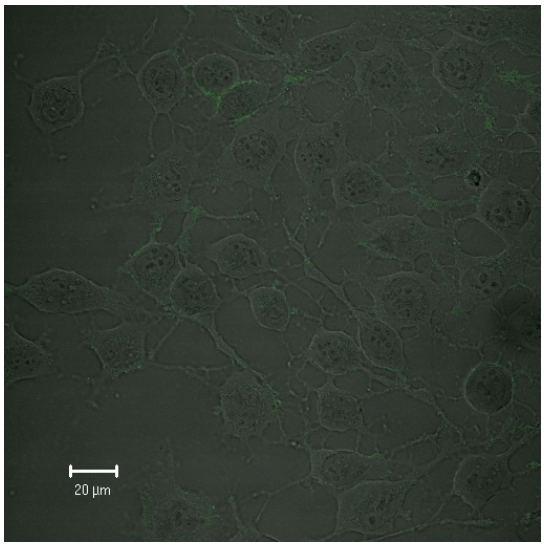

Figure 51a: MGH-U1 cells without FITC Anti-Pgp (Control). FITC fluorescence detection combined with DIC image. Zoom x1; Gain 1000.

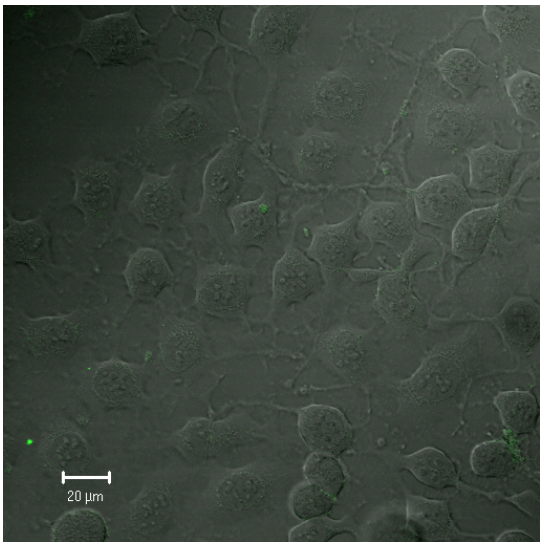

Figure 51b: MGH-U1 cells with FITC Anti-Pgp. FITC fluorescence detection combined with DIC image. Zoom x1; Gain 1000.

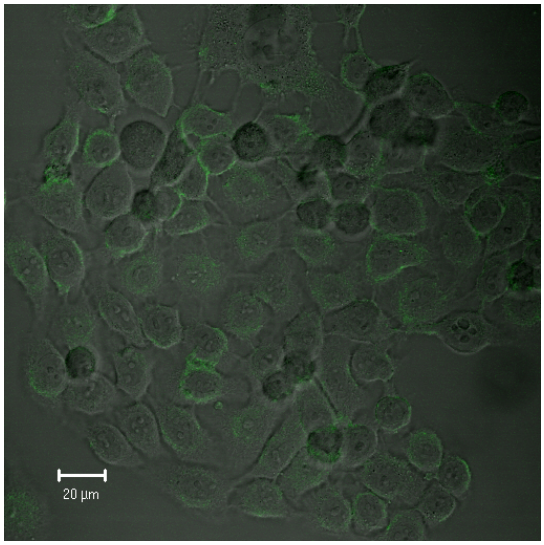

Figure 51c: RT112 cells without FITC Anti-Pgp (Control). FITC fluorescence detection combined with DIC image. Zoom x1; Gain 1000.

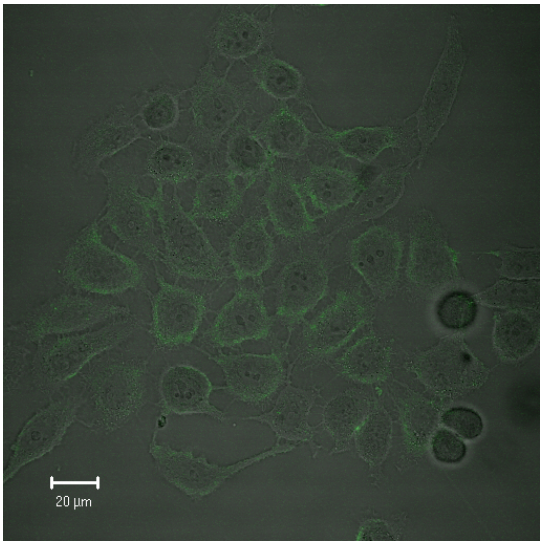

Figure 51d: RT112 cells with FITC Anti-Pgp. FITC fluorescence detection combined with DIC image. Zoom x1; Gain 1000.

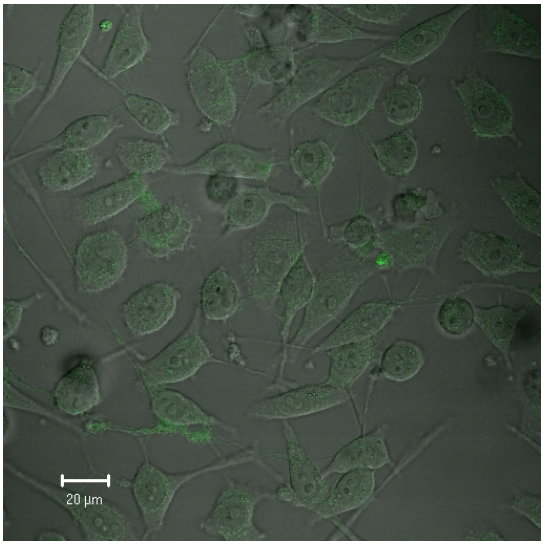

Figure 51e: MGH-U1R cells without FITC Anti-Pgp (Control). FITC fluorescence detection combined with DIC image. Zoom x1; Gain 1000.

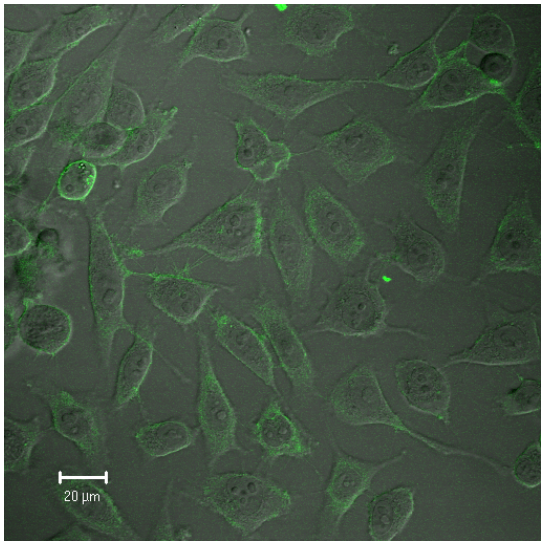

Figure 51f: MGH-U1R cells with FITC Anti-Pgp. FITC fluorescence detection combined with DIC image. Zoom x1; Gain 1000.

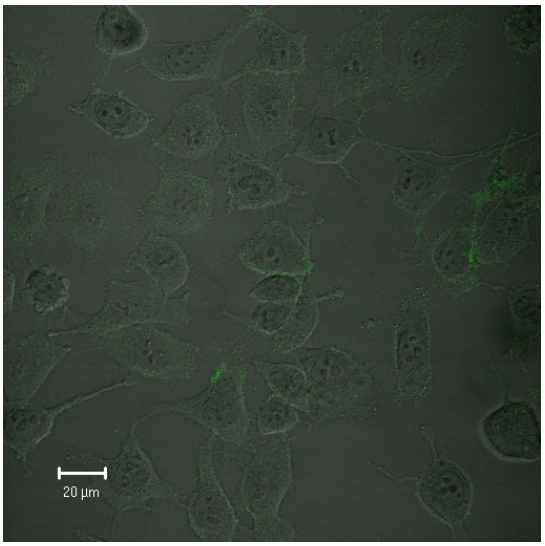

Figure 51g: MGHU-MMC cells without FITC Anti-Pgp (Control). FITC fluorescence detection combined with DIC image. Zoom x1; Gain 1000.

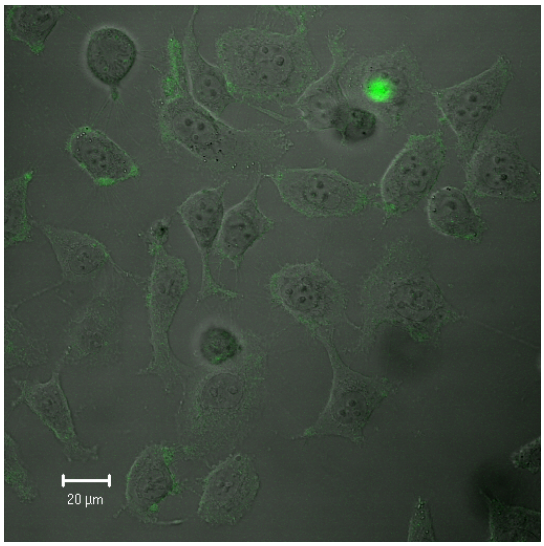

Figure 51h: MGHU-MMC cells with FITC Anti-Pgp. FITC fluorescence detection combined with DIC image. Zoom x1; Gain 1000.

Nuclear P-gp staining with a FITC conjugated Anti-P-gp antibody (17F9, BD Biosciences)

Nuclear isolates from MGH-U1 and MGH-U1R cells demonstrated very low levels of fluorescence at maximum gain setting, after exposure to a FITC-labelled anti-P-gp antibody (Figures 52a and b). Control nuclei (not shown) demonstrated similar low levels of green fluorescence at high gain settings. Given that we were unable to identify P-gp on the plasma membrane of MGH-U1R cells by confocal microscopy, it seemed unlikely that this represented any true nuclear fluorescence related to the anti-P-gp antibody.

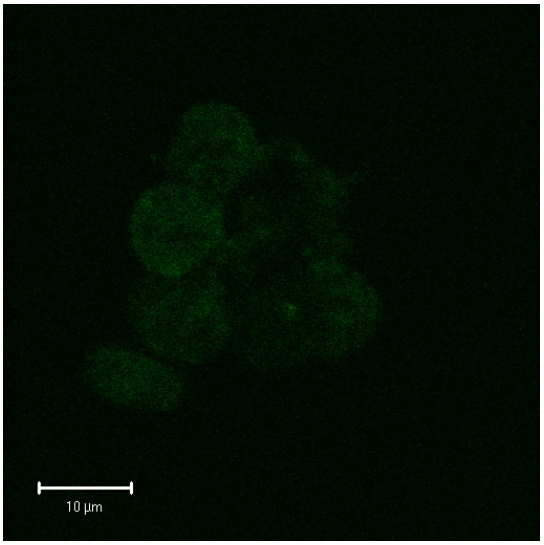

Figure 52a: MGH-U1 nuclei with FITC Anti-Pgp. FITC fluorescence detection only. Zoom x8; Gain 1250.

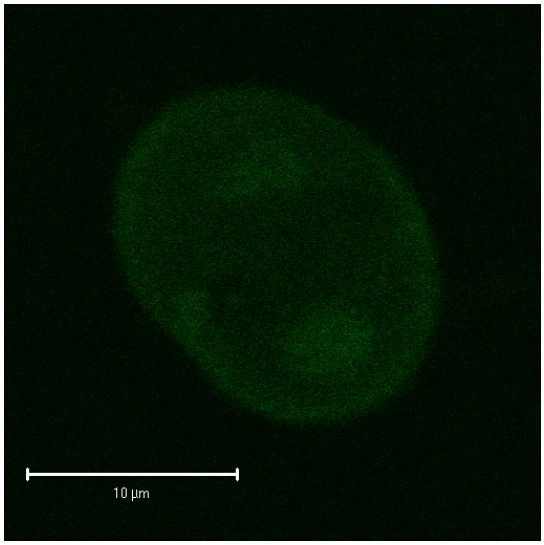

Figure 52b: MGH-U1R nucleus with FITC Anti-Pgp. FITC fluorescence detection only. Zoom x18; Gain 1250.

Membrane Leakiness Studies using FITC-dextrans

This experiment was performed to establish whether nuclear uptake of epirubicin in dead cells may be due to leaky membranes. Dead MGH-U1 and MGH-U1R cells showed cytoplasmic and nuclear fluorescence when incubated with a 77KDa FITC-dextran, which would not normally gain entry to cells through the plasma membrane or to the nucleus through the nuclear membrane (Figures 53a and b). This is highly suggestive that biological membranes become leaky after death and may account for the changes in epirubicin uptake and localisation observed in dead cells.

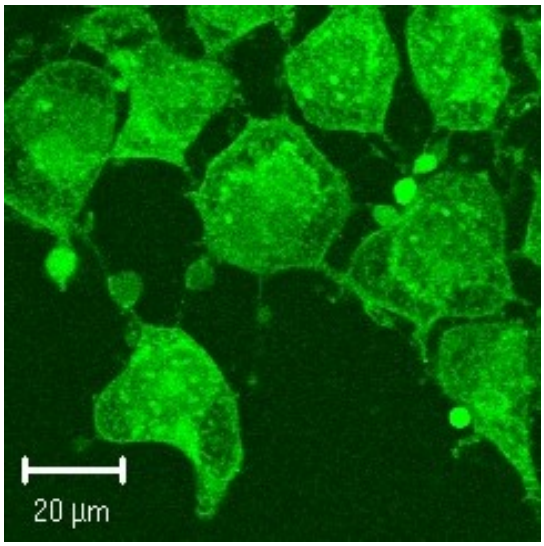

Figure 53a: Dead MGH-U1 cells incubated with 77KDa FITC-dextran. Fluorescence only image showing cytoplasmic and nuclear uptake.

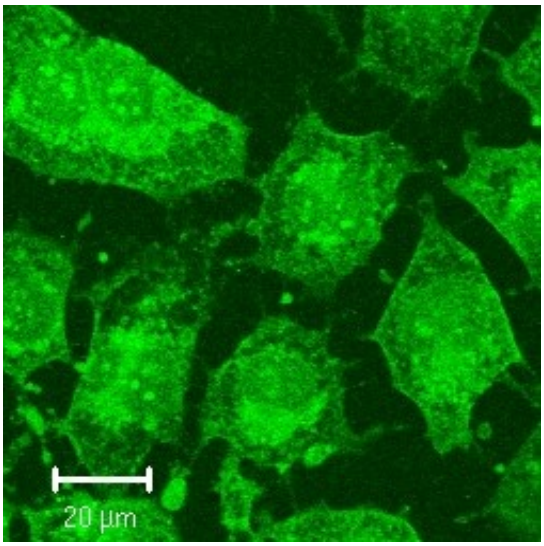

Figure 53b: Dead MGH-U1R cells incubated with 77KDa FITC-dextran. Fluorescence only image showing cytoplasmic and nuclear uptake.

Green Fluorescent Protein cell line experiments

Two Green fluorescent protein (GFP) cell lines had previously been derived from MGH-U1 and MGH-U1R cell lines in our research unit. We assessed the purity of frozen cultures and the MDR characteristics of these cells after being frozen at -180^{o}C, using confocal microscopy and later flow cytometry. We also assessed the potential of using GFP as a viability marker.

GFP cells – epirubicin uptake characteristics

MGH-U1-GFP and MGH-U1R-GFP cells maintained their usual epirubicin uptake characteristics following being frozen, as shown below. There was variability in the number of cells demonstrating GFP fluorescence between samples suggesting some frozen batches were purer that others (Figures 54a and b).

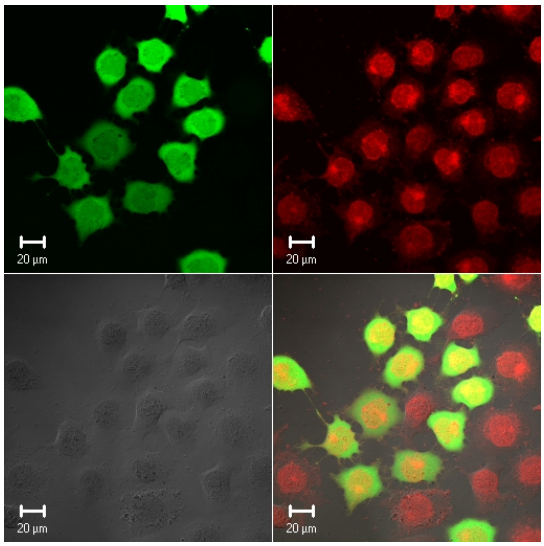

Figure 54a: MGH-U1-GFP cells (x40 Lens; Digital Zoom x1). Top Left: Green Fluorescent Protein (GFP) fluorescence (Green); Top Right: Epirubicin Fluorescence (Red); Bottom Left: Differential Interference Contrast Image (DIC); Bottom Right: Overlay image.

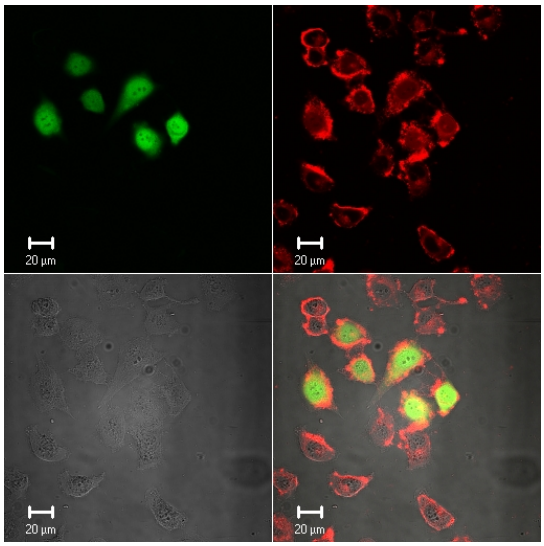

Figure 54b: MGH-U1R-GFP cells (x40 Lens; Digital Zoom x1). Top Left: Green Fluorescent Protein (GFP) fluorescence (Green); Top Right: Epirubicin Fluorescence (Red); Bottom Left: Differential Interference Contrast Image (DIC); Bottom Right: Overlay image.

Assessment of GFP as viability marker using time-lapse confocal microscopy

Green-fluorescent protein transfected cells fluoresce green when excited by laser light. It had been previously noted that dead GFP cells lose their fluorescence. We therefore decided to assess whether GFP could be used as a marker of cell viability.

MGH-U1-GFP and MGH-U1R-GFP were imaged after exposure to propidium iodide, this confirmed cell viability by the absence of PI from the nuclei of GFP

expressing cells (Figure 55a, b, d and e). GFP fluorescence almost disappeared by 1 minute after the addition of glutaraldehyde. Nuclear PI fluorescence gradually increased over a few minutes staining most nuclei quite strongly by 6 minutes, indicating that cell death had occurred. Interestingly in the MGH-U1R-GFP cells, one of the GFP cells and a couple of non-GFP expressing cells fail to take up propidium iodide. This GFP cell does lose its GFP fluorescence suggesting that loss of GFP expression may precede cell death. There is also some minor cross-over from the fluorescence signal of propidium iodide into the FITC detection range meaning that low level FITC fluorescence persists even after the cells are dead.

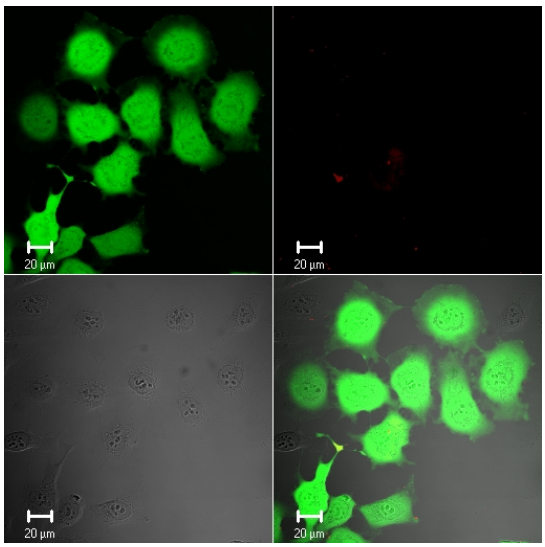

Figure 55a: Viable MGH-U1-GFP cells exposed to propidium iodide (x40 Lens; Digital Zoom x1). Top Left: Green Fluorescent Protein (GFP) fluorescence (Green); Top Right: Propidium Iodide Fluorescence (Red); Bottom Left: Differential Interference Contrast Image (DIC); Bottom Right: Overlay image.

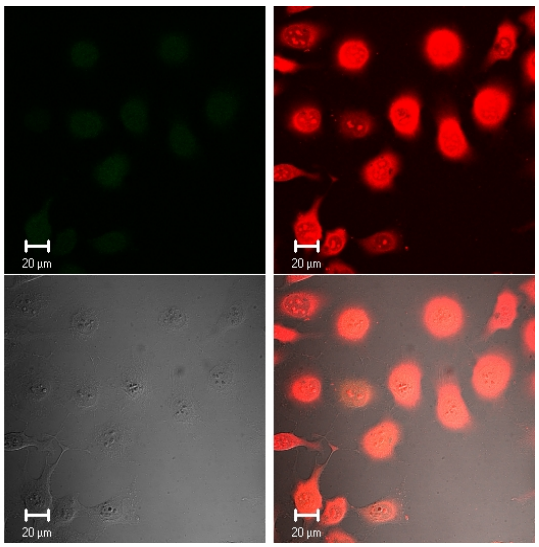

Figure 55b: MGH-U1-GFP cells exposed to propidium iodide and glutaraldehyde for 6 minutes (x40 Lens; Digital Zoom x1). Top Left: Green Fluorescent Protein (GFP) fluorescence (Green); Top Right: Propidium Iodide Fluorescence (Red); Bottom Left: Differential Interference Contrast Image (DIC); Bottom Right: Overlay image.

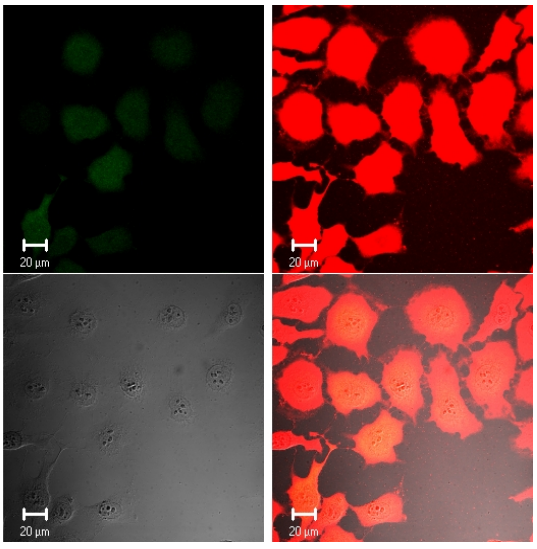

Figure 55c: MGH-U1-GFP cells exposed to propidium iodide and glutaraldehyde for 30 minutes (x40 Lens; Digital Zoom x1). Top Left: Green Fluorescent Protein (GFP) fluorescence (Green); Top Right: Propidium Iodide Fluorescence (Red); Bottom Left: Differential Interference Contrast Image (DIC); Bottom Right: Overlay image.

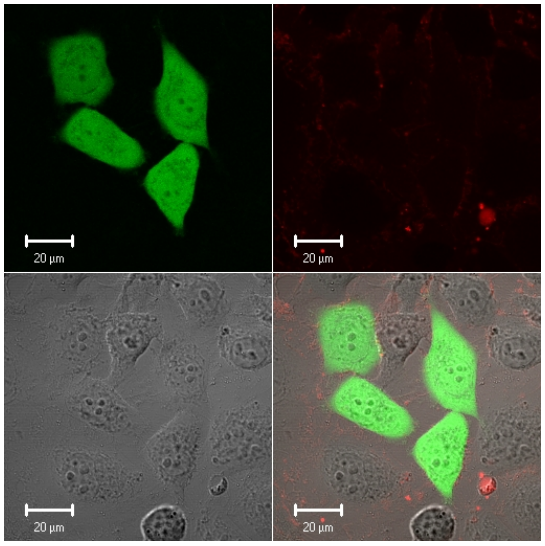

Figure 55d: Viable MGH-U1R-GFP cells exposed to propidium iodide (x40 Lens; Digital Zoom x1). Top Left: Green Fluorescent Protein (GFP) fluorescence (Green); Top Right: Propidium Iodide Fluorescence (Red); Bottom Left: Differential Interference Contrast Image (DIC); Bottom Right: Overlay image.

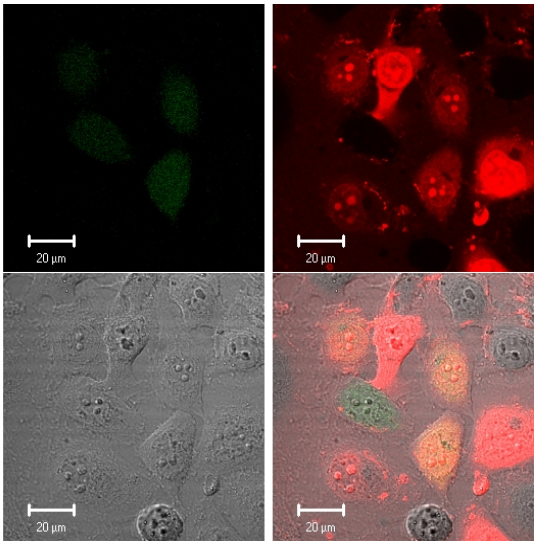

Figure 55e: MGH-U1R-GFP cells exposed to propidium iodide and glutaraldehyde for 6 minutes (x40 Lens; Digital Zoom x1). Top Left: Green Fluorescent Protein (GFP) fluorescence (Green); Top Right: Propidium Iodide Fluorescence (Red); Bottom Left: Differential Interference Contrast Image (DIC); Bottom Right: Overlay image.

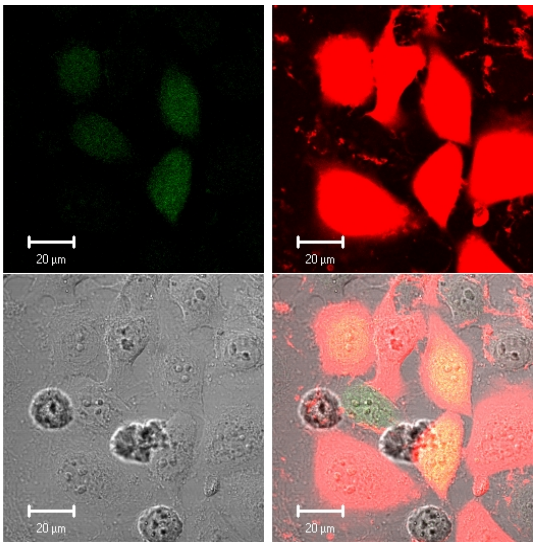

Figure 55f: MGH-U1R-GFP cells exposed to propidium iodide and glutaraldehyde for 30 minutes (x40 Lens; Digital Zoom x1). Top Left: Green Fluorescent Protein (GFP) fluorescence (Green); Top Right: Propidium Iodide Fluorescence (Red); Bottom Left: Differential Interference Contrast Image (DIC); Bottom Right: Overlay image.

Control time series of GFP fluorescence showed very minimal reduction in GFP fluorescence over a 30 minutes period, suggesting that any large reduction in GFP fluorescence over time is caused by cell death rather than bleaching of this fluophore (Figures 55g and h).

We conclude that GFP cell fluorescence is dramatically and immediately reduced as a result of cell death and could therefore be used as a marker of cell viability *in vitro*.

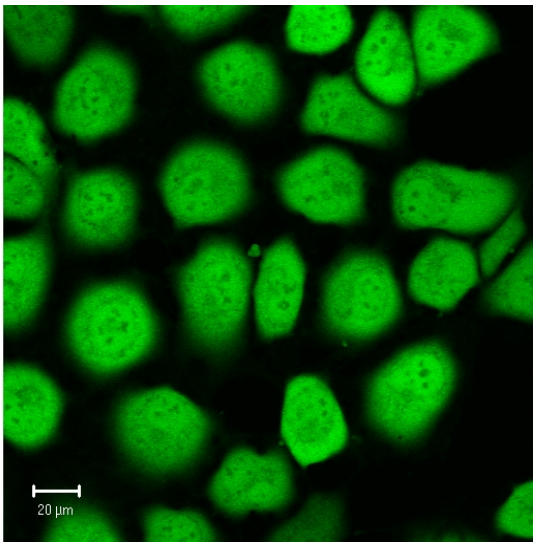

Figure 55g: MGH-U1-GFP cells at 0 minutes (x40 Lens; Digital Zoom x1). Green Fluorescent Protein (GFP) fluorescence only.

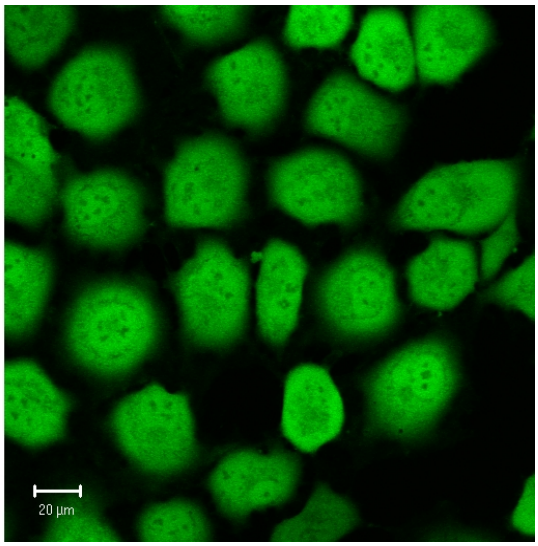

Figure 55h: MGH-U1-GFP cells at 30 minutes (x40 Lens; Digital Zoom x1). Green Fluorescent Protein (GFP) fluorescence only.

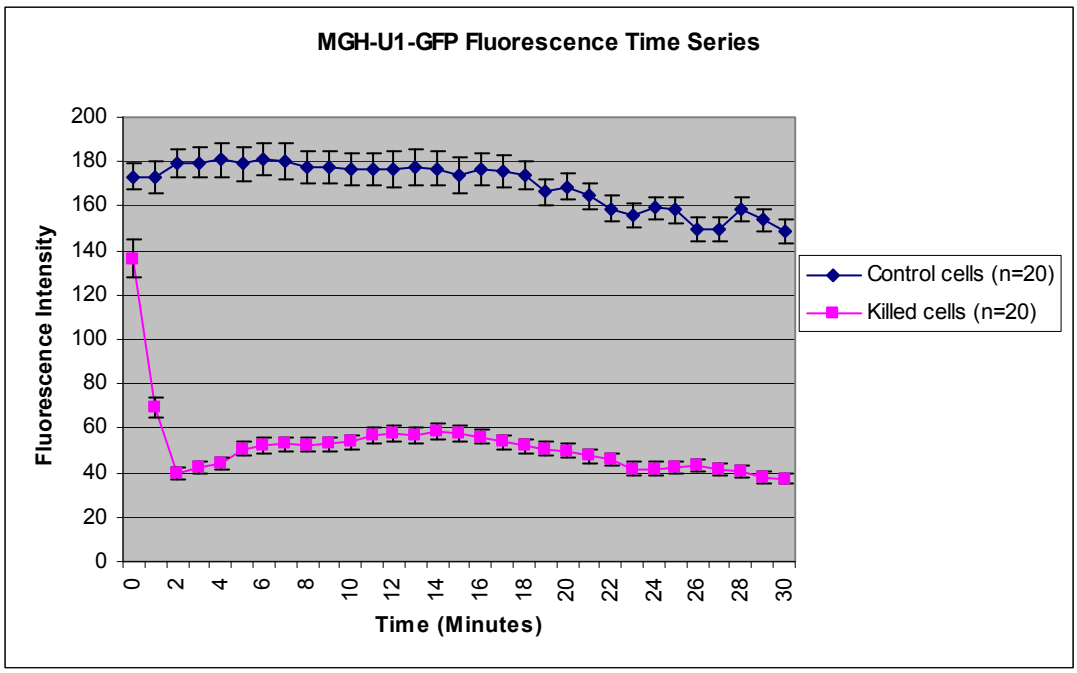

Figure 56: Time series of MGH-U1-GFP cell fluorescence for live and killed cells over 30 minutes (with 95% confidence intervals)

3.2: Flow cytometry experiments

Flow cytometric experiments were performed using a BD FACScaliber flow cytometer. Early experiments were analysed using WinMDI version 2.8, which generated values for geomean and median fluorescence and coefficients of variation (CV) for each sample. Later experiments were analysed using the BD FACScaliber software package generating values for geomean and median fluorescence and standard deviations, from which we were able to calculate 95% confidence intervals.

Cellular epirubicin dose response

Flow cytometric dose responses for epirubicin in MGH-U1 and MGH-U1R cells are shown in Figures 57 and 58. Statistics generated for each sample are shown in table 20 and 21.

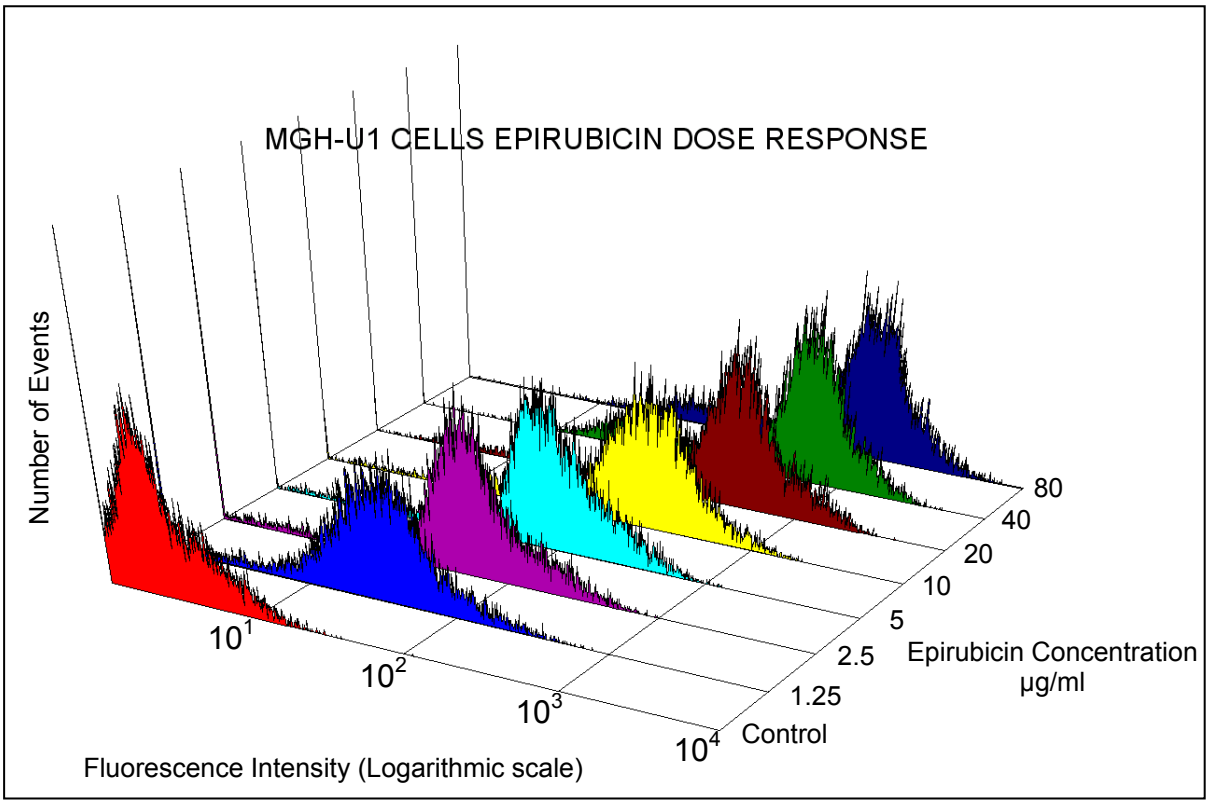

Figure 57: MHG-U1: Flow cytometric epirubicin dose response

Epirubicin Concentration	Geomean Fluorescence	Median Fluorescence	CV
Control	2.43	2.15	76.35
1.25	26.21	29.69	34.07
2.5	49.88	53.76	28.02
5	82.38	87.38	23.9
10	155.68	184.34	22.11
20	293.64	365.17	21.69
40	399.41	562.34	20.79
80	554.48	763.51	19.13

Table 20: MGH-U1 cells: Flow cytometric epirubicin dose response statistics: Geomean and median fluorescence and coefficient of variation (CV)

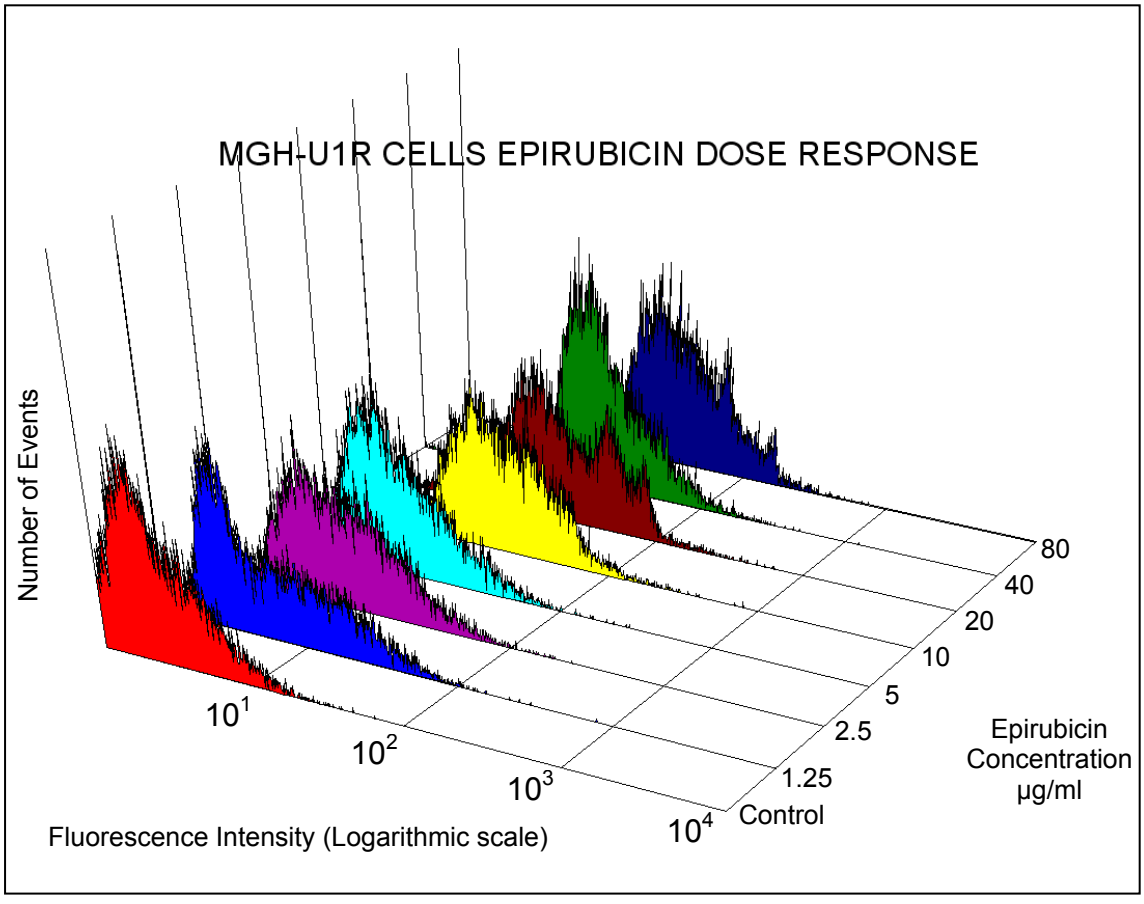

Figure 58: MHG-U1R cells: Flow cytometric epirubicin dose response

Epirubicin Concentration	Geomean Fluorescence	Median Fluorescence	CV
Control	2.54	2.25	70.11
1.25	5.74	4.61	54.99
2.5	7.41	6.92	42.25
5	7.90	7.04	36.08
10	17.77	17.00	27.54
20	21.39	20.17	29.27
40	21.33	19.11	22.59
80	36.33	33.68	20.81

Table 21: MGH-U1R cells: Flow cytometric epirubicin dose response statistics: Geomean and median fluorescence and coefficient of variation (CV)

Both cell lines demonstrated a clear dose response in epirubicin uptake, but this was much less pronounced in the MGH-U1R cells. At the highest dose of epirubicin exposure, cellular uptake in MGH-U1 cells was over 15 times greater than in the MGH-U1R cells.

Cellular idarubicin dose response

Flow cytometric idarubicin dose responses for MGH-U1 and MGH-U1R cells are shown in figures 59 and 60. Statistics generated for these samples are shown in tables 22 and 23.

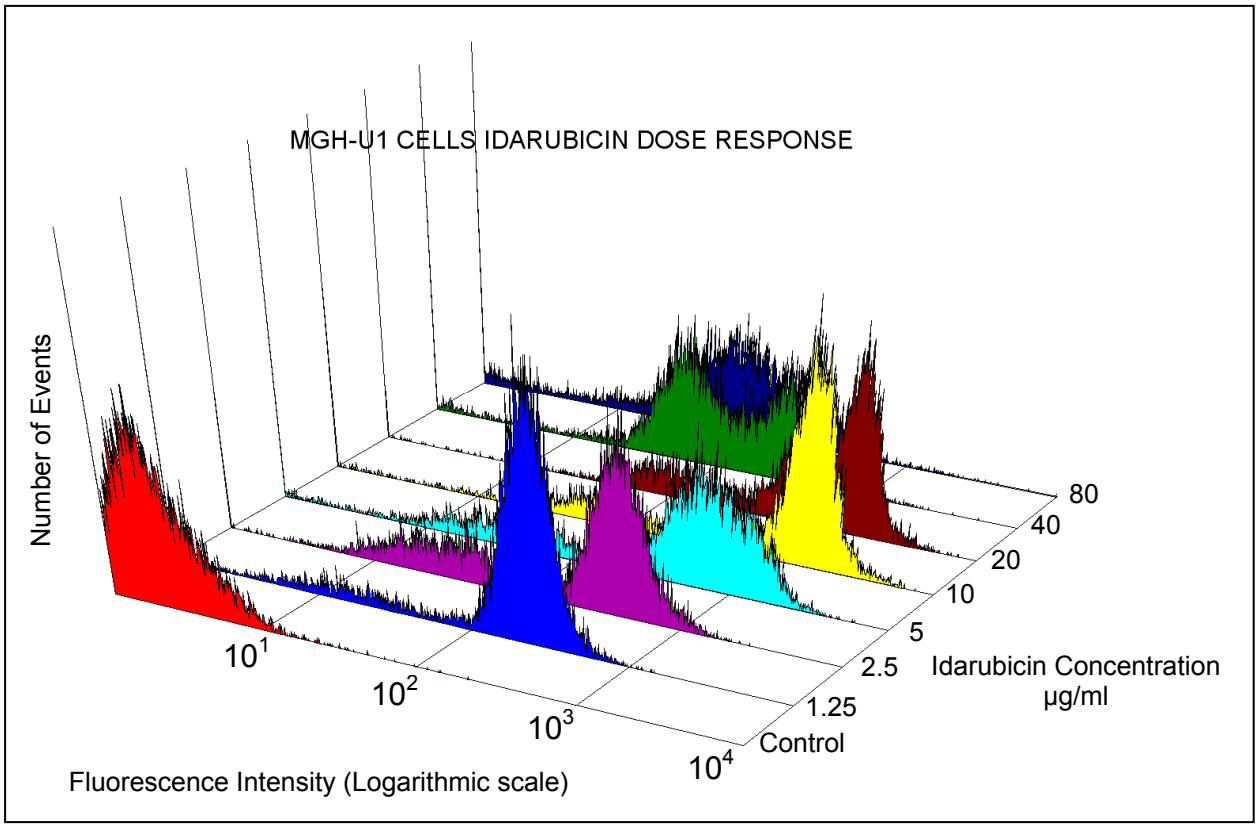

Figure 59: MGH-U1: Flow cytometric idarubicin dose response

Idarubicin Concentration	Geomean Fluorescence	Median Fluorescence	CV
Control	2.22	2.0	76.28
1.25	150.19	218.7	24.86
2.5	166	310.59	27.82
5	299.34	547.37	29.69
10	694.56	1321.58	23.41
20	695.70	1000	18.47
40	92.96	94.75	27.56
80	54.21	37.36	69.78

Table 22: MGH-U1: Flow cytometric idarubicin dose response statistics: Geomean and median fluorescence and coefficient of variation (CV)

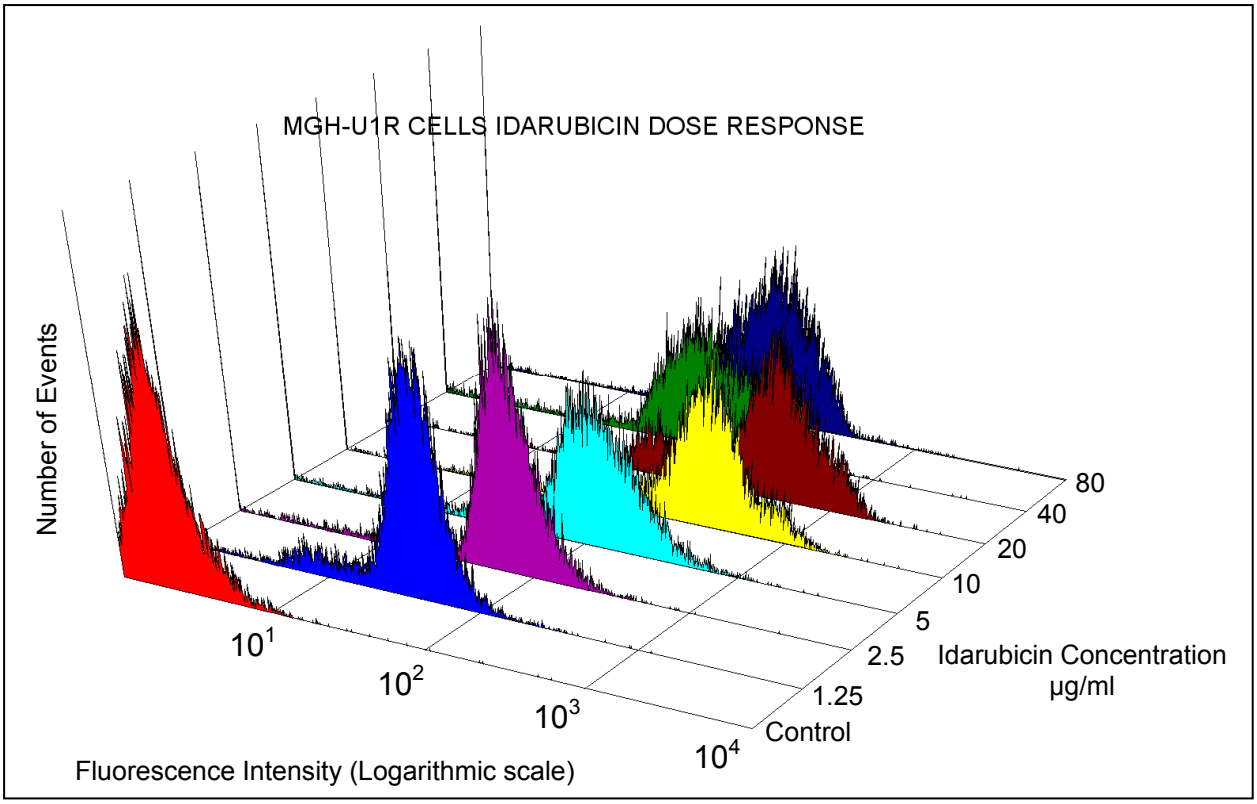

Figure 60: MGH-U1R cells: Flow cytometric idarubicin dose response

Idarubicin Concentration	Geomean Fluorescence	Median Fluorescence	CV
Control	2.21	2.15	61.13
1.25	32.69	38.54	23.43
2.5	57.94	65.52	21.47
5	89.2	104.6	23.66
10	198.37	257.13	21.6
20	298.51	381.97	20.1
40	72.66	78.44	25.86
80	90.56	99.1	19.32

Table 23: MGH-U1R cells: Flow cytometric idarubicin dose response statistics: Geomean and median fluorescence and coefficient of variation (CV)

Both cell lines demonstrated a clear dose response in idarubicin uptake up to 20µg/ml. At higher doses of idarubicin the samples were relatively acellular and demonstrated reduced levels of drug fluorescence. This is probably as a result of cell death in the higher concentration samples, meaning that cells taking up the most drug in these samples died and were lost during sample preparation. Hence the cells left behind were those with lower levels of drug uptake and fluorescence. At the lowest concentration of idarubicin (1.25µg/ml), sensitive cells demonstrated over 5 times more intracellular drug fluorescence than the resistant cells. At 20µg/ml, this gap in fluorescence is reduced, but the MGH-U1 cells still exhibit 2.33 times more fluorescence than the MGH-U1R cells.

Effects of WGA pre-incubation on cellular epirubicin dose response

The effects of WGA on cellular epirubicin uptake in MGH-U1 and MGH-U1R cells were examined using flow cytometry. The dose response histograms are shown in Figures 61 – 64 and the statistics generated for these samples are shown in tables 24 and 25.

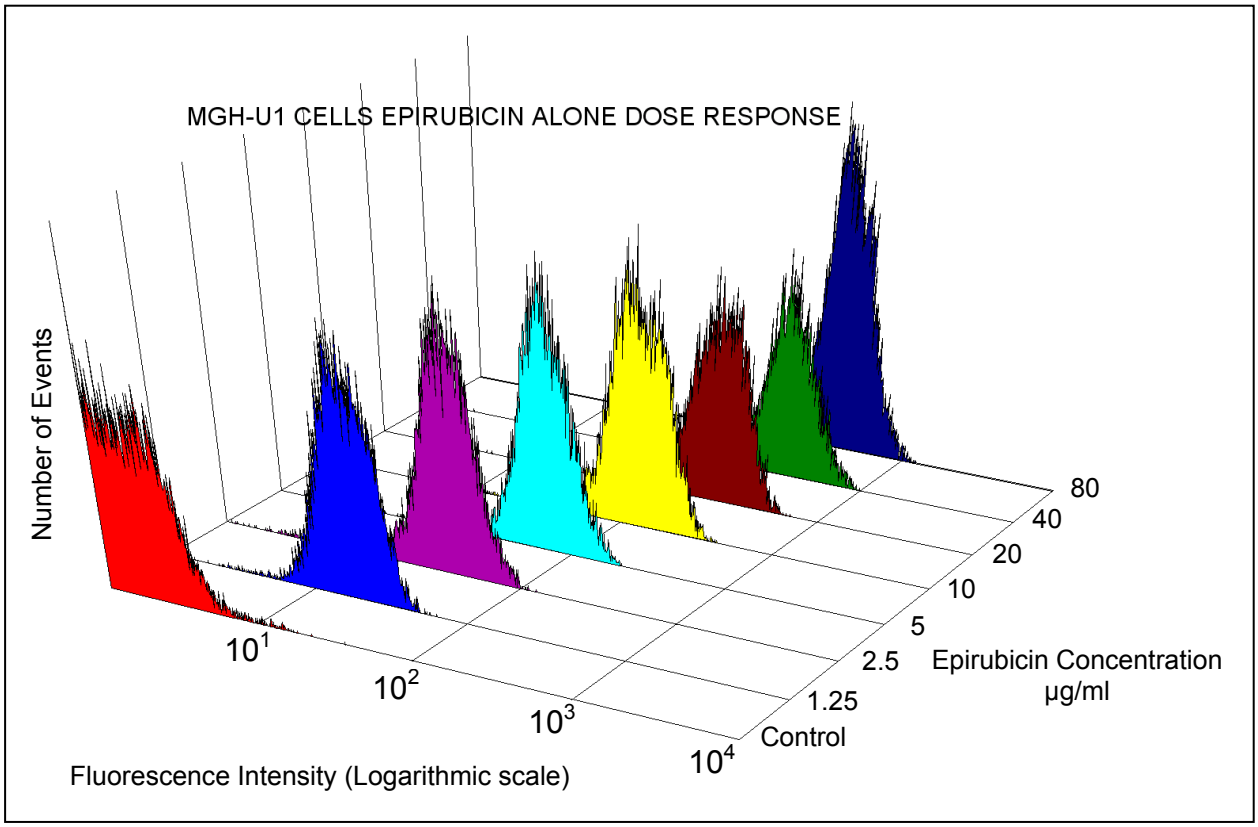

Figure 61: MGH-U1 cells: Flow cytometric epirubicin alone dose response

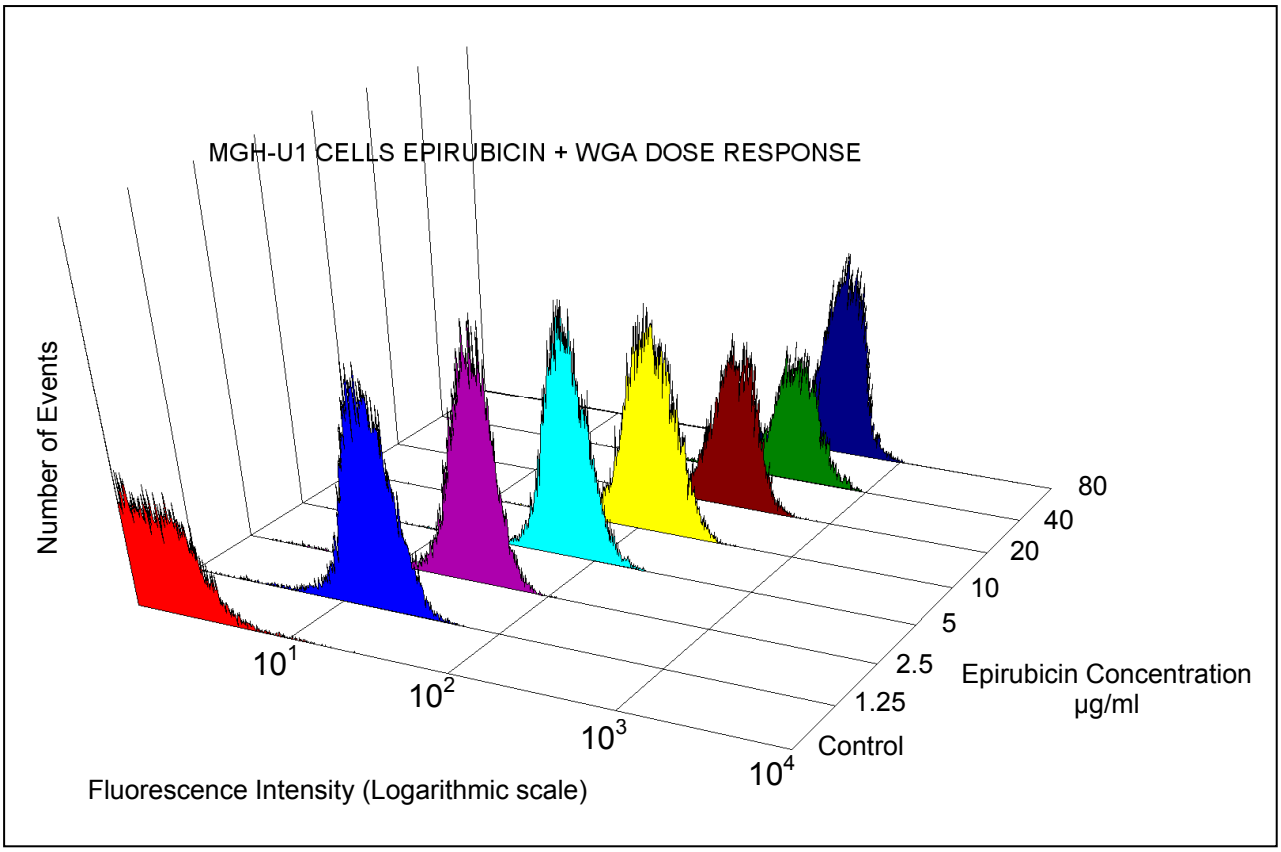

Figure 62: MGH-U1 cells: Flow cytometric epirubicin + WGA dose response

	MGH-U1 cells – No WGA			MGH-U1 cells – with WGA		
Epirubicin Concentration	Geomean	Median	CV	Geomean	Median	CV
Control	1.73	1.61	89.34	1.65	1.53	91.64
1.25	17.63	17.78	14.17	16.33	16.4	13.54
2.5	33.87	34.6	13.05	33.61	34.91	10.98
5	66.91	66.71	10.17	66.41	66.71	8.96
10	128.34	128.64	9.09	117.59	117.57	8.34
20	200.67	210.97	9.10	214.94	220.67	7.23
40	297.43	310.59	8.74	311.14	319.08	7.18
80	363.52	365.17	7.12	358.66	349.8	6.53

Table 24: MGH-U1 cells: Flow cytometric epirubicin dose response statistics with and without WGA: Geomean and median fluorescence and coefficient of variation (CV)

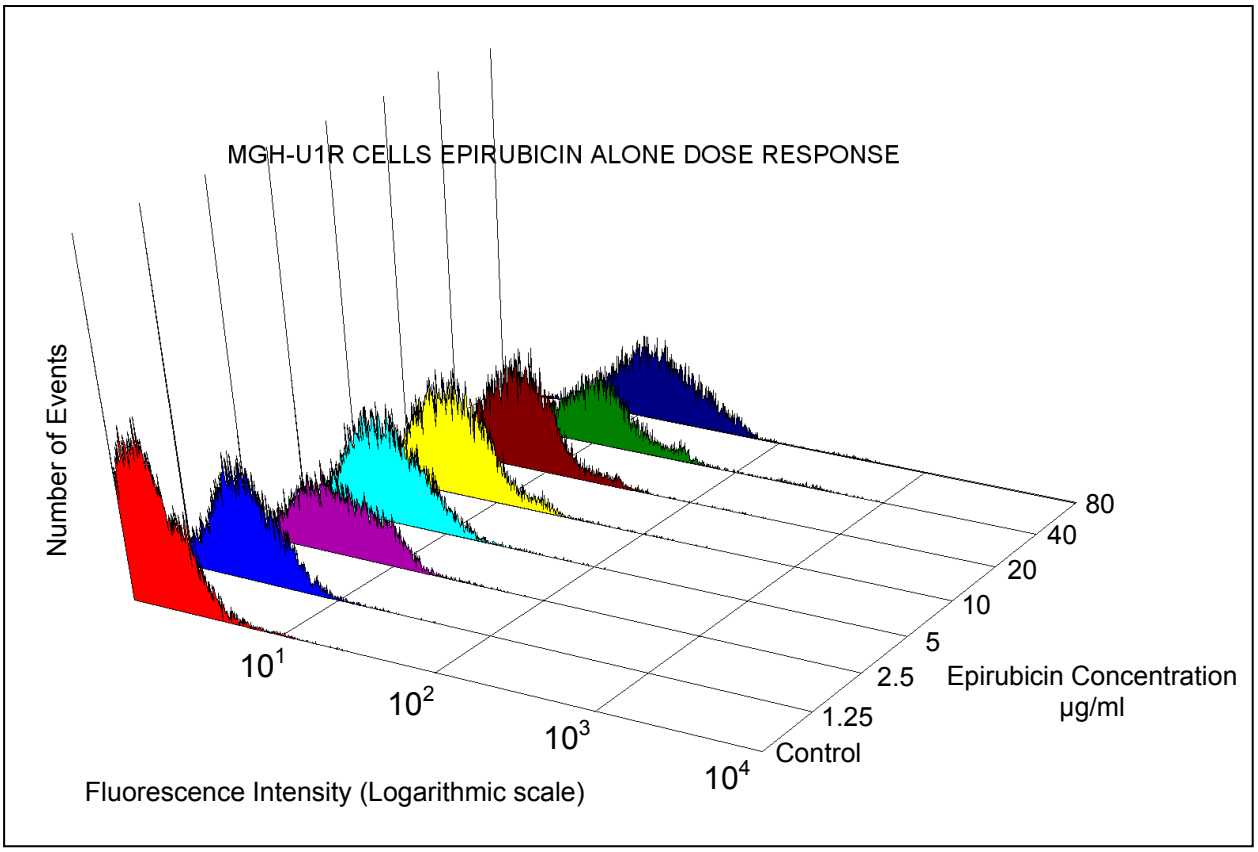

Figure 63: MGH-U1R cells: Flow cytometric epirubicin alone dose response

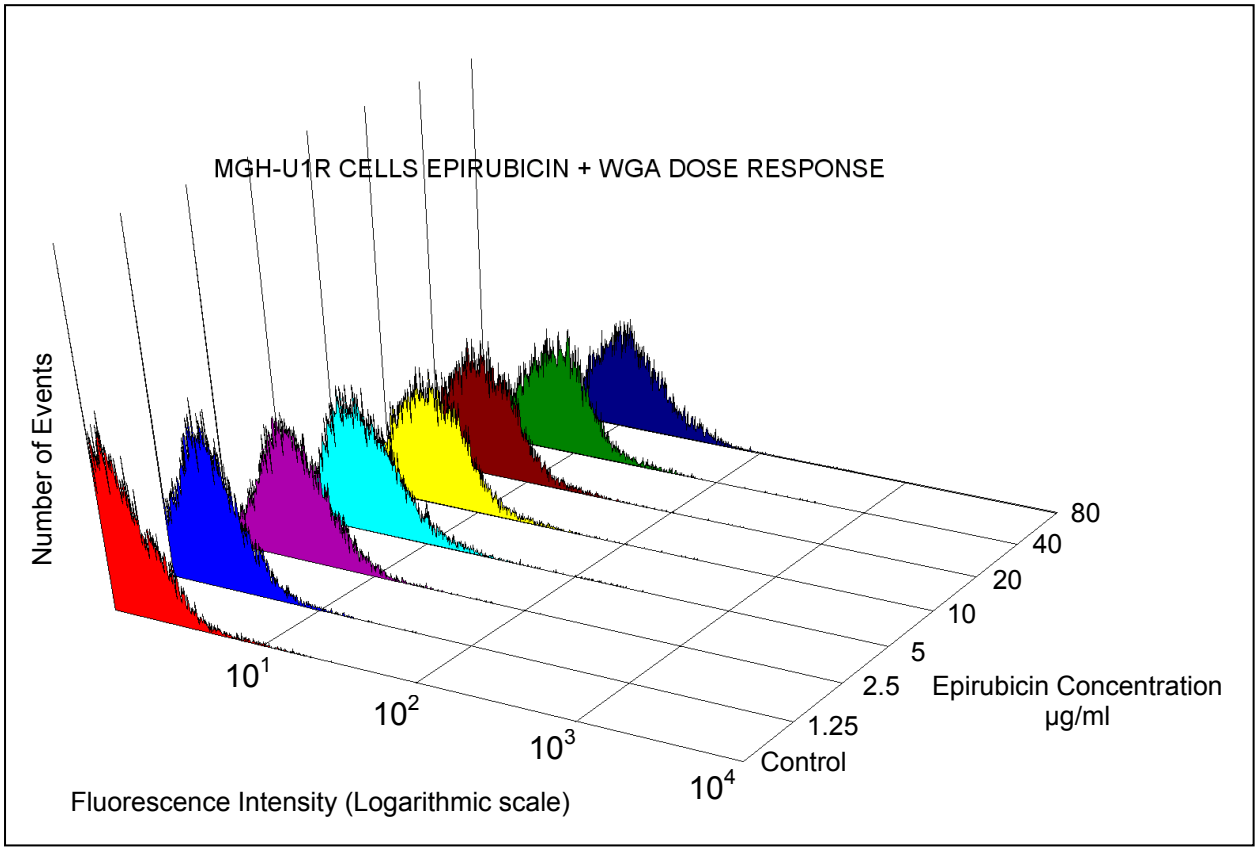

Figure 64: MGH-U1R cells: Flow cytometric epirubicin + WGA dose response

	MGH-U1R cells – No WGA			MGH-U1R cells – with WGA		
Epirubicin Concentration	Geomean	Median	CV	Geomean	Median	CV
Control	1.64	1.53	86.45	1.49	1.33	105.86
1.25	2.54	2.5	54.29	2.04	1.98	66.69
2.5	4.4	4.29	43.29	2.57	2.5	54.39
5	3.97	3.89	43.14	3.02	2.97	48.59
10	5.06	4.96	37.73	3.9	3.72	43.01
20	6.65	6.55	32.13	4.91	4.83	35.05
40	11.26	10.75	31.45	7.26	7.3	28.25
80	13.87	13.34	27.08	11.22	10.94	25.56

Table 25: MGH-U1R cells: Flow cytometric epirubicin dose response statistics with and without WGA: Geomean and median fluorescence and coefficient of variation (CV)

A clear dose response in epirubicin uptake was seen in both MGH-U1 and MGH-U1R cells with and without prior WGA exposure. The MGH-U1R cells showed much lower levels of epirubicin uptake across all concentrations, with the MGH-U1 cells demonstrating over 26 times more epirubicin fluorescence at the highest dose of 80µg/ml.

In addition WGA did not increase the cellular uptake of epirubicin in either MGH-U1 or MGH-U1R cells, with epirubicin uptake levels at the highest concentrations being slightly lower if anything.

Effects of WGA pre-incubation on nuclear epirubicin dose response

The effects of WGA on epirubicin uptake in nuclear isolates from MGH-U1 and MGH-U1R cells exposed to epirubicin before nuclear fractionation were also examined using flow cytometry. The dose response histograms are shown in Figures 65 – 68 and the statistics generated for these samples are shown in tables 26 and 27.

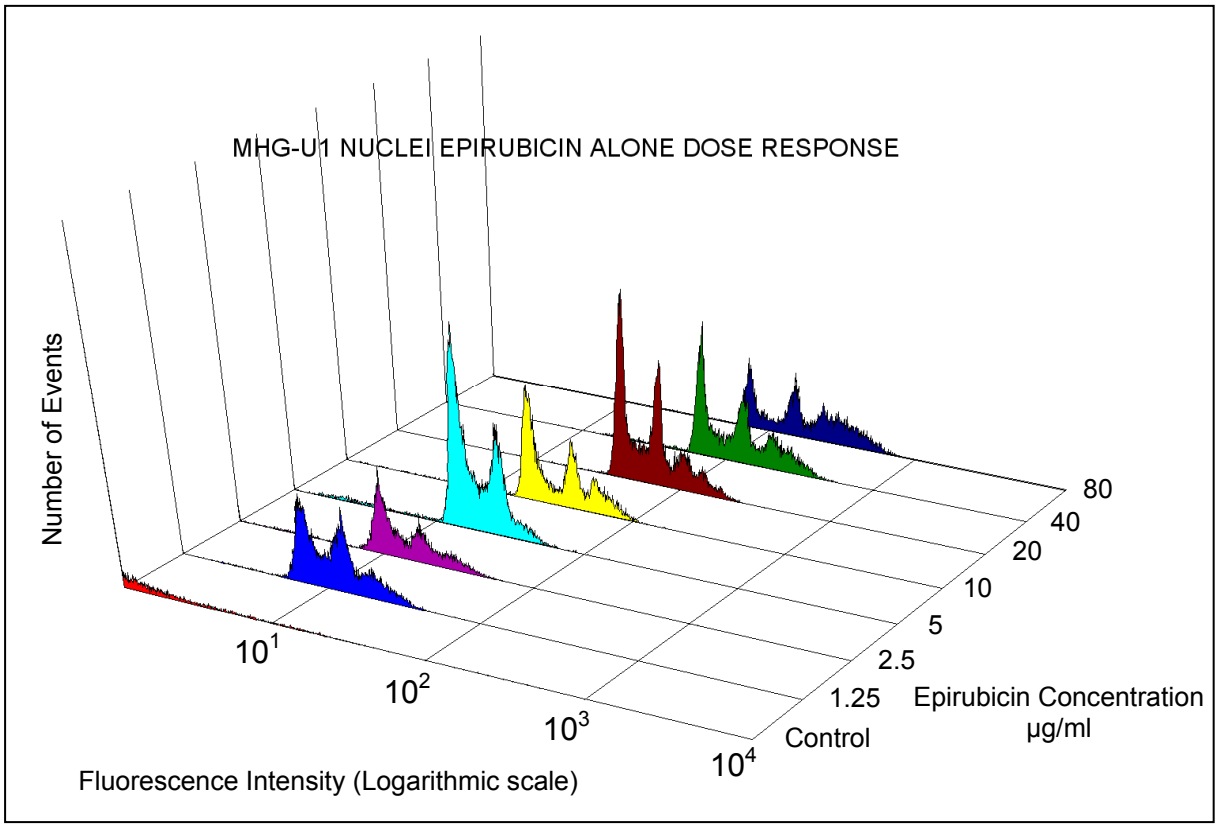

Figure 65: MGH-U1 nuclei: Flow cytometric epirubicin alone dose response

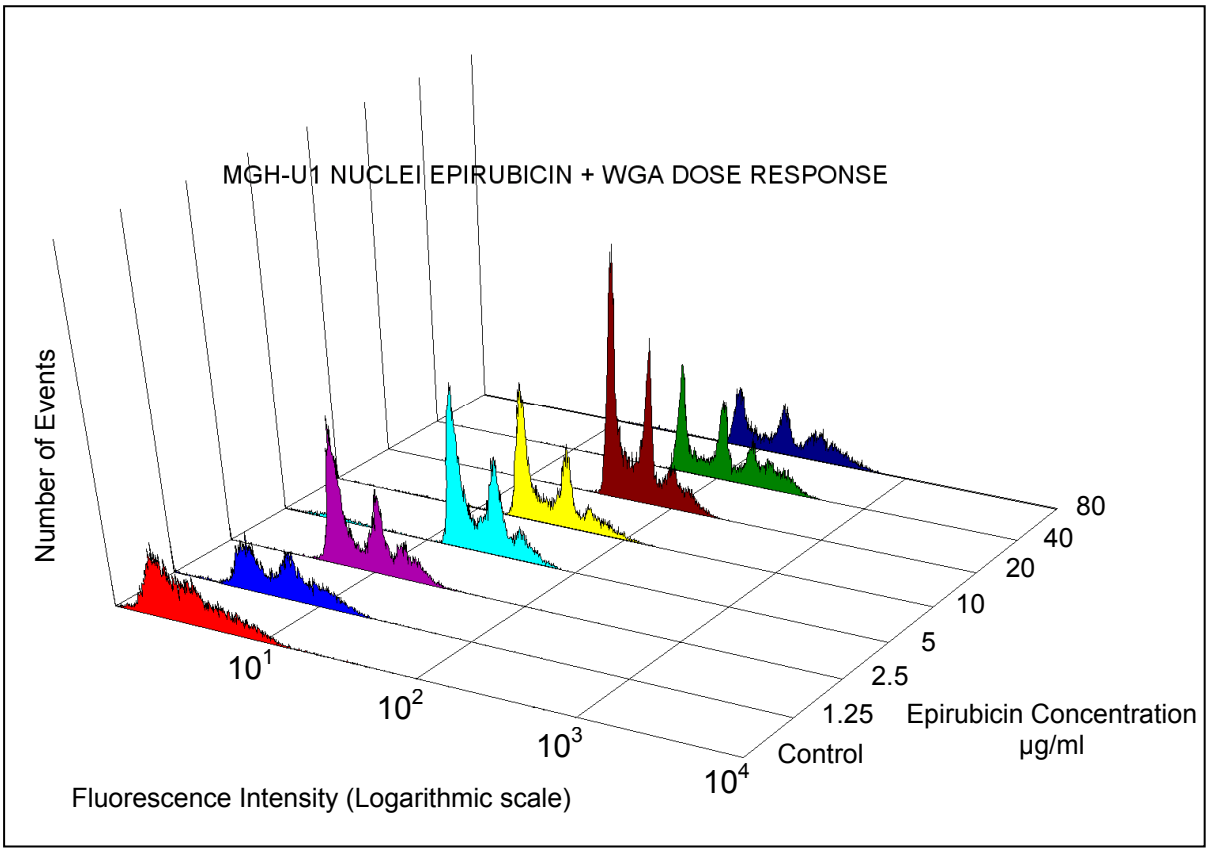

Figure 66: MGH-U1 nuclei: Flow cytometric epirubicin + WGA dose response

	MGH-U1 nuclei – No WGA			MGH-U1 nuclei – with WGA		
Epirubicin Concentration	Geomean	Median	CV	Geomean	Median	CV
Control	1.26	1.0	262.34	3.28	2.97	48.72
1.25	11.08	11.04	19.57	5.52	5.62	33.2
2.5	13.59	12.52	21.69	8.63	7.77	22.63
5	18.2	17.0	16.83	21.16	20.35	19.41
10	30.78	28.39	15.2	30.68	27.88	15.12
20	60.93	60.43	11.45	57.61	55.73	10.37
40	115.78	117.57	12.11	112.8	108.43	12.65
80	167.84	159.63	13.27	139.91	142.02	13.81

Table 26: MGH-U1 nuclei: Flow cytometric epirubicin dose response statistics with and without WGA: Geomean and median fluorescence and coefficient of variation (CV)

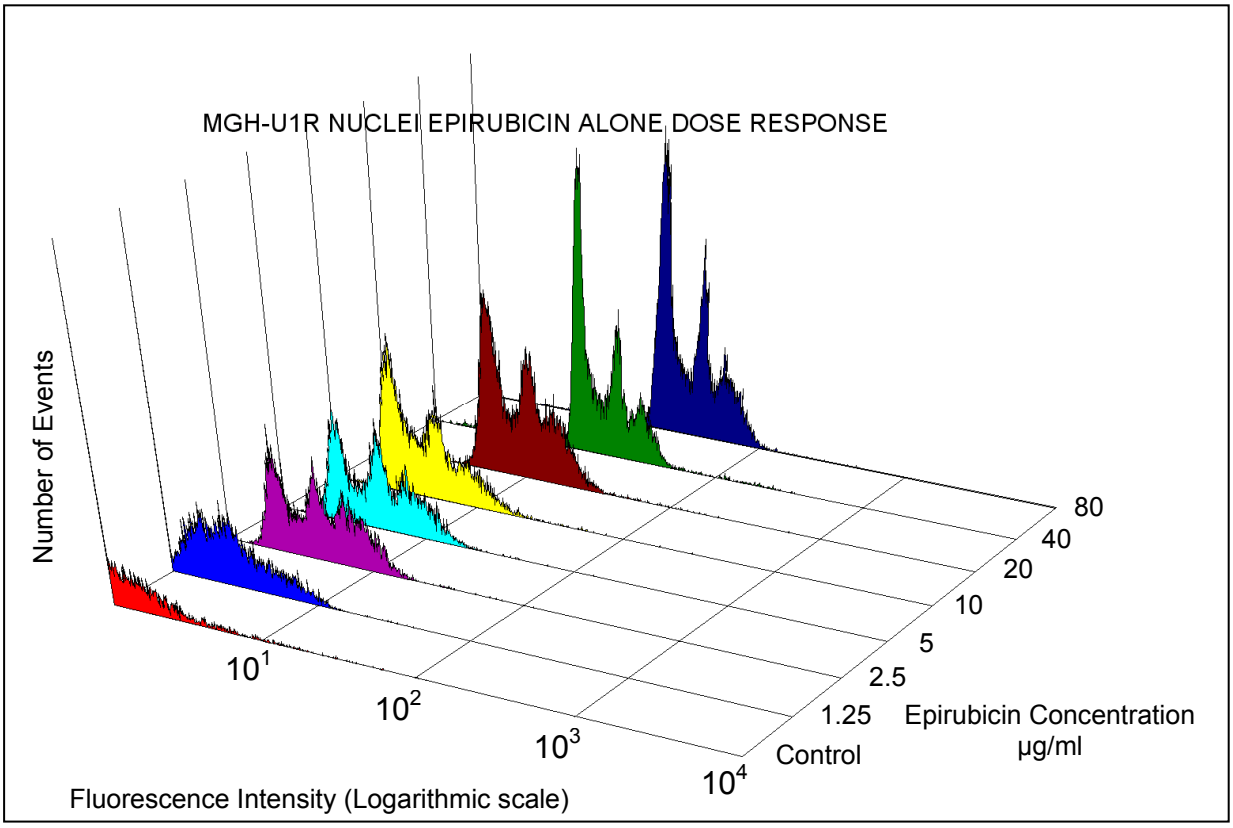

Figure 67: MGH-U1R nuclei: Flow cytometric epirubicin alone dose response

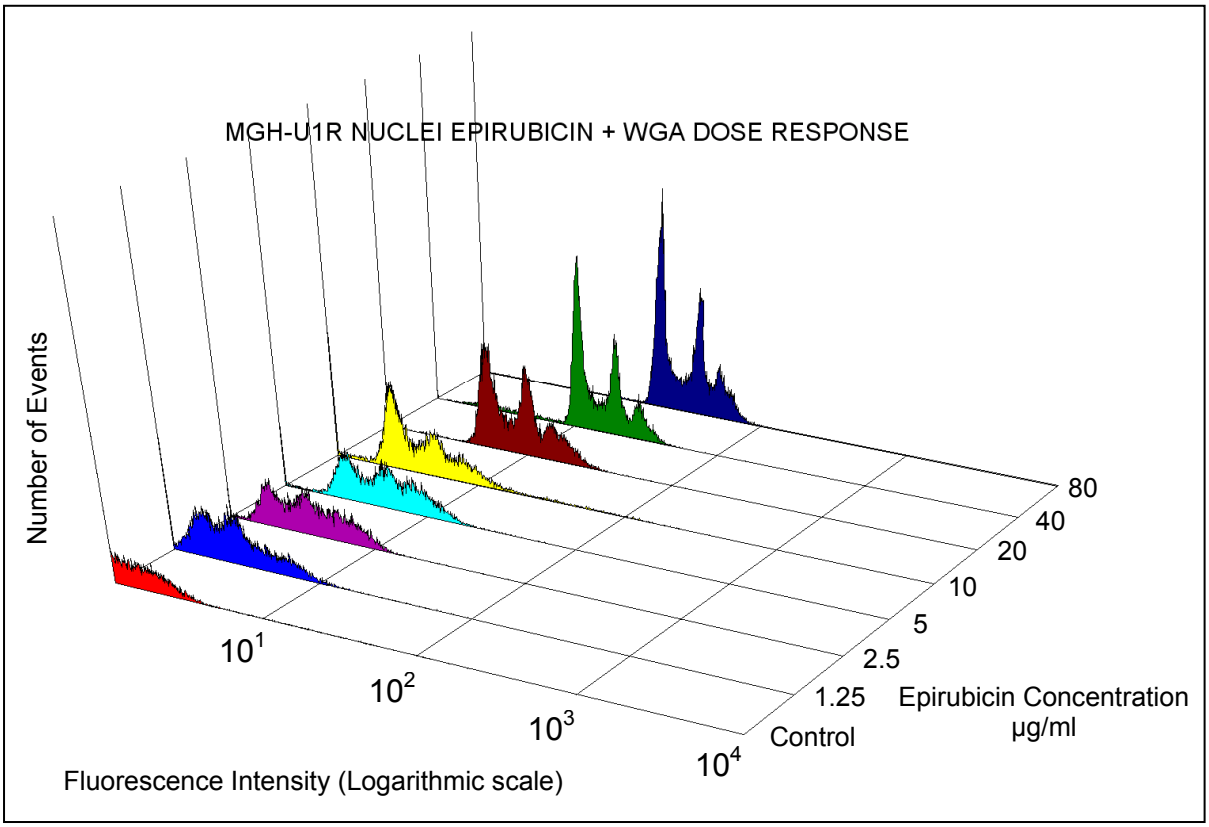

Figure 68: MGH-U1 nuclei: Flow cytometric epirubicin + WGA dose response

	MGH-U1R nuclei – No WGA			MGH-U1R nuclei – with WGA		
Epirubicin Concentration	Geomean	Median	CV	Geomean	Median	CV
Control	1.29	1.0	195.31	1.36	1.06	151.52
1.25	2.63	2.46	60.86	2.72	2.57	56.98
2.5	4.36	4.29	39.76	3.57	3.49	44.12
5	4.65	4.66	36.86	4.85	4.87	36.29
10	4.3	3.92	38.28	4.11	3.65	46.93
20	9.07	8.91	23.71	8.48	8.51	23.08
40	15.4	13.95	20.5	13.91	13.10	20.87
80	31.37	28.9	14.13	28.31	27.63	14.02

Table 27: MGH-U1R nuclei: Flow cytometric epirubicin dose response statistics with and without WGA: Geomean and median fluorescence and coefficient of variation (CV)

Again the nuclear isolates demonstrated a clear dose response in epirubicin uptake, which was more pronounced in the MGH-U1 cells. Without WGA MGH-U1 nuclei demonstrated more than 5 times more epirubicin fluorescence that the MGH-U1R cells. WGA did not affect nuclear epirubicin uptake levels across the range of epirubicin concentrations.

Mitomycin C dose response

We looked for evidence of mitomycin C fluorescence across a range of excitation and emission wavelengths. We excited the cells with 488 and 633nm laser excitation and tried to detect fluorescence with all detectors (FL-1, FL-2 and FL-3). The results are shown below in tables 28 and 29.

Mitomycin C Concentration µg/ml	FL-1 Geomean	FL-2 Geomean	FL-3 Geomean
Control	1.57	3.68	2.57
125	1.43	3.26	2.28
250	1.38	3.15	2.17
500	1.50	3.72	2.6
1000	1.97	5.34	3.64

Table 28: MGH-U1 cells: Mitomycin C fluorescence dose response

Mitomycin C Concentration µg/ml	FL-1 Geomean	FL-2 Geomean	FL-3 Geomean
Control	1.74	4.34	2.99
125	1.63	4.03	2.74
250	1.56	3.81	2.61
500	1.57	3.79	2.5
1000	2.76	7.99	5.67

Table 29: MGH-U1R cells: Mitomycin C fluorescence dose response

We were unable to detect any mitomycin C fluorescence between wavelengths of 505nm to over 650nm, in either the MGH-U1 or MGH-U1R cells.

Assessing Mitomycin C dose response by reduction acridine orange fluorescence

We tried an indirect method to assess the cellular uptake of mitomycin C, by looking for a reduction in cellular acridine orange (AO) uptake. To detect acridine orange fluorescence we used an excitation wavelength of 488nm and detected fluorescence using the FL-1 detector (515 – 545nm) (Table 30).

Mitomycin C (MMC) concentration µg/ml	MGH-U1 FL-1 Geomean AO Fluorescence	MGH-U1R FL-1 Geomean AO Fluorescence
Control – No MMC and no AO	2.02	1.44
Control – AO only	1192.39	498.63
125 MMC + AO	480.29	828.60
250 MMC + AO	797.17	1483.78
500 MMC + AO	1651.85	1293.19

Table 30: Acridine orange fluorescence dose response to mitomycin C in MGH-U1 and MGH-U1R cells

The cell samples exposed to 1000µg/ml of mitomycin C were not evaluable due to low cell numbers, presumably because of cell killing. There appeared to be no inverse dose response in acridine orange fluorescence as a result of prior exposure to mitomycin C in either cell type. It is possible that looking at the reduction of AO uptake in isolated nuclei would have been a more accurate surrogate marker of mitomycin C uptake, as it is the competition between these two agents to bind to DNA that is the basis of this assay. It seems likely that cellular AO contamination may have skewed our results.

Effects of verapamil on epirubicin dose response

MGH-U1

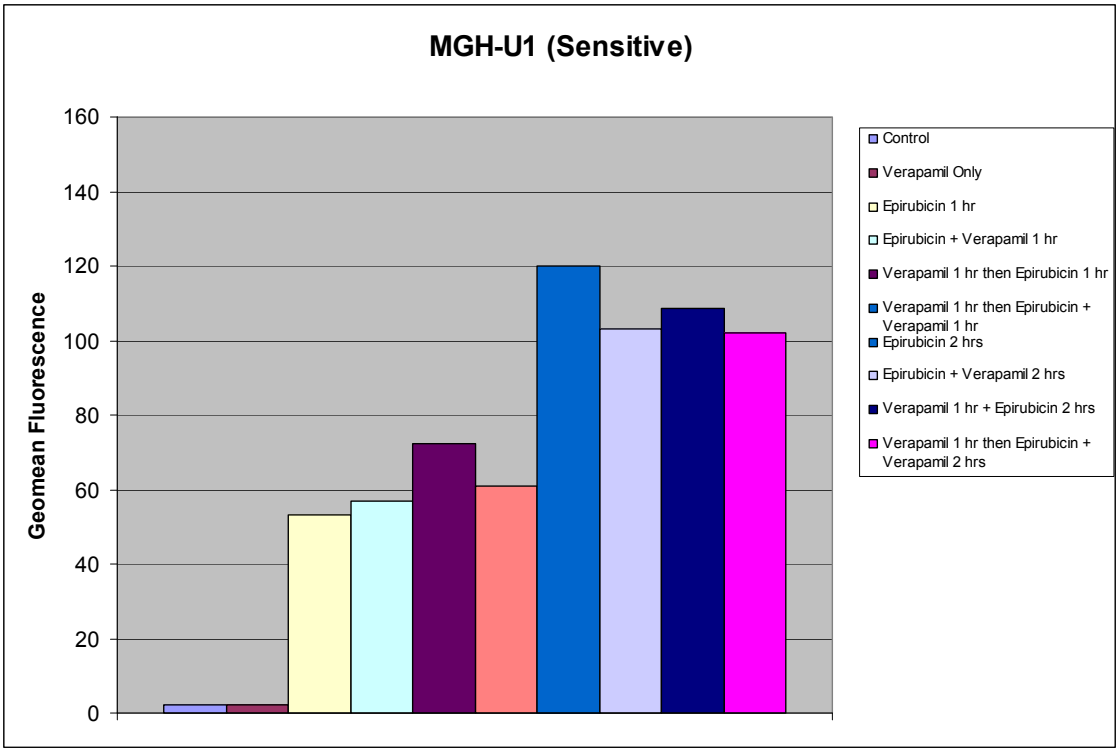

Figure 69: MGH-U1 cells: Geomean fluorescence values for various combinations of epirubicin with and without verapamil

MGH-U1 Samples n = 10,000	Geomean Fluorescence	Median Fluorescence	95% Confidence Interval
Control – No epirubicin and no verapamil	2.3	2.29	0.02
Control – Verapamil only	2.38	2.41	0.02
Epirubicin 1hr	53.11	52.8	0.65
Epirubicin + Verapamil 1hr	57	55.73	0.63
Verapamil 1hr then Epirubicin 1hr	72.43	66.12	1.10
Verapamil 1hr then Epirubicin and Verapamil 1hr	60.98	58.29	0.75
Epirubicin 2hrs	120.15	61.82	2.02
Epirubicin and Verapamil 2hrs	103.01	93.9	1.66
Verapamil 1hr then Epirubicin 2hrs	108.79	85.82	2.25
Verapamil 1hr then Epirubicin + Verapamil 2hrs	102.18	96.47	1.34

Table 31: MGH-U1 cells: Flow cytometric assessment of epirubicin uptake in combinations with and without verapamil

RT112:

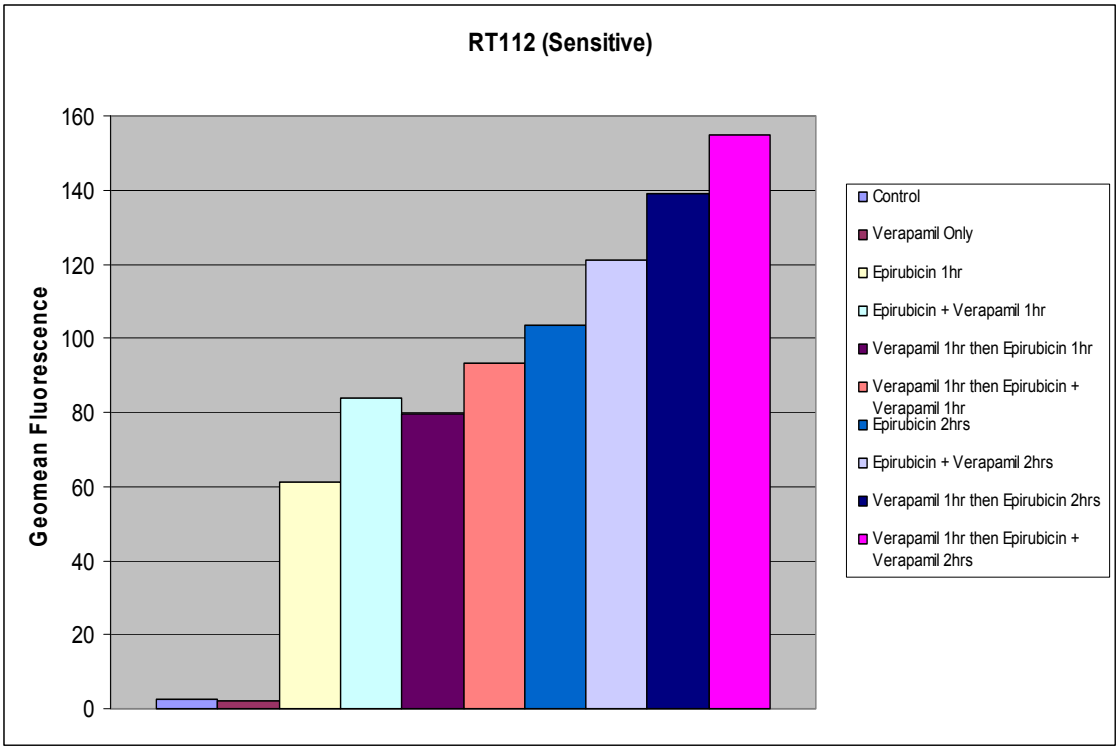

Figure 70: RT112 cells: Geomean fluorescence values for various combinations of epirubicin with and without verapamil

RT112 Samples n = 10,000	Geomean Fluorescence	Median Fluorescence	95% Confidence Interval
Control – No epirubicin and no verapamil	2.36	2.25	0.22
Control – Verapamil only	1.98	1.91	0.03
Epirubicin 1hr	61.03	62.08	0.38
Epirubicin + Verapamil 1hr	83.69	87.38	0.63
Verapamil 1hr then Epirubicin 1hr	79.55	86.6	0.64
Verapamil 1hr then Epirubicin and Verapamil 1hr	93.1	97.34	0.68
Epirubicin 2hrs	103.37	104.6	0.75
Epirubicin and Verapamil 2hrs	120.92	128.64	0.99
Verapamil 1hr then Epirubicin 2hrs	139.25	159.63	1.36
Verapamil 1hr then Epirubicin + Verapamil 2hrs	155.06	149.89	0.95

Table 32: RT112 cells: Flow cytometric assessment of epirubicin uptake in combinations with and without verapamil

MGH-U1R

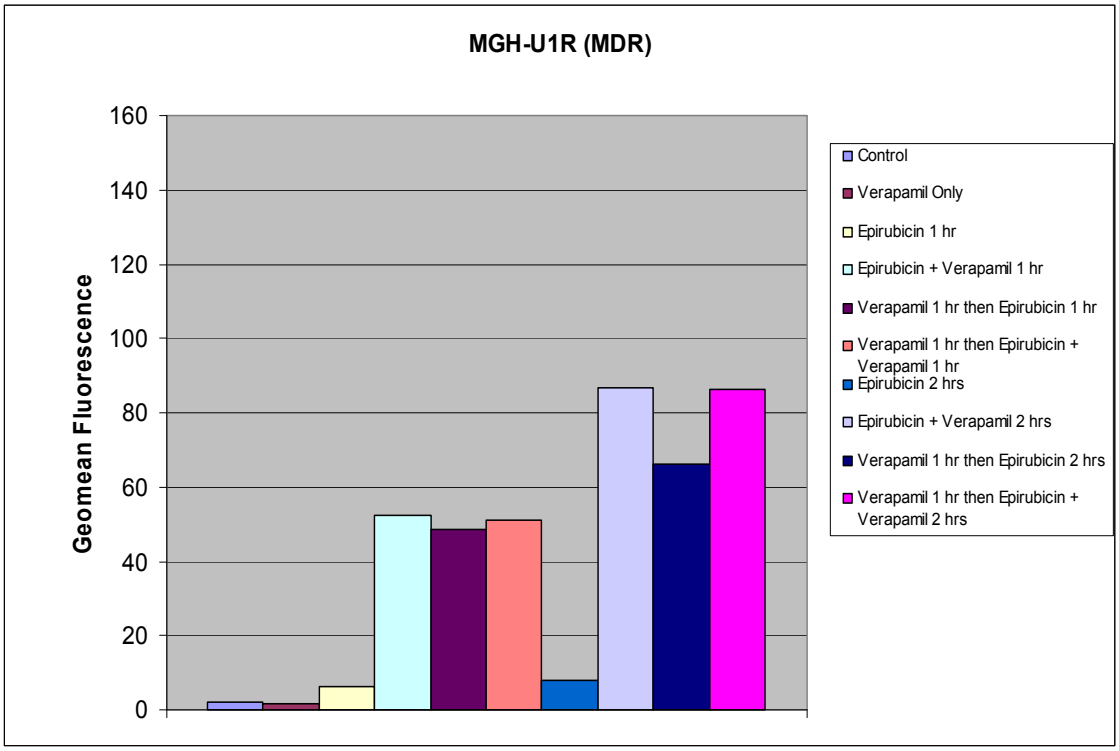

Figure 71: MGH-U1R cells: Geomean fluorescence values for various combinations of epirubicin with and without verapamil

MGH-U1R Samples n = 10,000	Geomean Fluorescence	Median Fluorescence	95% Confidence Interval
Control – No epirubicin and no verapamil	2.05	2.02	0.03
Control – Verapamil only	1.57	1.49	0.02
Epirubicin 1hr	6.17	5.99	0.12
Epirubicin + Verapamil 1hr	52.35	52.8	0.31
Verapamil 1hr then Epirubicin 1hr	48.47	48.7	0.55
Verapamil 1hr then Epirubicin and Verapamil 1hr	51.28	51.86	0.38
Epirubicin 2hrs	8.12	8.9	0.14
Epirubicin and Verapamil 2hrs	86.66	86.6	0.69
Verapamil 1hr then Epirubicin 2hrs	66.06	6.71	0.57
Verapamil 1hr then Epirubicin + Verapamil 2hrs	86.33	86.6	0.66

Table 33: MGH-U1R cells: Flow cytometric assessment of epirubicin uptake in combinations with and without verapamil

MGHU-MMC

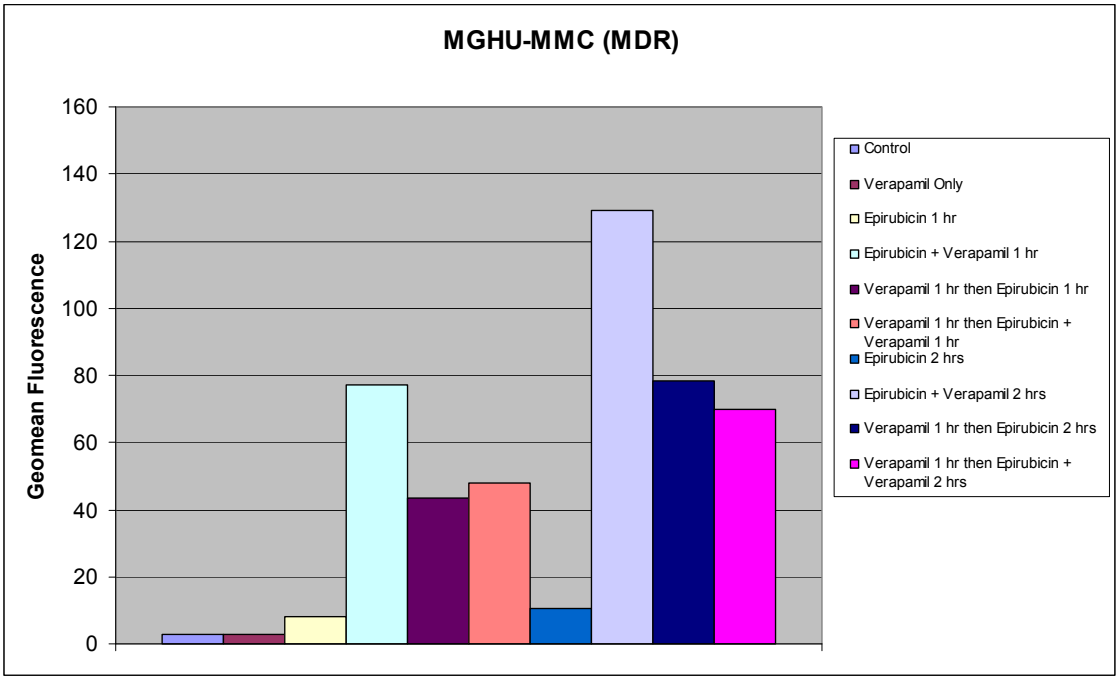

Figure 72: MGHU-MMC cells: Geomean fluorescence values for various combinations of epirubicin with and without verapamil

MGHU-MMC Samples n = 10,000	Geomean Fluorescence	Median Fluorescence	95% Confidence Interval
Control – No epirubicin and no verapamil	2.64	2.5	0.04
Control – Verapamil only	2.65	2.5	0.04
Epirubicin 1hr	8.14	7.7	0.19
Epirubicin + Verapamil 1hr	77.14	77.74	0.51
Verapamil 1hr then Epirubicin 1hr	43.38	45.73	0.41
Verapamil 1hr then Epirubicin and Verapamil 1hr	48.12	49.58	0.36
Epirubicin 2hrs	10.54	9.82	0.21
Epirubicin and Verapamil 2hrs	129.09	132.16	0.96
Verapamil 1hr then Epirubicin 2hrs	78.51	77.74	0.59
Verapamil 1hr then Epirubicin + Verapamil 2hrs	69.69	69.78	0.55

Table 34: MGHU-MMC cells: Flow cytometric assessment of epirubicin uptake in combinations with and without verapamil

Flow studies of MGH-U1 cells showed that drug fluorescence levels at 1 hour were similar for cells incubated with epirubicin alone and epirubicin and verapamil, these results were consistent with confocal time series results. However, for 2 hour exposures fluorescence levels were higher for epirubicin alone compared to epirubicin and verapamil, which did not fit with our confocal time series results (Figure 50a).

RT112 cells showed that 1 hour drug fluorescence was higher when epirubicin and verapamil were used in combination, which conflicted with the results of our confocal studies. At 2 hours this difference persisted with maximum drug uptake being shown in cells pre-incubated with verapamil followed by co-incubation with epirubicin and verapamil for 2 hours, again contrary to our confocal results (Figure 50b).

Flow cytometry showed that MGH-U1R cells had a 10.7-fold increase in cellular epirubicin fluorescence at 2 hours when co-incubated with epirubicin and verapamil compared with epirubicin alone. Pre-incubation with verapamil did not contribute any further increase in drug uptake (Figure 71).

Epirubicin uptake in MGHU-MMC cells was maximised by co-incubation with verapamil for 2 hours, showing a 12-fold increase over epirubicin alone at 2 hours (Figure 72).

Verapamil appeared to pre-sensitize MDR cells to epirubicin uptake for both 1 and 2 hour exposures to epirubicin, but overall for MDR cells co-incubation for 2 hours appeared to be the most advantageous regimen.

Interestingly the RT112 cells also showed beneficial effects from combination regimens with 1 and 2 hour exposure to epirubicin, whereas in MGH-U1 cells there was only a benefit for 1 hour co-incubation regimens but not for 2 hour exposures.

Overall, our results suggest that optimal reversal of MDR by verapamil, would be achieved by a combination of epirubicin and verapamil for a 2 hour exposure.

Effect of verapamil pre-exposure on epirubicin uptake in isolated nuclei

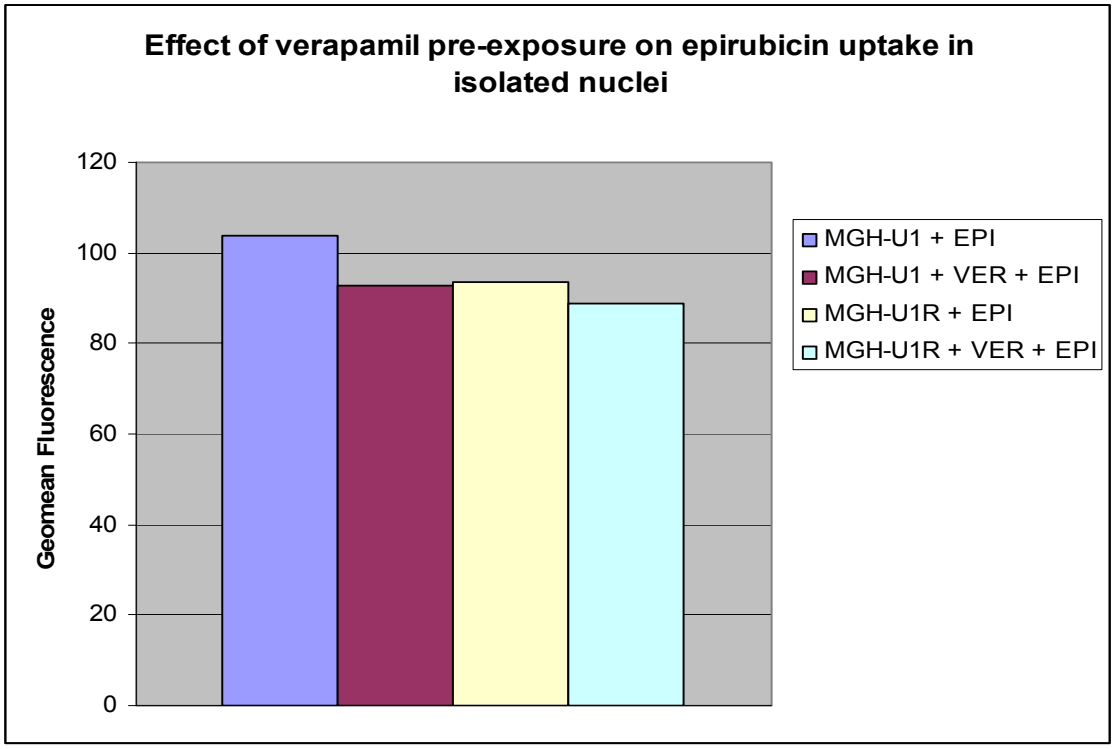

Figure 73: Effect of pre-exposure to verapamil on nuclear epirubicin uptake

Sample (n = 10,000)	Geomean Fluorescence	Median Fluorescence	CV
MGH-U1 + Epirubicin	103.98	99.1	11.63
MGH-U1 + Verapamil + Epirubicin	92.92	87.38	13.29
MGH-U1R + Epirubicin	93.61	89.77	9.98
MGH-U1R + Verapamil + Epirubicin	89.01	81.31	11.16

Table 35: Effect of pre-exposure to verapamil on nuclear epirubicin uptake

Pre-exposure to verapamil did not appear to have any effect on epirubicin uptake in isolated nuclei, if anything causing a slight reduction in nuclear epirubicin fluorescence.

Cellular P-gp staining with a FITC conjugated anti-P-gp antibody (17F9, BD Biosciences)

Histograms of green fluorescence (FL-1 detector) are shown for BSA control, FITC control and the FITC anti-P-gp antibody samples for each cell type (Figures 74 – 77). The geomean and median fluorescence values for each sample are shown in table 36.

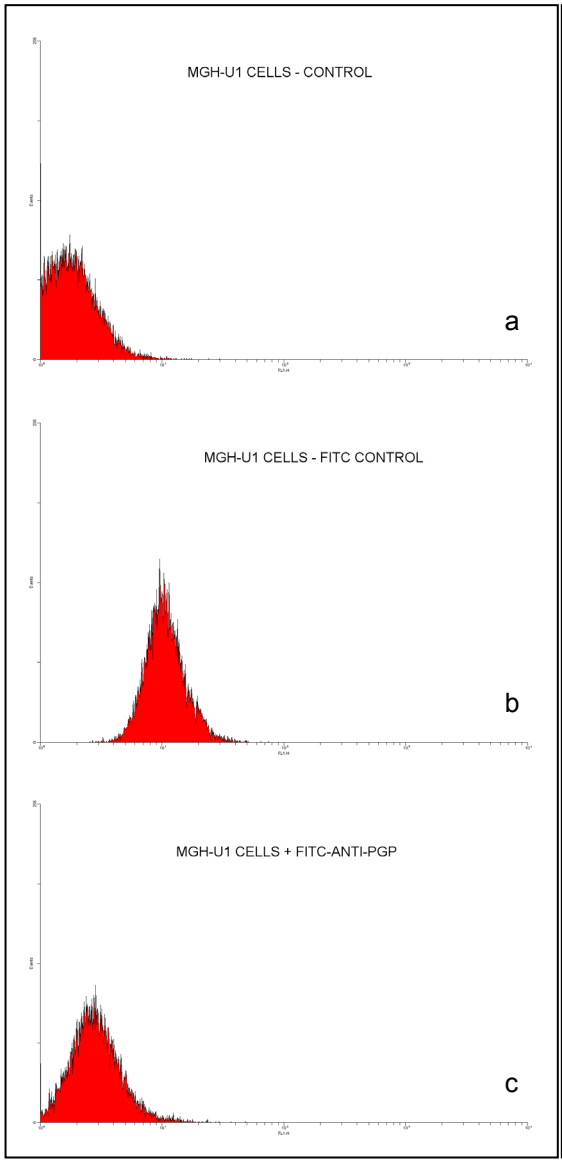

Figure 74: MGH-U1 cells FITC fluorescence detection for a: BSA control; b: FITC IgG control; c: FITC Anti-Pgp

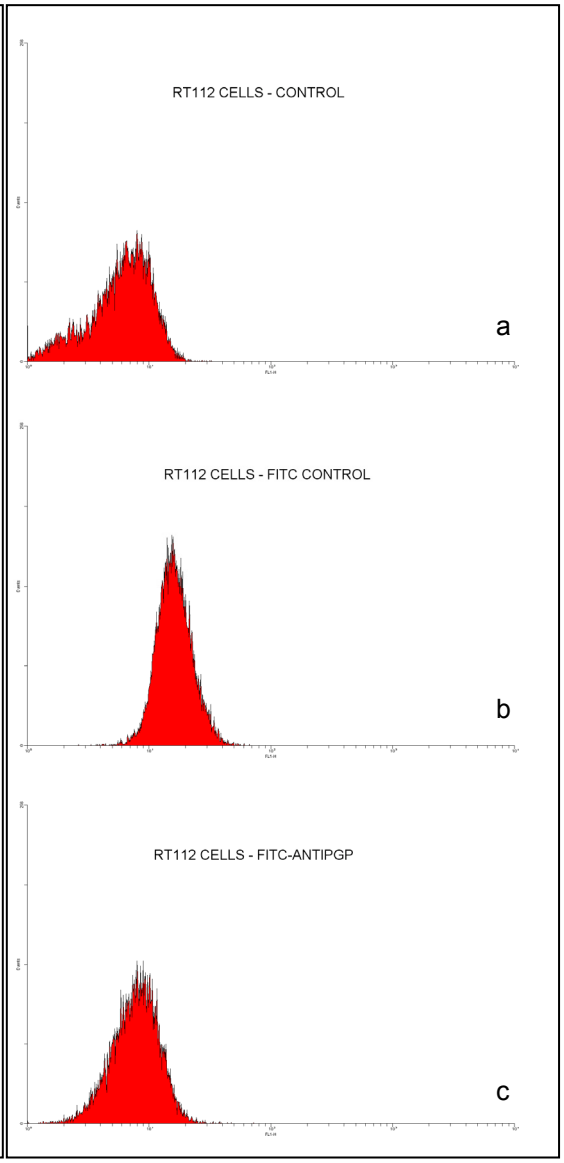

Figure 75: RT112 cells FITC fluorescence detection for a: BSA control; b: FITC IgG control; c: FITC Anti-Pgp

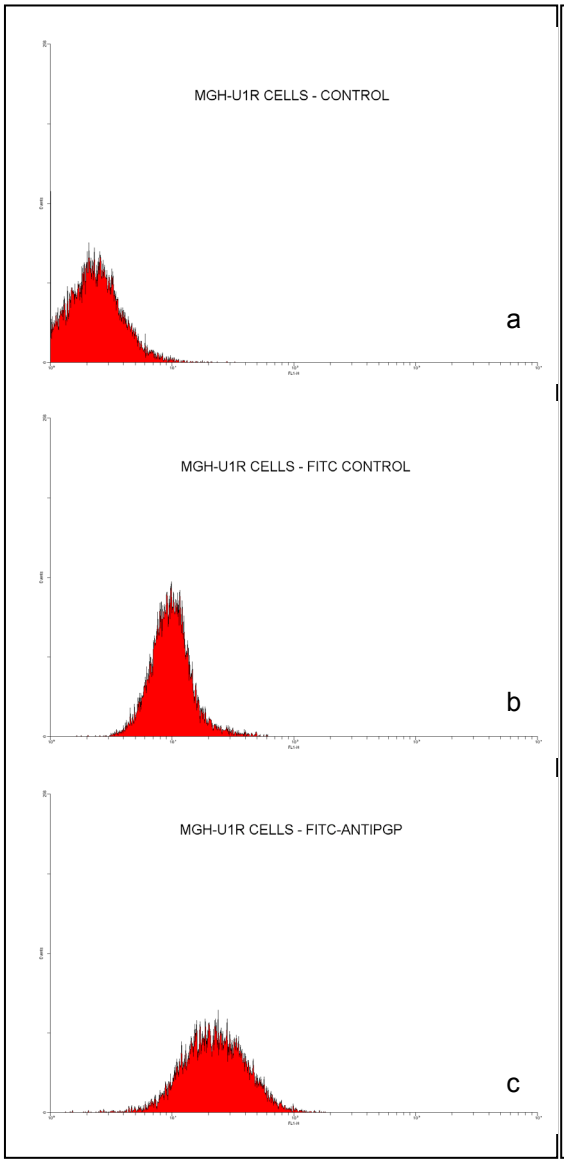

Figure 76: MGH-U1R cells: FITC fluorescence detection for a: BSA control; b: FITC IgG control; c: FITC Anti-Pgp

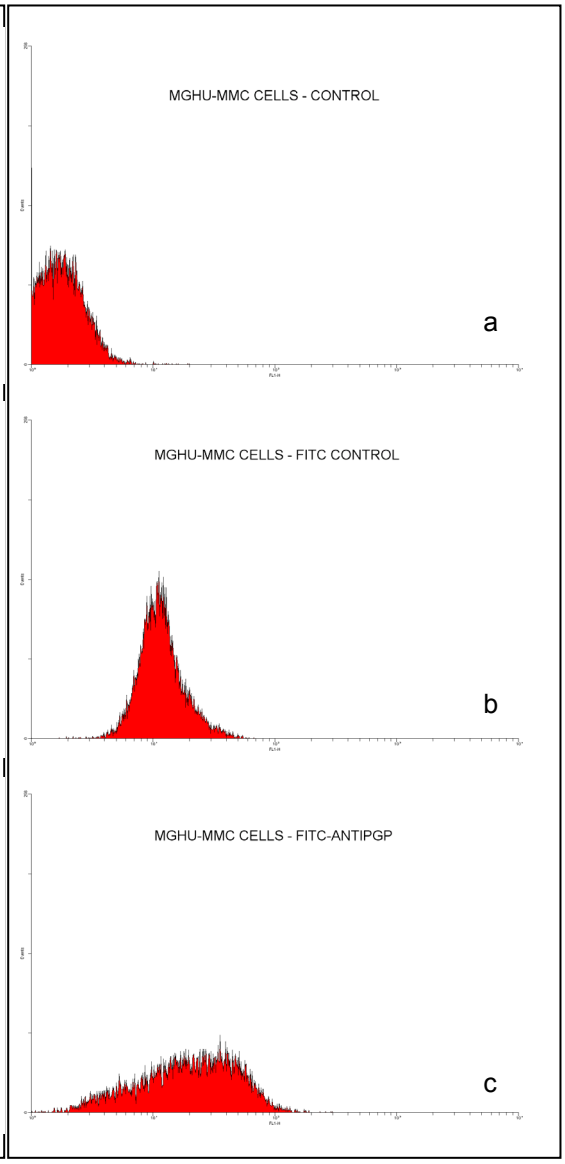

Figure 77: MGHU-MMC cells: FITC fluorescence detection for a: BSA control; b: FITC IgG control; c: FITC Anti-Pgp

These results show that MGH-U1R and MGHU-MMC cells demonstrate a significant increase in FITC fluorescence when incubated with the FITC Anti-Pgp antibody when compared to both the BSA control and the FITC IgG control, suggesting that both of these cell lines are positive for P-gp expression. The MGH-U1 and RT112 cell lines both demonstrated reduced levels of FITC Anti-P-gp fluorescence when compared to a FITC-IgG control, suggesting that they are negative for P-gp expression.

Cell Sample (n = 10,000)	Geomean Fluorescence	Median Fluorescence	CV
MGH-U1			
BSA Control	1.84	1.75	74.91
FITC Control	10.66	10.37	15.92
FITC Anti-Pgp	2.85	2.76	45.66
RT112			
BSA Control	5.74	6.38	34.2
FITC Control	16.16	15.96	12.03
FITC Anti-Pgp	7.68	7.91	21.94
MGH-U1R			
BSA Control	2.32	2.29	59.73
FITC Control	9.87	9.73	17.51
FITC Anti-Pgp	22.34	22.47	19.19
MGHU-MMC			
BSA Control	1.74	1.68	75.71
FITC Control	11.68	11.24	17.32
FITC Anti-Pgp	19.01	20.72	31.17

Table 36: Cellular FITC fluorescence levels for BSA control, FITC IgG control and FITC Anti-Pgp for each cell type

Nuclear P-gp staining with a FITC conjugated Anti-P-gp antibody (17F9, BD Biosciences)

Histograms of green fluorescence (FL-1 detector) are shown for BSA control, FITC IgG control and the FITC anti-P-gp antibody samples for each nuclear preparation sample (Figures 78 – 81).

The geomean and median fluorescence values for each sample are shown in table 37.

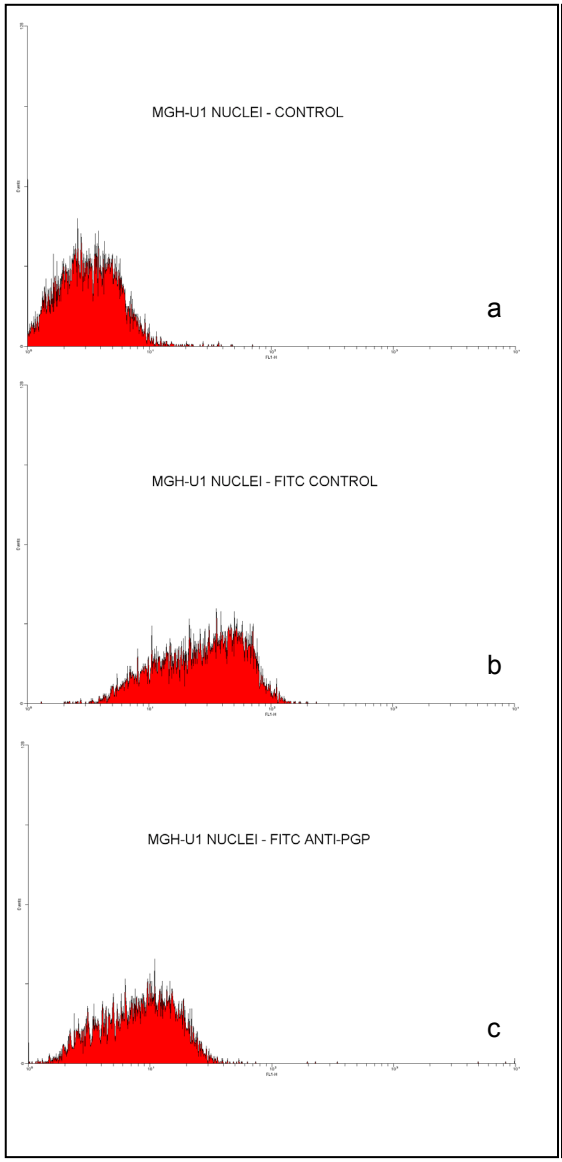

Figure 78: MGH-U1 nuclei: FITC fluorescence detection for a: BSA control; b: FITC IgG control; c: FITC Anti-Pgp

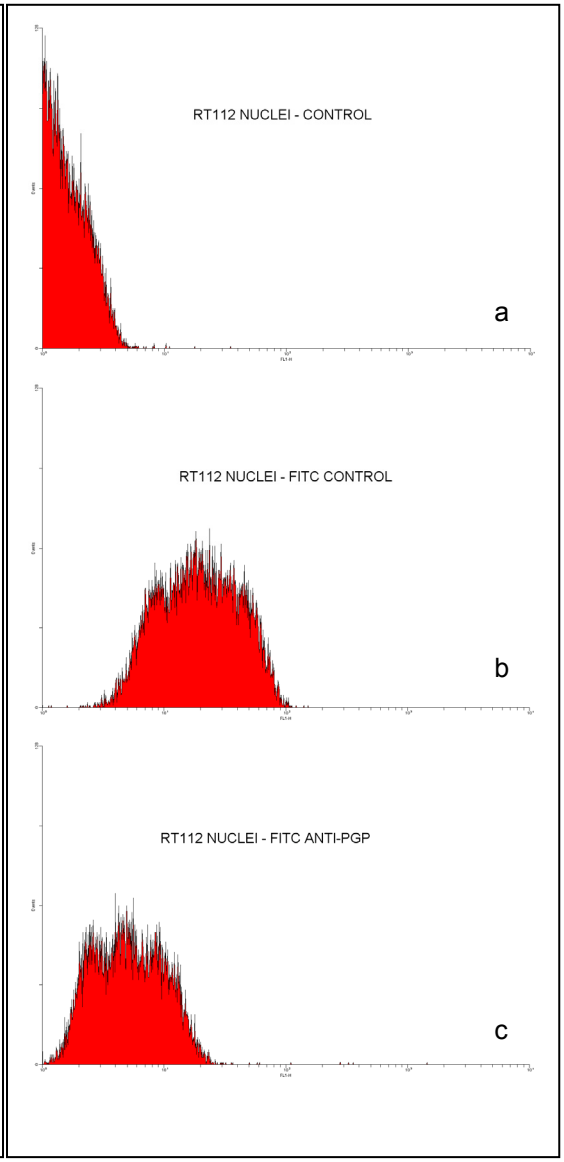

Figure 79: RT112 nuclei: FITC fluorescence detection for a: BSA control; b: FITC IgG control; c: FITC Anti-Pgp

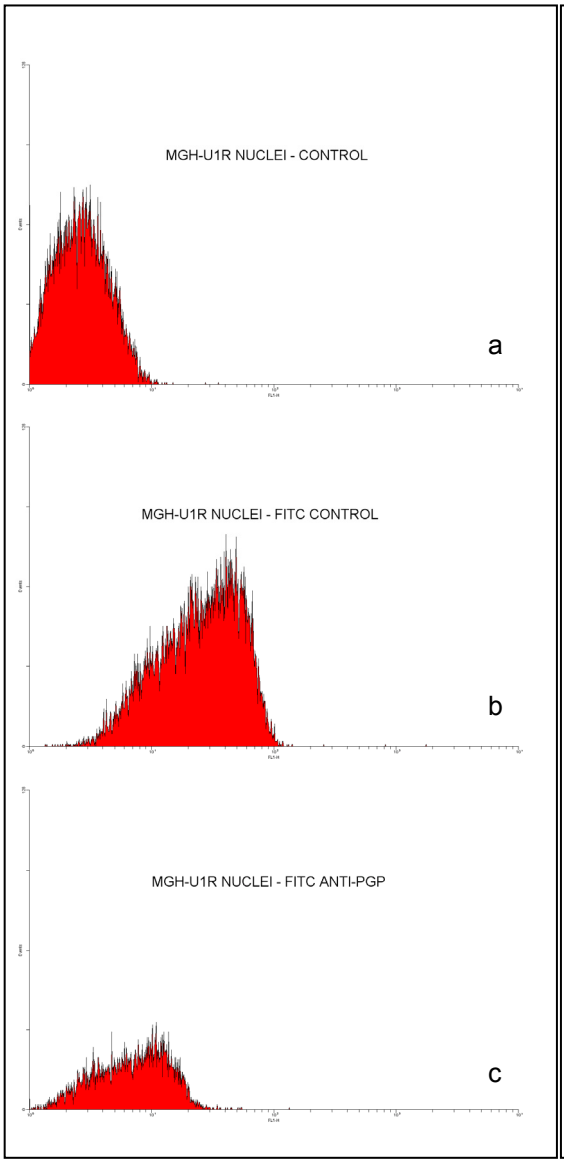

Figure 80: MGH-U1R nuclei: FITC fluorescence detection for a: BSA control; b: FITC IgG control; c: FITC Anti-Pgp

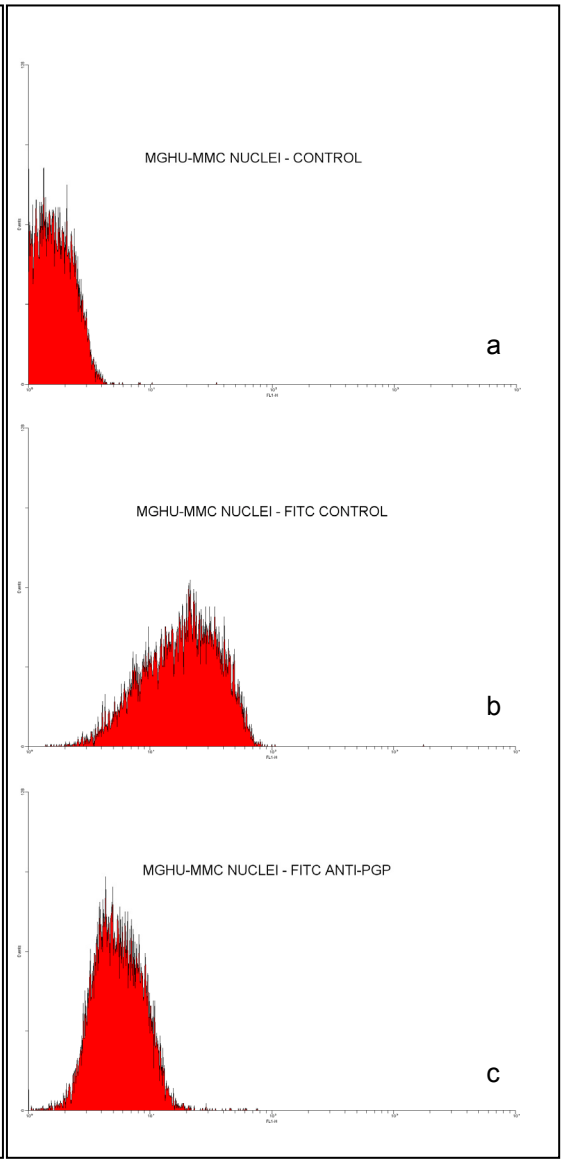

Figure 81: MGHU-MMC nuclei: FITC fluorescence detection for a: BSA control; b: FITC IgG control; c: FITC Anti-Pgp

Nuclear FITC fluorescence with FITC Anti-Pgp antibody is reduced in all nuclei compared to FITC IgG controls, suggesting that P-gp is not expressed on the nuclear membrane of any of these cells.

Nuclei Samples	N =	Geomean Fluorescence	Median Fluorescence	CV
MGH-U1				
Control	5761	3.38	3.34	46.31
FITC Control	5814	29.96	32.78	21.68
FITC Anti-Pgp	5794	8.88	9.39	31.84
RT112				
Control	14085	1.44	1.25	110.89
FITC Control	13868	19.32	19.46	25.56
FITC Anti-Pgp	11032	5.17	5.05	40.7
MGH-U1R				
Control	10420	2.66	2.64	52.14
FITC Control	14456	24.58	27.14	24.03
FITC Anti-Pgp	4682	6.96	7.5	34.94
MGHU-MMC				
Control	8130	1.8	1.68	88.62
FITC Control	7911	16.36	18.27	27.86
FITC Anti-Pgp	10243	5.26	6.32	48.52

Table 37: Nuclear FITC fluorescence levels for BSA control, FITC IgG control and FITC Anti-Pgp for each nuclear type

3.3: Microinjection experiments

Cytoplasmic microinjection with epirubicin at 37°C

Following microinjection with epirubicin, the sensitive cell lines, MGH-U1 and RT112, demonstrated a clear nuclear uptake pattern of epirubicin (Figures 82a and b) consistent with their incubated uptake characteristics. The MDR bladder cancer cell lines, MGH-U1R and MGH-U1-MMC, demonstrated characteristic nuclear sparing of epirubicin following microinjection, again consistent with their usual incubated uptake characteristics (Figures 82c and d).

The 77KDa FITC-dextran allowed clear identification of injected cells, especially resistant ones, which otherwise had low levels of fluorescence. This size of FITC-dextran was excluded from the nuclei of all injected cells, allowing clear visualisation of nuclear epirubicin uptake, if present. Characteristically the epirubicin fluorescence associated with resistant cells was punctuate and on the surface or even outside the cells. The dextran fluorescence was evenly distributed through the cytoplasm.

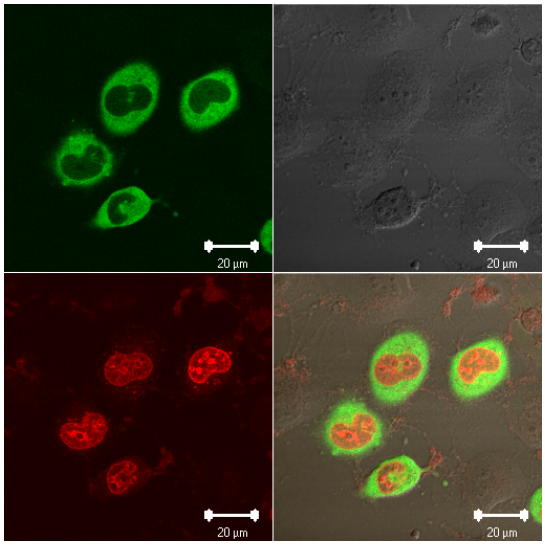

Figure 82a: MGH-U1 cells co-injected with epirubicin (0.5mg/ml) and 77KDa FITC-dextran (0.5mg/ml) (x40 lens; Zoom x2; Gain 1050). Bottom left: Epirubicin fluorescence (Red) showing nuclear uptake pattern. Top left: FITC-dextran fluorescence (Green) excluded from nucleus. Top right: DIC image. Bottom right: Integrated image.

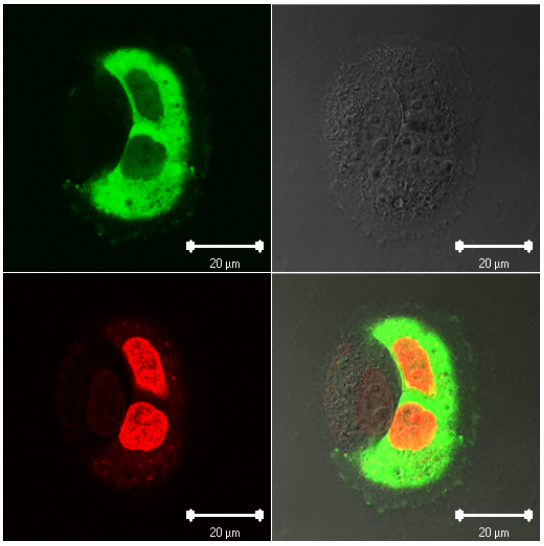

Figure 82b: RT112 cells co-injected with epirubicin (0.5mg/ml) and 77KDa FITC-dextran (0.5mg/ml) (x40 lens; Zoom x3; Gain 1050). Bottom left: Epirubicin fluorescence (Red) showing nuclear uptake pattern. Top left: FITC-dextran fluorescence (Green) excluded from nucleus. Top right: DIC image. Bottom right: Integrated image.

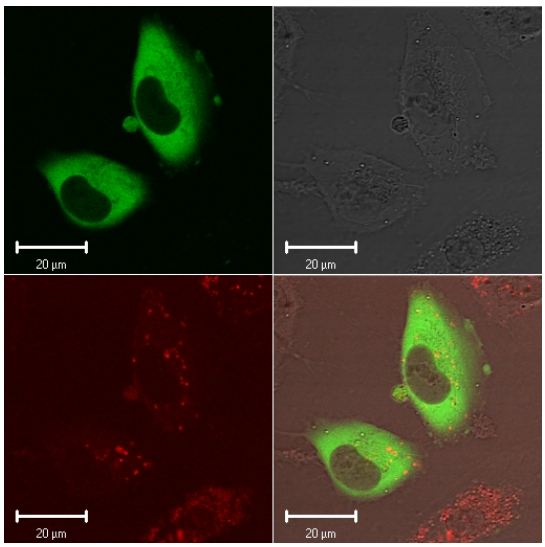

Figure 82c: MGH-U1R cells co-injected with epirubicin (0.5mg/ml) and 77KDa FITC-dextran (0.5mg/ml) (x40 lens; Zoom x3; Gain 1150). Bottom left: Epirubicin fluorescence (Red) showing nuclear sparing pattern with cytoplasmic vesicular staining. Top left: FITC-dextran fluorescence (Green) excluded from nucleus. Top right: DIC image. Bottom right: Integrated image.

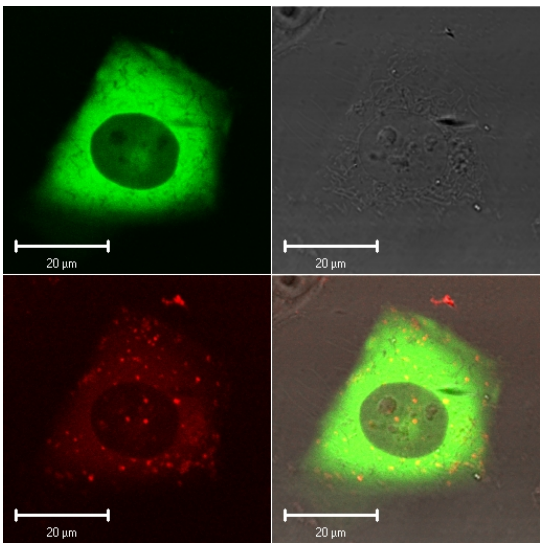

Figure 82d: MGHU-MMC cell co-injected with epirubicin (0.5mg/ml) and 77KDa FITC-dextran (0.5mg/ml) (x40 lens; Zoom x4; Gain 1150). Bottom left: Epirubicin fluorescence (Red) showing nuclear sparing pattern with cytoplasmic vesicular staining. Top left: FITC-dextran fluorescence (Green) excluded from nucleus. Top right: DIC image. Bottom right: Integrated image.

Subsequent addition of acridine orange (3µg/ml) demonstrated strong nuclear staining, confirming the viability of all injected cells (Figures 83a – d).

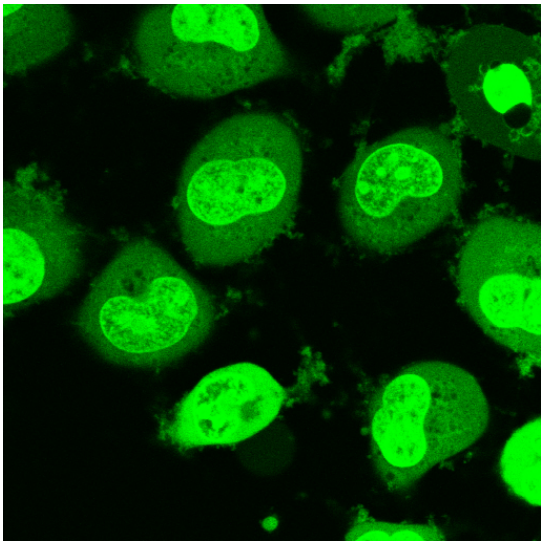

Figure 83a: MGH-U1 cells (same cells as Figure 82a) Fluorescence only image with acridine orange staining (Green) confirming cell viability.

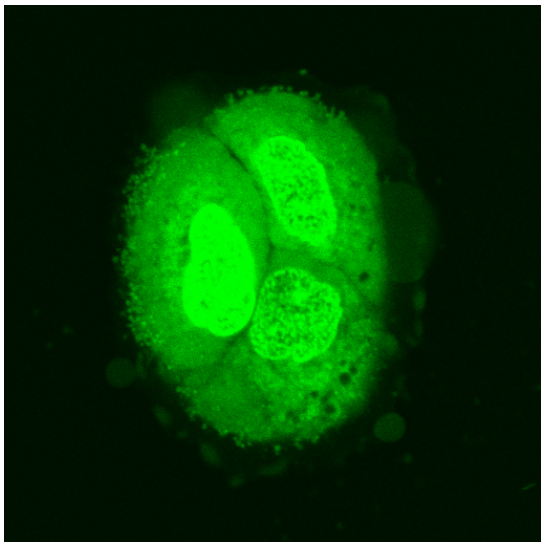

Figure 83b: RT112 cells (same cells as Figure 82b) Fluorescence only image with acridine orange staining (Green) confirming cell viability.

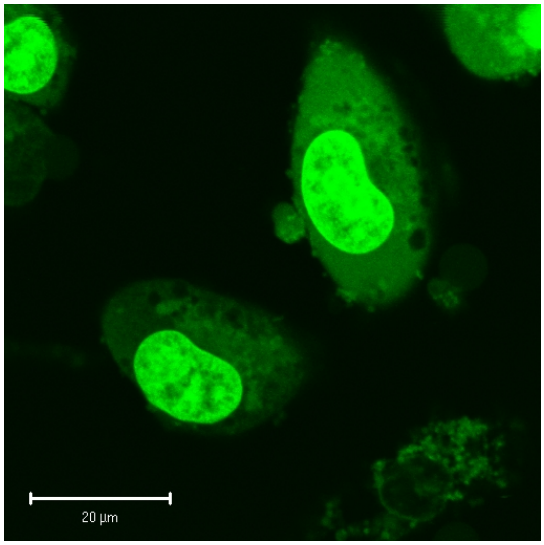

Figure 83c: MGH-U1R cells (same cells as Figure 82c) (x40 lens; Zoom x3) Fluorescence only image with acridine orange staining (Green) confirming cell viability.

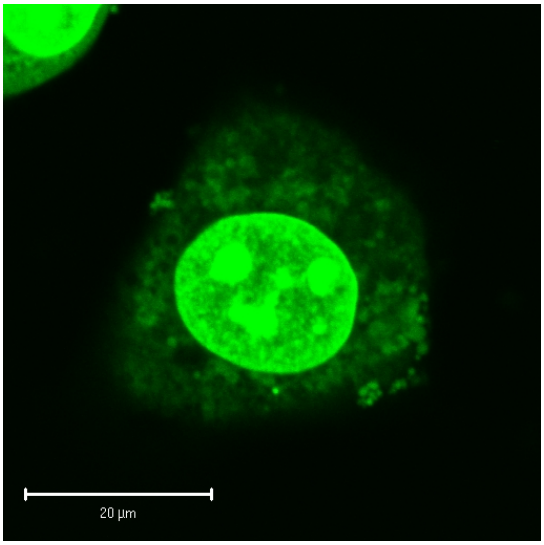

Figure 83d: MGHU-MMC cell (same cell as Figure 82d) (x40 lens; Zoom x4). Fluorescence only image with acridine orange staining (Green) confirming cell viability.

Cytoplasmic Microinjection with Epirubicin on Ice

By placing cells on ice any energy dependant processes in the cells are abolished. MGH-U1 cells microinjected with epirubicin at 0 – 4 degrees maintained their usual nuclear uptake characteristics, but nuclear epirubicin fluorescence levels were much lower than usual and there were higher levels of cytoplasmic fluorescence that normally seen in sensitive cells (Figures 84a – c).

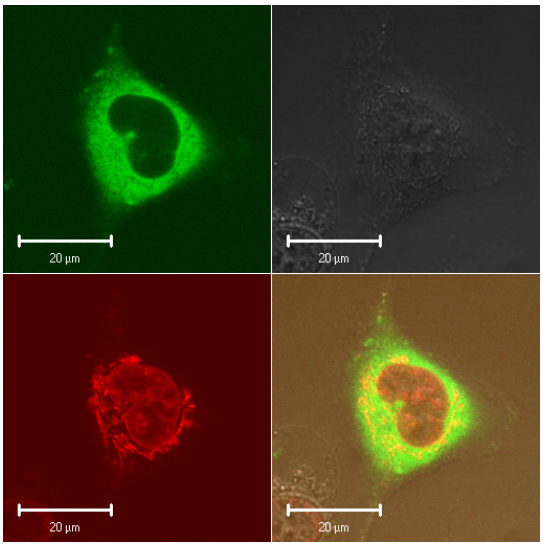

Figures 84a: MGH-U1 cells co-injected with epirubicin (0.5mg/ml) and 77KDa FITC dextran (0.5mg/ml) on ice (x40 Lens; Zoom x4; Gain 1150). Bottom left: Epirubicin fluorescence (Red) showing nuclear uptake pattern. Top left: FITC-dextran fluorescence (Green) excluded from nucleus. Top right: DIC image. Bottom right: Integrated image.

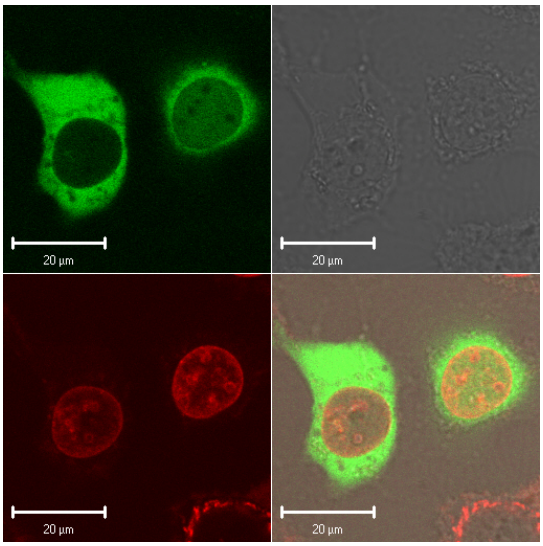

Figures 84b: MGH-U1 cells co-injected with epirubicin (0.5mg/ml) and 77KDa FITC dextran (0.5mg/ml) on ice (x40 Lens; Zoom x4; Gain 1150). Bottom left: Epirubicin fluorescence (Red) showing nuclear uptake pattern. Top left: FITC-dextran fluorescence (Green) excluded from nucleus. Top right: DIC image. Bottom right: Integrated image.

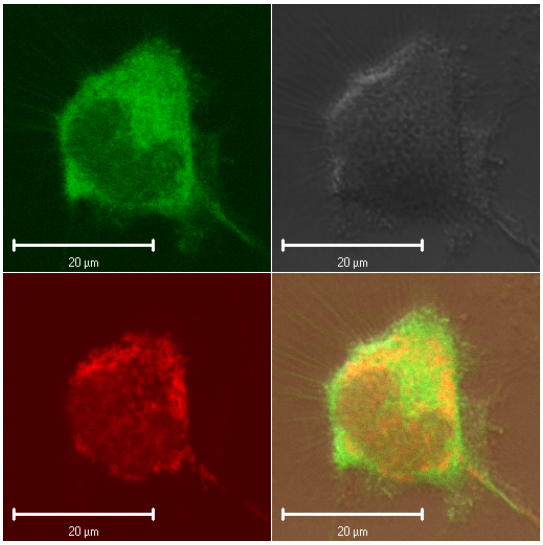

Figures 84c: MGH-U1 cells co-injected with epirubicin (0.5mg/ml) and 77KDa FITC dextran (0.5mg/ml) on ice (x40 Lens; Zoom x6; Gain 1150). Bottom left: Epirubicin fluorescence (Red) showing nuclear uptake pattern. Top left: FITC-dextran fluorescence (Green) excluded from nucleus. Top right: DIC image. Bottom right: Integrated image.

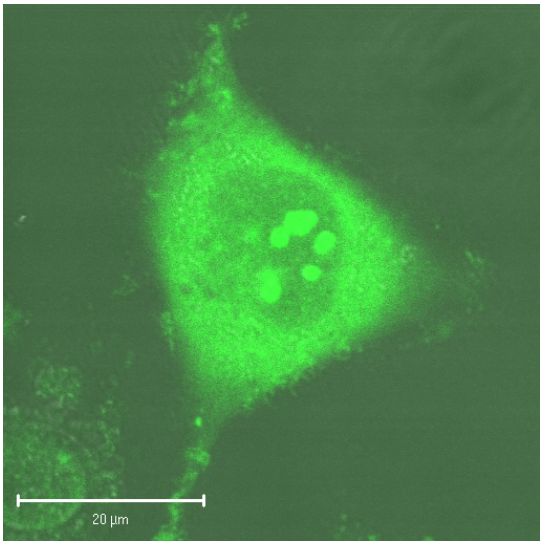

Figure 85a: MGH-U1 cell (same cell as Figure 84a) Acridine orange fluorescence (Green) confirming cell viability. Fluorescence image combine with DIC image

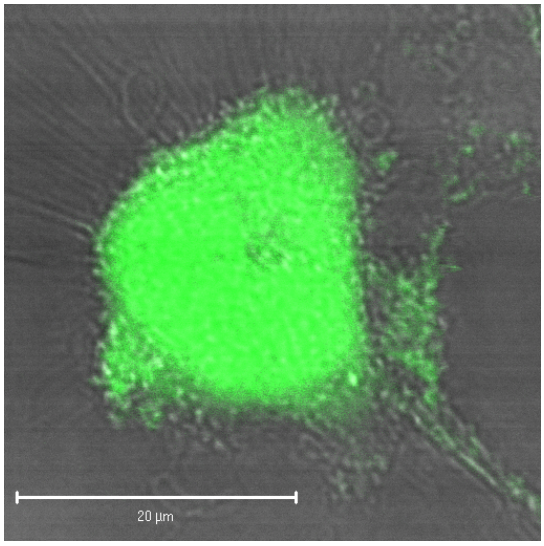

Figure 85b: MGH-U1 cell (same cell as Figure 84c) Acridine orange fluorescence (Green) confirming cell viability. Fluorescence image combine with DIC image

MGH-U1R cells reversed to a nuclear uptake pattern with microinjection of epirubicin on ice (Figures 86a-c). This is suggestive that some energy dependant process prevents nuclear epirubicin uptake. This could either be through reduced excretion via energy dependant vesicular uptake and exocytosis or some energy dependant efflux mechanism on the nuclear membrane. There appears to be a lot of epirubicin in vesicles within the cytoplasm of these cells which may suggest that cellular export by this mechanism is reduced.

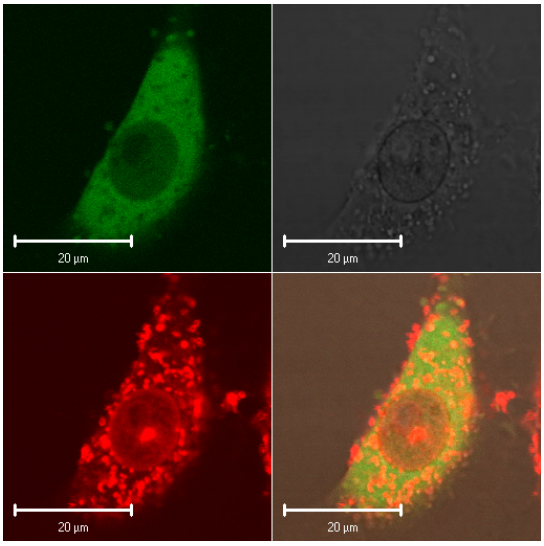

Figures 86a: MGH-U1R cells co-injected with epirubicin (0.5mg/ml) and 77KDa FITC dextran (0.5mg/ml) on ice (x40 Lens; Zoom x5; Gain 1100). Bottom left: Epirubicin fluorescence (Red) showing nuclear uptake pattern. Top left: FITC-dextran fluorescence (Green) excluded from nucleus. Top right: DIC image. Bottom right: Integrated image.

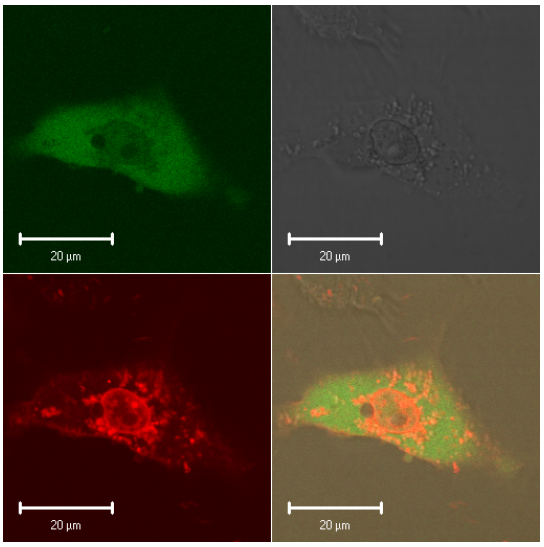

Figures 86b: MGH-U1R cells co-injected with epirubicin (0.5mg/ml) and 77KDa FITC dextran (0.5mg/ml) on ice (x40 Lens; Zoom x5; Gain 1100). Bottom left: Epirubicin fluorescence (Red) showing nuclear uptake pattern. Top left: FITC-dextran fluorescence (Green) excluded from nucleus. Top right: DIC image. Bottom right: Integrated image.

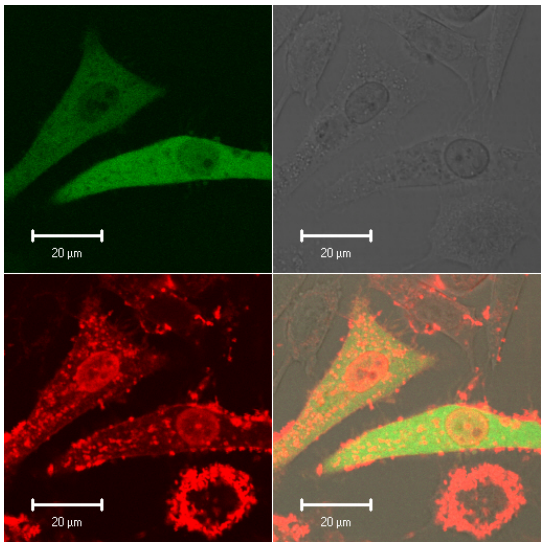

Figures 86c: MGH-U1R cells co-injected with epirubicin (0.5mg/ml) and 77KDa FITC dextran (0.5mg/ml) on ice (x40 Lens; Zoom x3; Gain 1100). Bottom left: Epirubicin fluorescence (Red) showing nuclear uptake pattern. Top left: FITC-dextran fluorescence (Green) excluded from nucleus. Top right: DIC image. Bottom right: Integrated image.

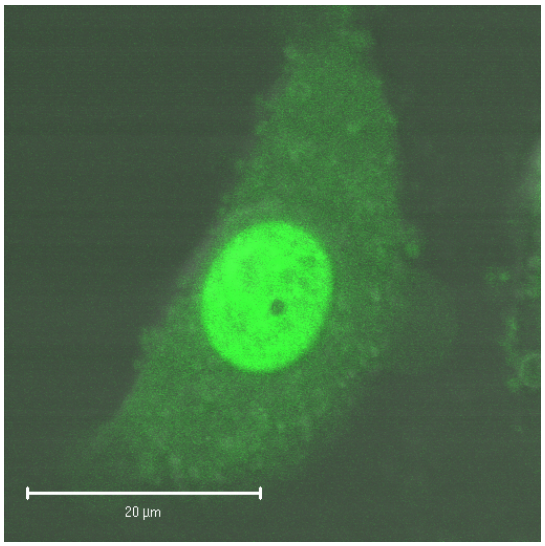

Figure 87a: MGH-U1 cell (same cell as Figure 86a) Acridine orange fluorescence (Green) confirming cell viability. Fluorescence image combine with DIC image

Acridine orange (3µg/ml) again demonstrated that both sensitive and MDR cells were viable (Figures 85a – b and 87a – c).

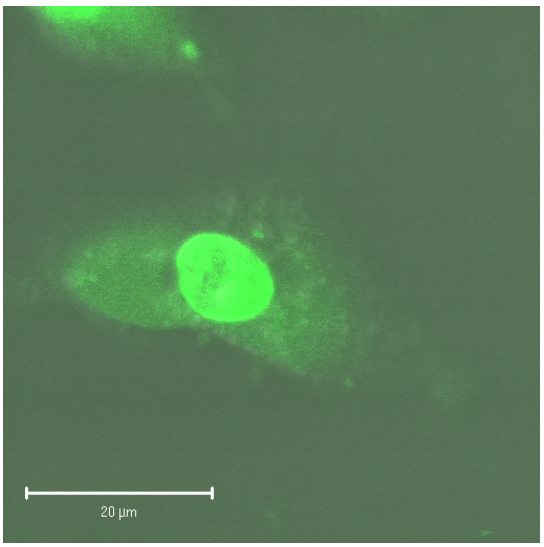

Figure 87b: MGH-U1 cell (same cell as Figure 86b) Acridine orange fluorescence (Green) confirming cell viability. Fluorescence image combine with DIC image

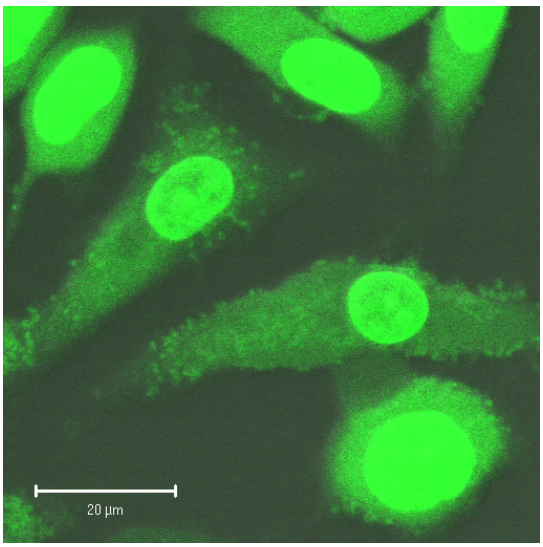

Figure 87c: MGH-U1 cell (same cell as Figure 86c) Acridine orange fluorescence (Green) confirming cell viability. Fluorescence image combine with DIC image

Nuclear pore sizing by cytoplasmic microinjection of various sized FITC-dextrans

Microinjection was a more successful means of delivering FITC-dextrans into the cytoplasm of cells. It can be seen clearly that FITC-dextrans of 4.4KDa and 19.5KDa are able to passively diffuse through the nuclear pores of both MGH-U1 and MGH-U1R cells, although the 19.5KDa dextran may not pass as readily across the MGH-U1R nuclear membrane, as evidenced by a mild degree of nuclear sparing (Figures 88a – d and 89a – d). The 43KDa and 77KDa FITC-dextrans are excluded from the nuclei of both cell types suggesting they are too large to passively diffuse through nuclear membrane pores (Figures 88e – h and 89e – h).

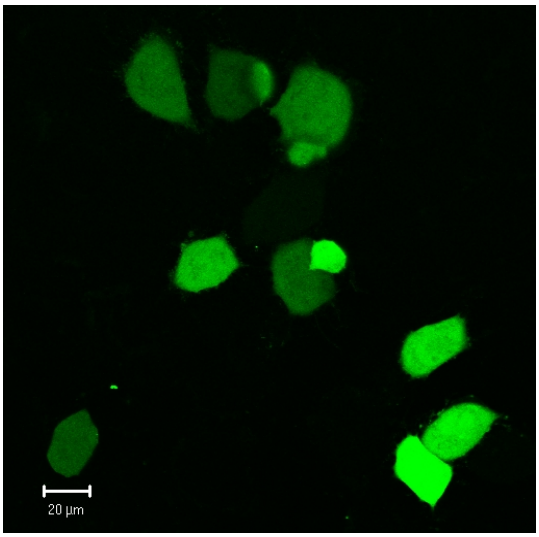

Figure 88a: MGH-U-1 cells microinjected with 4.4KDa FITC-Dextran (x40 Lens; Zoom x1). FITC-fluoresence only (Green), showing nuclear uptake of the dextran.

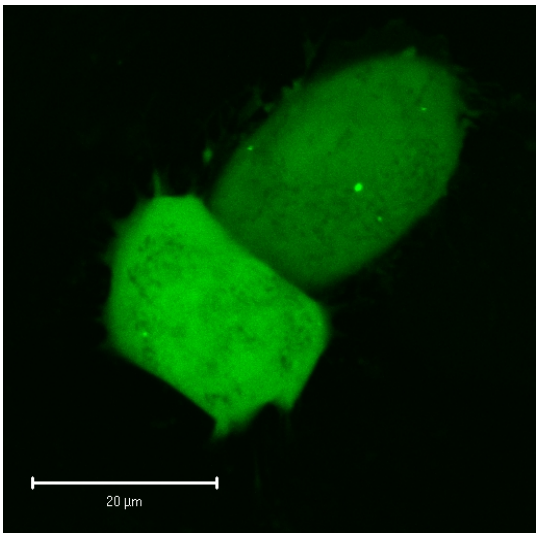

Figure 88b: MGH-U-1 cells microinjected with 4.4KDa FITC-Dextran (x40 Lens; Zoom x4). FITC-fluoresence only (Green), showing nuclear uptake of the dextran.

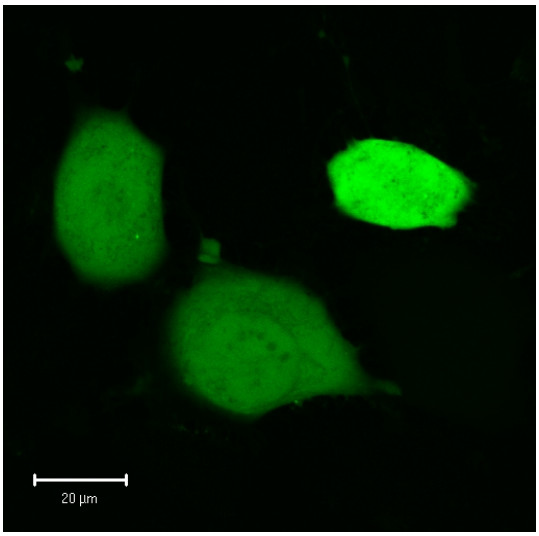

Figure 88c: MGH-U-1S cells microinjected with 19.5KDa FITC-Dextran (x40 Lens; Zoom x2). FITC-fluoresence only (Green), showing nuclear uptake of the dextran.

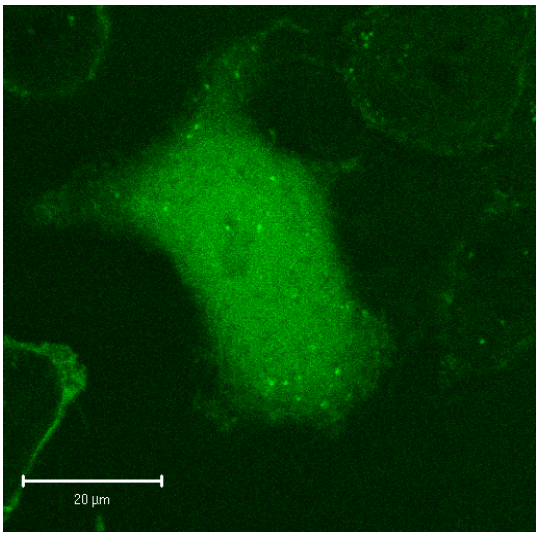

Figure 88d: MGH-U1 cell microinjected with 19.5KDa FITC-Dextran (x40 Lens; Zoom x3). FITC-fluoresence only (Green), showing nuclear uptake of the dextran.

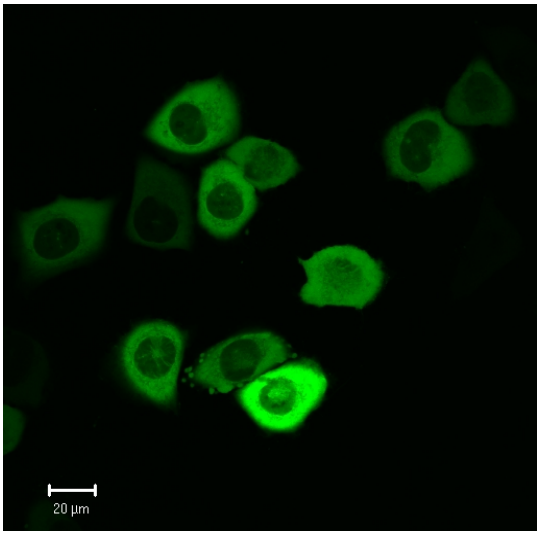

Figure 88e: MGH-U-1 cells microinjected with 42KDa FITC-Dextran (x40 Lens; Zoom x1). FITC-fluoresence only (Green), showing nuclear exclusion of the dextran.

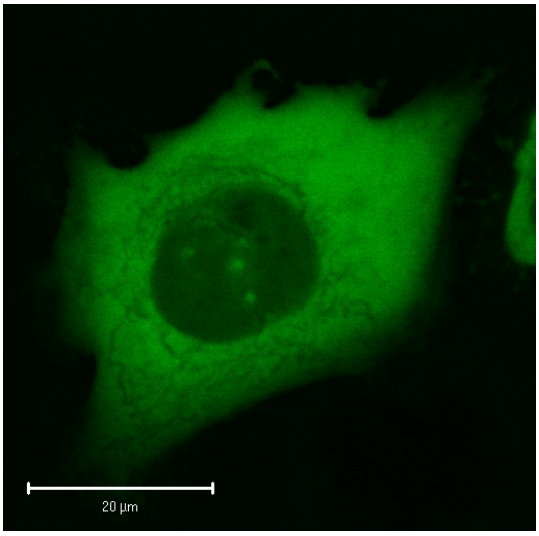

Figure 88f: MGH-U-1 cell microinjected with 42KDa FITC-Dextran (x40 Lens; Zoom x4). FITC-fluoresence only (Green), showing nuclear exclusion of the dextran.

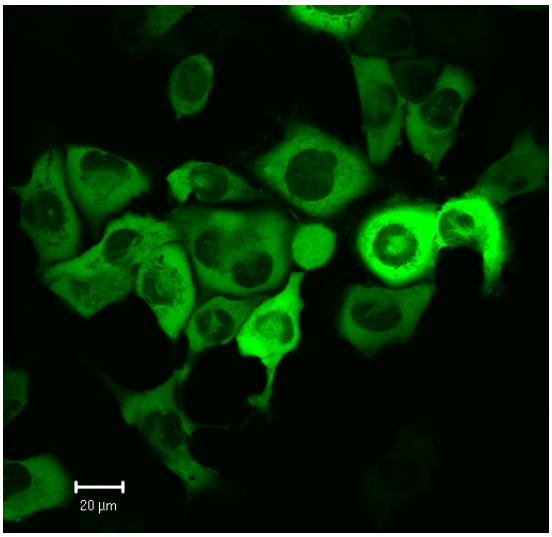

Figure 88g: MGH-U-1 cells microinjected with 77KDa FITC-Dextran (x40 Lens; Zoom x1). FITC-fluoresence only (Green), showing nuclear exclusion of the dextran.

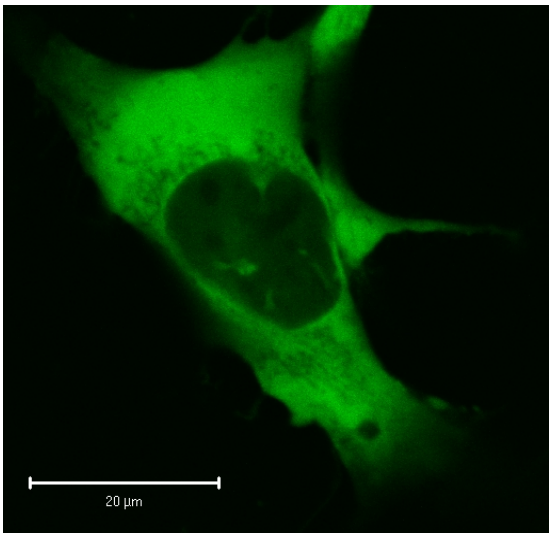

Figure 88h: MGH-U-1S cell microinjected with 77KDa FITC-Dextran (x40 Lens; Zoom x1). FITC-fluoresence only (Green), showing nuclear exclusion of the dextran.

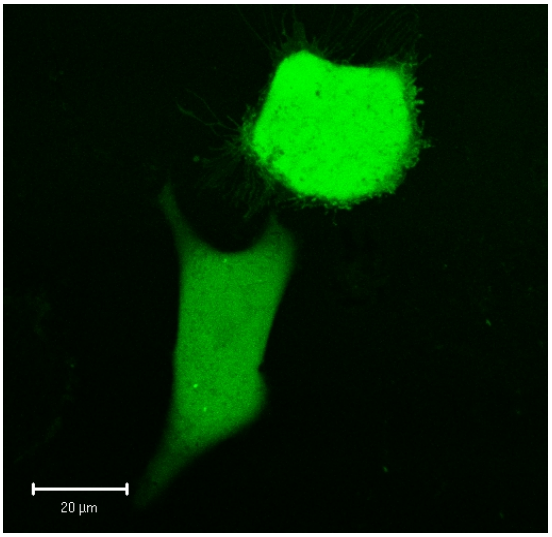

Figure 89a: MGH-U1R cells microinjected with 4.3KDa FITC-Dextran (x40 Lens; Zoom x2). FITC-fluoresence only (Green), showing nuclear uptake of the dextran.

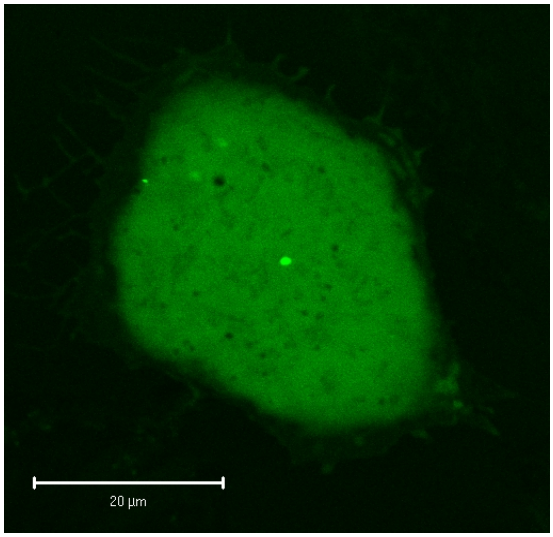

Figure 89b: MGH-U1R cell microinjected with 4.3KDa FITC-Dextran (x40 Lens; Zoom x4). FITC-fluoresence only (Green), showing nuclear uptake of the dextran.

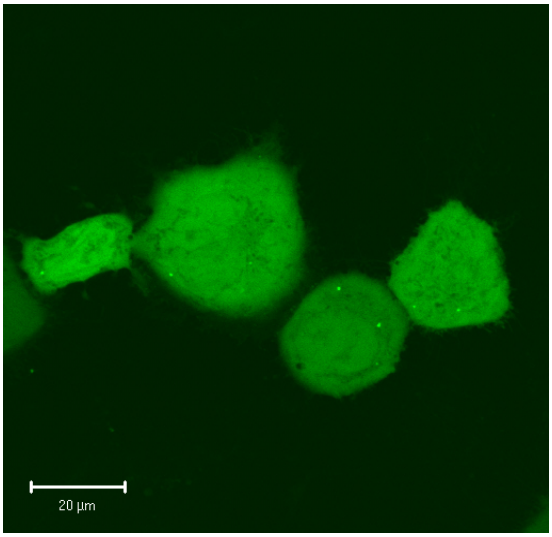

Figure 89c: MGH-U1R cells microinjected with 19.5KDa FITC-Dextran (x40 Lens; Zoom x2). FITC-fluoresence only (Green), showing nuclear uptake of the dextran.

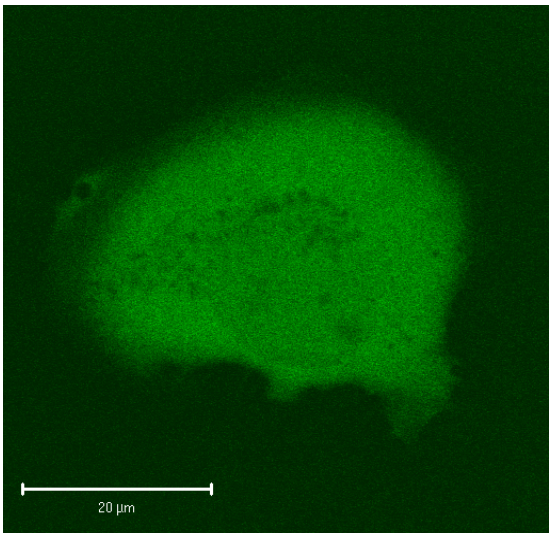

Figure 89d: MGH-U1R cell microinjected with 19.5KDa FITC-Dextran (x40 Lens; Zoom x4). FITC-fluoresence only (Green), showing nuclear uptake of the dextran.

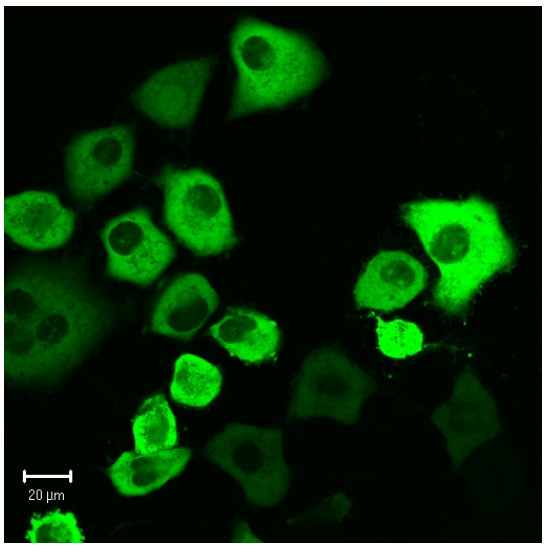

Figure 89e: MGH-U1R cells microinjected with 42KDa FITC-Dextran (x40 Lens; Zoom x 2). FITC-fluoresence only (Green), showing nuclear exclusion of the dextran.

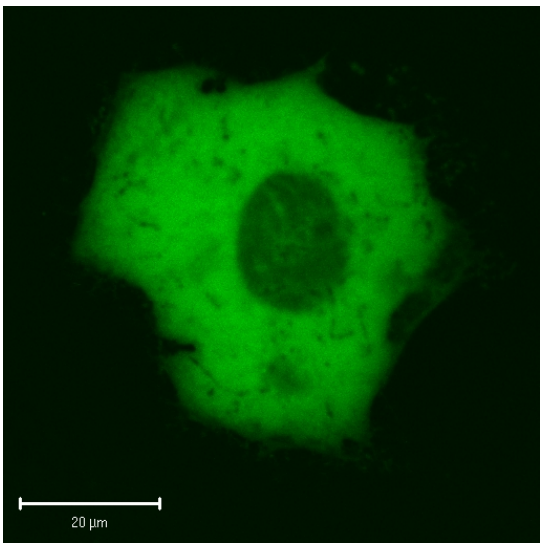

Figure 89f: MGH-U1R cell microinjected with 42KDa FITC-Dextran (x40 Lens; Zoom x 4). FITC-fluoresence only (Green), showing nuclear exclusion of the dextran.

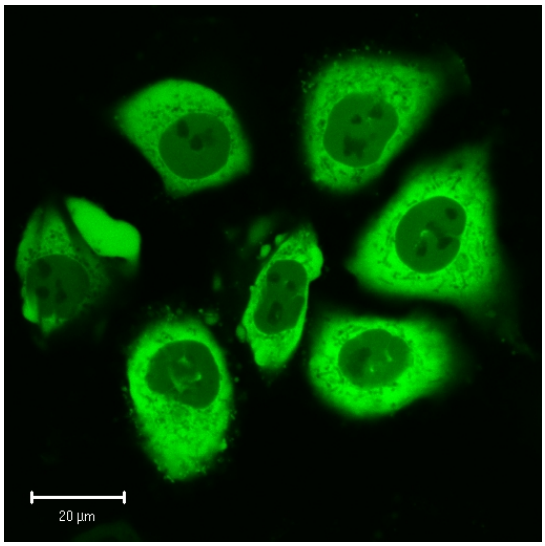

Figure 89g: MGH-U1R cells microinjected with 77KDa FITC-Dextran (x40 Lens; Zoom x1). FITC-fluoresence only (Green), showing nuclear exclusion of the dextran.

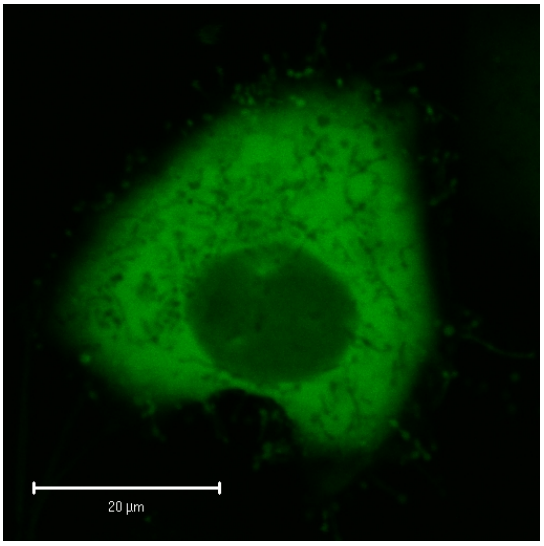

Figure 89h: MGH-U1R cell microinjected with 77KDa FITC-Dextran (x40 Lens; Zoom x3). FITC-fluoresence only (Green), showing nuclear exclusion of the dextran.

3.4: Cytotoxicity experiments:

Epirubicin Cytotoxicity Curves

Individual epirubicin cytotoxicity curves are plotted below for all cell lines (Figures 90a – d). The IC50 values (concentration of the drug required to inhibit cell growth by 50%) were calculated from the cytotoxicity curves. The IC50 for the sensitive cell lines, MGH-U1 and RT112, were similar at 0.2 and 0.6µg/ml respectively.

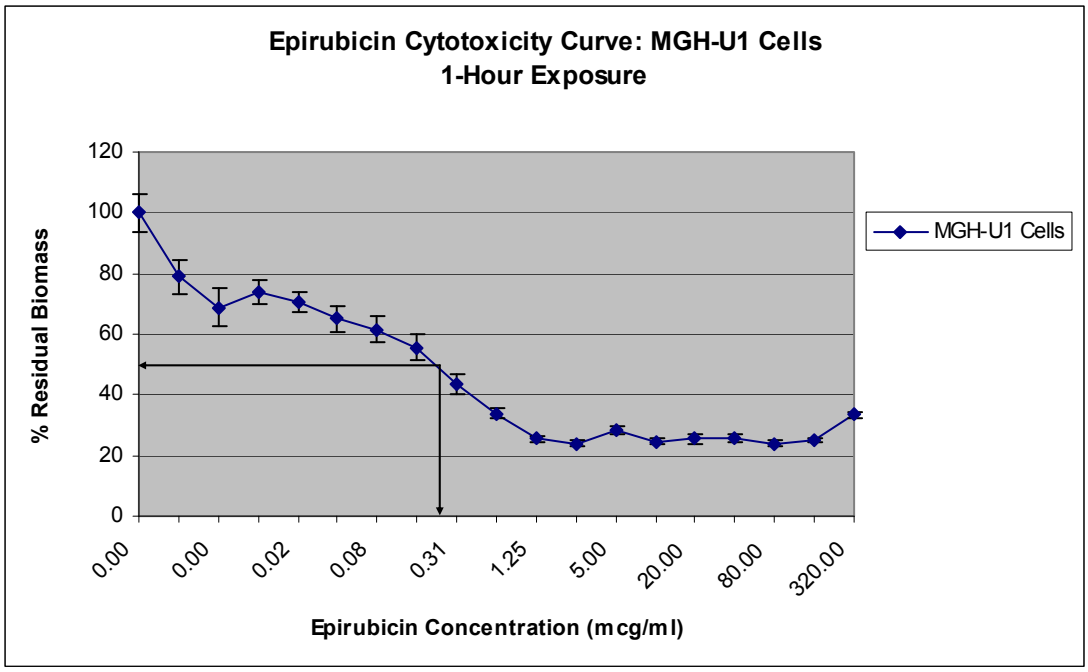

Figure 90a: MGH-U1 epirubicin cytotoxicity curve

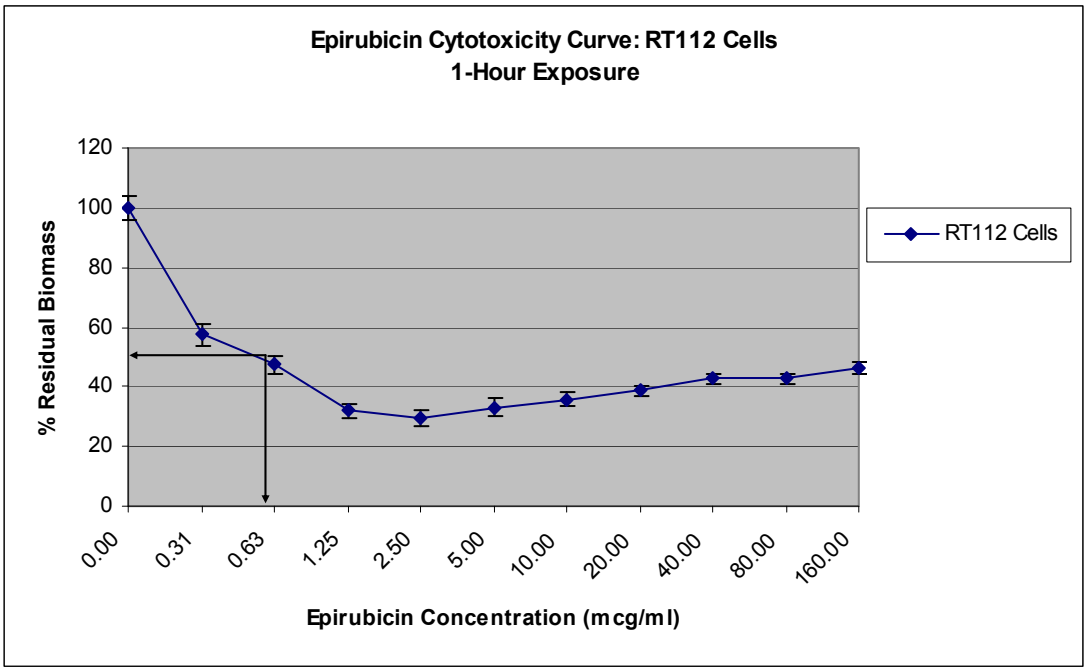

Figure 90b: RT112 epirubicin cytotoxicity curve

The IC50 values for the MDR cell lines, MGH-U1R and MGHU-MMC, were also similar at 120 and 160 µg/ml respectively.

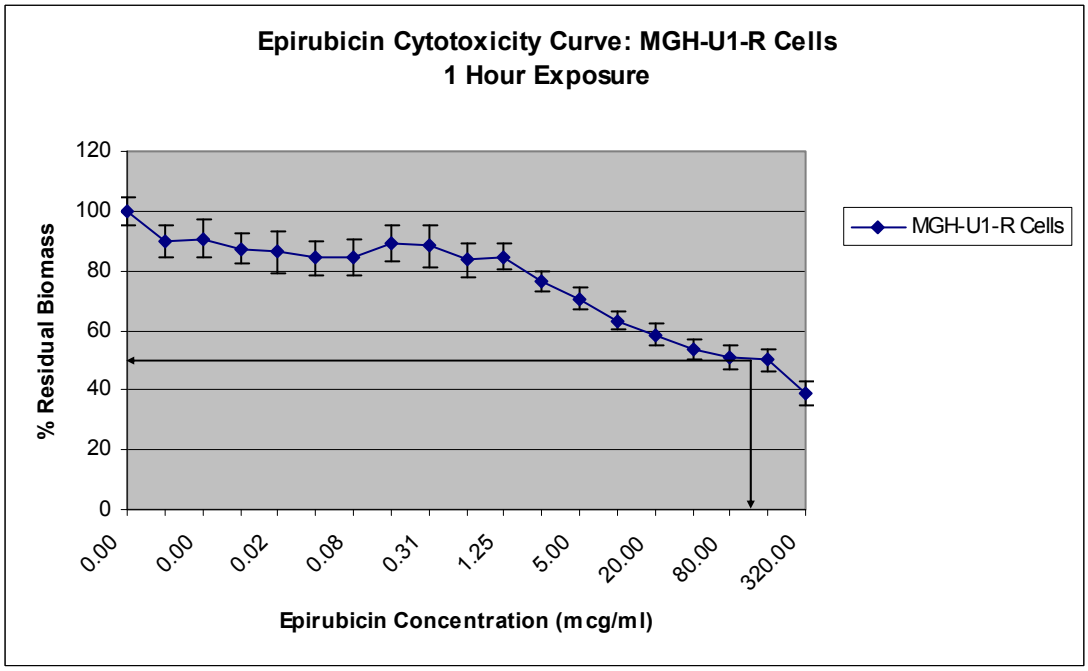

Figure 90c: MGH-U1R epirubicin cytotoxicity curve

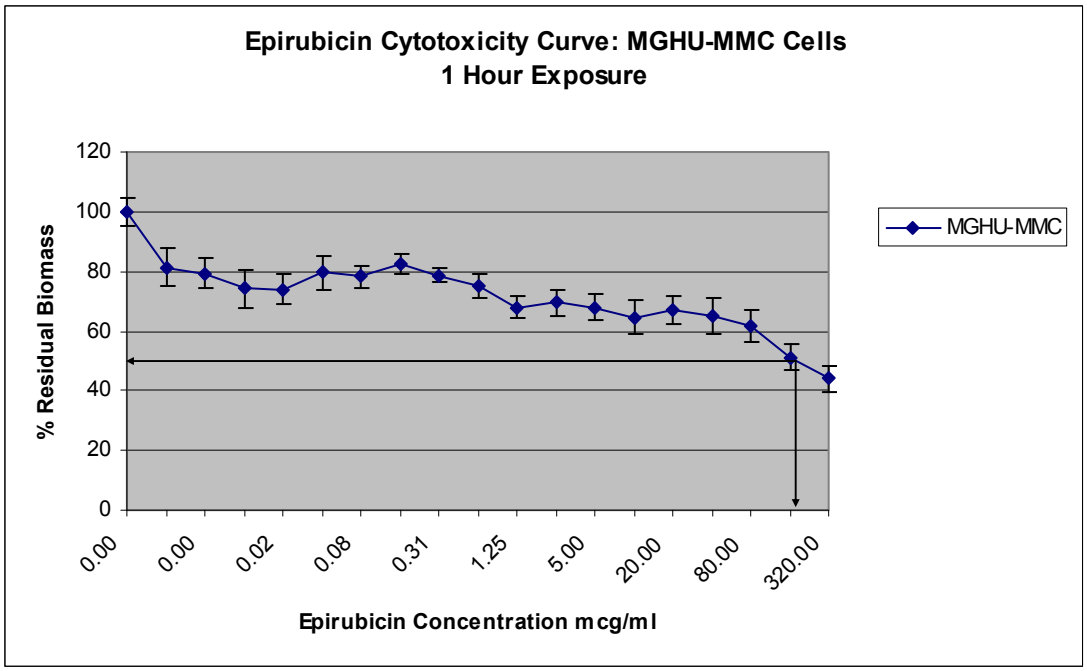

Figure 90d: MGHU-MMC epirubicin cytotoxicity curve

Idarubicin cytotoxicity curves

Idarubicin cytotoxicity curves were plotted for MGH-U1 and MGH-U1R cells Figures 91a and b). Their IC50 values were <0.08 and 2µg/ml respectively.

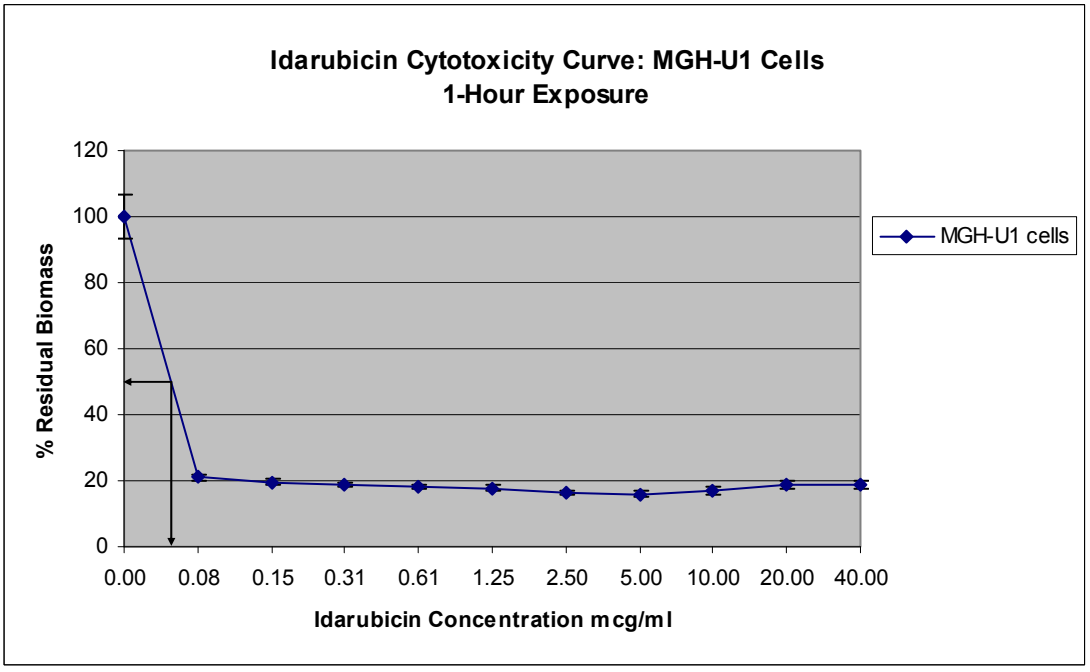

Figure 91a: MGH-U1 idarubicin cytotoxicity curve

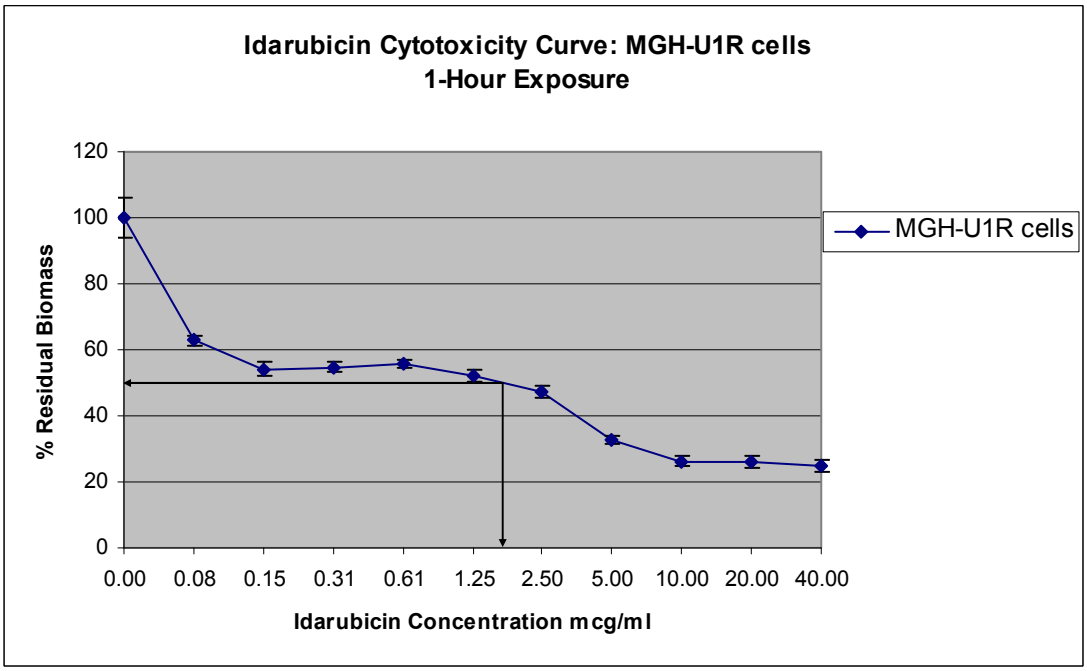

Figure 91b: MGH-U1R idarubicin cytotoxicity curve

Mitomycin C cytotoxicity curves

Mitomycin C cytotoxicity curves were plotted for MGH-U1 and MGH-U1R cells (Figures 92a and b). Their IC50 values were 7 and 75µg/ml respectively.

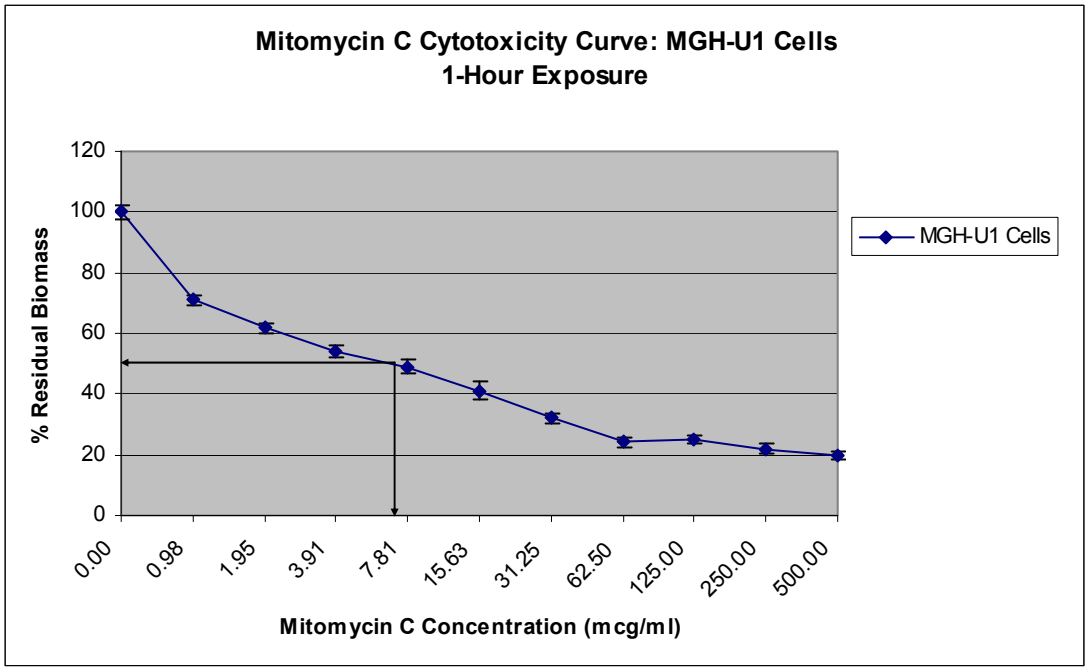

Figure 92a: MGH-U1 mitomycin C cytotoxicity curve

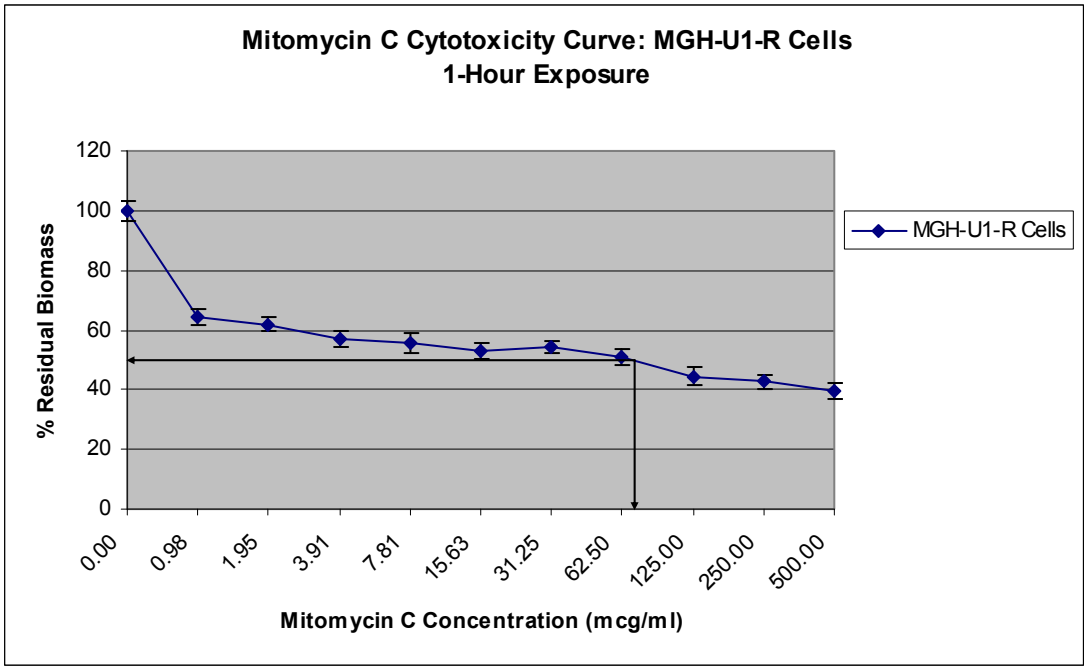

Figure 92b: MGH-U1R mitomycin C cytotoxicity curve

Wheat germ agglutinin (WGA) cytotoxicity curves

WGA cytotoxicity curves were plotted for MGH-U1 and MGH-U1R cells (Figures 93a – d). For 1-hour exposures IC50 values were not reached for either cell type.

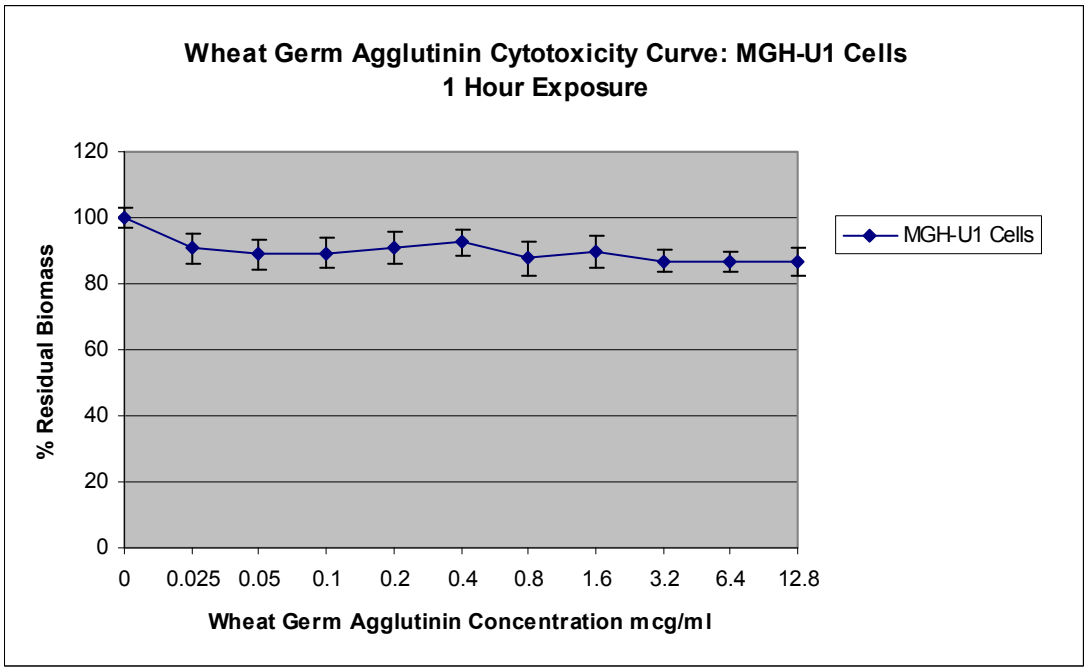

Figure 93a: MGH-U1 WGA cytoxicity curve – 1 hour exposure

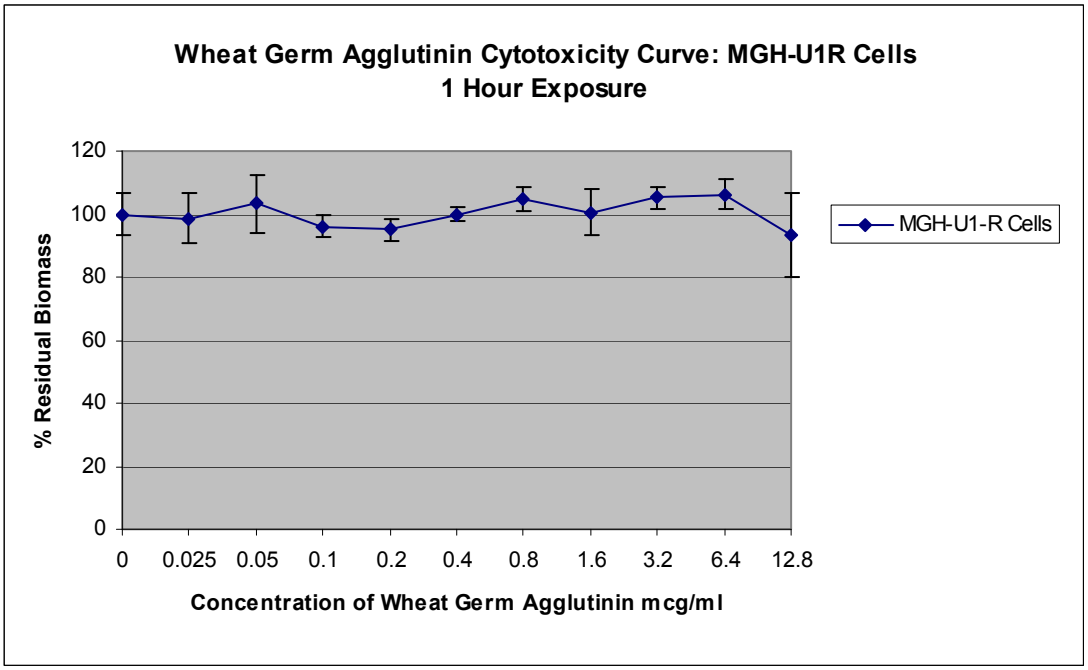

Figure 93b: MGH-U1R WGA cytotoxicity curve – 1 hour exposure

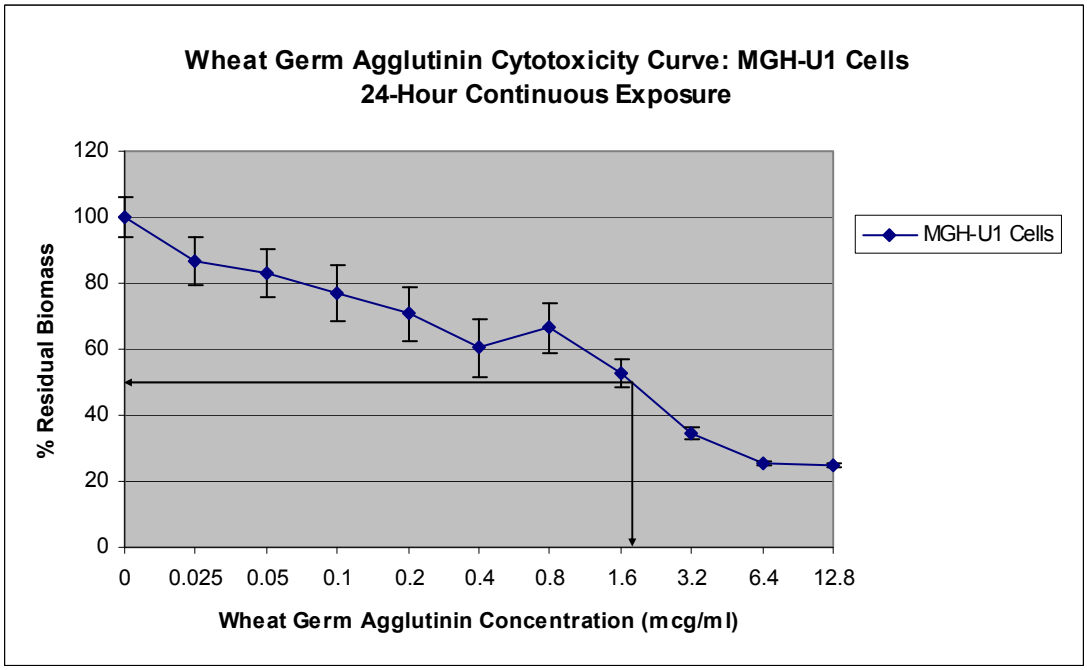

Figure 93c: MGH-U1 WGA cytotoxicity curve – 24 hour continuous exposure

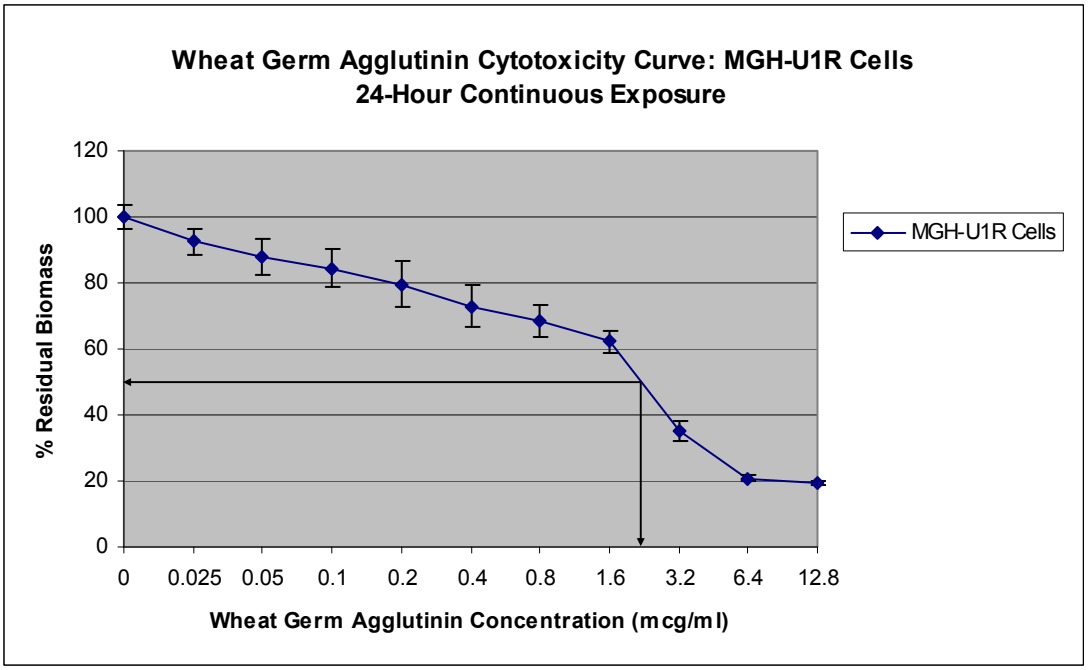

Figure 93d: MGH-U1R WGA cytotoxicity curve – 24 hour continuous exposure

Continuous exposure to WGA for 24 hours demonstrated some cytotoxicity in both MGH-U1 and MGH-U1R cells with IC50 values of around 2µg/ml.

Drug Combinations

Epirubicin and WGA

The combination of WGA with epirubicin did not alter epirubicin cytotoxicity in MGH-U1 cells, although the IC50 was not determined accurately because we did not look at concentrations of epirubicin below 0.31µg/ml (Figure 94a).

The MGH-U1R cells did demonstrate increased cytotoxicity of epirubicin in combination with WGA with a reduction in IC50 values from 80 to 3.75µg/ml. Some of this increased cytotoxicity is a direct result of WGA cytotoxicity but in the centre of this graph the curves diverge suggesting there may be some additive effect (Figure 94b).

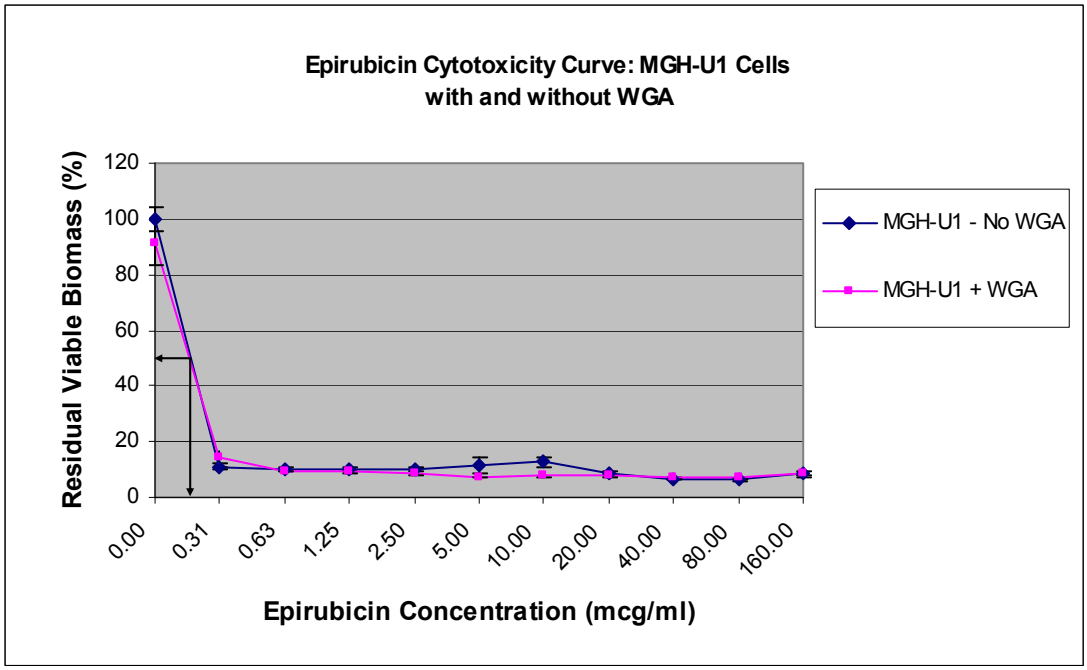

Figure 94a: MGH-U1 Cytotoxicity of epirubicin in combination with WGA

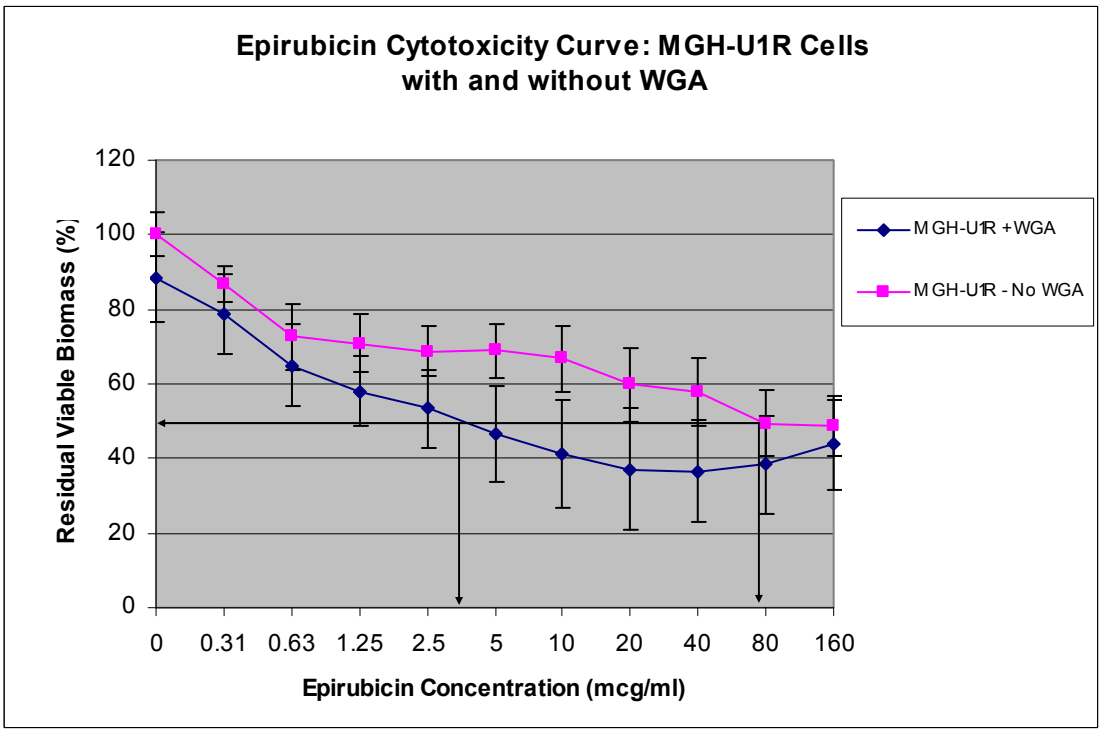

Figure 94b: MGH-U1R Cytotoxicity of epirubicin in combination with WGA

Epirubicin and Demecolcine

Demecolcine appears to be cytotoxic in its own right, with sensitive cells being killed at very low doses and epirubicin having very little additional effect (Figure 95a). Combination of demecolcine and epirubicin appears to have a concentration dependent additive effect in MGH-U1R cells (Figure 95b). At the highest concentration of demecolcine the IC-50 value for epirubicin is reduced to around 2µg/ml. This suggests that cells arrested in metaphase with their chromosomal material exposed are more susceptible to epirubicin. It may also imply that the nuclear membrane plays a role in excluding epirubicin from its nuclear site of action.

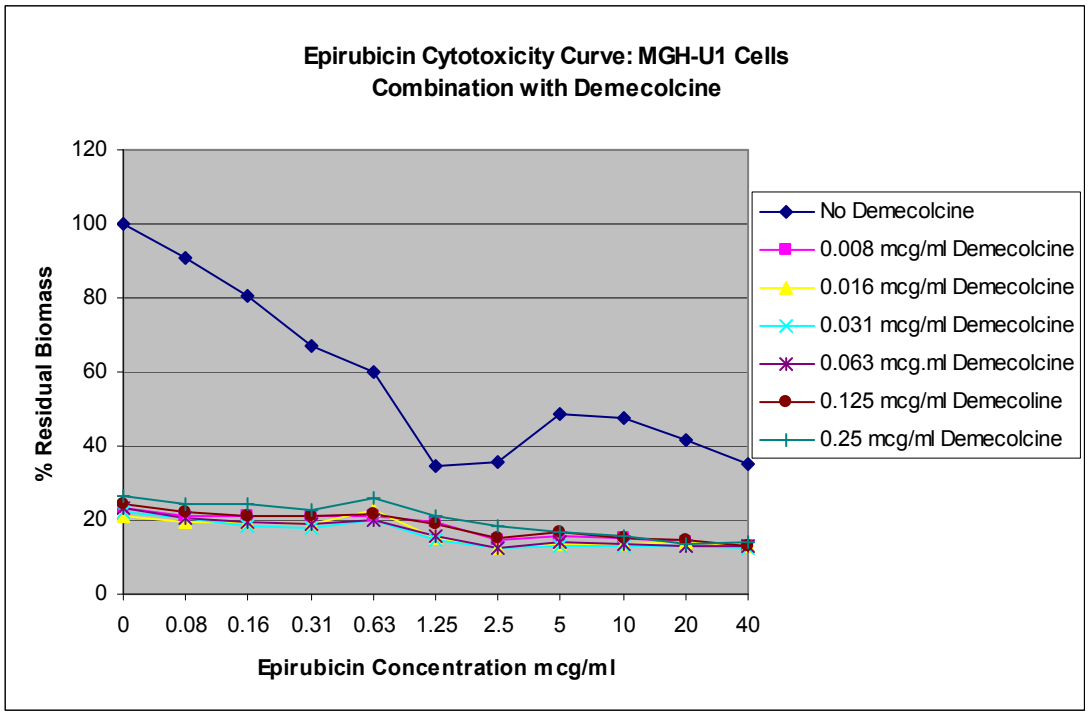

Figure 95a: MGH-U1 cytotoxicity with a combination of epirubicin and demecolcine

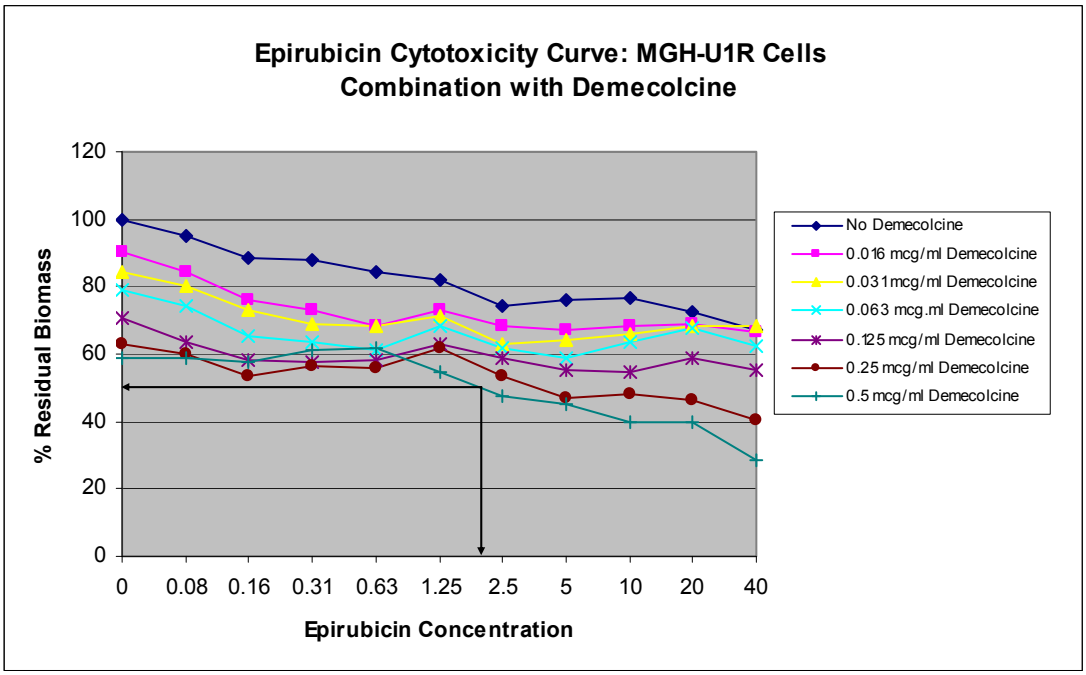

Figure 95b: MGH-U1R cytotoxicity with a combination of epirubicin and demecolcine

3.5: Summary of results:

Hypothesis 1:

"The nuclear membrane is responsible for nuclear sparing of epirubicin uptake in MDR bladder cancer cells."

1. The nuclear epirubicin staining characteristics of sensitive and MDR bladder cancer cell lines were determined. Sensitive cells showed strong nuclear uptake of epirubicin whereas MDR cells demonstrated a clear nuclear sparing pattern of epirubicin uptake.
2. Cell fusion experiments failed to demonstrate any cell fusion products containing nuclei of different phenotypes. This suggests that when sensitive and MDR cells fuse, one of the nuclei changes its characteristic uptake pattern. There could be several explanations for this, all of which are examined in the following discussion section.
3. Metaphase arrest experiments: We were only able to demonstrate chromosomal epirubicin staining in viable MDR cells at higher epirubicin concentrations. This suggests that a combination of resistance factors including the nuclear membrane contribute to nuclear sparing.
4. Microinjection studies: Sensitive cells microinjected with epirubicin demonstrated their normal pattern of nuclear epirubicin staining. MDR cells microinjected with epirubicin continued to demonstrate nuclear sparing of epirubicin uptake suggesting that the nuclear membrane is responsible for the nuclear sparing phenomenon.

Hypothesis 2:

"An active efflux mechanism is responsible for nuclear sparing of epirubicin in MDR bladder cancer cells."

1. Cell death reversed the nuclear sparing pattern of MDR cells to a sensitive phenotype. When incubated with epirbicin on ice both sensitive and MDR cells demonstrated nuclear sparing of epirubicin uptake, which may have been due to slower diffusion times or due to abolition of an active transport process for nuclear epirubicin uptake in sensitive cells.
2. Epirubicin uptake in MDR nuclear isolates exposed to epirubicin pre- and post-nuclear fractionation demonstrated much lower levels of fluorescence in pre-exposed nuclei. This suggests that active cell processes are responsible

for reduced nuclear uptake of epirubicin as opposed to the nuclear membrane per se.

3. Nuclear pore sizing using various sized FITC-dextrans showed that molecules of 19.5KDa and less gained easy entry the nuclei of sensitive and MDR cells by passive diffusion. Molecules larger than 42KDa were excluded from the nuclei of both sensitive and MDR nuclei. This means that by size criteria alone epirubicin (0.58KDa) should gain easy access through the nuclear membrane of sensitive and MDR cells

4. Blockade of nuclear pores using WGA did not appear to influence the uptake of epirubicin by either sensitive or MDR cells when assessed using confocal microscopy and flow cytometric assays. Neither did it preclude entry of the 19.5KDa FITC-dextran to the nuclei of sensitive or MDR cells, suggesting that any reduction in nuclear pore diameter is irrelevant in terms of diffusion of small molecules.

5. Direct microinjection of cells that were cooled on ice demonstrated that whilst sensitive cells maintained their nuclear uptake pattern of epirubicin, MDR cells showed reversal of their nuclear sparing pattern to a nuclear uptake pattern. This strongly suggests that there may be an active efflux pump on the nuclear membrane of MDR cells that is responsible for the nuclear sparing phenomenon.

6. The MDR cell lines used in this study were known to express P-glycoprotein. Using a flow cytometric assay with a FITC-labelled anti-Pgp antibody we demonstrated that MDR cells expressed P-gp at a cellular level but that the nuclei of MDR cells did not express P-gp. This means that another active efflux pump on the nuclear membrane must be responsible for the nuclear sparing phenomenon.

7. Verapamil reverses the nuclear sparing pattern of MDR cells. Time series confocal microscopy demonstrated that increases in cellular uptake of epirubicin in MDR cells co-incubated with verapamil appeared to due to increased nuclear uptake rather than increased cytoplasmic levels. This suggests than verapamil may also have an effect at the nuclear membrane level as well as on P-gp at the cell membrane level.

Other results:

Hypothesis 3:

"The nuclear membrane is not responsible for nuclear exclusion of idarubicin in sensitive and MDR bladder cancer cells."

1. Both sensitive and MDR cells demonstrate nuclear sparing of idarubicin uptake.
2. Nuclear isolates from sensitive and MDR cells showed similar levels of idarubicin fluorescence and in addition the levels of fluorescence did not appear to be affected by whether the nuclei were exposed to idarubicin before or after nuclear fractionation.
3. During metaphase arrest there appeared to be a lack of chromosomal idarubicin staining as demonstrated by central areas without fluorescence. When examined with other DNA stains these areas were clearly seen to be chromosomes.

Hypothesis 4:

"Mitomycin C fluorescence can be detected using direct or indirect fluorescence methods, allowing us to study its cellular uptake and localisation."

1. We were unable to demonstrate any convincing evidence of Mitomycin C fluorescence in sensitive or MDR cells using confocal microscopy (including time series uptake studies) and flow cytometric analysis.
2. An indirect assay of Mitomycin C uptake in sensitive and MDR cells utilising displacement of acridine orange DNA staining, again did not demonstrate a dose response using confocal microscopy or flow cytometric analysis.

Hypothesis 5:

"GFP fluorescence can be used as a viability stain in cell lines."

1. GFP fluorescence appears to be lost immediately as a result of cell death and could therefore be used as a marker of cell death *in vitro*.

Hypothesis 6:

"Changes in the localisation of epirubicin in MDR bladder cancer cells following cell death are due to leakiness of the cell and nuclear membranes."

1. Following cell death MDR cells reverse their nuclear sparing pattern to a

nuclear uptake pattern. This may be due to abolition of energy dependent processes or increased leakiness of the cell and nuclear membrane.

2. After cell death, a 77KDa FITC-labelled dextran was shown to gain access to the cell and nucleus of sensitive and MDR cells suggesting that cell membranes become leaky following cell death and may account for changes in nuclear epirubicin uptake.

Discussion

Much has been published about the nuclear sparing phenomenon exhibited by MDR cells when incubated with various anthracyclines and anthraquinones [244,340,347,348,350]. It is likely that nuclear sparing of other cytotoxic drugs also occurs in MDR cells leading to reduced efficacy, but studies to support this assertion are currently lacking.

In addition, few investigations have been performed to look at the role of the nuclear membrane in this nuclear sparing phenomenon [352]. This study is the most comprehensive assessment of the role of the nuclear membrane in this phenomenon in viable, adherent bladder cancer cells *in situ* to date.

Epirubicin uptake characteristics of sensitive and MDR bladder cell lines: Temperature and viability studies

In drug-sensitive, viable bladder cancer cell lines a clear nuclear uptake pattern of epirubicin is seen at 37^{o}C, with comparatively little cytoplasmic drug uptake. In contrast when incubated on ice (0 – 4^{o}C), despite demonstrating good levels of cytoplasmic epirubicin uptake, sensitive cells exhibit nuclear sparing of drug uptake. These results were consistent with previously reported results for the same cell lines [199,199,347,348,386]. In sensitive cells, epirubicin most likely gains access to the nucleus via one or both of two mechanisms, passive diffusion and/or active transport. As diffusion processes tend to be slower at low temperatures, nuclear fluorescence may be reduced as a result of slower passive diffusion through the cell. In addition, if epirubicin is actively transported into the nucleus then this energy-requiring process will be abolished at low temperatures, which could also explain the lack of nuclear epirubicin uptake seen at low temperatures. If epirubicin is actively transported into the nucleus of sensitive cells, this would imply that the epirubicin has become bound to a protein or molecule larger than 40KDa, meaning that passive diffusion into the nucleus is no longer possible.

In contrast, viable MDR cell lines showed nuclear sparing of epirubicin at 37^{o}C, with drug being sequestered in cytoplasmic vesicles. In addition a rim of drug was seen around the periphery of some cells, suggesting that drug was being effluxed or ejected from the cells by exocytosis. The nuclear sparing demonstrated by these cells could result from one or more of the

following mechanisms; reduced intracellular drug levels as a result of P-gp mediated drug efflux, vesicular sequestration of drug, nuclear drug efflux or reduced nuclear import. When incubated on ice (0 – 4^{o}C) there was no apparent change in the intracellular distribution or levels of drug uptake in MDR cells. This finding is somewhat surprising, as it suggests that the abolition of energy dependent efflux mechanisms at low temperatures does not affect drug uptake. However, this result concurs with previously reported results, where epirubicin uptake was examined using flow cytometry, showing no difference in cellular uptake between MDR cells incubated with epirubicin at 0^{o}C and 37^{o}C [346].

Non-viable sensitive and MDR bladder cancer cell lines both demonstrated a nuclear uptake pattern of epirubicin. Increased “leakiness” of both cellular and nuclear membranes can be demonstrated following cell death, with a 77KDa FITC-dextran, not usually taken up into the intracellular compartment of viable intact cells, gaining entry to both the cytoplasm and nucleus of non-viable cells. This membrane “leakiness” is the most likely reason for the nuclear uptake of epirubicin in dead MDR cells, although energy dependent mechanisms of drug efflux or expulsion are also abolished by cell death. This observation clearly emphasizes the importance of determining cell viability in any experiments where it is claimed that the MDR status of cells has changed from a resistant to a sensitive nuclear uptake pattern, to ensure that nuclear staining is not the result of cell death.

Cell viability was confirmed in all experiments examining the MDR characteristics of cells, using either fluorescein diacetate or acridine orange fluorescence. Experiments looking at GFP expressing cell lines suggested that GFP could also be used as a marker of cell viability.

Flow cytometric studies of epirubicin uptake in sensitive and MDR cells demonstrated a clear dose response, which was much less pronounced in the MDR cell line. At the highest dose of epirubicin, the sensitive cells demonstrated over 15 times more drug fluorescence than the MDR cells.

Investigation of nuclear MDR factors:

Nuclear pore sizing studies:

Nuclear pore sizing experiments using scrape-loading and microinjection techniques showed that FITC-dextrans of 19.5KDa and less passed easily into the nuclei of sensitive and MDR cells by passive diffusion. In contrast FITC-dextrans larger than 42KDa did not gain entry to the nuclei of sensitive or resistant nuclei. Epirubicin is a tiny molecule approximately 0.58KDa in size, so that by size criteria it should easily diffuse through the nuclear pores of sensitive and MDR cells.

This result suggests that other mechanisms must be involved the cellular localisation of epirubicin in MDR cells, as it is spared from the nuclei of resistant cells even when microinjected directly into the cell cytoplasm. This implies that either epirubicin is getting into the nucleus and then being effluxed or that it is denied entry into the nucleus in some way.

Nuclear isolate studies:

In nuclei exposed to epirubicin after nuclear isolation, there appeared to be equivalent high levels of epirubicin uptake in sensitive and resistant nuclei. One assumes that the study of nuclear isolates allow us to examine any inherent nuclear mechanisms of MDR. Some studies have utilised nuclei suspended in cytosolic substitutes and have shown results that appear to demonstrate metabolic activity in isolated nuclei [234,352]. However, our nuclei were not suspended in cytosol substitute and are therefore unlikely to behave as “viable” nuclei. We know that non-viable cells demonstrate high levels of epirubicin nuclear uptake. Whether extracted nuclei can be classified as “viable” remains unknown. It is therefore possible that “leakiness” of the nuclear membrane could account for the high levels of nuclear fluorescence observed in nuclear isolates. In addition, by removing the cellular apparatus, we have abolished any cellular mechanisms of nuclear exclusion, as well as any energy dependent mechanisms of nuclear uptake or exclusion. If one assumes that the nuclear membrane remains intact in nuclear isolates, then the only mechanism of nuclear drug entry can be passive diffusion across the nuclear membrane. We can therefore conclude that diffusion of epirubicin across the nuclear membrane is equal in sensitive and resistant cells in the absence of other processes.

Flow cytometric studies looking at concentration dependent nuclear epirubicin uptake in sensitive and resistant nuclear isolates would be a more accurate way of studying drug uptake in nuclear isolates. If equivalent concentration dependant uptake was demonstrated in the different nuclei, this would confirm that diffusion is the main mechanism of nuclear transport being studied when exposing nuclear isolates to drug.

In addition, nuclear isolates exposed to epirubicin after nuclear fractionation demonstrated much higher levels of epirubicin uptake than nuclear isolates from cells exposed to epirubicin prior to nuclear fractionation, for both sensitive and MDR nuclei. This difference was more pronounced in MDR nuclei, but also present for sensitive nuclei, suggesting that the cellular apparatus reduces nuclear uptake of epirubicin in both cell types.

In nuclei exposed to epirubicin before nuclear fractionation, sensitive nuclei demonstrated higher levels of nuclear fluorescence than resistant nuclei, as expected. Flow cytometric studies showed that over a range of epirubicin concentrations from 1.25 – 80μg/ml, sensitive nuclei took up between 3.1 – 7.5 times more epirubicin. This result confirms that the cellular apparatus of MDR cells is more effective at excluding epirubicin from the nucleus than that of sensitive cells.

Nuclear pore blockade studies:

WGA binds to nuclear pores and has been shown to block some active transport processes across the nuclear membrane, including active nuclear transport of adriamycin (doxorubicin) in a drug sensitive lymphoblastic tumour cell line [352]. FITC-WGA was seen to clearly localise to the nuclear membrane within a few hours, reaching a plateau at 4 hours which persisted for up to 24 hours. Nuclear isolates also demonstrated clear ring enhancement following exposure to FITC-WGA suggesting nuclear pore binding of WGA. Nuclear pore blockade with WGA did not change the nuclear uptake of a 19.5KDa FITC-dextran, suggesting that by size criteria WGA should have no effect on nuclear epirubicin uptake occurring by passive diffusion. This meant that any alteration of epirubicin uptake mediated by WGA would have to be through blockade of active transport.

Confocal studies of epirubicin uptake in sensitive and MDR cells following WGA exposure showed no changes in the levels of cellular uptake or localisation of epirubicin. Confocal examination of nuclear isolates from cells exposed to WGA followed by epirubicin exposure either pre- or post-nuclear fractionation did not demonstrate any differences in nuclear epirubicin uptake attributable to WGA.

In sensitive and resistant cells with or without pre-exposure to WGA, flow cytometric studies of whole cells and nuclear isolates demonstrated no significant differences in epirubicin uptake attributable to WGA.

These results contradict previously published results that demonstrated reduced epirubicin uptake in isolated drug sensitive nuclei exposed to WGA followed by doxorubicin [352] and increased epirubicin uptake in the nuclei of MDR cells exposed to WGA [394].

Cell fusion studies:

Demonstration of a mixed cell fusion with phenotypically sensitive and resistant nuclei within the same cell environment would have provided clear evidence that the nuclear membrane also acts a barrier to nuclear drug uptake in resistant cells. However, no mixed cell fusion products were demonstrated despite numerous attempts. Instead numerous cell fusion products containing phenotypically similar nuclei were seen.

The lack of mixed cell fusion products suggests that fusion of sensitive and resistant cells results in a change in the nuclear epirubicin uptake characteristics of one of the nuclei, either the resistant nuclei taking on a sensitive phenotype or vice versa.

Sensitive type fusion products appeared to be more common than resistant cell fusions. A simple counting technique would have provided stronger evidence for this statement. If true, this would suggest that the resistant nucleus changes to a sensitive phenotype.

There are several possible explanations for failing to demonstrate a mixed cell fusion, the first and most obvious being that we had failed to fuse a sensitive with a resistant cell, but this seems unlikely given our numerous attempts.

There are several possible explanations for the change from resistant to sensitive phenotype. One explanation could be a dilution in the cellular levels of P-gp resulting in higher intracellular concentrations of epirubicin which in

turn leads to increased nuclear uptake, changing the resistant nucleus to a sensitive pattern. Another possibility would be a dilution of intracellular MDR mechanisms, for example P-gp, LRP or cytoplasmic vault mediated vesicular drug sequestration, increasing cytoplasmic drug concentrations and nuclear uptake. A reduction in a nuclear efflux mechanism mediated by vault complexes may also explain the change in nuclear phenotype.

MGH-U1R cells have been shown to express LRP (Personal communication, Matthew Hayes), so a dilution of LRP or vault structures may result in reduced intracytoplasmic vesicular sequestration of drug [285] or reduced efflux of epirubicin from the nuclear compartment, as has been suggest by other workers [286-288].

Another possible mechanism may involve the numerous nuclear pore complexes that allow “molecular trafficking” between the nucleus and the cytoplasm. Nuclear pore complexes are large 120 Megadalton supramolecular assemblies that straddle the double-membraned nuclear envelope [358] and share the presence of the LRP with cytoplasmic vaults [270]. These nuclear pores allow passive diffusion of molecules up to 40KDa molecular weight. They also allow the transport of larger molecules, up to several megadaltons, by energy dependant transport mechanisms, provided they carry a nuclear localisation sequence that facilitates nuclear pore binding and transport [358]. It has been suggested that cytoplasmic vaults may also constitute the central plugs of the NPC, and might mediate the transport of a variety of molecules between nucleus and cytoplasm [280]. It is possible vaults might be acting in some such regulatory capacity, mediating cytoplasmic/nucleocytoplasmic drug transport.

Epirubicin is known to have a high affinity for protein binding in serum, so one possible explanation may be that epirubucin binds to proteins within the cytoplasm and is excluded from the nucleus if these proteins do not carry the nuclear localisation sequence necessary for transport into the nucleus of MDR cells. This theory is partially supported by previous work looking at the role of the nuclear membrane in adriamycin (doxorubicin) uptake in isolated sensitive and MDR nuclei, from a lymphoblastic tumour cell line [352]. This work showed that in isolated nuclei, nuclear transport of adriamycin is reduced in MDR cells when compared to sensitive cells. Furthermore blockade of active

nuclear transport by Wheat Germ Agglutinin (WGA; Triticum vulgaris lectin) reduced sensitive nuclear uptake of adriamycin to approximately the level of MDR nuclear uptake, but had no effect on adriamycin accumulation in MDR nuclei. This suggests that sensitive cells have two mechanisms by which nuclear adriamycin uptake is achieved: passive diffusion and active transport. Adriamycin is thus transported into the nucleus of sensitive cells bound to proteins, whereas MDR cells allow adriamycin into their nuclei by passive diffusion only, with an absence of active transport. This absence of active transport in MDR nuclei has several possible explanations, the two most probable being either that adriamycin binds to different proteins that don't carry the necessary sequence for nuclear transport or that the nuclear localisation sequence receptor on the nuclear pore complex is different in MDR cells.

In a mixed cell fusion it is possible that epirubicin undergoes nuclear transport bound to proteins. This would involve some cytoplasmic-nuclear membrane interaction, suggesting that a certain cytoplasmic factor from the sensitive cell allows epirubicin to gain entry to the MDR nucleus. This could be either a factor that promotes for nuclear transport of epirubicin or a sensitive cytosolic protein that binds epirubicin and is recognised and transported by the nuclear pore complex of the MDR nucleus, converting it to a sensitive pattern.

Further evidence to support the theory that sensitive cells transport anthracyclines into their nuclei bound to proteins, comes from a study that demonstrated in sensitive leukaemic cells that adriamycin was transported into nuclei bound to proteasomes [395]. Proteasomes are intracellular proteinase complexes involved in nonlysosomal protein degradation. They can be localised in both the cytoplasm and the nucleus and hence carry the nuclear localisation sequence necessary for active transport from the cytoplasm into the nucleus.

The protein binding of anthracyclines in cells needs to be investigated further to assess if there are differences between sensitive and resistant cancer cells that may account for their differences in nuclear uptake.

Metaphase arrest studies:

Metaphase experiments were performed to see if the chromosomes of MDR cells could be stained during metaphase. Evidence of this would provide strong indirect evidence of the nuclear membrane's role in nuclear sparing, as the nuclear membrane is absent during metaphase.

Viable, sensitive cells showed clear chromosomal staining with epirubicin, whereas viable MDR cells did not demonstrate any chromosomal staining with epirubicin at lower doses. This finding was confirmed by the subsequent addition of acridine orange which showed numerous cells in metaphase that had not stained with epirubicin. However, at higher concentrations of epirubicin low level chromosomal staining could be seen, being confirmed by the addition of acridine orange. These results suggest that low intracellular levels of epirubicin in MDR cells along with some nuclear membrane mechanism both play a part in the nuclear sparing of epirubicin in MDR cells.

An important question is what happens to the nuclear membrane during metaphase? It seems inconceivable that a cell would leave its chromosomal material completely unprotected during cell division, although one recognises that most cytotoxic agents exert their effects during this phase of the cell cycle. It is possible that when the nuclear membrane disperses that the nuclear membrane pores or another efflux mechanism could be distributed in a peri-nuclear location and actually efflux epirubicin away from chromosomes. It is also possible that cytoplasmic vaults could redistribute to a peri-chromosal location, denying epirubicin access to chromosomes during metaphase.

Another explanation for the absence of chromosomal epirubicin staining at low drug concentrations might be that there is some electrostatic repulsion of drug from chromosomes. DNA is said to be negatively charged by virtue of its histones. It is possible that epirubicin entering MDR cells becomes similarly charged and is therefore repelled from the chromosomes. It is also possible that epirubicin becomes bound to negatively charged cytoplasmic proteins in MDR cells that are repelled from the chromosomes. Differences in protein binding between sensitive and resistant cells could explain the discrepancy between the two cell types. However, these two theories seem less likely

given the presence of low level chromosomal staining seen at higher epirubicin concentrations.

The increased cytotoxicity of epirubicin when combined with demecolcine could also suggest enhanced DNA binding of epirubicin in metaphase cells.

Microinjection studies:

Microinjection provided a novel means of investigating the nuclear sparing phenomenon associated with MDR. Previous investigators have questioned whether the nuclear sparing phenomenon is merely a reflection of low levels of drug accumulation in MDR cells, due to drug efflux by P-glycoprotein, or whether the nuclear membrane is also playing a role [244,340,346,348,352,394]. Microinjection of epirubicin bypasses the P-gp efflux pump on the plasma membrane, delivering a bolus of drug directly into the cell cytoplasm. The persistence of nuclear sparing following microinjection would be highly suggestive that the nuclear membrane plays a role in MDR.

Microinjection of sensitive cells at 37^{o}C demonstrated their usual nuclear uptake pattern of epirubicin. Microinjection of resistant cells at 37^{o}C demonstrated clear nuclear sparing of epirubicin uptake, suggesting that P-gp mediated cellular efflux does not account for this phenomenon.

Efflux of the drug still takes place to some degree, as evidenced by the differences in overall drug fluorescence between sensitive and resistant cells at 37^{o}C. This observation suggests that the plasma membrane P-gp pump effluxes drug from the cell cytoplasm, as well as excluding drug while it crosses the plasma membrane as has been suggested by previous studies [396,397]. There was some delay in visualising injected cells, owing to the location of microinjection and confocal facilities at our institution, thus allowing time for some efflux to occur in our MDR cell samples. This delay also allowed time for drug to be packaged in vesicles within the cytoplasm of MDR cells, as has been noted in previous confocal studies using standard anthracycline exposure methods [347].

These results showed that cells microinjected with epirubicin show the same basic pattern of nuclear drug uptake or exclusion to cells incubated with epirubicin in the external milieu. This strongly suggests that the nuclear

membrane acts as a barrier to nuclear epirubicin uptake in MDR cells and must therefore play a role in multidrug resistance.

We attempted to clarify the mechanism(s) by which the nuclear membrane excludes epirubicin from the nuclei of MDR cells by microinjecting cells whilst on ice, to inhibit energy dependant processes.

When microinjected with epirubicin at 0 – 4^{o}C sensitive cells demonstrated slightly reduced levels of nuclear fluorescence when compared to sensitive cells at 37^{o}C, but still showed a predominant nuclear uptake pattern. Resistant cells injected with epirubicin at 0 – 4^{o}C showed reversal of their usual epirubicin uptake pattern to a "sensitive" nuclear uptake pattern. They also demonstrated higher cytoplasmic levels of epirubicin.

These results suggest that some intracellular process is responsible for nuclear sparing of drug uptake in MDR cells. The fact that when energy dependent processes are abolished, epirubicin gains entry to the nucleus suggests the mechanism must involve some energy dependent process. The most likely explanation would be an energy dependent efflux pump associated with the nuclear membrane. One possible mechanism for this could be vaults associated with the nuclear pore complexes [280]. Other studies have demonstrated vault induced efflux of anthracyclines at nuclear membrane level [286,287] and MGH-U1R cells are known to express LRP, the human major vault protein (personal communication, Matthew Hayes). Another recent study of nuclear drug efflux in human leukaemic cell lines suggests that efflux occurs by an ATP independent, passive diffusion mechanism that follows extracellular drug clearance [398]. Other possibilities include other energy dependent mechanisms reducing intracytoplasmic drug concentrations by vesicular drug sequestration, such mechanisms could include vesicle bound P-gp, LRP or vault transporters.

Time series studies:

Confocal microscopy time series experiments provided an interesting insight to intracellular uptake and localisation of epirubicin in sensitive and resistant cells.

Cytoplasmic epirubicin levels were remarkably constant between sensitive and MDR cells lines of the same lineage, suggesting that P-gp does not alter cellular uptake of epirubicin greatly. Despite this, nuclear epirubicin uptake

levels were much higher in sensitive cells, with MDR nuclei showing much lower levels that were remarkably similar to cytoplasmic drug levels. If entry to the nucleus occurs by passive diffusion one might expect cytoplasmic and nuclear levels to equilibrate across the nuclear membrane. This appears to happen in MDR cells perhaps suggesting that diffusion accounts for the limited nuclear uptake in MDR cells and is thus ultimately controlled by P-gp. However, given the affinity of epirubicin for DNA binding one would expect epirubicin to bind to the DNA in MDR nuclei, hence reducing the nucleoplasmic epirubicin concentration creating a diffusion gradient across the nuclear membrane. This situation would result in increasing nuclear binding of epirubicin with increasing fluorescence levels, which does not occur. This again suggests that there is another transporter probably associated with nuclear membrane that is responsible for maintaining equilibrium across the nuclear membrane with passive diffusion being matched by drug efflux.

In sensitive cells, cytoplasmic epirubicin levels are fairly constant in one cell line (MGH-U1) and are certainly below nuclear levels in the other cell line (RT112). The fact that nuclear uptake exceeds cytoplasmic drug concentrations suggests that the mechanism of transport across the nuclear membrane is not solely due to passive diffusion, otherwise cytoplasmic and nuclear levels would equilibrate. This discrepancy in the rates of cytoplasmic and nuclear accumulation of drug, suggests that either there is some active transport mechanism is involved in nuclear epirubicin import in sensitive cells or that once epirubicin is bound to DNA in the nucleus that it no longer contributes to nucleoplasmic epirubicin concentration, so that passive diffusion occurs across the nuclear membrane at a rate determined by DNA binding.

Verapamil appears to exert a minimal effect on cytoplasmic uptake of epirubicin and yet increases nuclear uptake of epirubicin dramatically in MDR cells. The presumed mechanism of action of verapamil has always been through competitive inhibition of P-gp mediated drug efflux, but without clear evidence of increased cytoplasmic epirubicin levels these experiments do not seem to support this. It is possible that verapamil acts at the nuclear

membrane to increase nuclear epirubicin uptake by inhibition of a nuclear membrane export pump such as LRP or cytoplasmic vault structures.
It must be recognised that these time series experiments looked at a single levels through each cell which whilst representative of drug uptake in each cellular compartment may not reveal the full picture. Confocal microscopy is also only a semiquantitative method of fluorescence measurement making it less accurate than flow cytometry in terms of absolute fluorescence measurements.
Flow cytometric time series experiments demonstrated significant increases in epirubicin uptake in MDR cells when combined with verapamil exposure. Co-incubation of MDR cells with epirubicin and verapamil for 2 hours resulted in a 10.7 – 12 fold increase in intracellular fluorescence levels over epirubicin alone for 2 hours. Our confocal experiments suggest that most of this results from increased nuclear epirubicin uptake. Performing similar time series experiments followed by nuclear fractionation would have shown us if increases in nuclear uptake account for these large differences in overall uptake. These experiments suggest that combinations of epirubicin and verapamil instilled for longer periods may enhance MDR reversal and increase intracellular levels of epirubicin, resulting in improved cytotoxicity. Previous researchers have demonstrated increased cytotoxicity associated with epirubicin and verapamil co-incubation in cell lines [199].

P-gp studies

One possibility that might have accounted for a nuclear efflux mechanism is the expression of P-gp on the nuclear membrane. One previous study in the literature identified P-gp on the nuclear membrane of the MDR breast cancer cell line, MCF-7 DX [234]. This study used anti-P-gp monoclonal antibodies, MM4.17, MC57 and JSB-1 to immunolabel P-gp on the nuclear membrane using two methods. Firstly, they immunolabelled P-gp on isolated nuclei, followed by FITC-conjugated secondary antibody and either confocal or flow cytometric analysis. Secondly, they used immunoelectron microscopic imaging of fixed cells embedded in epoxy resin that had been exposed to the same primary antibodies, followed by gold-conjugated secondary reagents. Using flow cytometry, this study also demonstrated P-gp mediated doxorubicin efflux from isolated nuclei that had been exposed to doxorubicin

and then incubated in drug free medium containing 1mM ATP. However, another study showed P-gp was absent from the nuclear membrane of a lymphoblastic tumour cell line that exhibits the MDR phenotype [399].
We looked for cellular and nuclear expression of P-gp using a flow cytometric assay utilising a FITC labelled monoclonal antibody directed against P-gp (17F9) to determine whether P-gp was responsible for the nuclear efflux of epirubicin in our MDR cells. This showed that whilst both MDR cell lines used in this study expressed P-gp at a cellular level, there was no evidence of P-gp expression on the nuclear membrane to account for a drug efflux at this level. Our results were consistent with previous studies of P-gp distribution in the MGH-U1R cell line, using straightforward immunostaining of P-gp with cold acetone/ethanol fixation and JSB-1, another monoclonal antibody against P-gp (Claire Davies – personal communication).

Mitomycin C

We were unable to demonstrate any direct fluorescence from mitomycin C to determine whether similar reductions in cellular and nuclear accumulation of mitomycin C occur in MDR cells.
Confocal studies looking at an indirect method of examining nuclear uptake of mitomycin C using reduction in acridine orange DNA staining suggested that nuclear uptake was reduced in MDR cells compared to sensitive cells. Confocal microscopy is only a semiquantitative method of measuring fluorescence and measurements are only taken through a single level of the cells which may introduce some intersample variation.
A similar indirect flow cytometric assay looking at cellular uptake of mitomycin C using acridine orange showed no correlation between reduction in AO fluorescence and mitomycin C dose response. However, a flow cytometric study looking at reduction in nuclear acridine orange uptake secondary to mitomycin C exposure would have been a better assay, as the reduction in acridine orange DNA binding as a result of mitomycin C DNA binding is what we are really interested in.
The nuclear sparing of cytotoxic drugs has also been demonstrated in previous studies looking at nuclear uptake of anthraquinones in MDR cells by fluorescence methods [244,350,351]. This suggests that other drugs that are

susceptible to MDR mechanisms, such as mitomycin C, may also be subject to nuclear sparing.

Idarubicin

The fact that idarubicin appears to be excluded from the nuclei of viable, sensitive and MDR cells at both 37^{o}C and 0 – 4^{o}C and is also excluded from the nuclei of dead cells remains somewhat of an enigma.

Flow cytometric studies showed a clear dose response to idarubicin in both sensitive and MDR cells, with sensitive cells showing 2.3 – 5 times greater levels of drug fluorescence.

Isolated nuclei from sensitive and MDR cells incubated with idarubicin did demonstrate nuclear fluorescence, with similar levels being seen in sensitive and MDR cells. Nuclei exposed to idarubicin after nuclear extraction also have similar levels of idarubicin uptake to those exposed before nuclear fractionation. The fluorescence levels exhibited by nuclei exposed to idarubicin are lower than respective epirubicin fluorescence levels in isolated nuclei exposed before or after nuclear fractionation. This might suggest that idarubicin DNA binding may have a certain threshold above which no further binding can occur.

Confocal microscopic images are generally adjusted to look at the area of the cell with the highest levels of fluorescence. The very high levels of cytoplasmic idarubicin uptake could mean that when the cells are visualised and the gain settings adjusted to show cytoplasmic idarubicin levels, it gives the impression of a total absence of nuclear fluorescence when in fact there is just relative sparing of drug from the nucleus.

Metaphase experiments were also of interest, as they clearly demonstrated that chromosomes of both sensitive and resistant cells did not stain with idarubicin during metaphase despite high levels of cytoplasmic fluorescence. This suggests that the nuclear membrane is not responsible for the reduction in DNA staining.

It seems likely therefore that the reduced idarubicin DNA binding may be due to either a low idarubicin binding threshold over which no further drug can bind, or some electrostatic repulsion of idarubicin or repulsion once bound to a particular protein which may be similar in both sensitive and MDR cells.

An experiment that would help to determine if there is a saturation threshold for idarubicin binding would be to perform a dose response in nuclear isolates exposed to various concentrations of idarubicin pre- and post- nuclear fractionation. If this demonstrated saturation of nuclear fluorescence this would suggest nuclear idarubicin binding reaches a certain threshold and then can bind no more. It may also suggest quenching of drug fluorescence once bound to DNA, suggesting that nuclear fluorescence bears no relation to nuclear drug uptake for idarubicin.
As idarubicin's predominant cytotoxic actions are within the nucleus, quenching of idarubicin fluorescence may also be suggested by the fact that the IC50 value for idarubicin cytotoxicity in MDR cells is significantly lower than for epirubicin.

The lack of any formal statistical analysis may be viewed by some as a weakness of this thesis. Formal statistical analysis was not performed for confocal microscopy experiments as this is a semi-quantitative technique. There are a number of variables that can interfere with meaningful analysis of confocal images. We attempted to exclude variables between samples by standardising laser and detector gain settings. Despite this, there will always be some variation in the cross-section plane of the sample cells. This cannot be adequately controlled between samples making formal statistical analysis less meaningful. Many of our experiments were designed to detect large discrepancies in cellular uptake and localisation between cell types, or to determine the intracellular localisation of a substance, both of which can be viewed and commented on by direct observation alone.
In terms of flow cytometric data analysis, because of the large number of cells examined in each sample, even the smallest differences between samples are likely to be highly statistically significant. Whether these differences equate to meaningful biological effects is a matter for debate. The larger differences that were observed between samples are highly likely to represent biologically significant effects.

Future directions:

In addition to the potential lines of work highlighted throughout the discussion, the following areas of research follow-on from our studies and would be of additional interest.

As stated there is some evidence that anthracyclines may be transported into the nuclei of sensitive cells bound to proteins that are actively transported via nuclear pores [352,395]. We performed some very basic protein analysis on our sensitive and resistant cell lines to see if there were differences in protein expression (Appendix 4). It would be interesting to refine this protein analysis to see if it is possible to demonstrate whether the anthracyclines, epirubicin and idarubicin, bind to intracellular proteins. It would also be interesting to establish whether there are any differences in the binding of these drugs between sensitive and MDR cells, which might explain their differences in cellular localisation.

We also performed some preliminary experiments extracting cytoplasmic fractions from sensitive cells and co-injecting this cytoplasmic fraction with epirubicin into MDR cells. In these studies we were able to demonstrate reversal to a nuclear uptake pattern in viable MDR cells, suggesting that sensitive cell cytoplasm may contain some factor necessary for nuclear transport of epirubicin or indeed may contain a protein which binds epirubicin and undergoes nuclear transportation. Obviously these were uncontrolled experiments, so the results are highly speculative and have therefore not been included in the main body of work. However, these results certainly warrant further investigation and refinement. Perhaps with time it would be possible to define a specific cytoplasmic fraction or indeed a specific protein that would act as a nuclear transport carrier of epirubicin allowing entry to MDR nuclei (Appendix 5).

Following on from our microinjection experiments, it would be of interest to inject epirubicin into the cytoplasm or nuclei of sensitive and MDR cells and watch the movement of drug using real-time fluorescence video capture. This would provide a direct insight into drug handling at the cytoplasmic and nuclear level. Injection of cells or nuclei at 0 – 4^{o}C followed by cell warming with real-time imaging would also be of interest. This would allow us to determine whether nuclear epirubicin uptake is reversible or whether

demonstration of nuclear uptake indicates that irreversible DNA binding has occurred.

Some newer modified anthracyclines, annamycin and doxorubicin-peptide, do not act as substrates for ABC transporters including P-gp [400-402]. Visualisation of the cellular localisation of these drugs using confocal microscopy, would give a clear answer as to whether P-gp function bears any relation to the nuclear sparing of anthracyclines.

Appendix 1: Nuclear Preparation Protocol [390]:

Cells were cultured in 25cm^2 flasks until 90 – 95% confluent. Cells were then washed three times in PBS containing protease- and phosphatase-inhibitors (PBSI), comprising:

9.2mM Na_2HPO_4

10mM NaH_2PO_4

0.15M NaCl

1mM Na_3VO_4

1mM PMSF (phenylmethylsulphonyl fluoride)

5μgml^{-1} Leupeptin

1μgml^{-1} Aprotinin

Immediate release of nuclei from cells was then initiated in 2 mls lysis buffer (10mM HEPES, 1.5mM $MgCl_2$ pH5.5) by the addition of 10 drops of Zaponin (Coulter Electronics, UK). The supernatant was pipetted off immediately and layered over a 20% solution of sucrose in PBSI in polythene centrifuge test tubes. These samples were spun at 800g for five minutes, and the top phase was discarded. A further single PBSI wash was performed, and the suspension was re-spun through 20% sucrose/PBSI at 800g for five minutes, and again the top phase was discarded. The presence of fractionated nuclei was confirmed by phase contrast light microscopy.

Appendix 2: Scrape-loading protocol [391]:

McNeil described this method of incorporating large macromolecules into cells. We used this method in our initial attempts to determine the size of nuclear pores using FITC-labelled dextran molecules of various sizes. Dextrans do not usually gain access to the cell cytoplasm as they are large inert molecules. Temporary disruption of the plasma membrane allows these molecules to enter the cell cytoplasm, with subsequent closure of the plasma membrane preventing their escape. Once they have gained entry into the cells, the dextrans distribute throughout the cell and are slowly excreted by exocytosis.

Cells were cultured in 25ml flasks until 90% confluent. The medium was then tipped off and replaced with 2ml of 10mg/ml FITC-dextran solution, diluted in PBS. Flasks were laid on ice to cool the cells.

The cells were then gently scraped with a sterile rubber policeman until all the cells were in suspension, “scrape-loading” them with FITC-dextran. The cells were then covered with 8mls of ice-cold culture medium. Once all flasks were scrape-loaded the cells were centrifuged at 438g (1500rpm) for 3 minutes and resuspended in fresh culture medium. Cells were then plated out into 40mm Petri dishes and re-incubated. Cells were then viewed by confocal microscopy at various time points to assess the cellular distribution of the FITC-dextrans.

Appendix 3:

Optimisation of Cell fusion using Polyethylene Glycol (PEG):

Effect of time of PEG exposure:

MGH-U1 and MGH-U1R cells were cultured in 40mm Petri dishes as a mixed culture, 1ml of 10^5 cell/ml of each cell type at 37^{o}C until confluent.

Cell culture media was pipetted off and cells were then covered with 0.5mls of polyethylene glycol (PEG) 50% w/v and gently agitated for various exposure times of 2, 3, 5, 10, 20, 40 and 60 minutes. The PEG was then serially diluted by the addition of ice-cold culture medium. This was then pipetted off and replaced with fresh culture medium. The samples were then incubated for a further hour at 37^{o}C to allow cell fusion to complete and recover.

The culture medium was then tipped off and cells were fixed by covering them with buffered formalin saline for 60 minutes. The cells were then stained with methylene blue and fusions were counted in 9 random fields at x20 magnification.

Results:

Time of PEG exposure (minutes)	Number of cell fusions counted
2	99
3	62
5	125
10	144 – some cells damaged
20	Some fusions – cells damaged ++
40	Cells damaged +++
60	Cells damaged +++

At higher exposure times some cells demonstrated damage with disappearance of their plasma membranes.

Overall the optimal number of fusions with the fewest damaged cells was achieved with an exposure time of 5 minutes and this was used for all subsequent PEG fusion experiments.

Effect of incubation time following exposure to PEG:

MGH-U1 and MGH-U1R cells were cultured in 40mm Petri dishes as a mixed culture, 1ml of 10^5 cell/ml of each cell type at 37^{o}C until confluent.

Cell culture media was pipetted off and cells were then covered with 0.5mls of polyethylene glycol (PEG) 50% w/v and gently agitated for 5 minutes. The PEG was then serially diluted by the addition of ice-cold culture medium. This was then pipetted off and replaced with fresh culture medium. The samples were then incubated at 37^{o}C for various times to allow cell fusion to complete and recover. The times used were 30 minutes, 1, 2, 4, 8 and 24 hours. The culture medium was then tipped off and cells were fixed by covering them with buffered formalin saline for 60 minutes. The cells were then stained with methylene blue and fusions were counted in 9 random fields through at x20 magnification.

Results:

Time of incubation after PEG exposure	Number of cell fusions counted
30 minutes	92
1 hour	141
2 hours	189
4 hours	151
8 hours	142
24 hours	100

The optimum time of incubation post-PEG exposure was shown to be 2 hours and this was used for all future PEG fusion experiments.

Appendix 4: Basic protein analysis of sensitive and MDR cells

We performed some basic protein analysis using gel electrophoresis, to determine if there were any alterations in protein expression between the sensitive and resistant cell lines.

SDS Gel plates were prepared according to the following standardised protocol.

Preparation of SDS gel electrophoresis plates

Reagents

Solution A = Protogel (Ultra Pure): 30% w/v Acrylamide: 0.8% Bis-Acrylamide stock solution (37.5:1); National Diagnostics, UK

Solution B = Protogel Buffer: 1.5M Tris, 0.384% SDS, pH 8.8; National Diagnostics, UK

Solution C = Protogel Stacking Buffer: 0.5M Tris·HCl, 0.4% SDS, pH 6.8; National Diagnostics, UK

De-ionised, distilled H_2O (16.5 Ohm)

APS = Ammonium Persulphate; Fisher Bioreagents, Fischer Scientific UK): Dilute 0.1g in 1ml de-ionised H_2O

TEMED = N, N, N', N'- Tetramethylethylethylenediamine ($C_6H_{12}N_2$): Electrophoresis Reagent; (Sigma, UK)

Resolving Gel (10% SDS Gel) Mixture

Compound	1 Plate	2 Plates	4 Plates
Solution A	1.35mls	2.7mls	5.4mls
Solution B	1.0mls	2.0mls	4.0mls
De-I, dist H_2O	1.625mls	3.25mls	6.5mls
APS	38µl	75µl	150µl
TEMED	5µl	10µl	20µl

Stacking Gel (10% SDS Gel) Mixture

Compound	1 Plate	2 Plates	4 Plates
Solution A	188µl	375µl	750µl
Solution C	313µl	625µl	1.25ml
De-I, dist H_2O	0.75ml	1.5ml	3.0ml
APS	10µl	20µl	40µl
TEMED	2.5µl	5µl	10µl

Method for producing gel plates

1. Put together glass plates making sure bottom of plates are aligned and Biorad sign is at top of plate.
2. Place plates into green clamp and clamp in place making sure bottom of plates are aligned
3. Place plates in to plate holding clamp making sure the bottom of the plates are pushed firmly against the grey seal.
4. Using a pipette fill the gap between the plates with resolving gel mixture up to the lower level of green plastic clamp.
5. Using a pipette fill the remaining gap to level with top of plate with de-ionised, distilled H_2O.
6. Once resolving gel is set, 10-15 minutes. Tip off water.
7. Using a pipette fill the gap to the top of the plate with stacking gel mixture and insert Biorad 10 well comb. Allow to set, 10-15 minutes.

The gel plate is then ready for electrophoresis.

Protein Sample Preparation:

Cells were cultured in 25cm^2 flasks until confluent. Cells were then harvested into suspension using trypsin-EDTA. The suspension was then centrifuged at 1800rpm for 3 minutes and the Trypsin containing medium was pipetted off. The cells were washed with PBS and re-centrifuged twice. The cells were then re-suspended in 5mls of PBS and counted using a haemocytometer slide. Cell numbers were adjusted to 75,000 cells per sample. The samples were then placed into centrifuge tubes and centrifuged at 1800rpm for 3

minutes. The PBS was removed and cells were resuspended in 1ml of PBS and transferred into eppendorf tubes. Cells were then pelleted again by ultracentrifugation at 6000rpm for 3 minutes. The supernatant was pipetted off and cells were re-suspended in 25µl PBS. Cell suspension was then mixed thoroughly with 25µl SDS double strength loading buffer. Protein samples were then heated in a Grant Heater Block at 90^{o}C for 5 minutes to dissolve the cell membranes and denature the cell proteins. Protein samples were then ultrasonicated using a harmonic ultrasonicator. Samples were then re-centrifuged at 6000rpm for 2 minutes to separate out any precipitates. Samples were then loaded into gel plate wells.

Gel Electrophoresis

Two gel plates were clamped into the gel electrophoresis cradle and placed into the electrophoresis chamber.

Electrophoresis buffer was made up fresh as a 1:10 dilution of 10X TRIS/Glycine/SDS in distilled, deionised H_2O. The area between the plates was filled up to the top of the plates and the outer electrophoresis container was filled until approximately 2/5ths full. The Biorad comb was then removed and a sample injector guide was placed between the plates. The gel plate wells were filled by slowly pipetting 15µl of each sample into individual wells within the stacking gel. One well was reserved for protein marker sample in order to roughly size the electrophoresed proteins. The protein marker well was filled with 5µl of SigmaMarker^{TM} Wide Molecular Weight Range (Product No. 4038, Sigma, UK). The order of protein extracts added to each gel plate was noted. The lid was placed on the electrophoresis chamber and the electrical leads were connected to the Biorad Machine (Red – Red and Black – Black). The gel plate was run at a voltage of 150volts for 50 minutes.

The plates were then removed and the plates were unclamped and gently prised apart. The gels were then removed from the plate and placed in a wet plastic container ready for staining.

Gel Plate Staining

Gel plates were stained using Silver staining (Silver stain plus, Bio-rad, Catalog Number 161-0449) as per the following protocol.

SDS Gel Electrophoresis Staining protocol: Silver stain

The following preparations are adequate for staining two mini gels (8 x 10cm), 0.75 – 1mm thick.

1. Fixative step – 20 minutes

Fixative Enhancer Solution Preparation

Reagent Grade Methanol	200ml	50% v/v
Reagent Grade Acetic Acid	40ml	10% v/v
Fixative Enhancer Concentrate	40ml	10% v/v
Deionised Distilled Water	120ml	30% v/v
Total	400ml	100% v/v

After gel electrophoresis, place gels in the Fixative Enhancer Solution. With gentle agitation fix the gels for 20 minutes.

2. Rinse Step – 20 minutes

Decant the Fixative Enhancer Solution from the staining vessel. Rinse the gels in 400ml of deionised distilled water for 10 minutes with gentle agitation. After 10 minutes, decant water and replace with fresh rinse water. Rinse for an additional 10 minutes. Decant rinse water.

3. Staining and Developing Step – 20 minutes

Staining Solution Preparation and Procedure

The staining solution was prepared within 5 minutes of use.

Place 35ml deionised water into a large beaker and stir with a Teflon coated stirring bar. Add the following to the beaker in this order:

5.0 ml Silver complex solution

5.0 ml Reduction moderator solution

5.0 ml Image developer reagent

Immediately before use quickly add 50ml of the room temperature development accelerator solution to the beaker. Swirl well. Add the contents of the beaker to the staining vessel. Stain with gentle agitation. Stain the gels for approximately 20 minutes or until desired staining intensity is reached (Watch). It may take at least 15 minutes before the first bands become visible. After the desired staining is reached place the gels in 5% acetic acid to stop the reaction.

4. Stop Step – 15 minutes

Prepare a 5% acetic acid solution to stop the staining reaction. Place gels in stop solution for a minimum of 15 minutes. After stopping the reaction rinse the gels in high purity water for 5 minutes. The gels are then ready for imaging and storing.

This silver staining protocol is taken from Bio-Rad Silver Stain Plus technical data sheet (Bio-Rad, Catalog Number 161-0449).

Gel Plate Imaging and Analysis

Gels were then scanned using GeneSnap (Syngene) image acquisition software to produce a digital image. Gel plates were stored wet in plastic heat-sealed bags.

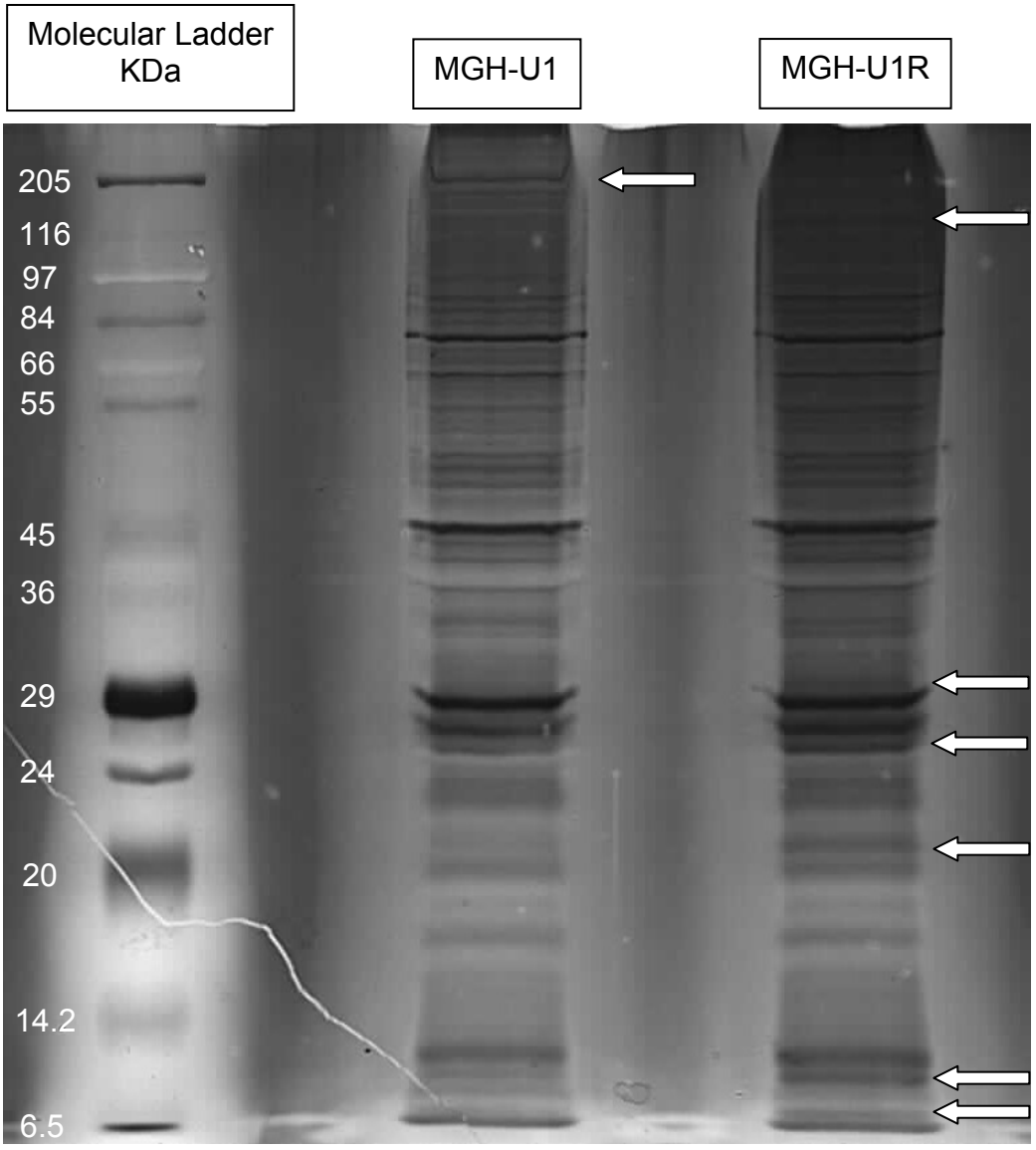

Figure 96: Analysis of differences in protein expression of MGH-U1 and MGH-UR cells (SDS Gel electrophoresis plate)

Very basic visual analysis reveals several differences of protein expression between sensitive and MDR cells from the same lineage. There are also many similarities in protein expression between samples. There appears to be a band of protein expression in the MGH-U1R cells between the 205 and 116KDa region which is likely to represent P-gp expression (170KDa). More detailed analysis using software packages such as GeneTools (Syngene) would have allowed more detailed analysis of the differences in the proteins expressed by each cell line. This software would allow identification of the molecular weight of the additional proteins expressed by the MDR cell line and quantify any differences in similar proteins expressed by each cell line.

Appendix 5: Co-injection of MDR cells with epirubicin and a sensitive cell cytosol extract

We postulated that our inability to demonstrate a mixed cell fusion may indicate some cytoplasmic-nuclear membrane interaction between sensitive cell cytoplasm and MDR nuclei, resulting in nuclear transport of epirubicin into MDR nuclei. We decided to co-inject epirubicin combined with a sensitive cell cytosol extract into MGH-U1R cells at 37^{o}C, to see if this reversed the nuclear sparing pattern of epirubicin uptake in MDR cells.

Method for cell cytosol preparation:

1. MGH-U1 (sensitive) cells were grown to confluence in a 75cm flask
2. Cells were then washed four times with PBS
3. Cells were harvested using a rubber policeman
4. Cells were pelleted by centrifuging at 1000rpm for 10 minutes and the supernatant was discarded
5. Cells were covered with 1ml of cold 0.02M TRIS buffer containing a protease inhibitor cocktail and agitated for 10 seconds every 5 minutes for 15 minutes
6. The sample was then centrifuged at 2000g for 20 minutes and the supernatant was transferred to an ultracentrifuge tube
7. The sample was then ultracentrifuged at 376,000g at 4C for 30 minutes.

The protease inhibitor cocktail used contained the following inhibitors:

AEBSF	104 millimolar	
Aprotinin	0.08 millimolar (80 micromolar)	
Leupeptin	2 millimolar	
Bestatin	4 millimolar	
Pepstatin A	1.5 millimolar	
E-64	1.4 millimolar	(Product No. 8340, Sigma, UK)

Method for injection:

MGH-U1R cells were cultured in low-sided 40mm Petri dishes (Orange Scientific, UK) until 50 – 75% confluent. Cell culture medium was changed to HEPES buffered medium (1:100 HEPES). The injection mixtured contained 0.05mls of epirubicin (2mg/ml), 0.1ml of a 77KDa FITC-dextran (1mg/ml) and 0.05mls of cytosol extract. This gave final concentrations of 0.5mg/ml for

epirubicin and FITC-dextran. These were then co-injected into the cytoplasm of MGH-U1R cells. The FITC-dextran allowed us to clearly identify our injected cell population. FITC-dextrans of 77KDa are ordinarily excluded from cells and cell nuclei, as they are too large to passively diffuse across these membranes. The injection buffer used was 48mM K_2HPO_4, 4.5mM KH_2PO_4, 14mM NaH_2PO_4, pH 7.2 (Eppendorf - personal communication). Once microinjected, cells were incubated for 60 minutes in normal culture conditions to allow cell recovery and time for epirubicin to distribute itself within the cells. Microinjected cells were then viewed by confocal microscopy. Injected cells were easily identified by their green FITC-dextran fluorescence, on direct fluorescence microscopy. Confocal microscopy allowed direct visualisation of the distribution of the various fluophores within the microinjected cells. Acridine orange (3µg/ml) stains the nuclei of viable cells green and was added after initial image capture in order to confirm cell viability.

Results:

The results of this experiment are shown below, with MGH-U1R cells showing a clear nuclear uptake pattern of epirubicin when microinjected with epirubicin in combination with sensitive cytosol extract. Cell viability was confirmed in all cells by strong nuclear acridine orange fluorescence.

These results suggest that some factor in sensitive cell cytosol allows epirubicin to gain entry into the nuclei of MDR cells. This may be a cytosolic nuclear transport factor which facilitated active transport of epirubicin or a protein that binds epirubicin and is recognised and transported by the NPCs of the MDR nucleus.

These experiments were uncontrolled, so clearly further work needs to be done to clarify the significance of these results. Future experiments would involve coinjecting epirubicin and similarly extracted resistant cell cytosol into MDR cells, to ensure that nuclear sparing of epirubicin uptake is preserved using the same technique.

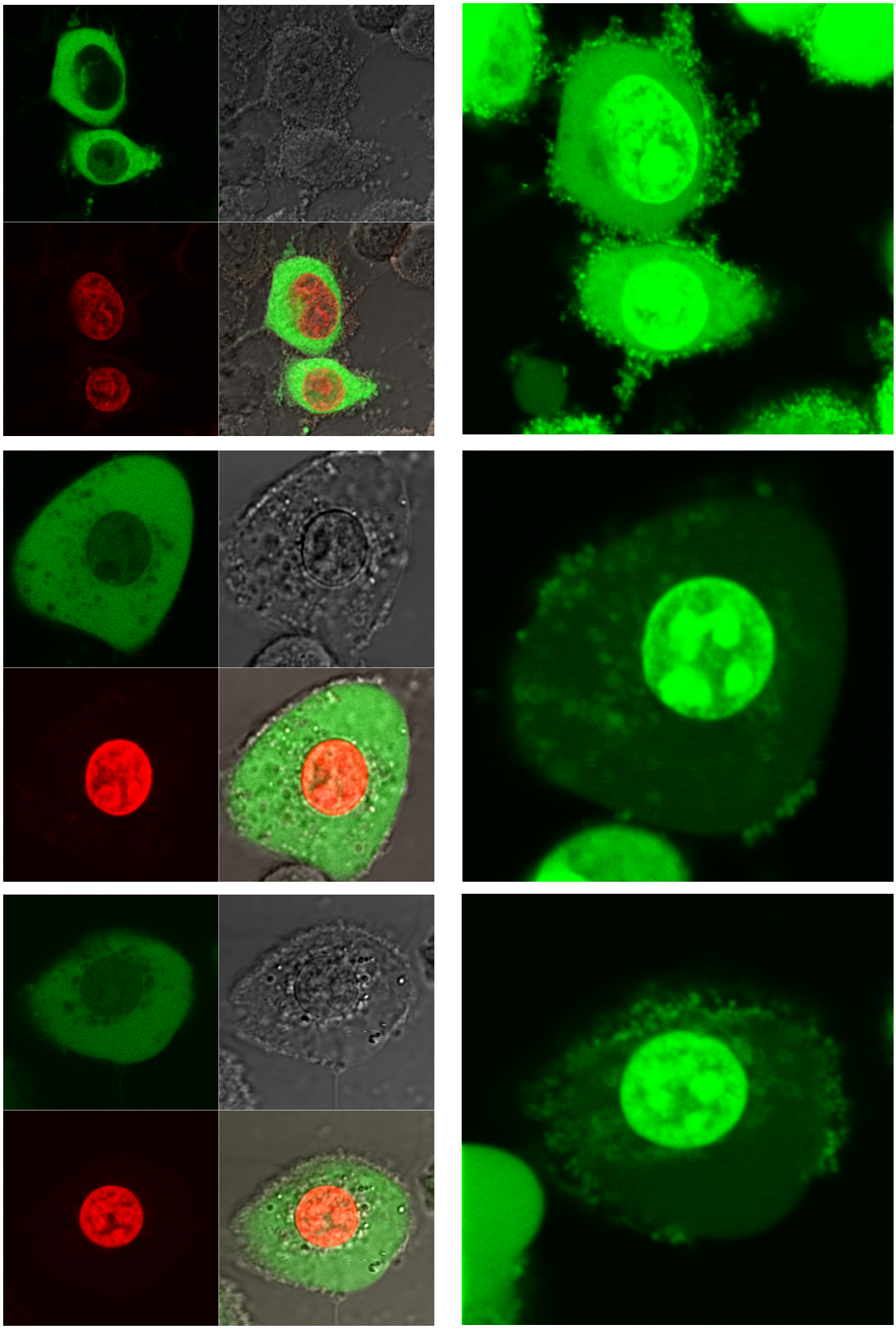

Figure 97: MGH-U1R cells co-injected with epirubicin and a sensitive cell cytosol extract showing string nuclear staining with epirubicin (Left hand side images). Viability of cells confirmed by strong nuclear acridine orange staining (Right hand side images).

References:

1 National Statistics. Series MB1 no.35: Cancer statistics registrations; Registrations of cancer diagnosed in 2004, England. 2005.
Ref Type: Report

2 National Statistics. Series DH2 no.31: Mortality Statistics Cause; Review of the Registrar General on deaths by cause, sex and age, in England and Wales, 2004. 2005.
Ref Type: Report

3 McLellan RA, French CG, Bell DG. Trends in the incidence of bladder cancer in Nova Scotia: a twenty-year perspective. *Can J Urol* 2003: **10**(3):1880-1884.

4 National Statistics. Cancer trends in England and Wales between 1950 and 1999. 2000.
Ref Type: Report

5 Matanoski GM, Elliott EA. Bladder cancer epidemiology. *Epidemiol Rev* 1981: **3**:203-229.

6 Rehn L. Blasengeschwultse bei fuchsinarbeitern. *Arch Clin Chir* 1895: **50**:588.

7 Hueper WC, Wiley FH, Wolfe HD. Experimental production of bladder tumours in dogs by administration of beta-naphthylamine. *J Industr Hyg Toxicol* 1938: **20**:46.

8 Case RAM, Hosker ME. Tumour of the urinary bladder as an occupational disease in the rubber industry in England and Wales. *Br J Prev Soc Med* 1954: **8**:39-50.

9 Case RAM, Hosker ME, McDonald DB, Pearson JT. Tumours of the urinary bladder in workmen engaged in the manufacture and use of certain dyestuff intermediates in the British chemical industry. *Brit J industr Med* 1954: **11**:75-104.

10 Johansson SL, Cohen SM. Epidemiology and etiology of bladder cancer. *Semin Surg Oncol* 1997: **13**(5):291-298.

11 Hoover R, Cole P. Population trends in cigarette smoking and bladder cancer. *Am J Epidemiol* 1971: **94**(5):409-418.

12 Talaska G, Schamer M, Skipper P, Tannenbaum S, Caporaso N, Unruh L et al. Detection of carcinogen-DNA adducts in exfoliated urothelial cells of cigarette smokers: association with smoking, hemoglobin adducts, and urinary mutagenicity. *Cancer Epidemiol Biomarkers Prev* 1991: **1**(1):61-66.

13 Talaska G, al Juburi AZ, Kadlubar FF. Smoking related carcinogen-DNA adducts in biopsy samples of human urinary bladder:

identification of N-(deoxyguanosin-8-yl)-4-aminobiphenyl as a major adduct. *Proc Natl Acad Sci U S A* 1991: **88**(12):5350-5354.

14 Cohen SM, Johansson SL. Epidemiology and etiology of bladder cancer. *Urol Clin North Am* 1992: **19**(3):421-428.

15 Wynder EL, Goldsmith R. The epidemiology of bladder cancer: a second look. *Cancer* 1977: **40**(3):1246-1268.

16 Sorahan T, Lancashire RJ, Sole G. Urothelial cancer and cigarette smoking: findings from a regional case-controlled study. *Br J Urol* 1994: **74**(6):753-756.

17 Brennan P, Bogillot O, Cordier S, Greiser E, Schill W, Vineis P et al. Cigarette smoking and bladder cancer in men: a pooled analysis of 11 case-control studies. *Int J Cancer* 2000: **86**(2):289-294.

18 Bengtsson U, Johansson S, Angervall L. Malignancies of the urinary tract and their relation to analgesic abuse. *Kidney Int* 1978: **13**(1):107-113.

19 Charbit L, Gendreau MC, Mee S, Cukier J. Tumors of the upper urinary tract: 10 years of experience. *J Urol* 1991: **146**(5):1243-1246.

20 Huben RP, Mounzer AM, Murphy GP. Tumor grade and stage as prognostic variables in upper tract urothelial tumors. *Cancer* 1988: **62**(9):2016-2020.

21 Worth PH. Cyclophosphamide and the bladder. *Br Med J* 1971: **3**(5767):182.

22 Travis LB, Curtis RE, Glimelius B, Holowaty EJ, van Leeuwen FE, Lynch CF et al. Bladder and kidney cancer following cyclophosphamide therapy for non-Hodgkin's lymphoma. *J Natl Cancer Inst* 1995: **87**(7):524-530.

23 Jung I, Messing E. Molecular mechanisms and pathways in bladder cancer development and progression. *Cancer Control* 2000: **7**(4):325-334.

24 Knowles MA. The genetics of transitional cell carcinoma: progress and potential clinical application. *BJU Int* 1999: **84**(4):412-427.

25 Knowles MA. Molecular pathogenesis of bladder cancer. *Int J Clin Oncol* 2008: **13**:287-297.

26 Coombs LM, Pigott DA, Sweeney E, Proctor AJ, Eydmann ME, Parkinson C et al. Amplification and over-expression of c-erbB-2 in transitional cell carcinoma of the urinary bladder. *Br J Cancer* 1991: **63**(4):601-608.

27 Sato K, Moriyama M, Mori S, Saito M, Watanuki T, Terada K et al. An immunohistologic evaluation of C-erbB-2 gene product in patients with urinary bladder carcinoma. *Cancer* 1992: **70**(10):2493-2498.

28 Sauter G, Moch H, Moore D, Carroll P, Kerschmann R, Chew K et al. Heterogeneity of erbB-2 gene amplification in bladder cancer. *Cancer Res* 1993: **53**(10 Suppl):2199-2203.

29 Underwood M, Bartlett J, Reeves J, Gardiner DS, Scott R, Cooke T. C-erbB-2 gene amplification: a molecular marker in recurrent bladder tumors? *Cancer Res* 1995: **55**(11):2422-2430.

30 Mellon JK, Lunec J, Wright C, Horne CH, Kelly P, Neal DE. C-erbB-2 in bladder cancer: molecular biology, correlation with epidermal growth factor receptors and prognostic value. *J Urol* 1996: **155**(1):321-326.

31 Mellon K, Wright C, Kelly P, Horne CH, Neal DE. Long-term outcome related to epidermal growth factor receptor status in bladder cancer. *J Urol* 1995: **153**(3 Pt 2):919-925.

32 Proctor AJ, Coombs LM, Cairns JP, Knowles MA. Amplification at chromosome 11q13 in transitional cell tumours of the bladder. *Oncogene* 1991: **6**(5):789-795.

33 Bringuier PP, Tamimi Y, Schuuring E, Schalken J. Expression of cyclin D1 and EMS1 in bladder tumours; relationship with chromosome 11q13 amplification. *Oncogene* 1996: **12**(8):1747-1753.

34 Oya M, Schmidt B, Schmitz-Drager BJ, Schulz WA. Expression of G1-->S transition regulatory molecules in human urothelial cancer. *Jpn J Cancer Res* 1998: **89**(7):719-726.

35 Shin KY, Kong G, Kim WS, Lee TY, Woo YN, Lee JD. Overexpression of cyclin D1 correlates with early recurrence in superficial bladder cancers. *Br J Cancer* 1997: **75**(12):1788-1792.

36 Masters JR, Vesey SG, Munn CF, Evan GI, Watson JV. c-myc oncoprotein levels in bladder cancer. *Urol Res* 1988: **16**(5):341-344.

37 Kotake T, Saiki S, Kinouchi T, Shiku H, Nakayama E. Detection of the c-myc gene product in urinary bladder cancer. *Jpn J Cancer Res* 1990: **81**(12):1198-1201.

38 Lipponen PK, Eskelinen MJ. Reduced expression of E-cadherin is related to invasive disease and frequent recurrence in bladder cancer. *J Cancer Res Clin Oncol* 1995: **121**(5):303-308.

39 Czerniak B, Deitch D, Simmons H, Etkind P, Herz F, Koss LG. Ha-ras gene codon 12 mutation and DNA ploidy in urinary bladder carcinoma. *Br J Cancer* 1990: **62**(5):762-763.

40 Meyers FJ, Gumerlock PH, Kokoris SP, deVere White RW, McCormick F. Human bladder and colon carcinomas contain activated ras p21. Specific detection of twelfth codon mutants. *Cancer* 1989: **63**(11):2177-2181.

41 Kallioniemi A, Kallioniemi OP, Citro G, Sauter G, DeVries S, Kerschmann R et al. Identification of gains and losses of DNA sequences in primary bladder cancer by comparative genomic hybridization. *Genes Chromosomes Cancer* 1995: **12**(3):213-219.

42 Richter J, Jiang F, Gorog JP, Sartorius G, Egenter C, Gasser TC et al. Marked genetic differences between stage pTa and stage pT1 papillary bladder cancer detected by comparative genomic hybridization. *Cancer Res* 1997: **57**(14):2860-2864.

43 Hovey RM, Chu L, Balazs M, DeVries S, Moore D, Sauter G et al. Genetic alterations in primary bladder cancers and their metastases. *Cancer Res* 1998: **58**(16):3555-3560.

44 Richter J, Beffa L, Wagner U, Schraml P, Gasser TC, Moch H et al. Patterns of chromosomal imbalances in advanced urinary bladder cancer detected by comparative genomic hybridization. *Am J Pathol* 1998: **153**(5):1615-1621.

45 Cordon-Cardo C, Wartinger D, Petrylak D, Dalbagni G, Fair WR, Fuks Z et al. Altered expression of the retinoblastoma gene product: prognostic indicator in bladder cancer. *J Natl Cancer Inst* 1992: **84**(16):1251-1256.

46 Logothetis CJ, Xu HJ, Ro JY, Hu SX, Sahin A, Ordonez N et al. Altered expression of retinoblastoma protein and known prognostic variables in locally advanced bladder cancer. *J Natl Cancer Inst* 1992: **84**(16):1256-1261.

47 Xu HJ, Cairns P, Hu SX, Knowles MA, Benedict WF. Loss of RB protein expression in primary bladder cancer correlates with loss of heterozygosity at the RB locus and tumor progression. *Int J Cancer* 1993: **53**(5):781-784.

48 Grossman HB, Liebert M, Antelo M, Dinney CP, Hu SX, Palmer JL et al. p53 and RB expression predict progression in T1 bladder cancer. *Clin Cancer Res* 1998: **4**(4):829-834.

49 Cote RJ, Dunn MD, Chatterjee SJ, Stein JP, Shi SR, Tran QC et al. Elevated and absent pRb expression is associated with bladder cancer progression and has cooperative effects with p53. *Cancer Res* 1998: **58**(6):1090-1094.

50 Olumi AF, Tsai YC, Nichols PW, Skinner DG, Cain DR, Bender LI et al. Allelic loss of chromosome 17p distinguishes high grade from

low grade transitional cell carcinomas of the bladder. *Cancer Res* 1990: **50**(21):7081-7083.

51 Wright C, Mellon K, Johnston P, Lane DP, Harris AL, Horne CH et al. Expression of mutant p53, c-erbB-2 and the epidermal growth factor receptor in transitional cell carcinoma of the human urinary bladder. *Br J Cancer* 1991: **63**(6):967-970.

52 Habuchi T, Ogawa O, Kakehi Y, Ogura K, Koshiba M, Sugiyama T et al. Allelic loss of chromosome 17p in urothelial cancer: strong association with invasive phenotype. *J Urol* 1992: **148**(5):1595-1599.

53 Lorenzo-Romero JG, Salinas-Sanchez AS, Gimenez-Bachs JM, Sanchez-Sanchez F, Escribano-Martinez J, Segura-Martin M et al. Prognostic implications of p53 gene mutations in bladder tumors. *J Urol* 2003: **169**(2):492-499.

54 Esrig D, Elmajian D, Groshen S, Freeman JA, Stein JP, Chen SC et al. Accumulation of nuclear p53 and tumor progression in bladder cancer. *N Engl J Med* 1994: **331**(19):1259-1264.

55 Ow K, Delprado W, Fisher R, Barrett J, Yu Y, Jackson P et al. Relationship between expression of the KAI1 metastasis suppressor and other markers of advanced bladder cancer. *J Pathol* 2000: **191**(1):39-47.

56 Jackson P, Kingsley EA, Russell PJ. Inverse correlation between KAI1 mRNA levels and invasive behaviour in bladder cancer cell lines. *Cancer Lett* 2000: **156**(1):9-17.

57 Tsai YC, Nichols PW, Hiti AL, Williams Z, Skinner DG, Jones PA. Allelic losses of chromosomes 9, 11, and 17 in human bladder cancer. *Cancer Res* 1990: **50**(1):44-47.

58 Orlow I, Lacombe L, Hannon GJ, Serrano M, Pellicer I, Dalbagni G et al. Deletion of the p16 and p15 genes in human bladder tumors. *J Natl Cancer Inst* 1995: **87**(20):1524-1529.

59 Balazs M, Carroll P, Kerschmann R, Sauter G, Waldman FM. Frequent homozygous deletion of cyclin-dependent kinase inhibitor 2 (MTS1, p16) in superficial bladder cancer detected by fluorescence in situ hybridization. *Genes Chromosomes Cancer* 1997: **19**(2):84-89.

60 Cheng L, Bostwick DG, Li G, Zhang S, Vortmeyer AO, Zhuang Z. Conserved genetic findings in metastatic bladder cancer: a possible utility of allelic loss of chromosomes 9p21 and 17p13 in diagnosis. *Arch Pathol Lab Med* 2001: **125**(9):1197-1199.

61 Cairns P, Evron E, Okami K, Halachmi N, Esteller M, Herman JG et al. Point mutation and homozygous deletion of PTEN/MMAC1 in primary bladder cancers. *Oncogene* 1998: **16**(24):3215-3218.

62 Aveyard JS, Skilleter A, Habuchi T, Knowles MA. Somatic mutation of PTEN in bladder carcinoma. *Br J Cancer* 1999: **80**(5-6):904-908.

63 McLellan RA, Oscarson M, Alexandrie AK, Seidegard J, Evans DA, Rannug A et al. Characterization of a human glutathione S-transferase mu cluster containing a duplicated GSTM1 gene that causes ultrarapid enzyme activity. *Mol Pharmacol* 1997: **52**(6):958-965.

64 Board P, Coggan M, Johnston P, Ross V, Suzuki T, Webb G. Genetic heterogeneity of the human glutathione transferases: a complex of gene families. *Pharmacol Ther* 1990: **48**(3):357-369.

65 Bell DA, Taylor JA, Paulson DF, Robertson CN, Mohler JL, Lucier GW. Genetic risk and carcinogen exposure: a common inherited defect of the carcinogen-metabolism gene glutathione S-transferase M1 (GSTM1) that increases susceptibility to bladder cancer. *J Natl Cancer Inst* 1993: **85**(14):1159-1164.

66 Brockmoller J, Kerb R, Drakoulis N, Staffeldt B, Roots I. Glutathione S-transferase M1 and its variants A and B as host factors of bladder cancer susceptibility: a case-control study. *Cancer Res* 1994: **54**(15):4103-4111.

67 Hirata Y, Orth DN. Epidermal growth factor (urogastrone) in human fluids: size heterogeneity. *J Clin Endocrinol Metab* 1979: **48**(4):673-679.

68 Messing EM, Murphy-Brooks N. Recovery of epidermal growth factor in voided urine of patients with bladder cancer. *Urology* 1994: **44**(4):502-506.

69 Messing EM, Hanson P, Ulrich P, Erturk E. Epidermal growth factor--interactions with normal and malignant urothelium: in vivo and in situ studies. *J Urol* 1987: **138**(5):1329-1335.

70 Rao JY, Hemstreet GP, III, Hurst RE, Bonner RB, Jones PL, Min KW et al. Alterations in phenotypic biochemical markers in bladder epithelium during tumorigenesis. *Proc Natl Acad Sci U S A* 1993: **90**(17):8287-8291.

71 Theodorescu D, Laderoute KR, Calaoagan JM, Guilding KM. Inhibition of human bladder cancer cell motility by genistein is dependent on epidermal growth factor receptor but not p21ras gene expression. *Int J Cancer* 1998: **78**(6):775-782.

72 Bringuier PP, Umbas R, Schaafsma HE, Karthaus HF, Debruyne FM, Schalken JA. Decreased E-cadherin immunoreactivity correlates with poor survival in patients with bladder tumors. *Cancer Res* 1993: **53**(14):3241-3245.

73 Shimazui T, Schalken JA, Giroldi LA, Jansen CF, Akaza H, Koiso K et al. Prognostic value of cadherin-associated molecules (alpha-, beta-, and gamma-catenins and p120cas) in bladder tumors. *Cancer Res* 1996: **56**(18):4154-4158.

74 Liebert M, Washington R, Wedemeyer G, Carey TE, Grossman HB. Loss of co-localization of alpha 6 beta 4 integrin and collagen VII in bladder cancer. *Am J Pathol* 1994: **144**(4):787-795.

75 Folkman J, Cole P, Zimmerman S. Tumor behavior in isolated perfused organs: in vitro growth and metastases of biopsy material in rabbit thyroid and canine intestinal segment. *Ann Surg* 1966: **164**(3):491-502.

76 Folkman J, Klagsbrun M. Angiogenic factors. *Science* 1987: **235**(4787):442-447.

77 Dickinson AJ, Fox SB, Persad RA, Hollyer J, Sibley GN, Harris AL. Quantification of angiogenesis as an independent predictor of prognosis in invasive bladder carcinomas. *Br J Urol* 1994: **74**(6):762-766.

78 Bochner BH, Cote RJ, Weidner N, Groshen S, Chen SC, Skinner DG et al. Angiogenesis in bladder cancer: relationship between microvessel density and tumor prognosis. *J Natl Cancer Inst* 1995: **87**(21):1603-1612.

79 Guirguis R, Schiffmann E, Liu B, Birkbeck D, Engel J, Liotta L. Detection of autocrine motility factor in urine as a marker of bladder cancer. *J Natl Cancer Inst* 1988: **80**(15):1203-1211.

80 Lokeshwar VB, Obek C, Soloway MS, Block NL. Tumor-associated hyaluronic acid: a new sensitive and specific urine marker for bladder cancer. *Cancer Res* 1997: **57**(4):773-777.

81 Grossfeld GD, Ginsberg DA, Stein JP, Bochner BH, Esrig D, Groshen S et al. Thrombospondin-1 expression in bladder cancer: association with p53 alterations, tumor angiogenesis, and tumor progression. *J Natl Cancer Inst* 1997: **89**(3):219-227.

82 Mohr DN, Offord KP, Owen RA, Melton LJ, III. Asymptomatic microhematuria and urologic disease. A population-based study. *JAMA* 1986: **256**(2):224-229.

83 Canadian task force on the period health examination: the period health examination. *Can Med Assoc J* 1994: **130**:1278-1285.

84 Badalament RA, Fair WR, Whitmore WF, Jr., Melamed MR. The relative value of cytometry and cytology in the management of bladder cancer: the Memorial Sloan-Kettering Cancer Center experience. *Semin Urol* 1988: **6**(1):22-30.

85 Shaaban AA, Tribukait B, el Bedeiwy AF, Ghoneim MA. Prediction of lymph node metastases in bladder carcinoma with deoxyribonucleic acid flow cytometry. *J Urol* 1990: **144**(4):884-887.

86 Soloway MS, Murphy W, Rao MK, Cox C. Serial multiple-site biopsies in patients with bladder cancer. *J Urol* 1978: **120**(1):57-59.

87 Kiemeney LA, Witjes JA, Heijbroek RP, Koper NP, Verbeek AL, Debruyne FM. Should random urothelial biopsies be taken from patients with primary superficial bladder cancer? A decision analysis. Members of the Dutch South-East Co-Operative Urological Group. *Br J Urol* 1994: **73**(2):164-171.

88 Oosterlinck W, Kurth KH, Schroder F, Sylvester R, Hammond B. A plea for cold biopsy, fulguration and immediate bladder instillation with Epirubicin in small superficial bladder tumors. Data from the EORTC GU Group Study 30863. *Eur Urol* 1993: **23**(4):457-459.

89 Solsona E, Iborra I, Ricos JV, Dumont R, Casanova JL, Calabuig C. Upper urinary tract involvement in patients with bladder carcinoma in situ (Tis): its impact on management. *Urology* 1997: **49**(3):347-352.

90 Malmstrom PU, Lonnemark M, Busch C, Magnusson A. Staging of bladder carcinoma by computer tomography-guided transmural core biopsy. *Scand J Urol Nephrol* 1993: **27**(2):193-198.

91 Davey P, Merrick MV, Duncan W, Redpath AT. Bladder cancer: the value of routine bone scintigraphy. *Clin Radiol* 1985: **36**(1):77-79.

92 Sobin DH, Wittekind C. TNM Classification of Malignant Tumours, 6th ed. New York: Wiley-Liss, 2002.

93 Waters WB. Invasive bladder cancer--where do we go from here? *J Urol* 1996: **155**(6):1910-1911.

94 Herr HW. Tumour progression and survival in patients with T1G3 bladder tumours: 15-year outcome. *Br J Urol* 1997: **80**(5):762-765.

95 Cookson MS, Herr HW, Zhang ZF, Soloway S, Sogani PC, Fair WR. The treated natural history of high risk superficial bladder cancer: 15-year outcome. *J Urol* 1997: **158**(1):62-67.

96 Soloway MS. Evaluation and management of patients with superficial bladder cancer. *Urol Clin North Am* 1987: **14**(4):771-780.

97 Althausen AF, Prout GR, Jr., Daly JJ. Non-invasive papillary carcinoma of the bladder associated with carcinoma in situ. *J Urol* 1976: **116**(5):575-580.

98 Epstein JI, Amin MB, Reuter VR, Mostofi FK. The World Health Organization/International Society of Urological Pathology consensus

classification of urothelial (transitional cell) neoplasms of the urinary bladder. Bladder Consensus Conference Committee. *Am J Surg Pathol* 1998: **22**(12):1435-1448.

99 Sauter G, Alagaba F, Amin M, Busch G, Cheville J, Gasser T et al. Tumours of the urinary system: non-invasive urothelial neoplasias. In: Eble JN, Sauter G, Epstein JI, Sesterhenn I, eds, WHO classification of classification of tumours of the urinary system and male genital organs. Lyon: IARCC Press, 2004: 29-34.

100 Abel PD, Hall RR, Williams G. Should pT1 transitional cell cancers of the bladder still be classified as superficial? *Br J Urol* 1988: **62**(3):235-239.

101 Birch BR, Harland SJ. The pT1 G3 bladder tumour. *Br J Urol* 1989: **64**(2):109-116.

102 Mulders PF, Hoekstra WJ, Heybroek RP, Schapers ER, Verbeek AL, Oosterhof GO et al. Prognosis and treatment of T1G3 bladder tumours. A prognostic factor analysis of 121 patients. Dutch South Eastern Bladder Cancer Study Group. *Eur J Cancer* 1994: **30A**(7):914-917.

103 Sylvester RJ, van der Meijden AP, Oosterlinck W, Witjes JA, Bouffioux C, Denis L et al. Predicting recurrence and progression in individual patients with stage Ta T1 bladder cancer using EORTC risk tables: a combined analysis of 2596 patients from seven EORTC trials. *Eur Urol* 2006: **49**(3):466-5.

104 Pawinski A, Sylvester R, Kurth KH, Bouffioux C, Van Der MA, Parmar MK et al. A combined analysis of European Organization for Research and Treatment of Cancer, and Medical Research Council randomized clinical trials for the prophylactic treatment of stage TaT1 bladder cancer. European Organization for Research and Treatment of Cancer Genitourinary Tract Cancer Cooperative Group and the Medical Research Council Working Party on Superficial Bladder Cancer. *J Urol* 1996: **156**(6):1934-40, discussion.

105 Kurth KH, Denis L, Bouffioux C, Sylvester R, Debruyne FM, Pavone-Macaluso M et al. Factors affecting recurrence and progression in superficial bladder tumours. *Eur J Cancer* 1995: **31A**(11):1840-1846.

106 Parmar MK, Freedman LS, Hargreave TB, Tolley DA. Prognostic factors for recurrence and followup policies in the treatment of superficial bladder cancer: report from the British Medical Research Council Subgroup on Superficial Bladder Cancer (Urological Cancer Working Party). *J Urol* 1989: **142**(2 Pt 1):284-288.

107 Kurth K, Denis L, Sylvester R, de Pauw M. The natural history and the prognosis of treated superficial bladder cancer. EORTC GU Group. *Prog Clin Biol Res* 1992: **378**:1-7.

108 Allard P, Bernard P, Fradet Y, Tetu B. The early clinical course of primary Ta and T1 bladder cancer: a proposed prognostic index. *Br J Urol* 1998: **81**(5):692-698.

109 Fujii Y, Fukui I, Kihara K, Tsujii T, Ishizaka K, Kageyama Y et al. Significance of bladder neck involvement on progression in superficial bladder cancer. *Eur Urol* 1998: **33**(5):464-468.

110 Tolley DA, Parmar MK, Grigor KM, Lallemand G, Benyon LL, Fellows J et al. The effect of intravesical mitomycin C on recurrence of newly diagnosed superficial bladder cancer: a further report with 7 years of follow up. *J Urol* 1996: **155**(4):1233-1238.

111 Oosterlinck W, Kurth KH, Schroder F, Bultinck J, Hammond B, Sylvester R. A prospective European Organization for Research and Treatment of Cancer Genitourinary Group randomized trial comparing transurethral resection followed by a single intravesical instillation of epirubicin or water in single stage Ta, T1 papillary carcinoma of the bladder. *J Urol* 1993: **149**(4):749-752.

112 Bouffioux C, Kurth KH, Bono A, Oosterlinck W, Kruger CB, de Pauw M et al. Intravesical adjuvant chemotherapy for superficial transitional cell bladder carcinoma: results of 2 European Organization for Research and Treatment of Cancer randomized trials with mitomycin C and doxorubicin comparing early versus delayed instillations and short-term versus long-term treatment. European Organization for Research and Treatment of Cancer Genitourinary Group. *J Urol* 1995: **153**(3 Pt 2):934-941.

113 Lamm DL, Blumenstein BA, Crawford ED, Montie JE, Scardino P, Grossman HB et al. A randomized trial of intravesical doxorubicin and immunotherapy with bacille Calmette-Guerin for transitional-cell carcinoma of the bladder. *N Engl J Med* 1991: **325**(17):1205-1209.

114 Malmstrom PU, Wijkstrom H, Lundholm C, Wester K, Busch C, Norlen BJ. 5-year followup of a randomized prospective study comparing mitomycin C and bacillus Calmette-Guerin in patients with superficial bladder carcinoma. Swedish-Norwegian Bladder Cancer Study Group. *J Urol* 1999: **161**(4):1124-1127.

115 Herr HW, Laudone VP, Badalament RA, Oettgen HF, Sogani PC, Freedman BD et al. Bacillus Calmette-Guerin therapy alters the progression of superficial bladder cancer. *J Clin Oncol* 1988: **6**(9):1450-1455.

116 Lamm DL, Blumenstein BA, Crissman JD, Montie JE, Gottesman JE, Lowe BA et al. Maintenance bacillus Calmette-Guerin immunotherapy for recurrent TA, T1 and carcinoma in situ transitional cell carcinoma of the bladder: a randomized Southwest Oncology Group Study. *J Urol* 2000: **163**(4):1124-1129.

117 Pagano F, Bassi P, Piazza N, Abatangelo G, Drago Ferrante GL, Milani C. Improving the efficacy of BCG immunotherapy by dose reduction. *Eur Urol* 1995: **27 Suppl 1**:19-22.

118 Martinez-Pineiro JA, Solsona E, Flores N, Isorna S. Improving the safety of BCG immunotherapy by dose reduction. Cooperative Group CUETO. *Eur Urol* 1995: **27 Suppl 1**:13-18.

119 Mack D, Frick J. Low-dose bacille Calmette-Guerin (BCG) therapy in superficial high-risk bladder cancer: a phase II study with the BCG strain Connaught Canada. *Br J Urol* 1995: **75**(2):185-187.

120 Lamm DL. Long-term results of intravesical therapy for superficial bladder cancer. *Urol Clin North Am* 1992: **19**(3):573-580.

121 Klan R, Loy V, Huland H. Residual tumor discovered in routine second transurethral resection in patients with stage T1 transitional cell carcinoma of the bladder. *J Urol* 1991: **146**(2):316-318.

122 Abel PD. Follow-up of patients with "superficial" transitional cell carcinoma of the bladder: the case for a change in policy. *Br J Urol* 1993: **72**(2):135-142.

123 Morris SB, Gordon EM, Shearer RJ, Woodhouse CR. Superficial bladder cancer: for how long should a tumour-free patient have check cystoscopies? *Br J Urol* 1995: **75**(2):193-196.

124 Holmang S, Hedelin H, Anderstrom C, Johansson SL. The relationship among multiple recurrences, progression and prognosis of patients with stages Ta and T1 transitional cell cancer of the bladder followed for at least 20 years. *J Urol* 1995: **153**(6):1823-1826.

125 Thompson RA, Jr., Campbell EW, Jr., Kramer HC, Jacobs SC, Naslund MJ. Late invasive recurrence despite long-term surveillance for superficial bladder cancer. *J Urol* 1993: **149**(5):1010-1011.

126 Frazier HA, Robertson JE, Dodge RK, Paulson DF. The value of pathologic factors in predicting cancer-specific survival among patients treated with radical cystectomy for transitional cell carcinoma of the bladder and prostate. *Cancer* 1993: **71**(12):3993-4001.

127 Ghoneim MA, el Mekresh MM, el Baz MA, el Attar IA, Ashamallah A. Radical cystectomy for carcinoma of the bladder: critical evaluation of the results in 1,026 cases. *J Urol* 1997: **158**(2):393-399.

128 Hellsten S, Rintala E, Wahlqvist R, Malmstrom PU. Nordic prospective trials of radical cystectomy and neoadjuvant chemotherapy. The Nordic Cooperative Bladder Cancer Study Group. *Eur Urol* 1998: **33 Suppl 4**:35-38.

129 Neoadjuvant cisplatin, methotrexate, and vinblastine chemotherapy for muscle-invasive bladder cancer: a randomised

controlled trial. International collaboration of trialists. *Lancet* 1999: **354**(9178):533-540.

130 Johnson DE, Lamy SM. Complications of a single stage radical cystectomy and ileal conduit diversion: review of 214 cases. *J Urol* 1977: **117**(2):171-173.

131 Frazier HA, Robertson JE, Paulson DF. Complications of radical cystectomy and urinary diversion: a retrospective review of 675 cases in 2 decades. *J Urol* 1992: **148**(5):1401-1405.

132 Bjerre BD, Johansen C, Steven K. Sexological problems after cystectomy: bladder substitution compared with ileal conduit diversion. A questionnaire study of male patients. *Scand J Urol Nephrol* 1998: **32**(3):187-193.

133 Pagano F, Bassi P, Galetti TP, Meneghini A, Milani C, Artibani W et al. Results of contemporary radical cystectomy for invasive bladder cancer: a clinicopathological study with an emphasis on the inadequacy of the tumor, nodes and metastases classification. *J Urol* 1991: **145**(1):45-50.

134 Thrasher JB, Frazier HA, Robertson JE, Paulson DF. Does of stage pT0 cystectomy specimen confer a survival advantage in patients with minimally invasive bladder cancer? *J Urol* 1994: **152**(2 Pt 1):393-396.

135 Waehre H, Ous S, Klevmark B, Kvarstein B, Urnes T, Ogreid P et al. A bladder cancer multi-institutional experience with total cystectomy for muscle-invasive bladder cancer. *Cancer* 1993: **72**(10):3044-3051.

136 Bassi P, Ferrante GD, Piazza N, Spinadin R, Carando R, Pappagallo G et al. Prognostic factors of outcome after radical cystectomy for bladder cancer: a retrospective study of a homogeneous patient cohort. *J Urol* 1999: **161**(5):1494-1497.

137 Bernardini S, Adessi GL, Billerey C, Chezy E, Carbillet JP, Bittard H. Immunohistochemical detection of p53 protein overexpression versus gene sequencing in urinary bladder carcinomas. *J Urol* 1999: **162**(4):1496-1501.

138 Gao JP, Uchida T, Wang C, Jiang SX, Matsumoto K, Satoh T et al. Relationship between p53 gene mutation and protein expression: clinical significance in transitional cell carcinoma of the bladder. *Int J Oncol* 2000: **16**(3):469-475.

139 Mead GM, Roberts JT. The role of the nonsurgical oncologist in the management of advanced transitional cell cancer. Part I: locally advanced disease. *BJU Int* 2004: **94**(7):977-980.

140 Duncan W, Williams JR, Kerr GR, Arnott SJ, Quilty PM, Rodger A et al. An analysis of the radiation related morbidity observed in a randomized trial of neutron therapy for bladder cancer. *Int J Radiat Oncol Biol Phys* 1986: **12**(12):2085-2092.

141 Gospodarowicz MK, Hawkins NV, Rawlings GA, Connolly JG, Jewett MA, Thomas GM et al. Radical radiotherapy for muscle invasive transitional cell carcinoma of the bladder: failure analysis. *J Urol* 1989: **142**(6):1448-1453.

142 Smaaland R, Akslen LA, Tonder B, Mehus A, Lote K, Albrektsen G. Radical radiation treatment of invasive and locally advanced bladder carcinoma in elderly patients. *Br J Urol* 1991: **67**(1):61-69.

143 Quilty PM, Duncan W. Primary radical radiotherapy for T3 transitional cell cancer of the bladder: an analysis of survival and control. *Int J Radiat Oncol Biol Phys* 1986: **12**(6):853-860.

144 Sauer R, Dunst J, Altendorf-Hofmann A, Fischer H, Bornhof C, Schrott KM. Radiotherapy with and without cisplatin in bladder cancer. *Int J Radiat Oncol Biol Phys* 1990: **19**(3):687-691.

145 Little FA, Howard GC. Sexual function following radical radiotherapy for bladder cancer. *Radiother Oncol* 1998: **49**(2):157-161.

146 Pollack A, Zagars GZ. Radiotherapy for stage T3b transitional cell carcinoma of the bladder. *Semin Urol Oncol* 1996: **14**(2):86-95.

147 Greven KM, Solin LJ, Hanks GE. Prognostic factors in patients with bladder carcinoma treated with definitive irradiation. *Cancer* 1990: **65**(4):908-912.

148 Borgaonkar S, Jain A, Bollina P, McLaren DB, Tulloch D, Kerr GR et al. Radical radiotherapy and salvage cystectomy as the primary management of transitional cell carcinoma of the bladder. Results following the introduction of a CT planning technique. *Clin Oncol (R Coll Radiol)* 2002: **14**(2):141-147.

149 Rodel C, Grabenbauer GG, Kuhn R, Papadopoulos T, Dunst J, Meyer M et al. Combined-modality treatment and selective organ preservation in invasive bladder cancer: long-term results. *J Clin Oncol* 2002: **20**(14):3061-3071.

150 Gschwend JE, May F, Paiss T, Gottfried HW, Hautmann RE. High-dose pelvic irradiation followed by ileal neobladder urinary diversion: complications and long-term results. *Br J Urol* 1996: **77**(5):680-683.

151 Sengelov L, Klintorp S, Havsteen H, Kamby C, Hansen SL, von der MH. Treatment outcome following radiotherapy in elderly patients with bladder cancer. *Radiother Oncol* 1997: **44**(1):53-58.

152 Arias F, Duenas M, Martinez E, Dominguez MA, Illarramendi JJ, Villafranca E et al. Radical chemoradiotherapy for elderly patients with bladder carcinoma invading muscle. *Cancer* 1997: **80**(1):115-120.

153 Hoskin PJ, Saunders MI, Phillips H, Cladd H, Powell ME, Goodchild K et al. Carbogen and nicotinamide in the treatment of bladder cancer with radical radiotherapy. *Br J Cancer* 1997: **76**(2):260-263.

154 Coppin CM, Gospodarowicz MK, James K, Tannock IF, Zee B, Carson J et al. Improved local control of invasive bladder cancer by concurrent cisplatin and preoperative or definitive radiation. The National Cancer Institute of Canada Clinical Trials Group. *J Clin Oncol* 1996: **14**(11):2901-2907.

155 Jakse G, Frommhold H, zur ND. Combined radiation and chemotherapy for locally advanced transitional cell carcinoma of the urinary bladder. *Cancer* 1985: **55**(8):1659-1664.

156 Sauer R, Birkenhake S, Kuhn R, Wittekind C, Schrott KM, Martus P. Efficacy of radiochemotherapy with platin derivatives compared to radiotherapy alone in organ-sparing treatment of bladder cancer. *Int J Radiat Oncol Biol Phys* 1998: **40**(1):121-127.

157 Neoadjuvant chemotherapy in invasive bladder cancer: a systematic review and meta-analysis. *Lancet* 2003: **361**(9373):1927-1934.

158 Sternberg CN, Raghaven D, Ohi Y, Bajorin D, Herr H, Kato T et al. Neoadjuvant and adjuvant chemotherapy in advanced disease--what are the effects on survival and prognosis? *Int J Urol* 1995: **2 Suppl 2**:76-88.

159 von der MH, Sengelov L, Roberts JT, Ricci S, Dogliotti L, Oliver T et al. Long-term survival results of a randomized trial comparing gemcitabine plus cisplatin, with methotrexate, vinblastine, doxorubicin, plus cisplatin in patients with bladder cancer. *J Clin Oncol* 2005: **23**(21):4602-4608.

160 Donat SM, Herr HW, Bajorin DF, Fair WR, Sogani PC, Russo P et al. Methotrexate, vinblastine, doxorubicin and cisplatin chemotherapy and cystectomy for unresectable bladder cancer. *J Urol* 1996: **156**(2 Pt 1):368-371.

161 Duchesne GM, Bolger JJ, Griffiths GO, Trevor RJ, Graham JD, Hoskin PJ et al. A randomized trial of hypofractionated schedules of palliative radiotherapy in the management of bladder carcinoma: results of medical research council trial BA09. *Int J Radiat Oncol Biol Phys* 2000: **47**(2):379-388.

162 Grossman HB, Natale RB, Tangen CM, Speights VO, Vogelzang NJ, Trump DL et al. Neoadjuvant chemotherapy plus

cystectomy compared with cystectomy alone for locally advanced bladder cancer. *N Engl J Med* 2003: **349**(9):859-866.

163 Splinter TA, Scher HI, Denis L, Bukowski R, Simon S, Klimberg I et al. The prognostic value of the pathological response to combination chemotherapy before cystectomy in patients with invasive bladder cancer. European Organization for Research on Treatment of Cancer--Genitourinary Group. *J Urol* 1992: **147**(3):606-608.

164 Sternberg CN, Pansadoro V, Calabro F, Marini L, van Rijn A, Carli PD et al. Neo-adjuvant chemotherapy and bladder preservation in locally advanced transitional cell carcinoma of the bladder. *Ann Oncol* 1999: **10**(11):1301-1305.

165 Herr HW, Bajorin DF, Scher HI. Neoadjuvant chemotherapy and bladder-sparing surgery for invasive bladder cancer: ten-year outcome. *J Clin Oncol* 1998: **16**(4):1298-1301.

166 Kachnic LA, Kaufman DS, Heney NM, Althausen AF, Griffin PP, Zietman AL et al. Bladder preservation by combined modality therapy for invasive bladder cancer. *J Clin Oncol* 1997: **15**(3):1022-1029.

167 Tester W, Caplan R, Heaney J, Venner P, Whittington R, Byhardt R et al. Neoadjuvant combined modality program with selective organ preservation for invasive bladder cancer: results of Radiation Therapy Oncology Group phase II trial 8802. *J Clin Oncol* 1996: **14**(1):119-126.

168 Tester W, Porter A, Asbell S, Coughlin C, Heaney J, Krall J et al. Combined modality program with possible organ preservation for invasive bladder carcinoma: results of RTOG protocol 85-12. *Int J Radiat Oncol Biol Phys* 1993: **25**(5):783-790.

169 Orsatti M, Curotto A, Canobbio L, Guarneri D, Scarpati D, Venturini M et al. Alternating chemo-radiotherapy in bladder cancer: a conservative approach. *Int J Radiat Oncol Biol Phys* 1995: **33**(1):173-178.

170 Shipley WU, Winter KA, Kaufman DS, Lee WR, Heney NM, Tester WR et al. Phase III trial of neoadjuvant chemotherapy in patients with invasive bladder cancer treated with selective bladder preservation by combined radiation therapy and chemotherapy: initial results of Radiation Therapy Oncology Group 89-03. *J Clin Oncol* 1998: **16**(11):3576-3583.

171 Logothetis CJ, Johnson DE, Chong C, Dexeus FH, Sella A, Ogden S et al. Adjuvant cyclophosphamide, doxorubicin, and cisplatin chemotherapy for bladder cancer: an update. *J Clin Oncol* 1988: **6**(10):1590-1596.

172 Logothetis CJ, Johnson DE, Chong C, Dexeus FH, Ogden S, von Eschenbach A et al. Adjuvant chemotherapy of bladder cancer: a preliminary report. *J Urol* 1988: **139**(6):1207-1211.

173 Skinner DG, Daniels JR, Russell CA, Lieskovsky G, Boyd SD, Nichols P et al. The role of adjuvant chemotherapy following cystectomy for invasive bladder cancer: a prospective comparative trial. *J Urol* 1991: **145**(3):459-464.

174 Stockle M, Meyenburg W, Wellek S, Voges G, Gertenbach U, Thuroff JW et al. Advanced bladder cancer (stages pT3b, pT4a, pN1 and pN2): improved survival after radical cystectomy and 3 adjuvant cycles of chemotherapy. Results of a controlled prospective study. *J Urol* 1992: **148**(2 Pt 1):302-306.

175 Freiha F, Reese J, Torti FM. A randomized trial of radical cystectomy versus radical cystectomy plus cisplatin, vinblastine and methotrexate chemotherapy for muscle invasive bladder cancer. *J Urol* 1996: **155**(2):495-499.

176 Huncharek M, Muscat J, Geschwind JF. Planned preoperative radiation therapy in muscle invasive bladder cancer; results of a meta-analysis. *Anticancer Res* 1998: **18**(3B):1931-1934.

177 Zeegers MP, Kellen E, Buntinx F, van den Brandt PA. The association between smoking, beverage consumption, diet and bladder cancer: a systematic literature review. *World J Urol* 2004: **21**(6):392-401.

178 Bochner BH, Kattan MW, Vora KC. Postoperative nomogram predicting risk of recurrence after radical cystectomy for bladder cancer. *J Clin Oncol* 2006: **24**(24):3967-3972.

179 Glick SH, Howell LP, White RW. Relationship of p53 and bcl-2 to prognosis in muscle-invasive transitional cell carcinoma of the bladder. *J Urol* 1996: **155**(5):1754-1757.

180 Sarkis AS, Bajorin DF, Reuter VE, Herr HW, Netto G, Zhang ZF et al. Prognostic value of p53 nuclear overexpression in patients with invasive bladder cancer treated with neoadjuvant MVAC. *J Clin Oncol* 1995: **13**(6):1384-1390.

181 Cote RJ, Esrig D, Groshen S, Jones PA, Skinner DG. p53 and treatment of bladder cancer. *Nature* 1997: **385**(6612):123-125.

182 JONES HC, SWINNEY J. Thiotepa in the treatment of tumours of the bladder. *Lancet* 1961: **2**:615-618.

183 Gavrell GJ, Lewis RW, Meehan WL, Leblanc GA. Intravesical thio-tepa in the immediate postoperative period in patients with recurrent transitional cell carcinoma of the bladder. *J Urol* 1978: **120**(4):410-411.

184 The effect of intravesical thiotepa on tumour recurrence after endoscopic treatment of newly diagnosed superficial bladder cancer. A further report with long-term follow-up of a Medical Research Council randomized trial. Medical Research Council Working Party on Urological Cancer, Subgroup on Superficial Bladder Cancer. *Br J Urol* 1994: **73**(6):632-638.

185 Bouffioux C, Denis L, Oosterlinck W, Viggiano G, Vergison B, Keuppens F et al. Adjuvant chemotherapy of recurrent superficial transitional cell carcinoma: results of a European organization for research on treatment of cancer randomized trial comparing intravesical instillation of thiotepa, doxorubicin and cisplatin. The European Organization for Research on Treatment of Cancer Genitourinary Group. *J Urol* 1992: **148**(2 Pt 1):297-301.

186 Nielsen HV, Thybo E. Epodyl treatment of bladder tumours. *Scand J Urol Nephrol* 1979: **13**(1):59-63.

187 Arcamone F, Cassinelli G, Fantini G, Grein A, Orezzi P, Pol C et al. Adriamycin, 14-hydroxydaunomycin, a new antitumor antibiotic from S. peucetius var. caesius. *Biotechnol Bioeng* 1969: **11**(6):1101-1110.

188 Di Marco A, Gaetani M, Scarpinato B. Adriamycin (NSC-123,127): a new antibiotic with antitumor activity. *Cancer Chemother Rep* 1969: **53**(1):33-37.

189 Kurth K, Tunn U, Ay R, Schroder FH, Pavone-Macaluso M, Debruyne F et al. Adjuvant chemotherapy for superficial transitional cell bladder carcinoma: long-term results of a European Organization for Research and Treatment of Cancer randomized trial comparing doxorubicin, ethoglucid and transurethral resection alone. *J Urol* 1997: **158**(2):378-384.

190 Di Marco A, Casazza AM, Giuliani F, Pratesi G, Arcamone F, Bernardi L et al. Synthesis and antitumor activity of 4-demethoxyadriamycin and 4-demethoxy-4' -epiadriamycin. *Cancer Treat Rep* 1978: **62**(3):375-380.

191 Matsumura Y, Tsushima T, Ozaki Y, Yoshimoto J, Akagi T, Obama T et al. Intravesical chemotherapy with 4'-epi-Adriamycin in patients with superficial bladder tumors. *Cancer Chemother Pharmacol* 1986: **16**(2):176-177.

192 IYER VN, SZYBALSKI W. MITOMYCINS AND PORFIROMYCIN: CHEMICAL MECHANISM OF ACTIVATION AND CROSS-LINKING OF DNA. *Science* 1964: **145**:55-58.

193 DeFuria MD, Bracken RB, Johnson DE, Soloway MS, Merrin CE, Morgan LR et al. Phase I-II study of mitomycin C topical therapy for

low-grade, low stage transitional cell carcinoma of the bladder: an interim report. *Cancer Treat Rep* 1980: **64**(2-3):225-230.

194 Heney NM, Koontz WW, Barton B, Soloway M, Trump DL, Hazra T et al. Intravesical thiotepa versus mitomycin C in patients with Ta, T1 and TIS transitional cell carcinoma of the bladder: a phase III prospective randomized study. *J Urol* 1988: **140**(6):1390-1393.

195 Huncharek M, Geschwind JF, Witherspoon B, McGarry R, Adcock D. Intravesical chemotherapy prophylaxis in primary superficial bladder cancer: a meta-analysis of 3703 patients from 11 randomized trials. *J Clin Epidemiol* 2000: **53**(7):676-680.

196 Huncharek M, McGarry R, Kupelnick B. Impact of intravesical chemotherapy on recurrence rate of recurrent superficial transitional cell carcinoma of the bladder: results of a meta-analysis. *Anticancer Res* 2001: **21**(1B):765-769.

197 Au JL, Badalament RA, Wientjes MG, Young DC, Warner JA, Venema PL et al. Methods to improve efficacy of intravesical mitomycin C: results of a randomized phase III trial. *J Natl Cancer Inst* 2001: **93**(8):597-604.

198 Cliff AM, Heatherwick B, Scoble J, Parr NJ. The effect of fasting or desmopressin before treatment on the concentration of mitomycin C during intravesical administration. *BJU Int* 2000: **86**(6):644-647.

199 Harris NM, Duffy PM, Crook TJ, Anderson WR, Sharpe P, Hayes MC et al. Intravesical pH: a potentially important variable affecting efficacy and the further development of anthracycline chemotherapy for superficial bladder cancer. *BJU Int* 2002: **90**(9):957-964.

200 Kuroda M, Niijima T, Kotake T, Akaza H, Hinotsu S. Effect of prophylactic treatment with intravesical epirubicin on recurrence of superficial bladder cancer--The 6th Trial of the Japanese Urological Cancer Research Group (JUCRG): a randomized trial of intravesical epirubicin at dose of 20mg/40ml, 30mg/40ml, 40mg/40ml. *Eur Urol* 2004: **45**(5):600-605.

201 Colombo R, Brausi M, Da Pozzo L, Salonia A, Montorsi F, Scattoni V et al. Thermo-chemotherapy and electromotive drug administration of mitomycin C in superficial bladder cancer eradication. a pilot study on marker lesion. *Eur Urol* 2001: **39**(1):95-100.

202 Di Stasi SM, Giannantoni A, Stephen RL, Capelli G, Navarra P, Massoud R et al. Intravesical electromotive mitomycin C versus passive transport mitomycin C for high risk superficial bladder cancer: a prospective randomized study. *J Urol* 2003: **170**(3):777-782.

203 Paroni R, Salonia A, Lev A, Da Pozzo LF, Cighetti G, Montorsi F et al. Effect of local hyperthermia of the bladder on mitomycin C pharmacokinetics during intravesical chemotherapy for the treatment of superficial transitional cell carcinoma. *Br J Clin Pharmacol* 2001: **52**(3):273-278.

204 Lukkarinen O, Paul C, Hellstrom P, Kontturi M, Nurmi M, Puntala P et al. Intravesical epirubicin with and without verapamil for the prophylaxis of superficial bladder tumours. *Scand J Urol Nephrol* 1991: **25**(1):25-28.

205 Naito S, Kotoh S, Omoto T, Osada Y, Sagiyama K, Iguchi A et al. Prophylactic intravesical instillation chemotherapy against recurrence after a transurethral resection of superficial bladder cancer: a randomized controlled trial of doxorubicin plus verapamil versus doxorubicin alone. The Kyushu University Urological Oncology Group. *Cancer Chemother Pharmacol* 1998: **42**(5):367-372.

206 Di Stasi SM, Giannantoni A, Giurioli A, Valenti M, Zampa G, Storti L et al. Sequential BCG and electromotive mitomycin versus BCG alone for high-risk superficial bladder cancer: a randomised controlled trial. *Lancet Oncol* 2006: **7**(1):43-51.

207 Okamura K, Ono Y, Kinukawa T, Matsuura O, Yamada S, Ando T et al. Randomized study of single early instillation of (2"R)-4'-O-tetrahydropyranyl-doxorubicin for a single superficial bladder carcinoma. *Cancer* 2002: **94**(9):2363-2368.

208 Hendricksen K, Witjes JA. Intravesical gemcitabine: an update of clinical results. *Curr Opin Urol* 2006: **16**(5):361-366.

209 Bartoletti R, Cai T, Gacci M, Giubilei G, Viggiani F, Santelli G et al. Intravesical gemcitabine therapy for superficial transitional cell carcinoma: results of a Phase II prospective multicenter study. *Urology* 2005: **66**(4):726-731.

210 Harris NM, Crook TJ, Dyer JP, Solomon LZ, Bass P, Cooper AJ et al. Intravesical meglumine gamma-linolenic acid in superficial bladder cancer: an efficacy study. *Eur Urol* 2002: **42**(1):39-42.

211 Uchio EM, Linehan WM, Figg WD, Walther MM. A phase I study of intravesical suramin for the treatment of superficial transitional cell carcinoma of the bladder. *J Urol* 2003: **169**(1):357-360.

212 Ord JJ, Streeter E, Jones A, Le Monnier K, Cranston D, Crew J et al. Phase I trial of intravesical Suramin in recurrent superficial transitional cell bladder carcinoma. *Br J Cancer* 2005: **92**(12):2140-2147.

213 Nseyo UO, DeHaven J, Dougherty TJ, Potter WR, Merrill DL, Lundahl SL et al. Photodynamic therapy (PDT) in the treatment of

patients with resistant superficial bladder cancer: a long-term experience. *J Clin Laser Med Surg* 1998: **16**(1):61-68.

214 Berger AP, Steiner H, Stenzl A, Akkad T, Bartsch G, Holtl L. Photodynamic therapy with intravesical instillation of 5-aminolevulinic acid for patients with recurrent superficial bladder cancer: a single-center study. *Urology* 2003: **61**(2):338-341.

215 Waidelich R, Beyer W, Knuchel R, Stepp H, Baumgartner R, Schroder J et al. Whole bladder photodynamic therapy with 5-aminolevulinic acid using a white light source. *Urology* 2003: **61**(2):332-337.

216 Manyak MJ, Ogan K. Photodynamic therapy for refractory superficial bladder cancer: long-term clinical outcomes of single treatment using intravesical diffusion medium. *J Endourol* 2003: **17**(8):633-639.

217 Kamuhabwa AA, Roskams T, D'Hallewin MA, Baert L, Van Poppel H, de Witte PA. Whole bladder wall photodynamic therapy of transitional cell carcinoma rat bladder tumors using intravesically administered hypericin. *Int J Cancer* 2003: **107**(3):460-467.

218 Asanuma H, Arai T, Morimoto Y, Kawauchi S, Satoh H, Seguchi K et al. Photodynamic therapy with PAD-S31, a new hydrophilic chlorin photosensitizer, in an orthotopic rat bladder tumor model. *J Urol* 2005: **174**(5):2016-2021.

219 Gasion JP, Cruz JF. Improving efficacy of intravesical chemotherapy. *Eur Urol* 2006: **50**(2):225-234.

220 Biedler JL, Riehm H. Cellular resistance to actinomycin D in Chinese hamster cells in vitro: cross-resistance, radioautographic, and cytogenetic studies. *Cancer Res* 1970: **30**(4):1174-1184.

221 Riordan JR, Ling V. Purification of P-glycoprotein from plasma membrane vesicles of Chinese hamster ovary cell mutants with reduced colchicine permeability. *J Biol Chem* 1979: **254**(24):12701-12705.

222 Inaba M, Kobayashi H, Sakurai Y, Johnson RK. Active efflux of daunorubicin and adriamycin in sensitive and resistant sublines of P388 leukemia. *Cancer Res* 1979: **39**(6 Pt 1):2200-2203.

223 Chen CJ, Chin JE, Ueda K, Clark DP, Pastan I, Gottesman MM et al. Internal duplication and homology with bacterial transport proteins in the mdr1 (P-glycoprotein) gene from multidrug-resistant human cells. *Cell* 1986: **47**(3):381-389.

224 Van der Bliek AM, Baas F, Van d, V, Biedler JL, Meyers MB, Ozols RF et al. Genes amplified and overexpressed in human multidrug-resistant cell lines. *Cancer Res* 1988: **48**(21):5927-5932.

225 Callen DF, Baker E, Simmers RN, Seshadri R, Roninson IB. Localization of the human multiple drug resistance gene, MDR1, to 7q21.1. *Hum Genet* 1987: **77**(2):142-144.

226 Gottesman MM, Pastan I. Biochemistry of multidrug resistance mediated by the multidrug transporter. *Annu Rev Biochem* 1993: **62**:385-427.

227 Ueda K, Cardarelli C, Gottesman MM, Pastan I. Expression of a full-length cDNA for the human "MDR1" gene confers resistance to colchicine, doxorubicin, and vinblastine. *Proc Natl Acad Sci U S A* 1987: **84**(9):3004-3008.

228 Chin JE, Soffir R, Noonan KE, Choi K, Roninson IB. Structure and expression of the human MDR (P-glycoprotein) gene family. *Mol Cell Biol* 1989: **9**(9):3808-3820.

229 Ueda K, Pastan I, Gottesman MM. Isolation and sequence of the promoter region of the human multidrug-resistance (P-glycoprotein) gene. *J Biol Chem* 1987: **262**(36):17432-17436.

230 Willingham MC, Richert ND, Cornwell MM, Tsuruo T, Hamada H, Gottesman MM et al. Immunocytochemical localization of P170 at the plasma membrane of multidrug-resistant human cells. *J Histochem Cytochem* 1987: **35**(12):1451-1456.

231 Molinari A, Cianfriglia M, Meschini S, Calcabrini A, Arancia G. P-glycoprotein expression in the Golgi apparatus of multidrug-resistant cells. *Int J Cancer* 1994: **59**(6):789-795.

232 Molinari A, Calcabrini A, Meschini S, Stringaro A, Del Bufalo D, Cianfriglia M et al. Detection of P-glycoprotein in the Golgi apparatus of drug-untreated human melanoma cells. *Int J Cancer* 1998: **75**(6):885-893.

233 Rajagopal A, Simon SM. Subcellular localization and activity of multidrug resistance proteins. *Mol Biol Cell* 2003: **14**(8):3389-3399.

234 Calcabrini A, Meschini S, Stringaro A, Cianfriglia M, Arancia G, Molinari A. Detection of P-glycoprotein in the nuclear envelope of multidrug resistant cells. *Histochem J* 2000: **32**(10):599-606.

235 Hyde SC, Emsley P, Hartshorn MJ, Mimmack MM, Gileadi U, Pearce SR et al. Structural model of ATP-binding proteins associated with cystic fibrosis, multidrug resistance and bacterial transport. *Nature* 1990: **346**(6282):362-365.

236 Sonveaux N, Shapiro AB, Goormaghtigh E, Ling V, Ruysschaert JM. Secondary and tertiary structure changes of reconstituted P-glycoprotein. A Fourier transform attenuated total reflection infrared spectroscopy analysis. *J Biol Chem* 1996: **271**(40):24617-24624.

237 Rosenberg MF, Velarde G, Ford RC, Martin C, Berridge G, Kerr ID et al. Repacking of the transmembrane domains of P-glycoprotein during the transport ATPase cycle. *EMBO J* 2001: **20**(20):5615-5625.

238 Rosenberg MF, Kamis AB, Callaghan R, Higgins CF, Ford RC. Three-dimensional structures of the mammalian multidrug resistance P-glycoprotein demonstrate major conformational changes in the transmembrane domains upon nucleotide binding. *J Biol Chem* 2003: **278**(10):8294-8299.

239 Rosenberg MF, Callaghan R, Ford RC, Higgins CF. Structure of the multidrug resistance P-glycoprotein to 2.5 nm resolution determined by electron microscopy and image analysis. *J Biol Chem* 1997: **272**(16):10685-10694.

240 Senior AE, Gadsby DC. ATP hydrolysis cycles and mechanism in P-glycoprotein and CFTR. *Semin Cancer Biol* 1997: **8**(3):143-150.

241 Shapiro AB, Ling V. Reconstitution of drug transport by purified P-glycoprotein. *J Biol Chem* 1995: **270**(27):16167-16175.

242 Gottesman MM. How cancer cells evade chemotherapy: sixteenth Richard and Hinda Rosenthal Foundation Award Lecture. *Cancer Res* 1993: **53**(4):747-754.

243 Higgins CF, Gottesman MM. Is the multidrug transporter a flippase? *Trends Biochem Sci* 1992: **17**(1):18-21.

244 Gervasoni JE, Jr., Fields SZ, Krishna S, Baker MA, Rosado M, Thuraisamy K et al. Subcellular distribution of daunorubicin in P-glycoprotein-positive and -negative drug-resistant cell lines using laser-assisted confocal microscopy. *Cancer Res* 1991: **51**(18):4955-4963.

245 Cole SP, Bhardwaj G, Gerlach JH, Mackie JE, Grant CE, Almquist KC et al. Overexpression of a transporter gene in a multidrug-resistant human lung cancer cell line. *Science* 1992: **258**(5088):1650-1654.

246 Zaman GJ, Versantvoort CH, Smit JJ, Eijdems EW, de Haas M, Smith AJ et al. Analysis of the expression of MRP, the gene for a new putative transmembrane drug transporter, in human multidrug resistant lung cancer cell lines. *Cancer Res* 1993: **53**(8):1747-1750.

247 Paul S, Breuninger LM, Tew KD, Shen H, Kruh GD. ATP-dependent uptake of natural product cytotoxic drugs by membrane vesicles establishes MRP as a broad specificity transporter. *Proc Natl Acad Sci U S A* 1996: **93**(14):6929-6934.

248 Hasegawa S, Abe T, Naito S, Kotoh S, Kumazawa J, Hipfner DR et al. Expression of multidrug resistance-associated protein (MRP),

MDR1 and DNA topoisomerase II in human multidrug-resistant bladder cancer cell lines. *Br J Cancer* 1995: **71**(5):907-913.

249 Schneider E, Cowan KH, Bader H, Toomey S, Schwartz GN, Karp JE et al. Increased expression of the multidrug resistance-associated protein gene in relapsed acute leukemia. *Blood* 1995: **85**(1):186-193.

250 Clifford SC, Neal DE, Lunec J. Alterations in expression of the multidrug resistance-associated protein (MRP) gene in high-grade transitional cell carcinoma of the bladder. *Br J Cancer* 1996: **73**(5):659-666.

251 Kruh GD, Belinsky MG. The MRP family of drug efflux pumps. *Oncogene* 2003: **22**(47):7537-7552.

252 Cole SP, Sparks KE, Fraser K, Loe DW, Grant CE, Wilson GM et al. Pharmacological characterization of multidrug resistant MRP-transfected human tumor cells. *Cancer Res* 1994: **54**(22):5902-5910.

253 Flens MJ, Izquierdo MA, Scheffer GL, Fritz JM, Meijer CJ, Scheper RJ et al. Immunochemical detection of the multidrug resistance-associated protein MRP in human multidrug-resistant tumor cells by monoclonal antibodies. *Cancer Res* 1994: **54**(17):4557-4563.

254 Eijdems EW, Zaman GJ, de Haas M, Versantvoort CH, Flens MJ, Scheper RJ et al. Altered MRP is associated with multidrug resistance and reduced drug accumulation in human SW-1573 cells. *Br J Cancer* 1995: **72**(2):298-306.

255 Breuninger LM, Paul S, Gaughan K, Miki T, Chan A, Aaronson SA et al. Expression of multidrug resistance-associated protein in NIH/3T3 cells confers multidrug resistance associated with increased drug efflux and altered intracellular drug distribution. *Cancer Res* 1995: **55**(22):5342-5347.

256 Ishikawa T, Akimaru K, Kuo MT, Priebe W, Suzuki M. How does the MRP/GS-X pump export doxorubicin? *J Natl Cancer Inst* 1995: **87**(21):1639-1640.

257 Zaman GJ, Flens MJ, van Leusden MR, de Haas M, Mulder HS, Lankelma J et al. The human multidrug resistance-associated protein MRP is a plasma membrane drug-efflux pump. *Proc Natl Acad Sci U S A* 1994: **91**(19):8822-8826.

258 Doyle LA, Yang W, Abruzzo LV, Krogmann T, Gao Y, Rishi AK et al. A multidrug resistance transporter from human MCF-7 breast cancer cells. *Proc Natl Acad Sci U S A* 1998: **95**(26):15665-15670.

259 Diestra JE, Scheffer GL, Catala I, Maliepaard M, Schellens JH, Scheper RJ et al. Frequent expression of the multi-drug resistance-associated protein BCRP/MXR/ABCP/ABCG2 in human tumours

detected by the BXP-21 monoclonal antibody in paraffin-embedded material. *J Pathol* 2002: **198**(2):213-219.

260 Candeil L, Gourdier I, Peyron D, Vezzio N, Copois V, Bibeau F et al. ABCG2 overexpression in colon cancer cells resistant to SN38 and in irinotecan-treated metastases. *Int J Cancer* 2004: **109**(6):848-854.

261 Knutsen T, Rao VK, Ried T, Mickley L, Schneider E, Miyake K et al. Amplification of 4q21-q22 and the MXR gene in independently derived mitoxantrone-resistant cell lines. *Genes Chromosomes Cancer* 2000: **27**(1):110-116.

262 Rocchi E, Khodjakov A, Volk EL, Yang CH, Litman T, Bates SE et al. The product of the ABC half-transporter gene ABCG2 (BCRP/MXR/ABCP) is expressed in the plasma membrane. *Biochem Biophys Res Commun* 2000: **271**(1):42-46.

263 Maliepaard M, Scheffer GL, Faneyte IF, van Gastelen MA, Pijnenborg AC, Schinkel AH et al. Subcellular localization and distribution of the breast cancer resistance protein transporter in normal human tissues. *Cancer Res* 2001: **61**(8):3458-3464.

264 Doyle LA, Ross DD. Multidrug resistance mediated by the breast cancer resistance protein BCRP (ABCG2). *Oncogene* 2003: **22**(47):7340-7358.

265 Scheper RJ, Broxterman HJ, Scheffer GL, Kaaijk P, Dalton WS, van Heijningen TH et al. Overexpression of a M(r) 110,000 vesicular protein in non-P-glycoprotein-mediated multidrug resistance. *Cancer Res* 1993: **53**(7):1475-1479.

266 Izquierdo MA, van der Zee AG, Vermorken JB, Van d, V, Belien JA, Giaccone G et al. Drug resistance-associated marker Lrp for prediction of response to chemotherapy and prognoses in advanced ovarian carcinoma. *J Natl Cancer Inst* 1995: **87**(16):1230-1237.

267 Izquierdo MA, Scheffer GL, Flens MJ, Giaccone G, Broxterman HJ, Meijer CJ et al. Broad distribution of the multidrug resistance-related vault lung resistance protein in normal human tissues and tumors. *Am J Pathol* 1996: **148**(3):877-887.

268 Kedersha NL, Rome LH. Isolation and characterization of a novel ribonucleoprotein particle: large structures contain a single species of small RNA. *J Cell Biol* 1986: **103**(3):699-709.

269 Kedersha NL, Heuser JE, Chugani DC, Rome LH. Vaults. III. Vault ribonucleoprotein particles open into flower-like structures with octagonal symmetry. *J Cell Biol* 1991: **112**(2):225-235.

270 Scheffer GL, Wijngaard PL, Flens MJ, Izquierdo MA, Slovak ML, Pinedo HM et al. The drug resistance-related protein LRP is the human major vault protein. *Nat Med* 1995: **1**(6):578-582.

271 Kong LB, Siva AC, Rome LH, Stewart PL. Structure of the vault, a ubiquitous celular component. *Structure* 1999: **7**(4):371-379.

272 Kickhoefer VA, Siva AC, Kedersha NL, Inman EM, Ruland C, Streuli M et al. The 193-kD vault protein, VPARP, is a novel poly(ADP-ribose) polymerase. *J Cell Biol* 1999: **146**(5):917-928.

273 Kickhoefer VA, Stephen AG, Harrington L, Robinson MO, Rome LH. Vaults and telomerase share a common subunit, TEP1. *J Biol Chem* 1999: **274**(46):32712-32717.

274 Collins K. Mammalian telomeres and telomerase. *Curr Opin Cell Biol* 2000: **12**(3):378-383.

275 de Murcia G, Menissier-de Murcia J, Schreiber V. Poly(ADP-ribose) polymerase: molecular biological aspects. *Bioessays* 1991: **13**(9):455-462.

276 de Murcia G, Schreiber V, Molinete M, Saulier B, Poch O, Masson M et al. Structure and function of poly(ADP-ribose) polymerase. *Mol Cell Biochem* 1994: **138**(1-2):15-24.

277 Ame JC, Rolli V, Schreiber V, Niedergang C, Apiou F, Decker P et al. PARP-2, A novel mammalian DNA damage-dependent poly(ADP-ribose) polymerase. *J Biol Chem* 1999: **274**(25):17860-17868.

278 Le Rhun Y, Kirkland JB, Shah GM. Cellular responses to DNA damage in the absence of Poly(ADP-ribose) polymerase. *Biochem Biophys Res Commun* 1998: **245**(1):1-10.

279 Kickhoefer VA, Rajavel KS, Scheffer GL, Dalton WS, Scheper RJ, Rome LH. Vaults are up-regulated in multidrug-resistant cancer cell lines. *J Biol Chem* 1998: **273**(15):8971-8974.

280 Chugani DC, Rome LH, Kedersha NL. Evidence that vault ribonucleoprotein particles localize to the nuclear pore complex. *J Cell Sci* 1993: **106 (Pt 1)**:23-29.

281 Hamill DR, Suprenant KA. Characterization of the sea urchin major vault protein: a possible role for vault ribonucleoprotein particles in nucleocytoplasmic transport. *Dev Biol* 1997: **190**(1):117-128.

282 Herrmann C, Golkaramnay E, Inman E, Rome L, Volknandt W. Recombinant major vault protein is targeted to neuritic tips of PC12 cells. *J Cell Biol* 1999: **144**(6):1163-1172.

283 Li JY, Volknandt W, Dahlstrom A, Herrmann C, Blasi J, Das B et al. Axonal transport of ribonucleoprotein particles (vaults). *Neuroscience* 1999: **91**(3):1055-1065.

284 Abbondanza C, Rossi V, Roscigno A, Gallo L, Belsito A, Piluso G et al. Interaction of vault particles with estrogen receptor in the MCF-7 breast cancer cell. *J Cell Biol* 1998: **141**(6):1301-1310.

285 Izquierdo MA, Scheffer GL, Flens MJ, Shoemaker RH, Rome LH, Scheper RJ. Relationship of LRP-human major vault protein to in vitro and clinical resistance to anticancer drugs. *Cytotechnology* 1996: **19**(3):191-197.

286 Kitazono M, Sumizawa T, Takebayashi Y, Chen ZS, Furukawa T, Nagayama S et al. Multidrug resistance and the lung resistance-related protein in human colon carcinoma SW-620 cells. *J Natl Cancer Inst* 1999: **91**(19):1647-1653.

287 Kitazono M, Okumura H, Ikeda R, Sumizawa T, Furukawa T, Nagayama S et al. Reversal of LRP-associated drug resistance in colon carcinoma SW-620 cells. *Int J Cancer* 2001: **91**(1):126-131.

288 Ohno N, Tani A, Uozumi K, Hanada S, Furukawa T, Akiba S et al. Expression of functional lung resistance--related protein predicts poor outcome in adult T-cell leukemia. *Blood* 2001: **98**(4):1160-1165.

289 Danks MK, Yalowich JC, Beck WT. Atypical multiple drug resistance in a human leukemic cell line selected for resistance to teniposide (VM-26). *Cancer Res* 1987: **47**(5):1297-1301.

290 Deffie AM, Batra JK, Goldenberg GJ. Direct correlation between DNA topoisomerase II activity and cytotoxicity in adriamycin-sensitive and -resistant P388 leukemia cell lines. *Cancer Res* 1989: **49**(1):58-62.

291 Deffie AM, McPherson JP, Gupta RS, Hedley DW, Goldenberg GJ. Multifactorial resistance to antineoplastic agents in drug-resistant P388 murine leukemia, Chinese hamster ovary, and human HeLa cells, with emphasis on the role of DNA topoisomerase II. *Biochem Cell Biol* 1992: **70**(5):354-364.

292 Friche E, Danks MK, Schmidt CA, Beck WT. Decreased DNA topoisomerase II in daunorubicin-resistant Ehrlich ascites tumor cells. *Cancer Res* 1991: **51**(16):4213-4218.

293 Ravdin PM. Anthracycline resistance in breast cancer: clinical applications of current knowledge. *Eur J Cancer* 1995: **31A Suppl 7**:S11-S14.

294 Batist G, Tulpule A, Sinha BK, Katki AG, Myers CE, Cowan KH. Overexpression of a novel anionic glutathione transferase in multidrug-resistant human breast cancer cells. *J Biol Chem* 1986: **261**(33):15544-15549.

295 Awasthi S, Singhal SS, Srivastava SK, Zimniak P, Bajpai KK, Saxena M et al. Adenosine triphosphate-dependent transport of

doxorubicin, daunomycin, and vinblastine in human tissues by a mechanism distinct from the P-glycoprotein. *J Clin Invest* 1994: **93**(3):958-965.

296 Muller M, Meijer C, Zaman GJ, Borst P, Scheper RJ, Mulder NH et al. Overexpression of the gene encoding the multidrug resistance-associated protein results in increased ATP-dependent glutathione S-conjugate transport. *Proc Natl Acad Sci U S A* 1994: **91**(26):13033-13037.

297 Tsuruo T, Iida H, Tsukagoshi S, Sakurai Y. Overcoming of vincristine resistance in P388 leukemia in vivo and in vitro through enhanced cytotoxicity of vincristine and vinblastine by verapamil. *Cancer Res* 1981: **41**(5):1967-1972.

298 Tsuruo T, Iida H, Yamashiro M, Tsukagoshi S, Sakurai Y. Enhancement of vincristine- and adriamycin-induced cytotoxicity by verapamil in P388 leukemia and its sublines resistant to vincristine and adriamycin. *Biochem Pharmacol* 1982: **31**(19):3138-3140.

299 Tsuruo T, Iida H, Tsukagoshi S, Sakurai Y. Increased accumulation of vincristine and adriamycin in drug-resistant P388 tumor cells following incubation with calcium antagonists and calmodulin inhibitors. *Cancer Res* 1982: **42**(11):4730-4733.

300 Yusa K, Tsuruo T. Reversal mechanism of multidrug resistance by verapamil: direct binding of verapamil to P-glycoprotein on specific sites and transport of verapamil outward across the plasma membrane of K562/ADM cells. *Cancer Res* 1989: **49**(18):5002-5006.

301 Lecureur V, Fardel O, Guillouzo A. The antiprogestatin drug RU 486 potentiates doxorubicin cytotoxicity in multidrug resistant cells through inhibition of P-glycoprotein function. *FEBS Lett* 1994: **355**(2):187-191.

302 Dayan G, Jault JM, Baubichon-Cortay H, Baggetto LG, Renoir JM, Baulieu EE et al. Binding of steroid modulators to recombinant cytosolic domain from mouse P-glycoprotein in close proximity to the ATP site. *Biochemistry* 1997: **36**(49):15208-15215.

303 Conseil G, Baubichon-Cortay H, Dayan G, Jault JM, Barron D, Di Pietro A. Flavonoids: a class of modulators with bifunctional interactions at vicinal ATP- and steroid-binding sites on mouse P-glycoprotein. *Proc Natl Acad Sci U S A* 1998: **95**(17):9831-9836.

304 Choi CH. ABC transporters as multidrug resistance mechanisms and the development of chemosensitizers for their reversal. *Cancer Cell Int* 2005: **5**:30.

305 Hagen K, Daly JJ, Kamali HM, Lin JC, Yu SC, Prout GR, Jr. New assay for cytotoxic agents in human bladder cancer. *Surg Forum* 1979: **30**:560-562.

306 Hepburn PJ, Oliver RT, Riley PA, Hill BT, Masters JR. Comparison of the cytotoxic activities of chemotherapeutic drugs using a human bladder cancer cell line. *Urol Res* 1985: **13**(1):27-34.

307 Simpson WG, Tseng MT, Anderson KC, Harty JI. Verapamil enhancement of chemotherapeutic efficacy in human bladder cancer cells. *J Urol* 1984: **132**(3):574-576.

308 McGovern F, Kachel T, Vijan S, Schiff S, Lin CW, Prout GR, Jr. Establishment and characterization of a doxorubicin-resistant human bladder cancer cell line (MGH-U1R). *J Urol* 1988: **140**(2):410-414.

309 Long JP, Jr., Prout GR, Jr., Wong YK, Lin CW. The effect of verapamil on a multi-drug resistant bladder carcinoma cell line and its potential as an intravesical chemotherapeutic agent. *J Urol* 1990: **143**(5):1053-1056.

310 Floyd JW, Lin CW, Prout GR, Jr. Multi-drug resistance of a doxorubicin-resistant bladder cancer cell line. *J Urol* 1990: **144**(1):169-171.

311 Popert RJ, Goodall J, Coptcoat MJ, Thompson PM, Parmar MK, Masters JR. Superficial bladder cancer: the response of a marker tumour to a single intravesical instillation of epirubicin. *Br J Urol* 1994: **74**(2):195-199.

312 Kimiya K, Naito S, Soejima T, Sakamoto N, Kotoh S, Kumazawa J et al. Establishment and characterization of doxorubicin-resistant human bladder cancer cell line, KK47/ADM. *J Urol* 1992: **148**(2 Pt 1):441-445.

313 Seemann O, Muscheck M, Siegsmund M, Pilch H, Nebe CT, Rassweiler J et al. Establishment and characterization of a multidrug-resistant human bladder carcinoma cell line RT112/D21. *Urol Res* 1995: **22**(6):353-360.

314 Guo H, Lu G, Xiong X, Dong J, Liu S. Establishment of doxorubicin-resistant human bladder cancer cell line (BUI-87/ADMR) and its mechanism of multidrug resistance. *Chin Med J (Engl)* 1997: **110**(3):167-172.

315 Naito S, Hasegawa S, Yokomizo A, Koga H, Kotoh S, Kuwano M et al. Non-P-glycoprotein-mediated atypical multidrug resistance in a human bladder cancer cell line. *Jpn J Cancer Res* 1995: **86**(11):1112-1118.

316 Kim WJ, Kakehi Y, Yoshida O. Multifactorial involvement of multidrug resistance-associated [correction of resistance] protein, DNA

topoisomerase II and glutathione/glutathione-S-transferase in nonP-glycoprotein-mediated multidrug resistance in human bladder cancer cells. *Int J Urol* 1997: **4**(6):583-590.

317 Thomas DJ, Birch PJ, Vickers J, Robinson M, Clifford S, Hall A et al. Glutathione-S-transferase pi expression in transitional cell carcinoma of the bladder. *Br J Urol* 1993: **72**(5 Pt 2):740-743.

318 Park J, Shinohara N, Liebert M, Noto L, Flint A, Grossman HB. P-glycoprotein expression in bladder cancer. *J Urol* 1994: **151**(1):43-46.

319 Petrylak DP, Scher HI, Reuter V, O'Brien JP, Cordon-Cardo C. P-glycoprotein expression in primary and metastatic transitional cell carcinoma of the bladder. *Ann Oncol* 1994: **5**(9):835-840.

320 Pu YS, Tsai TC, Cheng AL, Tsai CY, Tseng NF, Su IJ et al. Expression of MDR-1 gene in transitional cell carcinoma and its correlation with chemotherapy response. *J Urol* 1996: **156**(1):271-275.

321 Kim WJ, Kakehi Y, Wu WJ, Fukumoto M, Yoshida O. Expression of multidrug resistance-related genes (mdrl, MRP, GST-pi and DNA topoisomerase II) in urothelial cancers. *Br J Urol* 1996: **78**(3):361-368.

322 Gan Y, Wientjes MG, Badalament RA, Au JL. Pharmacodynamics of doxorubicin in human bladder tumors. *Clin Cancer Res* 1996: **2**(8):1275-1283.

323 Nakagawa M, Emoto A, Nasu N, Hanada T, Kuwano M, Cole SP et al. Clinical significance of multi-drug resistance associated protein and P-glycoprotein in patients with bladder cancer. *J Urol* 1997: **157**(4):1260-1264.

324 Tada Y, Wada M, Migita T, Nagayama J, Hinoshita E, Mochida Y et al. Increased expression of multidrug resistance-associated proteins in bladder cancer during clinical course and drug resistance to doxorubicin. *Int J Cancer* 2002: **98**(4):630-635.

325 Diestra JE, Condom E, Del Muro XG, Scheffer GL, Perez J, Zurita AJ et al. Expression of multidrug resistance proteins P-glycoprotein, multidrug resistance protein 1, breast cancer resistance protein and lung resistance related protein in locally advanced bladder cancer treated with neoadjuvant chemotherapy: biological and clinical implications. *J Urol* 2003: **170**(4 Pt 1):1383-1387.

326 Zhu Y, Kong C, Zeng Y, Sun Z, Gao H. Expression of lung resistance-related protein in transitional cell carcinoma of bladder. *Urology* 2004: **63**(4):694-698.

327 SILVESTRINI R, Gaetani M. [ACTION OF DAUNOMYCIN ON THE NUCLEIC METABOLISM OF EHRLICH ASCITES TUMOR.]. *Tumori* 1963: **49**:389-397.

328 Villani F, Comazzi R, Lacaita G, Genitoni V, Guindani A, Martini A. Preliminary echocardiographic and polygraphic evaluation of cardiac toxicity of 4'-epi-doxorubicin. *Int J Clin Pharmacol Ther Toxicol* 1983: **21**(4):203-208.

329 Facchinetti T, Mantovani A, Cantoni L, Cantoni R, Salmona M. Intercalation with DNA is a prerequisite for daunomycin, adriamycin and its congeners in inhibiting DNAase I. *Chem Biol Interact* 1978: **20**(1):97-102.

330 Taatjes DJ, Fenick DJ, Koch TH. Nuclear targeting and nuclear retention of anthracycline-formaldehyde conjugates implicates DNA covalent bonding in the cytotoxic mechanism of anthracyclines. *Chem Res Toxicol* 1999: **12**(7):588-596.

331 Young RC, Ozols RF, Myers CE. The anthracycline antineoplastic drugs. *N Engl J Med* 1981: **305**(3):139-153.

332 Salmon SE, Sartorelli AC. Chapter 58: Cancer chemotherapy. In: Katzung BG, ed, Basic and Clinical Pharmacology, Third edn. Chapt 58. Appleton and Lange, 1987: 665-699.

333 Solie TN, Yuncker C. Adriamycin induced changes in translocation of sodium ions in transporting epithelial cells. *Life Sci* 1978: **22**(21):1907-1919.

334 Ames MM, Spreafico F. Selected pharmacologic characteristics of idarubicin and idarubicinol. *Leukemia* 1992: **6 Suppl 1**:70-75.

335 Plosker GL, Faulds D. Epirubicin. A review of its pharmacodynamic and pharmacokinetic properties, and therapeutic use in cancer chemotherapy. *Drugs* 1993: **45**(5):788-856.

336 Tewey KM, Rowe TC, Yang L, Halligan BD, Liu LF. Adriamycin-induced DNA damage mediated by mammalian DNA topoisomerase II. *Science* 1984: **226**(4673):466-468.

337 Bodley A, Liu LF, Israel M, Seshadri R, Koseki Y, Giuliani FC et al. DNA topoisomerase II-mediated interaction of doxorubicin and daunorubicin congeners with DNA. *Cancer Res* 1989: **49**(21):5969-5978.

338 Capranico G, Zunino F, Kohn KW, Pommier Y. Sequence-selective topoisomerase II inhibition by anthracycline derivatives in SV40 DNA: relationship with DNA binding affinity and cytotoxicity. *Biochemistry* 1990: **29**(2):562-569.

339 Cummings J, Anderson L, Willmott N, Smyth JF. The molecular pharmacology of doxorubicin in vivo. *Eur J Cancer* 1991: **27**(5):532-535.

340 Coley HM, Amos WB, Twentyman PR, Workman P. Examination by laser scanning confocal fluorescence imaging

microscopy of the subcellular localisation of anthracyclines in parent and multidrug resistant cell lines. *Br J Cancer* 1993: **67**(6):1316-1323.

341 Schuurhuis GJ, Broxterman HJ, Cervantes A, van Heijningen TH, de Lange JH, Baak JP et al. Quantitative determination of factors contributing to doxorubicin resistance in multidrug-resistant cells. *J Natl Cancer Inst* 1989: **81**(24):1887-1892.

342 Bankusli I, Yin MB, Mazzoni A, Abdellah AJ, Rustum YM. Enhancement of adriamycin-induced cytotoxicity by increasing retention and inhibition of DNA repair in DOX-resistant P388 cell lines with new calcium channel blocker, DMDP. *Anticancer Res* 1989: **9**(3):567-574.

343 Krishan A, Ganapathi R. Laser flow cytometry and cancer chemotherapy: detection of intracellular anthracyclines by flow cytometry. *J Histochem Cytochem* 1979: **27**(12):1655-1656.

344 Krishan A, Ganapathi R. Laser flow cytometric studies on the intracellular fluorescence of anthracyclines. *Cancer Res* 1980: **40**(11):3895-3900.

345 Ganapathi R, Reiter W, Krishan A. Intracellular adriamycin levels and cytotoxicity in adriamycin-sensitive and adriamycin-resistant P388 mouse leukemia cells. *J Natl Cancer Inst* 1982: **68**(6):1027-1032.

346 Duffy PM, Hayes MC, Cooper A, Smart CJ. Determination and reversal of resistance to epirubicin intravesical chemotherapy. A flow cytometric model. *Br J Urol* 1996: **77**(6):819-823.

347 Duffy PM, Hayes MC, Gatrell SK, Cooper A, Smart CJ. Determination and reversal of resistance to epirubicin intravesical chemotherapy. A confocal imaging study. *Br J Urol* 1996: **77**(6):824-829.

348 Davies CL, Duffy PM, MacRobert AJ, Loizidou MC, Cooper AJ, Taylor I. Localization of anthracycline accumulation in sensitive and resistant urothelial tumor cell lines. *Cancer Detect Prev* 1996: **20**(6):625-633.

349 Cooper AJ, Hayes MC, Duffy PM, Davies CL, Smart CJ. Multidrug resistance evaluation by confocal microscopy in primary urothelial cancer explant colonies. *Cytotechnology* 1996: **19**(3):181-186.

350 Davies CL, Loizidou M, Cooper AJ, Taylor I. Effect of gamma-linolenic acid on cellular uptake of structurally related anthracyclines in human drug sensitive and multidrug resistant bladder and breast cancer cell lines. *Eur J Cancer* 1999: **35**(10):1534-1540.

351 Consoli U, Van NT, Neamati N, Mahadevia R, Beran M, Zhao S et al. Cellular pharmacology of mitoxantrone in p-glycoprotein-positive and -negative human myeloid leukemic cell lines. *Leukemia* 1997: **11**(12):2066-2074.

352 Bobichon H, Cailleret L, Ploton D, Belhoussine R, Jardillier JC. Nuclear transport as an ultimate step of multidrug resistance. *Life Sci* 1999: **65**(22):2343-2349.

353 Duffy PM, Hayes MC, Cooper A, Smart CJ. Confocal microscopy of idarubicin localisation in sensitive and multidrug-resistant bladder cancer cell lines. *Br J Cancer* 1996: **74**(6):906-909.

354 Gorlich D, Kutay U. Transport between the cell nucleus and the cytoplasm. *Annu Rev Cell Dev Biol* 1999: **15**:607-660.

355 Fahrenkrog B, Aebi U. The nuclear pore complex: nucleocytoplasmic transport and beyond. *Nat Rev Mol Cell Biol* 2003: **4**(10):757-766.

356 Pemberton LF, Paschal BM. Mechanisms of receptor-mediated nuclear import and nuclear export. *Traffic* 2005: **6**(3):187-198.

357 Conti E, Muller CW, Stewart M. Karyopherin flexibility in nucleocytoplasmic transport. *Curr Opin Struct Biol* 2006: **16**(2):237-244.

358 Pante N, Aebi U. Molecular dissection of the nuclear pore complex. *Crit Rev Biochem Mol Biol* 1996: **31**(2):153-199.

359 Yang Q, Rout MP, Akey CW. Three-dimensional architecture of the isolated yeast nuclear pore complex: functional and evolutionary implications. *Mol Cell* 1998: **1**(2):223-234.

360 Rout MP, Wente SR. Pores for thought: nuclear pore complex proteins. *Trends Cell Biol* 1994: **4**(10):357-365.

361 Rout MP, Aitchison JD, Suprapto A, Hjertaas K, Zhao Y, Chait BT. The yeast nuclear pore complex: composition, architecture, and transport mechanism. *J Cell Biol* 2000: **148**(4):635-651.

362 Cronshaw JM, Krutchinsky AN, Zhang W, Chait BT, Matunis MJ. Proteomic analysis of the mammalian nuclear pore complex. *J Cell Biol* 2002: **158**(5):915-927.

363 Stoffler D, Fahrenkrog B, Aebi U. The nuclear pore complex: from molecular architecture to functional dynamics. *Curr Opin Cell Biol* 1999: **11**(3):391-401.

364 Goldberg MW, Allen TD. The nuclear pore complex: three-dimensional surface structure revealed by field emission, in-lens scanning electron microscopy, with underlying structure uncovered by proteolysis. *J Cell Sci* 1993: **106 (Pt 1)**:261-274.

365 Ribbeck K, Gorlich D. Kinetic analysis of translocation through nuclear pore complexes. *EMBO J* 2001: **20**(6):1320-1330.

366 Bustamante JO, Liepins A, Hanover JA. Nuclear pore complex ion channels (review). *Mol Membr Biol* 1994: **11**(3):141-150.

367 Paine PL, Moore LC, Horowitz SB. Nuclear envelope permeability. *Nature* 1975: **254**(5496):109-114.

368 Smith A, Brownawell A, Macara IG. Nuclear import of Ran is mediated by the transport factor NTF2. *Curr Biol* 1998: **8**(25):1403-1406.

369 Conti E, Uy M, Leighton L, Blobel G, Kuriyan J. Crystallographic analysis of the recognition of a nuclear localization signal by the nuclear import factor karyopherin alpha. *Cell* 1998: **94**(2):193-204.

370 Li J, Meyer AN, Donoghue DJ. Nuclear localization of cyclin B1 mediates its biological activity and is regulated by phosphorylation. *Proc Natl Acad Sci U S A* 1997: **94**(2):502-507.

371 Yang J, Bardes ES, Moore JD, Brennan J, Powers MA, Kornbluth S. Control of cyclin B1 localization through regulated binding of the nuclear export factor CRM1. *Genes Dev* 1998: **12**(14):2131-2143.

372 Toyoshima F, Moriguchi T, Wada A, Fukuda M, Nishida E. Nuclear export of cyclin B1 and its possible role in the DNA damage-induced G2 checkpoint. *EMBO J* 1998: **17**(10):2728-2735.

373 Furnari B, Rhind N, Russell P. Cdc25 mitotic inducer targeted by chk1 DNA damage checkpoint kinase. *Science* 1997: **277**(5331):1495-1497.

374 Tomoda K, Kubota Y, Kato J. Degradation of the cyclin-dependent-kinase inhibitor p27Kip1 is instigated by Jab1. *Nature* 1999: **398**(6723):160-165.

375 Harris CC, Hollstein M. Clinical implications of the p53 tumor-suppressor gene. *N Engl J Med* 1993: **329**(18):1318-1327.

376 Moll UM, Riou G, Levine AJ. Two distinct mechanisms alter p53 in breast cancer: mutation and nuclear exclusion. *Proc Natl Acad Sci U S A* 1992: **89**(15):7262-7266.

377 Middeler G, Zerf K, Jenovai S, Thulig A, Tschodrich-Rotter M, Kubitscheck U et al. The tumor suppressor p53 is subject to both nuclear import and export, and both are fast, energy-dependent and lectin-inhibited. *Oncogene* 1997: **14**(12):1407-1417.

378 Ryan KM, Phillips AC, Vousden KH. Regulation and function of the p53 tumor suppressor protein. *Curr Opin Cell Biol* 2001: **13**(3):332-337.

379 Shaulsky G, Goldfinger N, Ben Ze'ev A, Rotter V. Nuclear accumulation of p53 protein is mediated by several nuclear localization

signals and plays a role in tumorigenesis. *Mol Cell Biol* 1990: **10**(12):6565-6577.

380 Yasuhara N, Eguchi Y, Tachibana T, Imamoto N, Yoneda Y, Tsujimoto Y. Essential role of active nuclear transport in apoptosis. *Genes Cells* 1997: **2**(1):55-64.

381 Ferrando-May E, Cordes V, Biller-Ckovric I, Mirkovic J, Gorlich D, Nicotera P. Caspases mediate nucleoporin cleavage, but not early redistribution of nuclear transport factors and modulation of nuclear permeability in apoptosis. *Cell Death Differ* 2001: **8**(5):495-505.

382 Lam DH, Aplan PD. NUP98 gene fusions in hematologic malignancies. *Leukemia* 2001: **15**(11):1689-1695.

383 Fornerod M, Ohno M, Yoshida M, Mattaj IW. CRM1 is an export receptor for leucine-rich nuclear export signals. *Cell* 1997: **90**(6):1051-1060.

384 Lin CW, Lin JC, Prout GR Jr. Establishment and characterization of four human bladder tumor cell lines and sublines with different degrees of malignancy. *Cancer Research* 1985: **45**(10):5070-5079.

385 Crook TJ, Hall IS, Solomon LZ, Birch BR, Cooper AJ. A model of superficial bladder cancer using fluorescent tumour cells in an organ-culture system. *BJU Int* 2000: **86**(7):886-893.

386 Hayes MC, Birch BR, Cooper AJ, Primrose JN. Cellular resistance to mitomycin C is associated with overexpression of MDR-1 in a urothelial cancer cell line (MGH-U1). *BJU International* 2001: **87**(3):245-250.

387 Geng YJ, Wu Q, Muszynski M, Hansson GK, Libby P. Apoptosis of vascular smooth muscle cells induced by in vitro stimulation with interferon-gamma, tumor necrosis factor-alpha, and interleukin-1 beta. *Arterioscler Thromb Vasc Biol* 1996: **16**(1):19-27.

388 Givan A. Flow cytometry: First principles. Wiley-Liss, NY., 2001.

389 Freshney R. Culture of animal cells. A manual of basic technique. Wiley-Liss, 1994.

390 Holt SJ, Alexander P, Inman CB, Davies D. **Epidermal growth factor induced tyrosine phosphorylation of nuclear proteins associated with translocation of epidermal growth factor receptor into the nucleus.** *Biochem Pharmacol* 1994: **47**(1):117-126.

391 Mcneil PL, Murphy F, Lanni F, Taylor DL. A method for incorporating macromolecules into adherent cells. *J Cell Biol* 1984: **98**(4):1556-1564.

392 Lane RD. A short duration polyethylene glycol fusion technique for increasing production of monoclonal antibody-secreting hybridomas. *J Immunol Methods* 1985: **81**(2):223-228.

393 Wardman P, Dennis MF, White J. A probe for intracellular concentrations of drugs: delayed fluorescence from acridine orange. *Int J Radiat Oncol Biol Phys* 1989: **16**(4):935-938.

394 Lewin JM, Lwaleed BA, Cooper AJ, Birch BR. The direct effect of nuclear pores on nuclear chemotherapeutic concentration in multidrug resistant bladder cancer: the nuclear sparing phenomenon. *J Urol* 2007: **177**(4):1526-1530.

395 Kiyomiya K, Matsuo S, Kurebe M. Mechanism of specific nuclear transport of adriamycin: the mode of nuclear translocation of adriamycin-proteasome complex. *Cancer Res* 2001: **61**(6):2467-2471.

396 Colin M, Madoulet C, Warren L, Jardillier JC. Alterations of vinblastine influx in multidrug-resistant lymphoblastic leukaemic CEM cells. *Anticancer Res* 1996: **16**(1):407-412.

397 Luker GD, Flagg TP, Sha Q, Luker KE, Pica CM, Nichols CG et al. MDR1 P-glycoprotein reduces influx of substrates without affecting membrane potential. *J Biol Chem* 2001: **276**(52):49053-49060.

398 Chen VY, Posada MM, Zhao L, Rosania GR. Rapid doxorubicin efflux from the nucleus of drug-resistant cancer cells following extracellular drug clearance. *Pharm Res* 2007: **24**(11):2156-2167.

399 Bobichon H, Colin M, Depierreux C, Liautaud-Roger F, Jardillier JC. Ultrastructural changes related to multidrug resistance in CEM cells: role of cytoplasmic vesicles in drug exclusion. *J Exp Ther Oncol* 1996: **1**(1):49-61.

400 Consoli U, Priebe W, Ling YH, Mahadevia R, Griffin M, Zhao S et al. The novel anthracycline annamycin is not affected by P-glycoprotein-related multidrug resistance: comparison with idarubicin and doxorubicin in HL-60 leukemia cell lines. *Blood* 1996: **88**(2):633-644.

401 Perez-Soler R, Neamati N, Zou Y, Schneider E, Doyle LA, Andreeff M et al. Annamycin circumvents resistance mediated by the multidrug resistance-associated protein (MRP) in breast MCF-7 and small-cell lung UMCC-1 cancer cell lines selected for resistance to etoposide. *Int J Cancer* 1997: **71**(1):35-41.

402 Mazel M, Clair P, Rousselle C, Vidal P, Scherrmann JM, Mathieu D et al. Doxorubicin-peptide conjugates overcome multidrug resistance. *Anticancer Drugs* 2001: **12**(2):107-116.